A

Presented to

the faculty of the School of Engineering and Applied Science

University of Virginia

in partial fulfillment

of the requirements for the degree

by

APPROVAL SHEET

This

is submitted in partial fulfillment of the requirements
for the degree of

Author:

Advisor:

Advisor:

Committee Member:

Committee Member:

Committee Member:

Committee Member:

Committee Member:

Committee Member:

Accepted for the School of Engineering and Applied Science:

Jennifer L. West [signature]

Jennifer L. West, School of Engineering and Applied Science

Acknowledgements

I would like to thank Dr. Jason Kerrigan for giving me the chance to be a part of the ongoing research at the Center for Applied Biomechanics. You have always been supportive not only of my work, but of my goals beyond CAB. For that I am extremely thankful.

I would also like to thank Dr. Bronislaw Gepner and John-Paul Donlon, who both spent a great deal of time showing me the ropes and teaching me how to be an efficient, organized researcher. Both of you have been incredible sounding boards every step of the way.

The staff and students at CAB have been incredibly important in my success over the last few years, and my achievements would be nothing without them.

Lastly, I would like to thank my fiancée, Rachel, for her love and support throughout the process.

Abstract

Introduction: Lap belt induced injuries to the region of the pelvis between the anterior superior iliac spine (ASIS) and anterior inferior iliac spine (AIIS) in frontal impacts have been denoted in literature for almost 50 years. While it is an uncommon injury in the field, this injury is one that can be found within the current fleet of vehicles. However, the risk of this injury may increase with the development of Highly Automated Vehicles (HAVs). New, unconventional seating configurations may occur due to the presence of open, spacious interiors. In some vehicle concepts, the instrument panel and knee bolster components would be moved farther away from the occupant to allow for better comfort. Such a position may lower the efficacy of airbags, and may even bring about their removal. However, if an occupant were to be in a crash in this style of vehicle, the seatbelt system will provide all of the restraint of the occupant. Increased lap belt forces would likely cause an increase of the occurrence of the iliac wing injuries; yet, no experimental studies have been conducted to specifically understand at what force these injuries are caused.

Goals of Study: The main goal of this study is to develop an injury criteria for the iliac wings under frontal lap belt loading conditions. To achieve the goal of developing an injury criteria, I first need to recreate similar fractures using a similar loading/injury mechanism. I will design an experiment to characterize belt-to-pelvis loading with the goal of recreating the same fracture at the same isolated lap-belt-to-pelvis orientation that caused fracture in Richardson et al 2020. After replicating these fractures on a full scale test, I will then design a component level test to measure the tolerance of fracture on isolated pelvic wings, and do so across a variety of pelvises. I will then use the tolerance data to perform a statistical analysis to predict risk across the population to achieve the desired injury criteria.

2

Methods of Study: I developed a test fixture that was capable of replicating mid-sled test postures where pelvic fractures occurred. Three whole-body PMHS tests were run; two sustained fracture between the ASIS and AIIS on one of the two iliac wings. From there, two, subinjurious tests were run on a fourth PMHS to capture iliac wing strain data at varying lap-belt-to-pelvis angles. I then created a simpler, component-level test environment to isolate loading on denuded iliac wings between the ASIS and AIIS at the same lap-belt-to-pelvis angles from the first set of tests. Testing was completed on the fourth PMHS pelvis to relate the boundary conditions and load response on the component-level test to the full-scale test environment. After that, 20 pelvis wings were loaded to failure, and development of an injury risk function was performed.

Results of Study: The lap belt loading rate and injury type sustained by the PMHS in the first testing environment matched those of the sled test series where the targets came from. Two of the three PMHS sustained pelvis injuries at the targeted location, while the third subject submarined. Twenty two pelvic wings were tested to failure at two lap-belt-to-pelvis angles; nineteen of them sustained injuries similar to those found in literature and the full-scale test environment. A survival analysis was completed using the tolerance data, and an injury risk function was developed using a Weibull distribution cumulative distribution function. From this analysis, a 50% probability of injury correlated to an iliac wing force of ~4500 N. While loading angle did not have a significant effect on the fracture tolerance of the pelvis, a weighted bone density metric was shown to be a significant predictor of injury risk.

Impact of Thesis: The testing in this thesis was the first to specifically investigate the tolerance of the iliac wings to lap belt loading. While the injury is not currently common in the field data, it has the potential to become much more common with the occupant environments predicted to be available with HAVs. Restraint manufacturers and automobile OEMs can begin to use the

results of this study, and specifically IRF developed in this thesis, to guide the development of occupant restraints and other injury countermeasures. Further work will be needed to relate load at the iliac wing to lap belt tension load; however this thesis provides the first injury tolerance data of the iliac wings under frontal loading.

Table of Contents

Table of Figures

Table of Tables

1.   Introduction

1.1. Motivation

Pelvis injuries due to lap belt loading in frontal impacts have been cited in sled test literature for almost the last 50 years, However, injuries to the iliac wings of the pelvis are not commonly seen in the field. A query of the Crash Injury Research Engineering Network (CIREN) database indicated 14 cases of iliac wing fractures from frontal impacts, determined to be caused by the lap belt. The lack of injury prevalence in the field may be due, in part, to the design of vehicle interiors that restrain the motion of the pelvis. The seat belt system and knee bolsters in the current fleet of vehicles tend to limit occupant pelvic motion, and thus the force applied to the occupant's pelvis is also limited. However, in the future, highly autonomous vehicles (HAVs) may create an environment where the occupant relies more on the seatbelt system to prevent motion than ever before.

The introduction of HAVs has the potential to provide enhanced safety for road users while also giving occupants extreme flexibility in the way they use the time that they spend travelling. Concept vehicles promise luxurious, open interiors where occupants will be able to use their commute to work, sleep, or socialize without dedicating effort to driving (Jörlov et al 2017, Östling 2019, Koppel et al 2019). While not all occupants may sit unconventionally, some of these configurations will provide new challenges for the successful restraint of occupants. For longer trips, it was found that two thirds of participants would prefer to sit in a non-traditional seating configuration (Östling 2019) (ie configurations B-E in Figure 1.1-1). In another study, occupants described the idea of HAVs as "luxurious… The car would have a limousine-feeling" (Jörlov et al 2017).
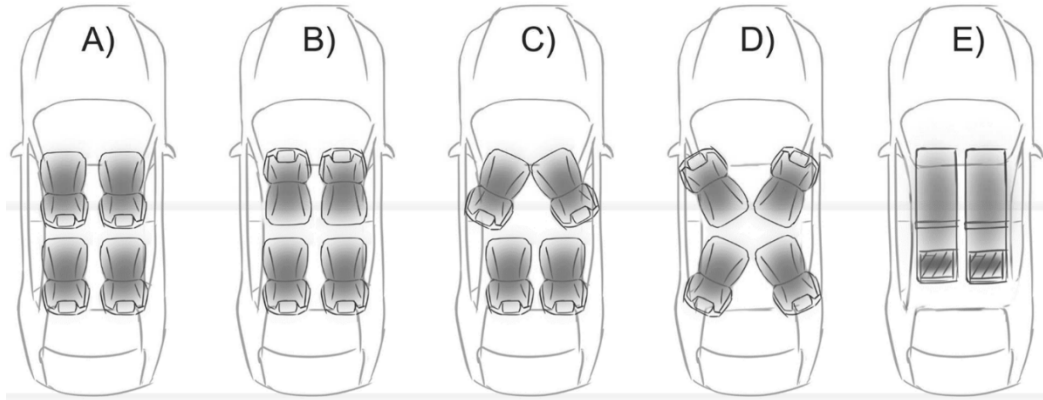
1.1-1 Östling 2019 Seating Configuration Options Diagram

The National Highway Traffic Safety Administration (NHTSA) has suggested that manufacturers should be testing any possible future seating configurations in HAVs to ensure occupants are safe (NHTSA 2017). However, the current restraint systems are certified only in conventional seating practices (Östling 2019). It is possible that new seating configurations will cause new problems in sufficiently engaging the pelvis with the lap belt to prevent the occurrence of submarining, or when the lap belt slides over the pelvis and loads the abdomen. In addition, it may put the pelvis under new magnitudes of load unseen in the current fleet of vehicles due to differences in the interior design (such as the removal of the knee bolster).

Human body models (HBMs) and finite element (FE) simulations have allowed for computational investigations of the wide range of possible seating configurations and vehicle interiors that may be present in the future. Modifications to the seatback angle, seat orientation, and restraint system have all been studied in an attempt to understand how occupant response changes with these factors. In studies looking at frontal impacts, it has been found that changing the seating direction relative to the impact direction changes the effectiveness of the seatbelt restraint system (Kitagawa 2017). The seatback and seat belt were both essential for occupant restraint (Kitagawa 2017). Increasing the seatback angle increases the occurrence of submarining

18

(Rawska 2019). Submarining occurrence has been shown to be correlated to occupant size, with smaller occupants submarining more often than larger occupants (Rawska 2019). This effect is tied together with the distance between the occupant's knees to the knee bolster; more distance between the knees and the knee bolster resulted in greater chance to submarine (Rawska 2019). In addition, the Global Human Body Model Consortium (GHMBC) Detailed HBM and Simplified HBM submarined in different seat and restraint configurations (Rawska 2019, Gepner 2020).

Testing post mortem human surrogates (PMHS) in physical tests can provide information to validate anthropomorphic test devices (ATDs) and HBMs. Sled impact tests replicate crash scenarios in simplified environments to allow for increased repeatability of environmental factors, such as seat configuration, restraint system, and/or subject positioning. Some ATDs, like the THOR 50-M and the HIII small female ATDs, have load cells at the anterior, superior iliac spines (ASIS) which could be used to understand how much force is being applied to the pelvis where the lap belt interacts with it. However, no validation of whether this is comparable to a human surrogate has been completed.

Thus, to get the closest to understanding how an occupant may respond in an unconventional seating configuration without testing live volunteers (which is impossible in high-severity crashes), full scale testing of PMHS in unconventional seating configurations is necessary. In 2019, a reference set of PMHS tests were conducted at University of Virginia. Five, mid-sized (in height) male PMHS were subjected to a 50 km/h impact pulse, each restrained with a custom restraint system consisting of dual lap belt pre-tensioners, shoulder belt pre-tensioner, and shoulder belt load limiter (Richardson 2020). This restraint system was aimed at preventing submarining of the occupant despite being reclined, which has been shown to increase the

likelihood of submarining (Rawska 2019, Gepner 2019, Forman 2018). Each PMHS torso was reclined to approximately 50 degrees from vertical. Of the five PMHS, two sustained pelvis fractures between the anterior superior iliac spine (ASIS) and the anterior inferior iliac spine (AIIS) on the outboard side (Figure 1.1-2), and one subject submarined on the inboard side (Richardson 2020). Peak lap belt loads for the two subjects that sustained fracture were 7.8 kN and 6.6 kN, respectively.
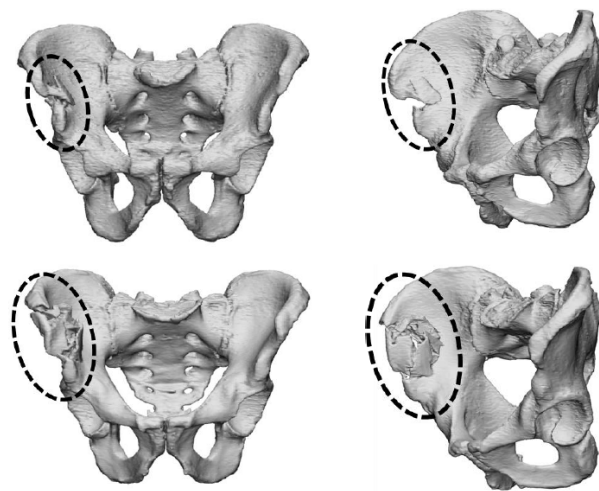
1.1-2 Pelvis Injuries from Richardson et al 2020

These reference PMHS tests were the first sled tests to investigate occupants to such extremes, and two of the five subjects sustained iliac wing fractures from lap belt loading. These fractures, however, have been seen before in recent frontal sled tests where occupants were upright, but no knee bolster was present to constrain the forward pelvis motion (Luet 2012, Uriot 2015, Trosseille 2018). Upon further investigation, it was found that such iliac wing injuries due to lap belt loading have actually be cited to occur in the literature since the 1970s (Schmidt 1974, Fayon 1975), yet no research has been conducted to understand why or how these injuries occur. Instead, there is a large stretch of studies over the last 50 years that focused on understanding the risk of injury to the chest in a conventional seating environment (ie, with the presence of a knee

bolster). Many of these studies either do not have pelvis injuries, or do not report pelvis injury data. If the restraint system of HAVs is to be optimized to protect occupants in unconventional seating configurations, further research is necessary to understand the fracture tolerance of the iliac wings. To do this, we need to take a sample of the human population to help us understand how that tolerance and such information could be used to design restraint systems.

1.2. Goals

As discussed above, it appears that the pelvis injuries due to lap belt loading occur most often in sled test series where no knee bolster is present. No current research exists in understanding the fracture tolerance of the pelvis in this region. The overall goal of this thesis is to develop the first injury risk function of isolated pelvic wings loaded under a distributed frontal load. The research studies presented in this thesis aim to understand how lap belt loading environments may cause fracture. In addition, possible external factors such as bone density and loading direction will be investigated to understand if these have any significant effect on the fracture tolerance of the pelvis.

The goals of this thesis are:

1) to design a "belt-pull" fixture that is capable of replicating the isolated lap belt loading environment from sled tests where iliac wing fractures occurred

2) Recreate the pelvis fractures seen in the sled tests on whole-body PMHS in the "belt-pull" environment

3) design a simplified experimental set up that isolates the same lap belt loading environment in 1) to create fractures on isolated pelvic wings

4) to create an injury risk function for distributed loading to the region of the pelvis just below the anterior superior iliac spine (ASIS) to understand the variation in fracture tolerance in a sub-population

The work in this thesis to achieve these goals will be broken into four tasks:

- Task 1 – Analysis of reference recline PMHS sled tests (Richardson 2020)
- Task 2 – Recreation of fractures on whole-body PMHS in a simplified, "belt-pull" (non-impact, dynamic) environment
- Task 3 – Recreation of fractures on isolated pelvic wings
- Task 4 – Injury risk function development

Each of these tasks is presented as its own chapter in addition to background information and conclusions drawn from this thesis. The following flow chart outlines the structure of the document:
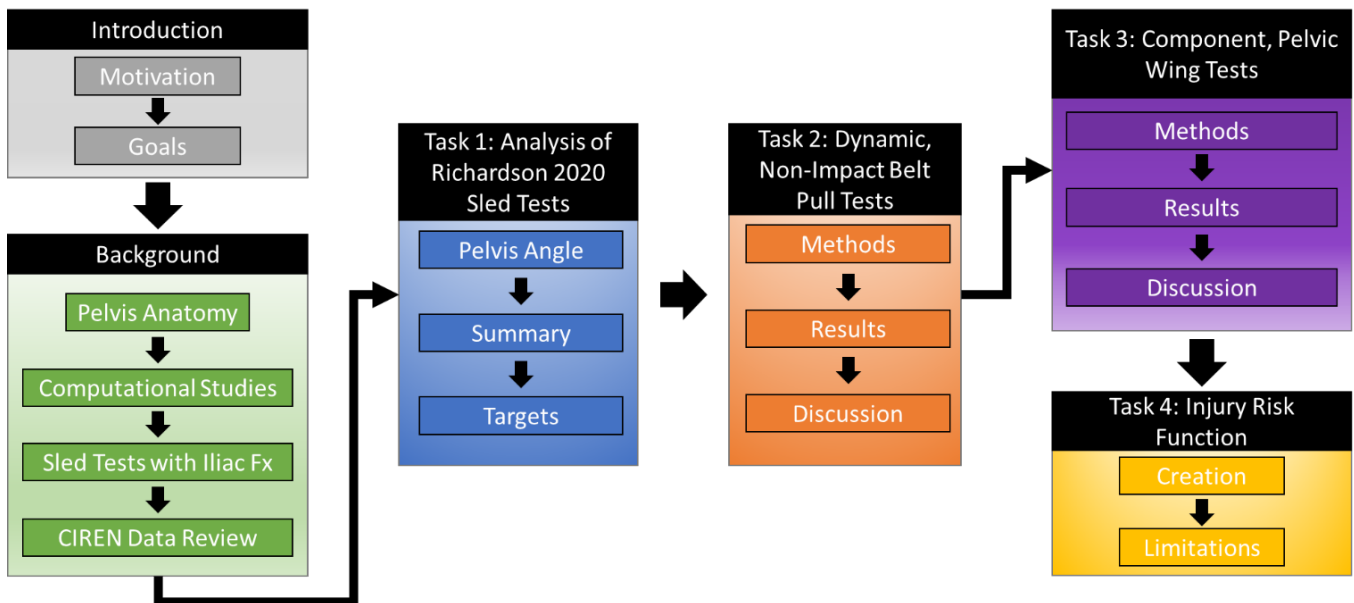
1.2-1 Flow Chart of Thesis Document

2. Background

The goal of this chapter is to illustrate the variety of conditions, both in the laboratory and in the field data, where pelvis fractures like those studied in this thesis have been produced. These cases are reviewed to broaden the description of the problem this study aims to address. While much of this thesis focuses on targets from a specific sled test series, my approach is not motivated solely by this single set of sled tests (discussed in Chapter 1). This chapter will help show the prevalence of these fractures in the field and in literature and show how these fractures could increase in likelihood as a result of new seating configurations. First, appropriate background information on the anatomy of the pelvis, along with common acronyms that will be used for the majority of the document, will be presented. Then, a summary of various computational studies completed will be summarized to show how the seat belt system interaction with occupants will change as a result of new seating configurations. Lastly, summaries of the major physical sled impact tests where pelvis injuries similar to Richardson 2020 were seen will be provided, as well as available field data from the CIREN network.

2.1. Pelvis Anatomy

The pelvis is comprised of two wings that create a bowl like structure that encases and protects the bowel. The two wings are attached to each other on the anterior side by the pubic symphysis (also called the pubic crest (PC)), which is a cartilaginous joint. On the posterior side, the pelvic wings are connected to the sacrum through cartilage and multiple muscle attachments. These connections help the pelvis stay extremely stable. The femoral head attaches to the pelvis through a ball and socket joint; the socket is denoted as the acetabulum. The relevant landmarks for lap-belt-to-pelvis interaction are located on the front of the pelvis. The anterior superior iliac spine (ASIS) is the attachment point to the largest muscle in the

23

human body (the Sartorius muscle). The anterior inferior iliac spine (AIIS) is the attachment point of the rectus femoris muscle, which is one of four quadriceps muscles. With a sagittal view of the pelvis, the ASIS and the AIIS create a "hook" in which a properly placed lap belt will engage the pelvic bone to restrain forward motion (Figure 2.1-1). Another landmark commonly used to track pelvis orientation in the automotive field is the posterior superior iliac spine (PSIS)
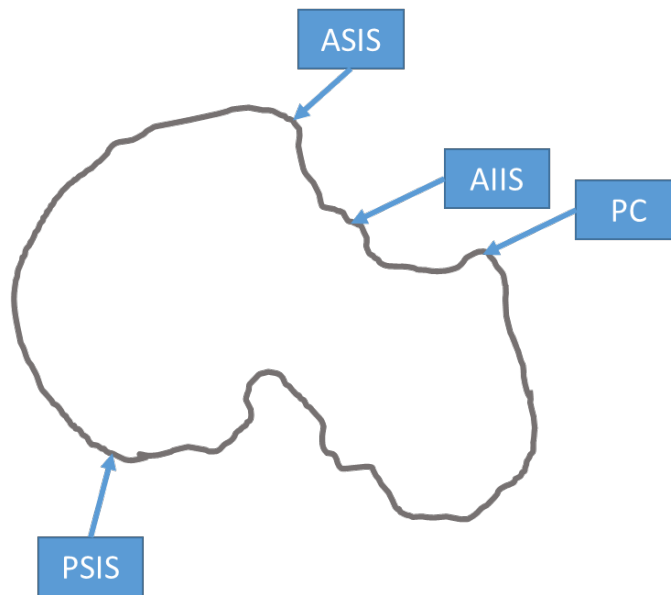
2.1-1 Sagittal View of Pelvis

2.2. Computational Studies

Much of the investigation of unconventional seating scenarios has been completed through computational, FE simulations using HBMs. In particular, the protection of reclined occupants has received large attention in the injury prevention field. Reclined occupants are primed for poor restraint interaction due to the possibility of greater forward excursion and a more rearward reclined pelvis – which has been shown to lead to an increased risk of submarining (Adomeit and Heger 1975). A key component in limiting the amount of

forward excursion an occupant experiences is the knee bolster; yet, it has been hypothesized through concept vehicles that the removal of the knee bolster may occur in future HAVs (Östling 2019). Increasing the distance between the occupant, or full removal of the knee bolster has been shown to increase the submarining likelihood of reclined occupants (Ji 2017, Gepner 2019, Rawska 2019, Rawska 2020). In addition, increasing the distance between the occupant and the knee bolster increases the overall lap belt forces applied due to the lack of an alternative load path, plus increased pelvis displacement (Gepner 2019). However, in most of these studies, kinematics were observed (with the main outcome being submarining). Changes in lap belt force as a result of change in knee bolster position was only provided in Gepner 2019. In Figure 2.2-1, it is clear that a larger distance between the occupant and knee bolster (nIP means no instrument panel, bIP means rearward instrument panel) was very well correlated with larger lap belt forces.
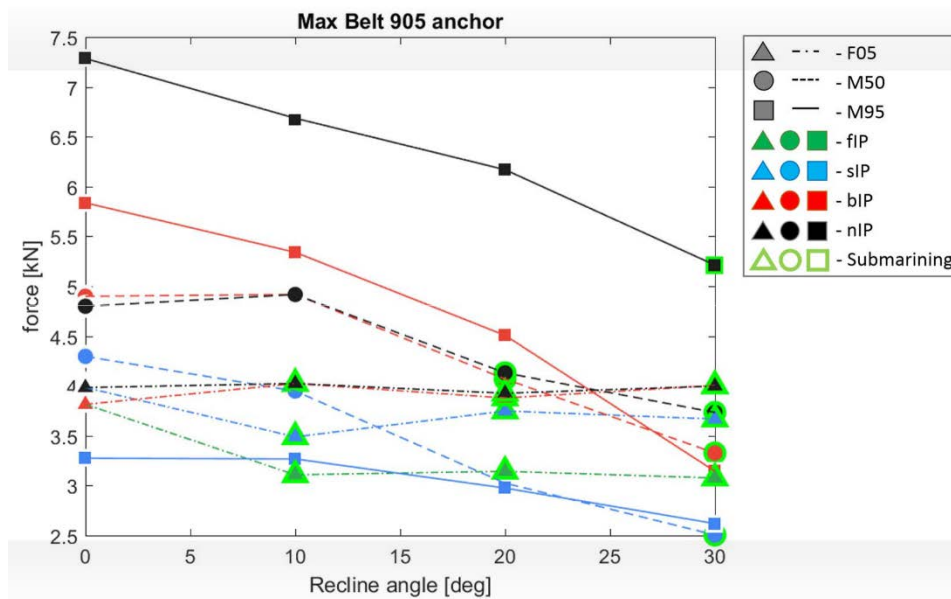
2.2-1 – Gepner 2019 Force vs Recline Angle plot. Plot clearly shows that a more forward knee bolster usually results in a much lower lap belt force.

In an attempt to combat this issue of increased lap belt force, various restrain system changes have been investigated, such as load limiters of the seat belt and in the seat track (Mroz 2020). Seat track load limiting was shown to reduce the ASIS resultant force by an average of 2.3 kN, while lap belt load limiting reduced pelvis forces by 2.2 kN (Mroz 2020). However, it is still unclear whether the forces obtained in the studies would result in fracture to the pelvis because no injury criteria exists.

2.3. Iliac Wing Injuries in Sled Tests

2.3.1. Schmidt 1974

In the 1970's, sled tests were conducted to understand the differences of two point and three point harnesses following changes in legislation requiring car manufacturers to implement three point harnesses. Schmidt et al completed a study on a 49 cadavers ranging in age from 12 – 82 years old in 1974. Using a deceleration sled with an optimal crash velocity of 50 km/h, 30 tests were run using a three point retractor belt and 19 tests were run using a two point belt and a knee bar. While much of the paper focuses on describing the differences in the thoracic response of the cadavers between configurations, it is noted that three of the thirty cadavers tested in the three point belt condition sustained fractures of the right ilium. It was noted that the lap belt forces ranged between 340-770 hp, but further detail of which cadavers sustained injuries and at what forces is not presented in the publication.

2.3.2. Fayon 1975

In 1975, Fayon et al tested 31 cadavers in frontal sled impacts where an entire car cabin was affixed to a sled and a 3 point safety belt was used to secure the cadaver. The cabin consisted of seats, instrument panel, steering wheel, and anchor points that all were

of specification of a fleet vehicle at the time. Crash severities ranged from 40-65 km/h. In addition, seven static seated belt tests were performed on different cadavers to measure chest deflection from lap belt loading. Much of the analysis presented in the paper surrounded the deformation of the thorax, with focus on sternum, rib, and clavicle fractures. However, it is noted in the "After Test Necropsies" tables that 5 of 31 cadavers in the frontal cabin impact sustained at least one iliac wing fracture, with lap belt forces peaking at upwards of 15 kN. Timing of fracture was not presented in this paper. None of the static belt pull cadavers sustained pelvis injuries, though it is unclear if the static belt test actually loaded the lap belt or only loaded the shoulder belt.

2.3.3.   Kent 2001

In 2001, the Center for Applied Biomechanics conducted ten, right-front passenger, 48 km/h cadaver sled tests in three different restraint configurations. The first tested restraint system was a force-limited belt with a depowered airbag. The second restraint system consisted of a non-depowered airbag and no torso belt. Then, the third restraint system consisted of a standard belt with a depowered airbag. The sled environment consisted of a full vehicle cabin that included an instrument panel but no steering wheel. Again, the focus of the paper was understanding how these three restraint systems changed observed injuries by the cadavers. It was noted that, in the second restraint configuration, one cadaver sustained a large iliac wing fracture on the right side. While timing of this fracture is not provided, the peak lap belt force at the buckle was noted to be around 4.1 kN.

2.3.4. Kent 2011

In 2011, the Center for Applied Biomechanics evaluated the three-point restraint system against an inflatable, force-limited shoulder belt with pre-tensioned lap belt. Volunteer data was used for the three-point restraint system, while cadaveric surrogates were tested in the inflatable system. The air-belt system consisted of a shoulder belt load limiter of 3 kN, and the lap belt had a nominal pre-tension load of 2.3 kN. Three cadavers were tested with an impact speed of 48 km/h in a buck that represented the rear seat of a U.S. mid-sized sedan, with the front seat removed. Of the three cadavers tested, all sustained some sort of pelvis fracture, but only one cadaver sustained an iliac wing fracture. This cadaver was subjected to the largest lap belt force of 6.1 kN.

2.3.5. Shaw 2018

In 2018, frontal sled tests were conducted to evaluate the effectiveness of pelvis restraint cushions (PRC) at preventing forward motion of the pelvis. Four cadavers were each tested three times. The first two tests were low severity tests of 20 km/h, while the third test was of higher severity of 58 km/h. A three-point harness with 4 kN load limited shoulder belt and pre-tensioner was used to restrain each cadaver. Each cadaver was palpated between each test to note for pelvis injuries. It was noted that the two cadavers tested with the PRC at high force did not sustained pelvis fractures, while both subjects who did not have the PRC sustained pelvis fractures. Of those two, one sustained an iliac wing fracture. Peak lap belt forces reached 7.9 kN for this subject. Since CT scans were not taken between tests, it is unsure whether small fractures were present before the third test where the large fracture was noted or not.

2.3.6.   Luet 2012

In 2012, a series of sled tests were conducted to understand the occurrence of submarining (where the lap belt slides over the pelvis and loads the abdomen) in Anthropomorphic Test Devices (ATDs) and cadavers. Three different configurations were tested: a 40 km/h pulse with a rearward lap belt anchor position, a 50 km/h pulse with forward lap belt anchor position, and a 50 km/h pulse with rearward lap belt anchor position and slightly inclined seat pan. Each subject was tested in a rigid seat with a restraint system consisting of a two point shoulder belt and two point lap belt. Because of the two point lap belt, lap belt loading was usually symmetric on both sides. Of the 9 cadavers tested, 5 sustained iliac wing fractures. The left iliac wing broke on three subjects, while the right iliac wing broke on the other two. The iliac wing fractures occurred in all three configurations of the sled test environment. Strain gauges were affixed to the pelvis pre-test to determine fracture timing. All fractures occur between 3-7 kN of lap belt force. The authors note that it was difficult to draw conclusions as to if the occurrence of submarining affected the fractures, or if the fractures could have possibly prevented the occurrence of submarining.
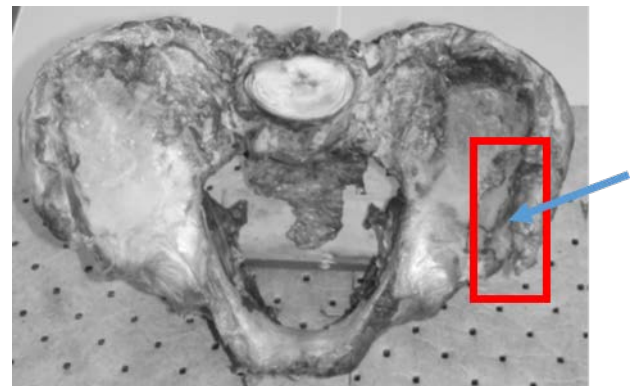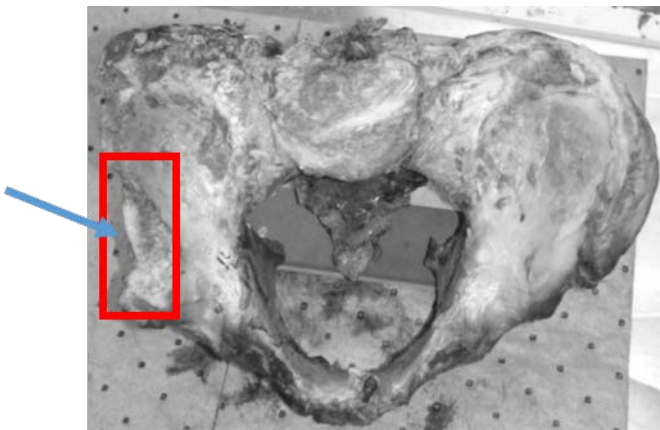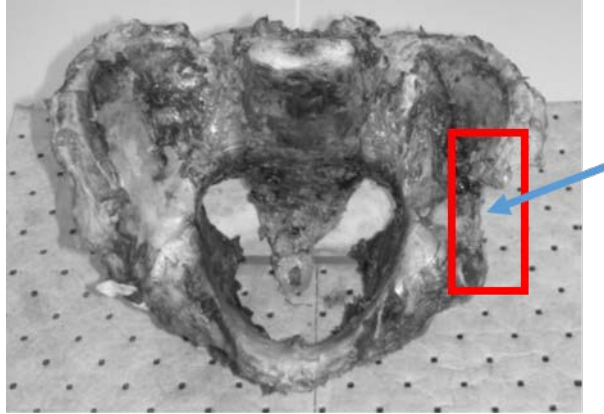
2.3.6-1 Pelvis Fractures from Luet 2012

2.3.7. Uriot 2015

In 2015, the investigation of submarining was expanded to include a semi-rigid seat with an anti-submarining ramp. Two test configurations were tested in an effort to represent a front seat and rear seat. The front seat configuration had more forward lap belt anchorage locations and different seat stiffness values than the rear seat configuration (which was supposed to be more representative of a rear seat bench). Both seat configurations used a similar two point shoulder belt and two point lap belt restraint system that was used in 2.3.6. The pulse used was a 50 km/h pulse, again similar to that of Luet et al 2012. Eight cadavers were tested, with four in each configuration. All cadavers in the rear seat configuration sustained iliac wing fractures. Peak lap belt forces ranged between 5-6.5 kN in the rear seat configuration. While similar peak lap belt forces were observed in the front seat configuration, no pelvis injuries occurred. The stark delineation between the two configurations was unexpected, as the lap belt was supposed to be load limited to 5 kN for all tests in all configurations; it is possible that the increase in force was a reason why fractures occurred only in the rear seat configuration. In addition, it was noted that the fractures could have also occurred because of the belt

position on the pelvis (all positions were "higher" in the rear seat configuration in comparison to the front seat configuration), as well as the direction of loading differences between the two configurations (the rear seat configuration had around a 15 degree more horizontal initial lap belt angle than the front seat configuration).
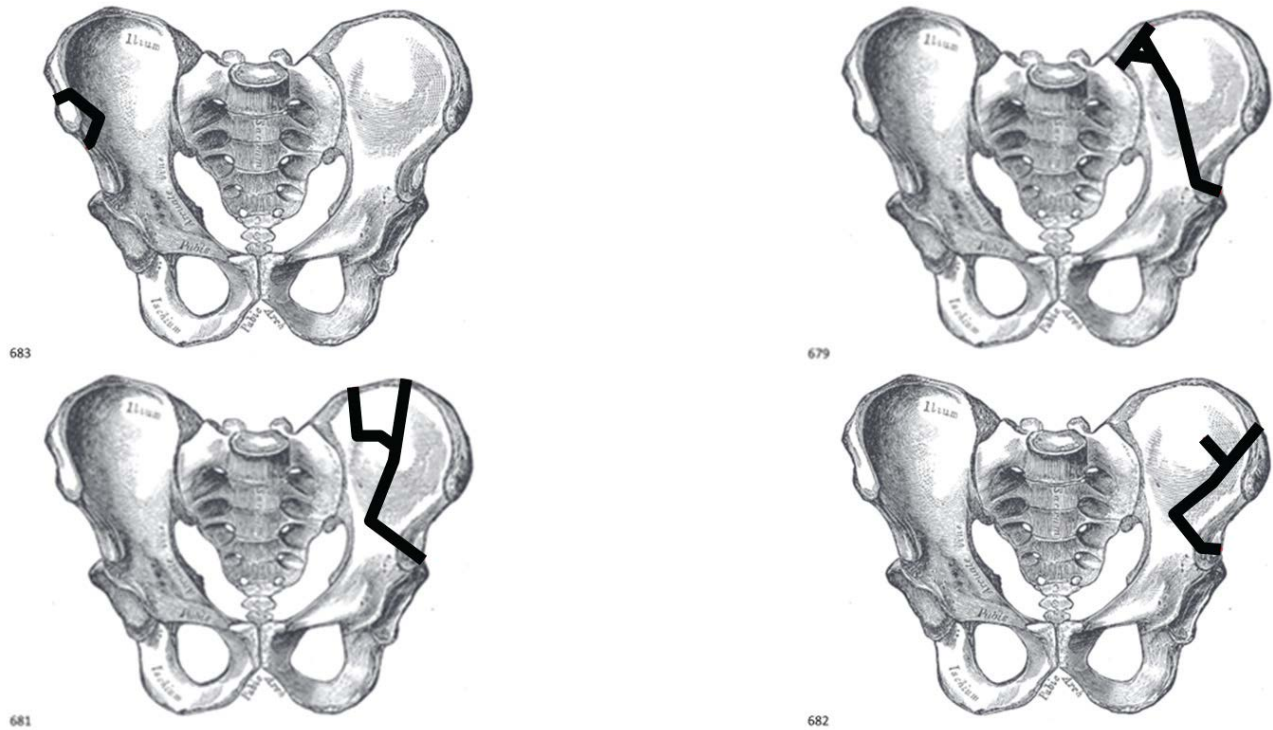
2.3.7-1 Pelvis Fractures from Uriot 2015

2.3.8. Trosseille 2018

In 2018, the same semi rigid seat and two point lap belt/two point shoulder belt restraint system from 2.3.7 was used to test nine small female cadavers in three different test configurations to assess submarining. The first configuration was the same geometrical configuration as the rear seat configuration from 2.3.7 except that the foot pan was moved closer to the seat pan due to the size of the subjects tested. A 29 km/h pulse was used. The other two configurations changed the location of the lap belt anchors and the stiffness of the semi rigid seat, and a higher severity impact pulse was used in

31

these two configurations (50 km/h pulse). The only differences between configuration 2 and 3 was the initial position of the belt relative to the pelvis, with configuration 2 having a much higher belt position. Pelvis fractures occurred in three of the nine cadavers where peak lap belt forces ranging from 2-4 kN were seen. No pelvis fractures occurred in configuration 2 despite higher lap belt forces compared to the other two configurations. This is most likely due to the fact the belt was placed higher up relative to the ASIS – so far up, that the belt slid over the pelvis well before peak belt force was reached.
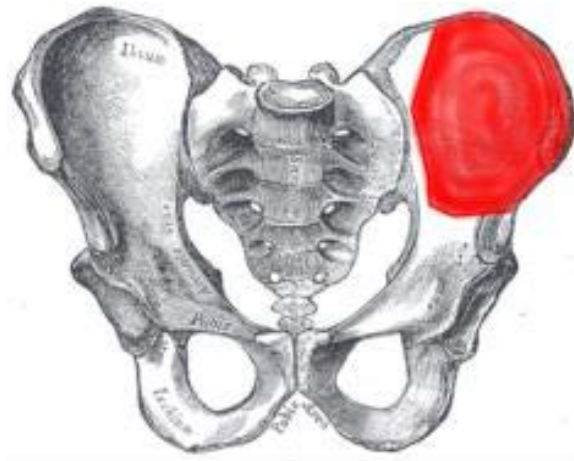
2.3.8-1 Location of Pelvis Fractures from Trosseille 2018

2.4. CIREN Database Review: AIS Code 856151.2

The CIREN database includes thousands of vehicle crash cases containing detailed injury information. Case inclusion require that the patient received treatment at a Level 1 trauma center. Usually, the minimum Maximum Abbreviated Injury Scale (MAIS) is a level 3. Each case contains crash data, as well as extensive information regarding injuries to occupants. However, because it is limited to such severe cases, only about 300-400 crashes are entered

into the database per year. Thus, it is not truly a representative sample of crashes in the population (Stitzel 2007).

The 856151.2 Abbreviated Injury Scale (AIS) code denotes any pelvis injury that does not interrupt the stability of the pelvic ring. A query of the CIREN database (circa June 2021) for this AIS code will provide 162 cases where an occupant had an injury under this AIS code. Analysis of these cases show that 42 (26%) of these cases were determined to have lap belt induced injuries. Of those 42 cases, 11 (26%) cases were determined to have a purely frontal impact crash direction. If the impact direction is expanded to 0 degrees +/- 20 degrees for a "mostly" frontal impact direction, the number of cases increases to 21 cases (50%). The breakdown of the cases with occupant information can be found in Table 2.4-1. Data was left blank where no information was provided. From this data table, 14 of the 21 cases (67%) saw injury at the ilium. Of the 14 cases, the injured occupant for these cases was mostly the driver (57%), then front passenger (29%), then rear right passenger (14%). The range of ages of affected occupants was from 3 years old up to 90 years old.

This means that, in the entirety of the CIREN database, **only 14 cases** are present where a purely frontal impact had a lap belt induced pelvis injury located at the iliac wing. While the CIREN database may not be representative of the entire population, it is one measure of how prevalent an injury is among fairly severe accidents among Level 1 trauma centers. Because only 14 cases are present in the entirety of the database, it can be concluded that this is not a common currently seen in the field; however, it is possible for this injury to occur in the modern fleet of vehicles.

Table 2.4-1 CIREN Cases: Frontal Impact with Lap Belt as an Injury Component

Sex	Age	Height (cm)	Weight (kg)	Seating Position	Delta V (km/h)	Injury Number	Component	Pelvis Injury Location	Impact Direction (Degrees)
Male	43	173	91	Front Passenger	60.00	3	Lap Belt	Sacrum	0
Male	75	177	68	Front Passenger	65.00	2	Lap Belt	Right Ilium	0
Female	55	138	64	Driver	65.00	8	Lap Belt	Right Ilium	0
Female	90	152	61	Front Passenger	76.00	4	Lap Belt	Right Ilium	0
Male	45	182	75	Driver	80.00	4	Lap Belt	Left Ilium	0
Male	77	183	80	Driver	89.00	16	Lap Belt	Right Pubic Ramus, Left Pubic Ramus	0
Female	61	160	59	Driver		8	Lap Belt	Left Ilium	0
Male	72	188	81	Driver		8	Lap Belt	Sacrum; Left Pubic Rami	0
Female	77	165	86	Driver	53.00	9	Lap Belt; Seat, back support	Sacrum	0
Male	53	193	111	Driver		1	Lap Belt; Seat, back support	Sacrum	0
Female	67	165	66	Driver	39.00	2	Center console first row; Lap belt	Sacrum	0
Female	47	168	52	Driver	32.00	1	Lap Belt	Right Ilium	10
Male	61	175	82	Driver	65.00	17	Lap Belt	Right Ilium, Left Ilium, Right Pubic Ramus, Left Pubic Ramus	10
Female	77	165	75	Front Passenger	28.00	5	Lap Belt	Right Ilium	20

Male	8	152	40	Rear Right Passenger	36.00	2	Lap Belt	Left Ilium	340
Male	3	101	18	Rear Right Passenger	65.00	1	Lap Belt	Right Ilium, Left Ilium	340
Male	23	173	62	Driver		5	Lap Belt	Right Pubic Rami	340
Female	46	178	55	Driver	77.00	3	Lap Belt	Left Ilium	350
Female	71	152	45	Driver	18.00	3	Lap Belt	Left Ilium	350
Female	27	170	88	Front Passenger		1	Lap Belt	Right Ilium	350
Female	68	170	54	Driver		34	Lap Belt	Right Ilium	355

2.5. Summary

This chapter presented summaries of various tests and field data cases where iliac wing injuries occurred due to lap belt loading of the pelvis. This illustrates that iliac wing injuries due to lap belt loading are currently occurring, and is a problem that has not been studied. To best understand how these fractures occur, I first need to define some target condition to test. The studies and field data presented in this chapter help provide some information for the tolerance of the pelvis; however, detailed specifics of pelvis orientation at the time of fracture would be difficult to identify. For this reason, I will review details of the Richardson et al sled tests in the next chapter to identify specific parameters to recreate iliac wing fractures in an experimental setting.

3.   Task 1: Analysis of Richardson 2020 Sled Tests

In the previous chapter, I showed that iliac wing fractures due to lap belt loading have been occurring in both the laboratory and the field, and have not been specifically studied. In this chapter, I will identify specific targets from the Richardson 2020 sled tests, where iliac wing fractures occurred. As a part of this, I will create a new way of describing pelvis orientation that describes the orientation of the location of these fractures over time. Then, I will reanalyze the available data from these sled tests in this new reference frame to understand how the lap belt was oriented relative to the pelvis. By understanding how the pelvis was loaded at the time of fracture, I can begin to develop an experimental fixture that can replicate this instance.

3.1. Defining Pelvis Angle

In Luet 2012, Uriot 2015, Trosseille 2018, and Richardson 2020, the pelvis orientation was described by the Nyquist plane/angle. The Nyquist plane is defined by a line connecting the anterior superior iliac spine (ASIS) and pubic crest (PC), and the global horizontal or vertical (Figure 3-1) (Nyquist and Patrick 1976). These points represent a gross measure of orientation of the anterior portion of the pelvis.
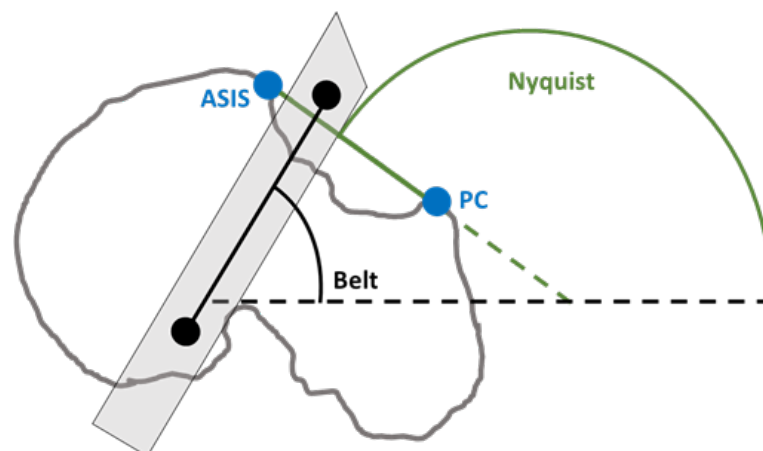
3.1-1 Nyquist Angle Definition

A new proposed measure of the pelvis angle was created as a part of this thesis. The fractures seen in the sled tests kept occurring between the ASIS and the anterior inferior iliac spine (AIIS). It was hypothesized that a better measure of the pelvis orientation relative to the belt would be defined by a line connecting these two landmarks. This measure, defined as the Notch Angle, incorporates subject specific geometry in addition to orientation of the pelvis relative to the world (Figure 3-2).
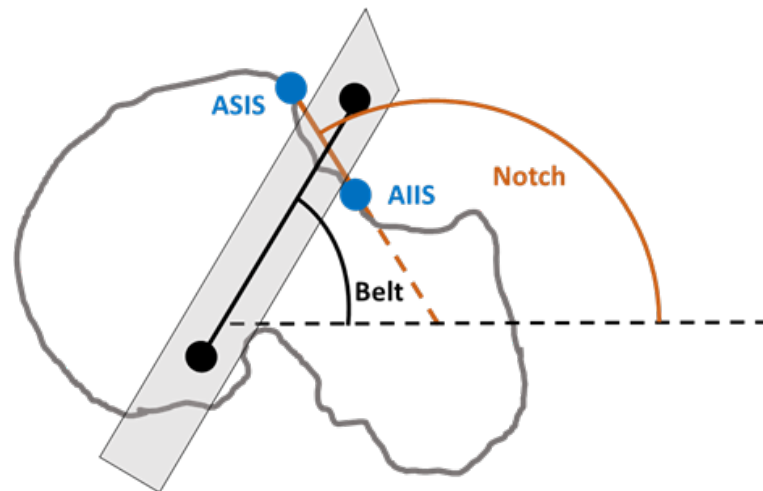
3.1-2 Notch Angle Definition

3.2. Summary of Sled Series

In 2018, a reference set of PMHS dynamic impact sled tests were completed by Richardson et al. In these tests, five PMHS were positioned at a target 50 degree recline angle from the vertical (measured at the sternum). Each PMHS was subjected to a 30 g, 50 km/h pulse (the same pulse used in Uriot 2015 described in section 2.3.7). A custom restraint system of dual lap belt pre-tensioners, shoulder pre-tensioner, and shoulder load limiter (4 kN) was used. A semi-rigid seat developed by LAB was used, which consisted of an independent seat pan and anti-submarining pan. 3-D motion tracking targets were mounted to various important anatomical

landmarks in order to obtain position and orientation time histories. Strain gauges were attached

to the pelvis in order to determine possible fracture timing. No knee bolster was present; in this

test series, two of five PMHS sustained iliac wing fractures. Peak lap belt forces ranged from 6.6

kN to 8.3 kN (Figure 3-3).

Table 3.2-1 Subject Information from Richardson et al 2020

Test	S0529	S0530	S0531	S0532	S0533
Subject Number	1	2	3	4	5
Age	66	53	72	25	55
Height (cm)	177.8	173	177.8	173	177.8
Weight (kg)	74.4	56.7	73.9	75	74.4
Peak Lap Belt Force (kN)	7.8	4.6	6.6	8.3	7.6
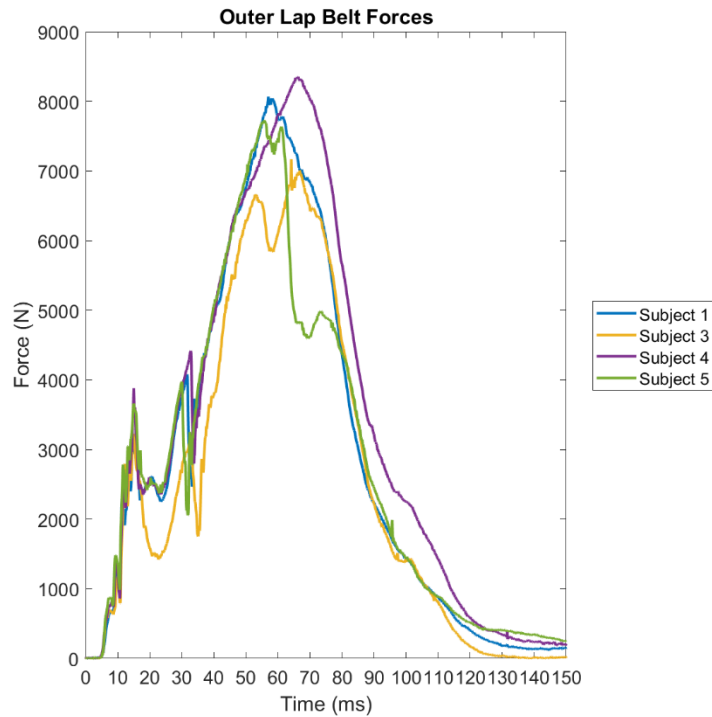
3.2-1 Lap Belt Forces from Richardson et al 2020

3.3. Development of Targets

Data presented in Richardson et al 2020 was reanalyzed to understand if the fractures seen in these tests could be attributed to the lap belt orientation relative to the pelvis. To do this, analysis of the Nyquist angle definition of the pelvis orientation was compared to analysis using the Notch Angle definition of the pelvis orientation to understand if there were any differences in conclusions drawn. Since this difference is a constant value for each unique pelvis, data collected was just shifted by the constant. In the five subjects, the Notch Angle was always more inclined than the Nyquist Angle (Table 3.3-1). In this analysis, only Subjects 1, 4, and 5 were of interest, as these were the three subjects of similar weight and height, and those that had pelvis tracking capabilities throughout the entirety of the test. While Subject 3 sustained an iliac wing fracture, pelvis orientation data is unavailable at the time of fracture due to mount interaction with the sled buck.

Table 3.3-1 Difference in Nyquist and Notch Angle

Subject	Difference in Nyquist and Notch Angle (Degrees)
1	26.88
2	27.35
3	29.75
4	27.14
5	39.4

In the sled tests, Subject 5 initially had the most rearward pitched pelvis with respect to the Nyquist Angle (most positive value) at 170 degrees. Throughout the entirety of the test, the Nyquist angle measurement was always the most positive, indicating that it was always the most rearward pitched pelvis (Figure 3.3-1). The difference in the Nyquist Angle and Lap Belt Angle (Nyquist to Belt Angle) was also the largest for Subject 5, indicating that the lap belt was oriented the most horizontal relative to the Nyquist plane (Figure 3.3-2). It was concluded that

this subject may have submarined partly because of the more rearward pitched pelvis in comparison to other subjects. Subject 1 sustained an iliac wing fracture, and had a more inclined pelvis (155 degrees,) at the time of fracture relative to Subject 4 (162 degrees), which sustained no injury or submarining. However, the Nyquist to Belt angle was more horizontal for Subject 1 (117 degrees) than for Subject 4 (106 degrees), indicating a more horizontal load path at this time. However, this still was not as horizontal of a load path for Subject 1 as it was for Subject 5 (125 degrees). This suggests that a more horizontal lap belt angle oriented with respect to the pelvis could cause submarining, with the threshold being somewhere between Subject 1 and Subject 5.
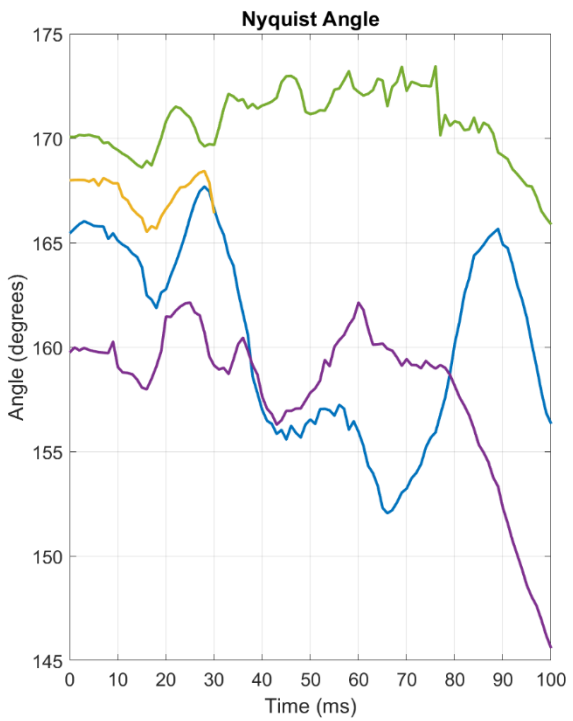
3.3-1 Nyquist Angle Time Histories from Richardson et al 2020
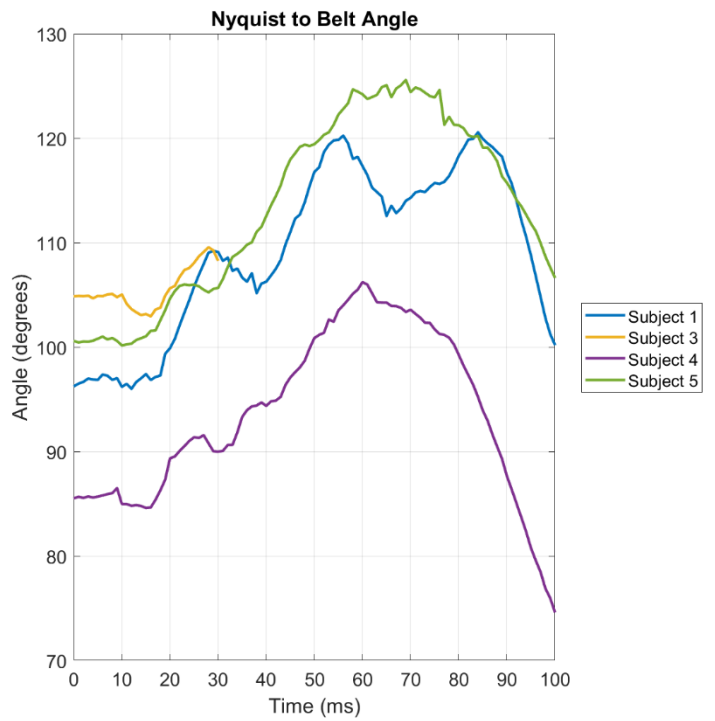
3.3-2 Nyquist to Belt Angle Time Histories from Richardson et al 2020
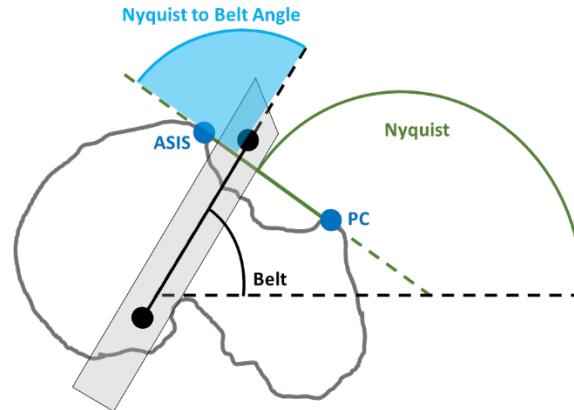
3.3-3 Nyquist to Belt Angle Definition

If this same analysis is completed with respect to the Notch Angle definition, a slight difference in conclusions can be drawn. First, Subject 5 no longer becomes the subject with the most rearward pelvis (Figure 3.3-4). Subject 5 actually had the most inclined pelvis with respect to the Notch Angle definition at the start of the test compared to the rest of the subjects. Subject 1 had the most rearward pitched pelvis at the start of the test, and had the largest Notch to Belt angle. This means that Subject 1 had the most horizontal belt angle relative to the Notch Plane at the start of the test. At the time of fracture, the Notch to Belt Angle for Subject 1 was 90 degrees, implying that the load path was perpendicular to the Notch Plane. At the time of submarining, Subject 5 had a Notch to Belt angle of 85 degrees; this is similar to the Notch to Belt angle of the subject that fractured. However, it is actually less than the subject that fractured, which is different than the conclusion drawn when using the Nyquist Plane reference frame (Figure 3.3-5). Subject 4, which did not sustain injury, had the lowest Notch to Belt angle, implying that the lap belt was more vertical relative to the Notch Plane. This may imply that loading angle could affect the fracture tolerance of the pelvis, with a more vertical lap belt angle allowing for more force to be applied.

While there may be many factors attributing why Subject 1 fractured, Subject 5 submarined, and Subject 4 withstood high forces with no fracture or submarining, the lap-belt-to-pelvis angle may be a large factor. Because UVA recently ran these tests, and they are one of the first sled tests in an unconventional seating configuration, there is large motivation to understand if reclined subjects are more apt to sustain fracture due to different lap-belt-to-pelvis orientations, and at what forces these pelvis fractures occur. Since extensive environmental data was available to use as targets, this thesis relies heavily on the information gathered from Subject 1, where full information regarding the lap belt orientation relative to the pelvis is available.

However, using these targets is purely due to the information available. Pelvis fractures may occur at different forces. For example, the Richardson et al 2020 sled tests had a custom restrain system with an aggressive, 3 kN lap belt pretensioner. While fractures did not occur as a result of the pretensioner in this study, fractures have occurred in other studies (Trosseille 2018) well under 3 kN of belt load. Or, perhaps the reason why Subject 4 did not fracture was because this subject had superior bone quality in comparison to the other subjects. Further experiments to aid in understanding lap-belt-to-pelvis engagement to investigate pelvis fractures will be presented in Chapters 4 and 5.
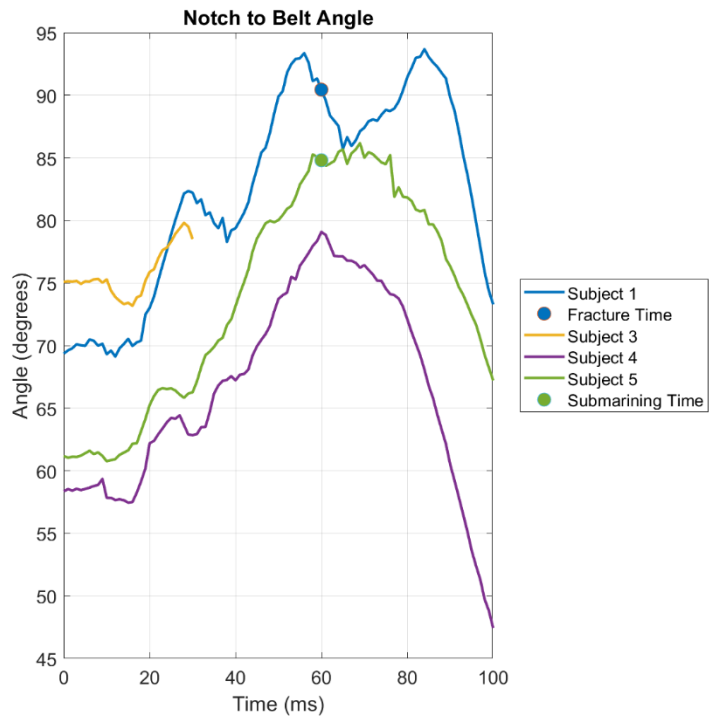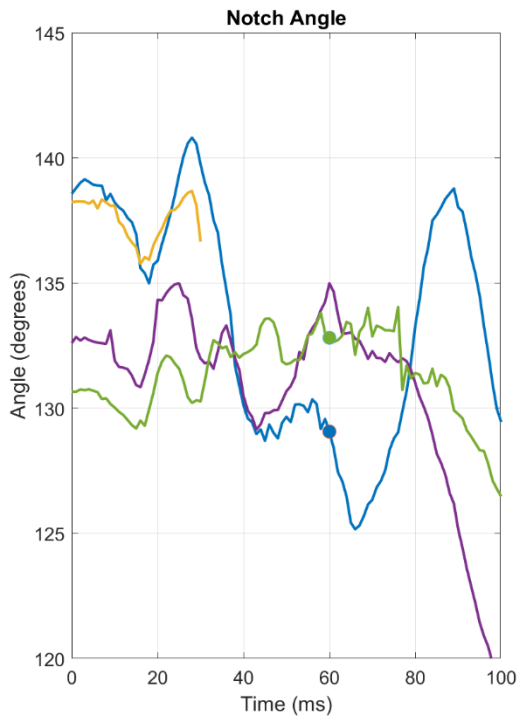
3.3-4 Notch Angle Time Histories Richardson et al 2020

3.3-5 Notch to Belt Angle Time Histories Richardson et al 2020
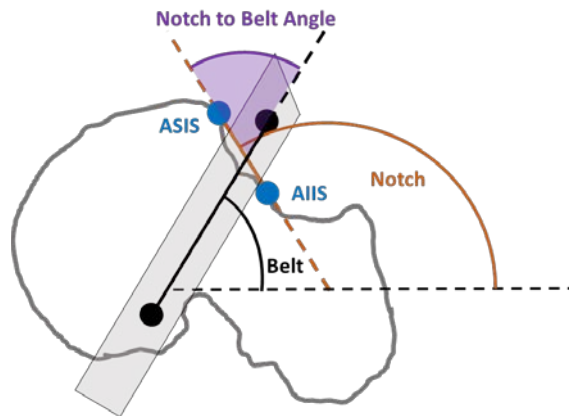
3.3-6 Notch to Belt Angle Definition

3.4. Flow Chart

Below details a flow chart of the steps taken in this thesis to connect the lap belt loading

environment of a sled test to the component level testing necessary to create an injury risk

function (Figure 3.4-1). Task 1 (this chapter) has detailed the lap belt loading targets derived

from sled tests, noted in blue in the flow chart. The details in green will be explained in Task 2

(Chapter 4), which details the methodology and results of testing whole-body PMHS in a

dynamic, non-impact environment by isolating a single lap belt loading instance. Then, based on

the results gathered in Task 2, an environment will be developed in Task 3 (outlined in orange,

Chapter 5) to re-create the loading environment that caused fractures in Task 2 on component

level wings.
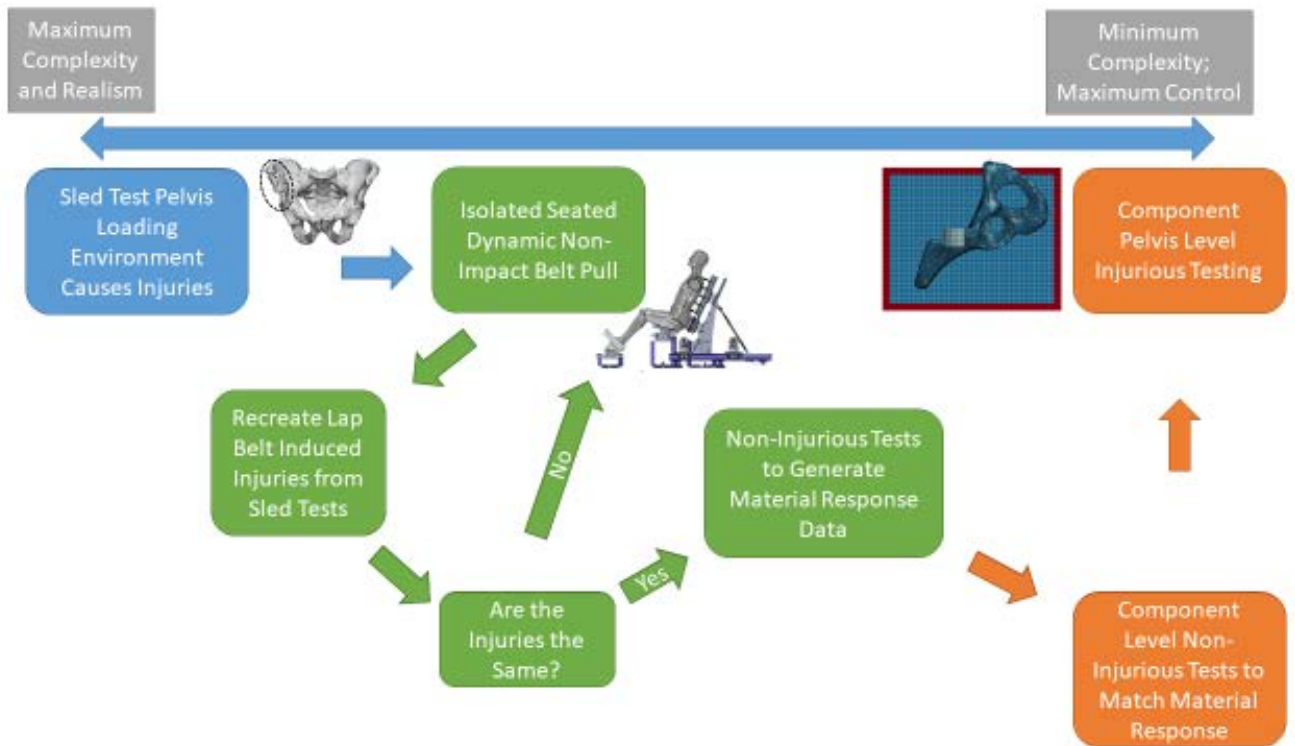
3.4-1 Flow Chart of Experimental Testing

4.   Task 2: Dynamic Non-Impact Belt Pull Tests

The main goal of this task is to develop a fixture that uses the targets of the isolated instance that was determined at the time of fracture in Chapter 3 to replicate these fractures in a more controlled environment. I will explain how the development of the test fixture occurred, as well as explain the two sets of test run. One set of tests will be to replicate fractures, and the second test will be to generate material response data of the pelvis to compare how the pelvis is loaded in this test environment to how the pelvis is loaded in the test environment that will be developed in Chapter 5. This chapter provides the main link between the sled test environment and component level environment that can be used to study the injury tolerance of the pelvis.

4.1. Methods

To connect the loading environment of a sled test to an isolated, component pelvic wing, a more controlled environment than a sled test needed to be developed. The environment needed to load the pelvis at the same rate and to a similar force as a sled test, but also needed to have better flexibility in positioning the lap belt and pelvis to dial in a specific Notch to Belt Angle. The following sections will detail how a test environment was created, along with the process of positioning whole-body PMHS in the environment to isolate the desired Notch to Belt Angle. Two types of tests were run in this environment. The first set of tests were designed to recreate fractures seen in the sled tests detailed in Section 3 by matching the Notch Angle, Belt Angle, Spine Angle, and Notch to Belt Angle at the time of fracture from Subject 1 from Richardson et al 2020. These tests will commonly be referred to as "High Force Tests." Three whole body PMHS were tested with this high force pulse. The second set of tests run were subinjurious tests to the same whole-body PMHS at different Notch to Belt Angles to understand the effect of load angle on the strain distribution of the pelvis. These tests will be referred to as "Low Force Tests,"

45

and we designed to provide information to connect the intermediate step between this less complex environment and the more controlled environment that would test component pelvic wings. Only one PMHS was tested with this low force pulse, but two tests were completed at different Notch to Belt Angles to capture differences in the strain distribution of the pelvis as a result of different loading angles. Note that the targets of these tests are not related to the pelvis kinematics from the sled tests. The intent was to design a fixture that would hold a target posture as still as possible throughout a lap belt loading event to isolate the lap-belt-to-pelvis angle that resulted in fracture in Richardson et al 2020.

Table 4.1-1 Test Matrix and Targets of Non-Impact Dynamic Tests

Test Number	Subject Number	Force Limit (kN)	Spine Angle (Deg)	Target Notch Angle (Deg)	Target Belt Angle (Deg)	Target Notch to Belt Angle (Deg)
D1525	UVA_663	8.0	45	130	40	90
D1527	UVA_1001	8.0	45	130	40	90
D1529	UVA_895	8.0	45	130	40	90
D1531	UVA_990	1.0	45	130	40	90
D1532	UVA_990	1.0	45	130	55	75

4.1.1. Impactor and Pulse Description

For both sets of tests, an acceleration pulse similar to the lap belt displacement relative to the pelvis displacement from Richardson et al 2020 was input into a feedback-controlled air over hydraulic impactor software. The control system would attempt to match the impactor's acceleration to the desired acceleration pulse using hydraulic brakes. The impactor (Dr. Steffan Datentechnik Advanced Side Impact System, Linz, Austria) was then attached to a drive cable that was wrapped around two sheaves to transfer the pushing force of the impactor into a pulling force to pull the lap belt. The system was displacement controlled; through tuning of the

acceleration pulse, desired forces could be replicated, but the system is not inherently force limited through feedback control.

The main drive cable was connected to a mechanical force limiting system to prevent extreme forces from being applied to the PMHS in the first set of tests, and to prevent injury all together in the second set of tests. In Richardson et al 2020, the PMHS experienced lap belt forces upwards of 8 kN (Figure 3.2-1); thus a force limit of 8 kN per side was chosen for the lap belt. To prevent injury in the subinjurious tests, a force limit of 1 kN per side was chosen. These force limits were achieved through the use of honeycomb. Honeycomb is a material that will hold its shape until a force is reached; at that force, it begins to crush. The mechanical force limiting system used honeycomb to stop the motion of the impactor ram relative to the lap belt cables. This meant that, once the force limit was reached, the lap belts would stop displacing relative to the PMHS while the impactor completed its displacement. A second set of honeycomb was placed behind the force limiting honeycomb, creating a gap of "free travel space." This free travel space determined the stroke length that the belt could be pulled before stopping if the force limit was not reached. Thus, if the force limit was not reached, there was a mechanical system that would stop the belt from being pulled too far. If the force limit was reached, the force limiting honeycomb would begin to crush and stop the motion of the lap belt relative to the occupant.
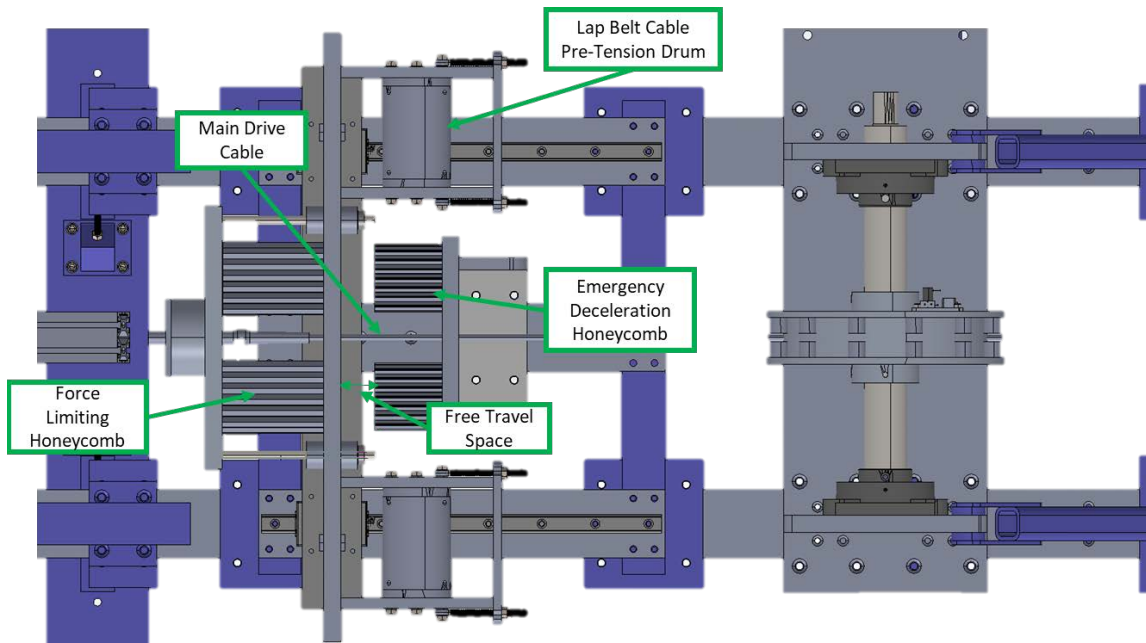
4.1.1-1 Mechanical Force Limiting Honeycomb System

Analysis of the sled tests showed that, on average, Subjects 1, 4, and 5 had around 80 mm of lap belt displacement relative to the pelvis coordinate system. This displacement occurred over a time of around 80 ms. Thus, the first trial pulse tested during tuning was an 80mm/80ms pulse (Figure 4.1.1-3). Because the impactor was rigidly affixed to the cable system, the impactor had to both accelerate and decelerate the system. Therefore, a sinusoidal pulse was created to achieve both acceleration and deceleration in a given time period. In order to check that this pulse was able to generate enough force to crush the honeycomb for the high force tests, UVA's uncertified HIII ATD was affixed to the system as a placeholder. The trial 80mm/80ms pulse was unable to generate enough force to crush the 8 kN honeycomb when trial testing with the HIII, but was able to accurately achieve the target 1 kN consistently. Because Subject 4 from the reclined sled tests was able to withstand 8 kN of force, it was decided to increase the displacement target of the high force pulse to ensure that the force limit was reached on the HIII. So, the displacement target was increased to 120mm over the same 80 ms. With this adjusted pulse, the force limit

was able to be reached, and the honeycomb crushed. Thus, for the injurious PMHS tests, it was decided to use the 120mm/80ms pulse as a precautionary measure to ensure enough force could be generated to fracture the pelvis (Figure 4.1.1-2). For the subinjurious tests, the smaller, 80 mm/80 ms pulse was chosen to ensure that no overshoot occurred in the system that would cause injury to the PMHS.

The DSD control system was tuned by ensuring the system input the maximum amount of energy into the pulse. This was achieved by setting the free travel distance to 0 mm, essentially forcing the system to have to put enough energy in to crush the force limiting honeycomb. By training the control system to generate enough energy to match the necessary displacement in this configuration, the DSD would be trained to achieve the required displacement despite if it was pulling the lap belts against a completely rigid object. By tuning the system in this way, it ensured that the system was capable of having enough energy to match the desired force limit. For the High Force tests, this meant that the DSD was trained to have enough energy to crush the 8 kN honeycomb. For the Low Force tests, this meant that the DSD was trained to avoid overshoot of the acceleration in the system due to the lower force limiting honeycomb that was present.
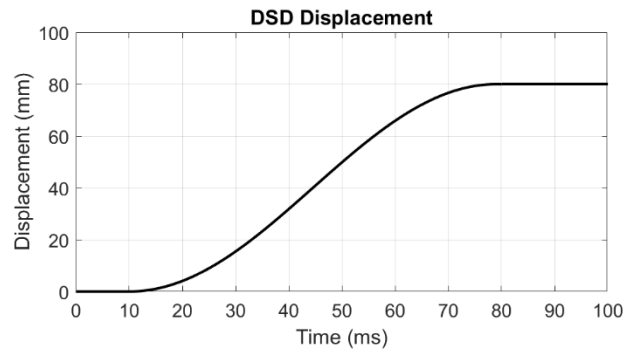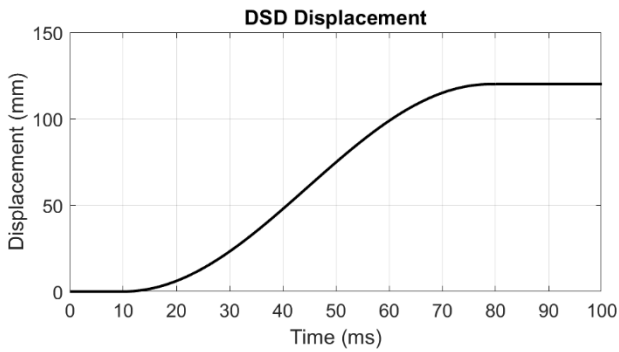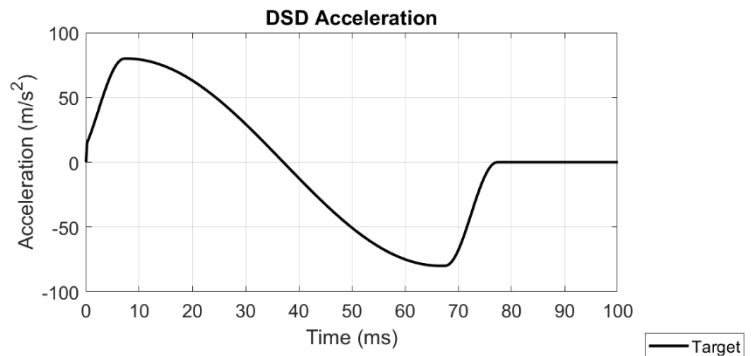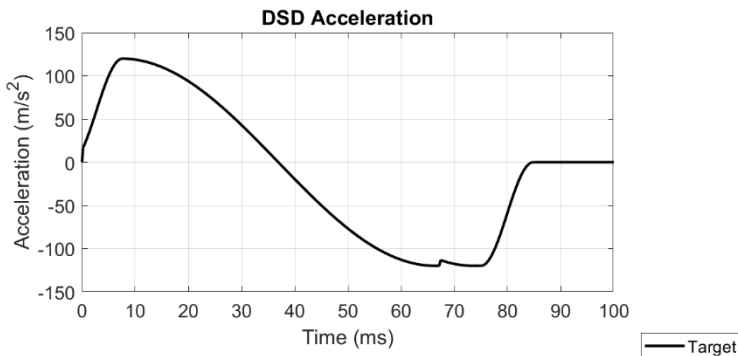
4.1.1-2 High Force Test Target Pulse Information

4.1.1-3 Low Force Test Target Pulse Information

4.1.2. Positioning Methodology and Seat Fixture Description

A rigid seat system was designed with multiple degrees of freedom to assist in positioning each PMHS to its target posture (Figure 4.1.2-1). Each PMHS targeted a Notch Angle of 130 degrees relative to the global horizontal and a spine angle (defined as the line between T8 and L1 vertebra of the spine) of 45 degrees from vertical. For all of the high force tests, the target Notch to Belt Angle was 90 degrees, which was the Notch to Belt Angle that caused fracture in the Richardson et al 2020 tests. In the low force tests, the target Notch to Belt Angles were 90 degrees and 75 degrees (which was the Notch to Belt Angle of Subject 4 at the time of peak force).
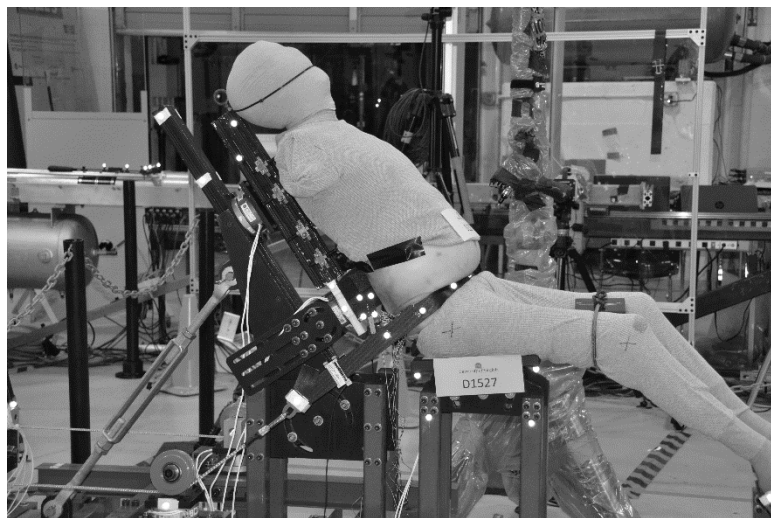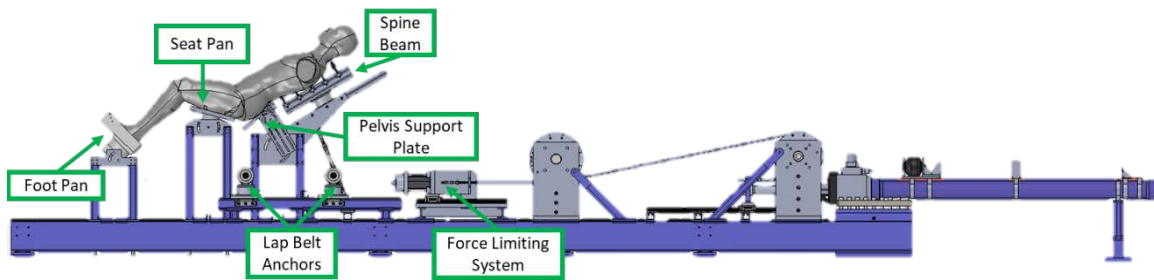
4.1.2-1 Full Seat Fixture

A consistent positioning procedure was followed to ensure that all the PMHS were

positioned as close to the target posture as possible. Computed tomography (CT) analysis was

completed before each test to obtain transformations from the pelvis to the pelvis mount and the

spine to the spine beam to calculate relative angles of the bones to the mounts. These

transformations were subject specific and depended on how each PMHS was mounted to the

spine beam and where the pelvis mount was placed. Then, the seatback was set to the necessary

angle to achieve a spine angle of 45 degrees. The spine beam was secured to the seatback

through a load cell adapter plate. At this point, the spine angle was set to the target, but the Notch

Angle was not. At this point, the pelvis was much too inclined. To achieve the target Notch Angle, two degrees of freedom were utilized. The first was the spine beam load cell. While the spine beam (attached to the PMHS) was rigidly attached to the load cell, the load cell was allowed to slide up and down the seatback while the pelvis was positioned. This means that the angle of the spine stayed the same, but the position on the seatback was able to change. Combining this with translating the seat pan away from the seatback allowed the pelvis to recline by creating a gap between the seatback and the seat pan. Once the target Notch Angle was achieved, the spine load cell was locked into place on the seatback, and the seat pan was locked into place on the impactor tracks.

The next step in positioning was to place the pelvis support plate into optimal position. Ideally, the goal of the pelvis support plate was to provide support above and below the pelvis mount to prevent translation of the pelvis relative to the seat pan during the pulse. This was to ensure that the pelvis orientation relative to the world stayed as constant as possible. However, the configuration of the plate was a subject specific variable and depended on where the pelvis mount was located relative to the seat pan. The pelvis support plate was designed to translate relative to the seatback to allow support of the pelvis regardless of the gap created to achieve the desired pelvis angle. In addition, the plate could rotate to best fit parallel to the posterior iliac wings of the pelvis. High density foam was added above and, when possible, below the pelvis mount to provide strong support to the pelvis while also preventing the pelvis mount from crushing into the seatback during the pulse. This way, minimal force was transferred to the screws of the pelvis mount. The idea here was to prevent any artificial injuries to the pelvis because of the hardware installed to position and track the pelvis. The pelvis support plate was pushed into the PMHS to displace some of the soft tissue to provide adequate support, but was

not used to move the pelvis as a part of positioning. At this stage, the pelvis should still be in the same position as it was before the pelvis support plate and accompanying foam were installed.
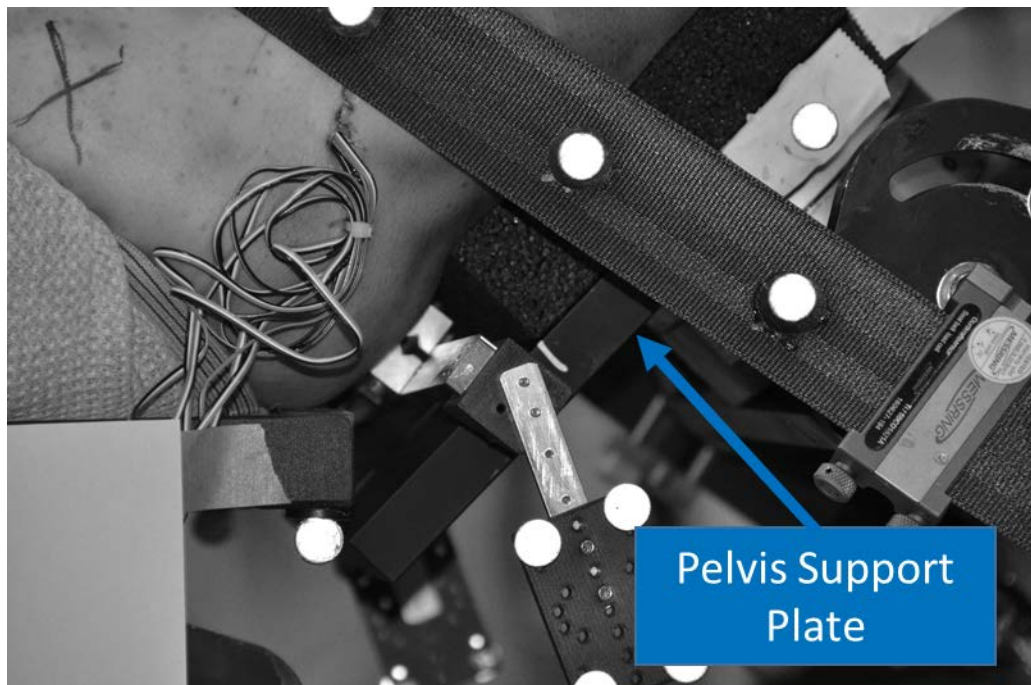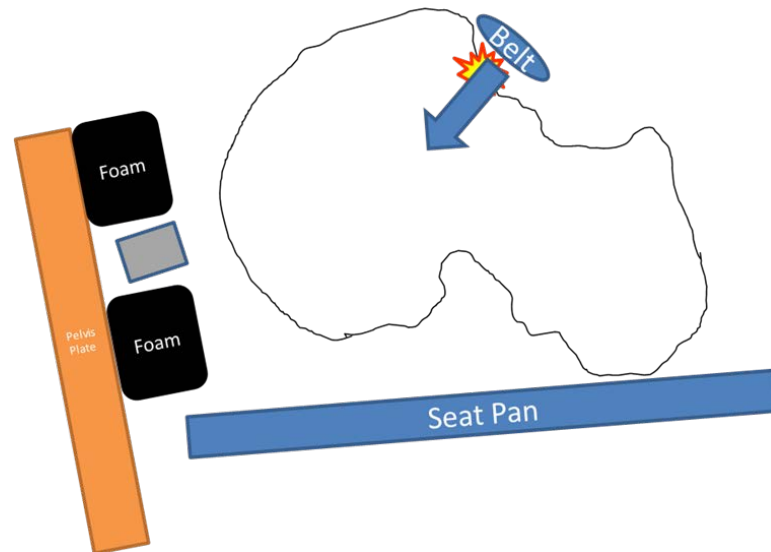
4.1.2-2 Pelvis Support Plate

The last step of the positioning procedure was to move the lap belt anchors into position.

Based on the pelvis angle, lap belt anchors were moved on their respective tracks to produce a

lap belt angle relative to world that was equal to the Notch Angle – 90. This was accomplished through a series of trials where the lap belts were manually pre-tensioned by pulling on the belt, and the angle of the belt was calculated through the use of 3-D motion tracking markers. Once the belt angle was correct and symmetric, the anchors were locked into place. Then, the seatbelt was pre-tensioned to a nominal value of 500N to seat the belt in its starting position. Pre-tensioning occurred by moving the lap belt cable drums along slots in the mechanical force limiting system by tightening threaded rods on the rear of the system. This pulled the drums rearward, giving the lap belt tension. This process was slow, and relaxation occurred, but the location of the lap belt stayed secure due to the length of the process. The seatbelt was placed as favorable as possible, meaning that in all attempts, the top edge of the belt was placed below the ASIS and held there as the pre-tensioning occurred. This was to promote better engagement with the Notch region of the pelvis, and avoid submarining.

Measurements of all the necessary components needed to reach the targets were constantly taken throughout the positioning procedure. This was not only to ensure that the positions stayed the same through the entirety of the positioning procedure. In addition, measurements were compared between manual devices (such as inclinometers) and the 3-D tracking markers attached to mounts and other parts of the rig such as the seatback, lap belt, etc.

4.1.3. Specimen and Rig Instrumentation

Each PMHS thorax was rigidly attached to an aluminum slotted beam through the use of spinal mounts (Kim 2015). This is accomplished through the use of external fixation (pedicle) connected to an adjustable bracket. The mounts were installed in every three or four vertebra from the cervical spine down through the thoracic spine. No spinal mounts were installed in the lumbar spine.
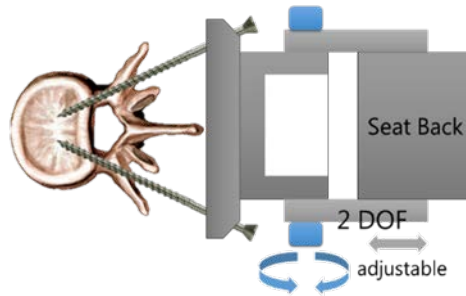
4.1.3-1 Spinal Mount Diagram

Pre-test positioning and kinematic data was collected at 1000 Hz using an optoelectronic motion capture system consisting of 10 cameras (Vicon TXTM, VICON, Centennial, CO, USA) that tracked the position of retro reflective spherical markers in a calibrated 3D space lying within the cameras' collective field of view. Four-marker clusters were secured posterior to the pelvis by attaching them to a mount secured to the left and right posterior superior iliac spines. Markers were also secured to the spine aluminum slotted beam for calculating the spine angle. Motion tracking markers were superglued the seatbelt to assist in positioning the lap belt angle relative to the pelvis. The seatbelt material used in these tests was the same as the material used in the Richardson et al 2020 sled tests to keep the loading environment as similar as possible.
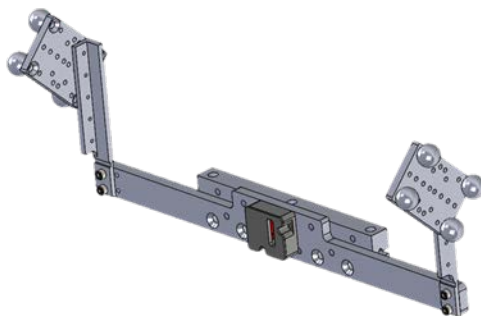
4.1.3-2 Pelvis Mount

Two Micro-Measurements ® C2A-06-062WW-350 strain gauge rosettes were affixed to the lateral surface of each iliac wing between the ASIS and AIIS landmarks. The resulting in-plane maximum and minimum principal strains and direction of principal strain were computed when possible. A computed tomography scan was taken after instrumentation to get orientations of the vertebra relative to the aluminum slotted beam, orientation of the notch angle relative to the pelvis mount, and orientation of the strain gauges relative to the pelvis. The strain gauges used were 45/90 gauge orientations.

Six-axis load cells were installed at the foot pan, seat pan, seat back (one at the pelvis plate and another at the spine beam), and one on each lap belt anchor sheave. Uniaxial seat belt gauge load cells were installed on each side of the lap belt between the corner of the seat pan and the buckle.

4.2. Results

4.2.1. High Force Tests

4.2.1.1. Positioning

Measurements of pre-test positioning data can be found in Table 4.2.1.1-1. Targets for positioning were Notch Angles of 130 degrees, Spine Angles of 45 degrees, and Notch to Belt Angles of 40 degrees. From this table, it can be shown that the Notch Angles ranged from 127-134 degrees, Spine Angle ranged between 45-46 degrees, and the Notch to Belt Angle ranged from 89-94 degrees.

Three-Dimensional reconstructions of the belt location relative to each pelvis can be found in Figure 4.2.1.1-1. From these initial position reconstructions, it can be seen that the midline of the lap belt was placed in the target location of the Notch in

test D1525 and test D1527. In test D1529, the midline of the belt was slightly higher

than the Notch, and the midline was closer to the ASIS itself.

Table 4.2.1.1-1 Pre-Test Positioning Data, High Force Tests

Test Number	Subject Number	Force Limit (kN per side)	Spine Angle (Deg)	Belt Angle (Deg)		Notch Angle (Deg)		Notch to Belt Angle (Deg)	
				Left:	Right:	Left:	Right:	Left:	Right:
D1525	UVA_663	8.0	46	34	38	128	127	94	89
D1527	UVA_1001	8.0	46	Left: 35	Right: 36	Left: 128	Right: 128	Left: 93	Right: 92
D1529	UVA_895	8.0	45	Left: 40	Right: 43	Left: 134	Right: 133	Left: 94	Right: 90
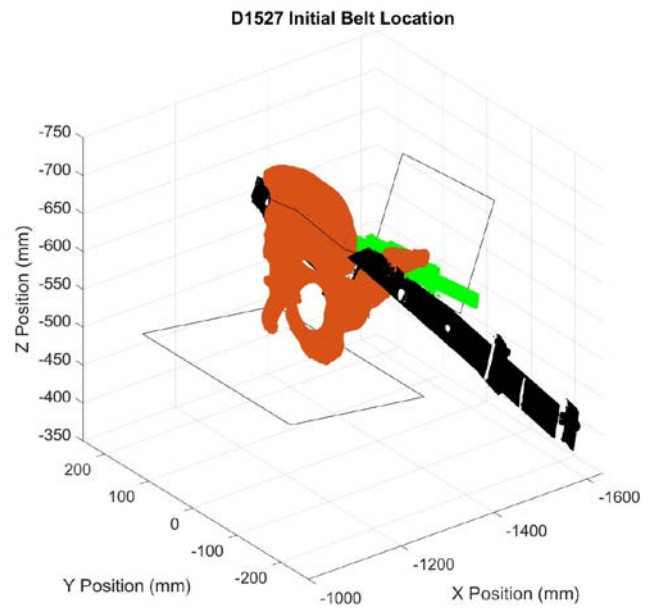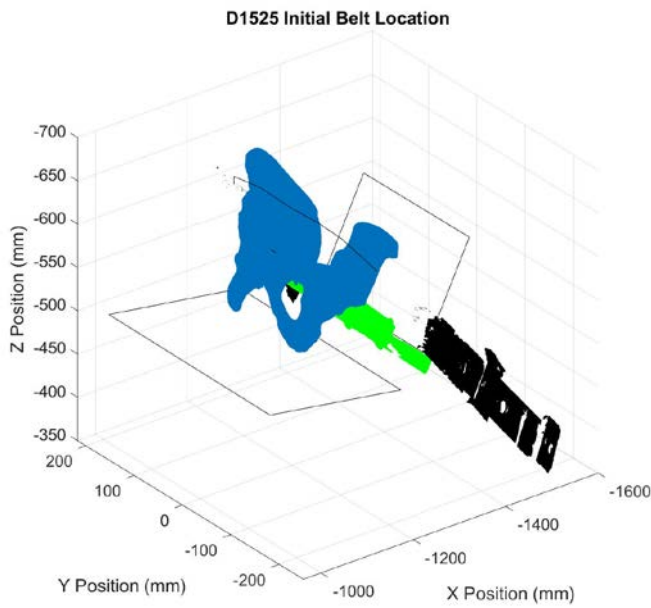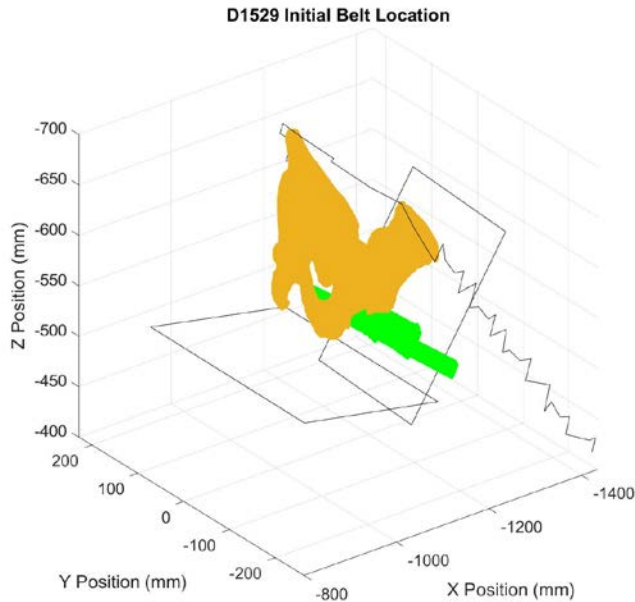
4.2.1.1-1 High Force Test Lap Belt Initial Positions. The green bar is the pelvis mount, each unique pelvis has been oriented to its position in space relative to the seat and pelvis support plate. Lines denote points taken using a 3-D digitizer, and scans of the actual lap belt were taken when possible.

4.2.1.2.   Data Traces

4.2.1.2.1.   Pelvis Kinematics

The goal of constraining the pelvis from translating was successfully achieved in two of the three tests. In tests D1525 and D1529, the pelvis support plate engaged with the posterior aspects of the pelvis, preventing translation of the pelvis. In test D1527, the posterior aspects of the pelvis were not supported sufficiently to prevent relative translation of the pelvis to the seatback. In test D1525, the pelvis pitched forward 1 degree relative to the sagittal plane on both the left and right sides before the pelvis mount interacted with the seatbelt, causing errors in data collection. In test D1527, larger forward rotation was seen as a result of large pelvis motion, pitching forward 8 degrees relative to the sagittal plane on the right side and 4 degrees on the left side before the

pelvis mount interacted with the seatback. In test D1529, the pelvis originally pitched forward for the first 20 ms of the pulse, but then pitched rearward, oscillating around 1 degree of rearward rotation relative to the sagittal plane on both sides (Figure 4.2.1.2.1-1). The Notch Angle time histories were cut off at the time where the mount interacted with the seatback or seatbelt, due to errors in the data collection.

In all tests except D1527, the Notch to Belt Angle deviated 5 degrees or less from the initial starting point (Figure 4.2.1.2.1-2). The Notch to Belt Angle was always larger on the left side than on the right side by an average of two degrees. In tests D1527 and D1529, the Notch to Belt Angle follows roughly the same change over time on both sides of the lap belt. In test D1529, the lap belt angle tracking markers were blocked on the right side after 50 ms, so data traces stop at that time.
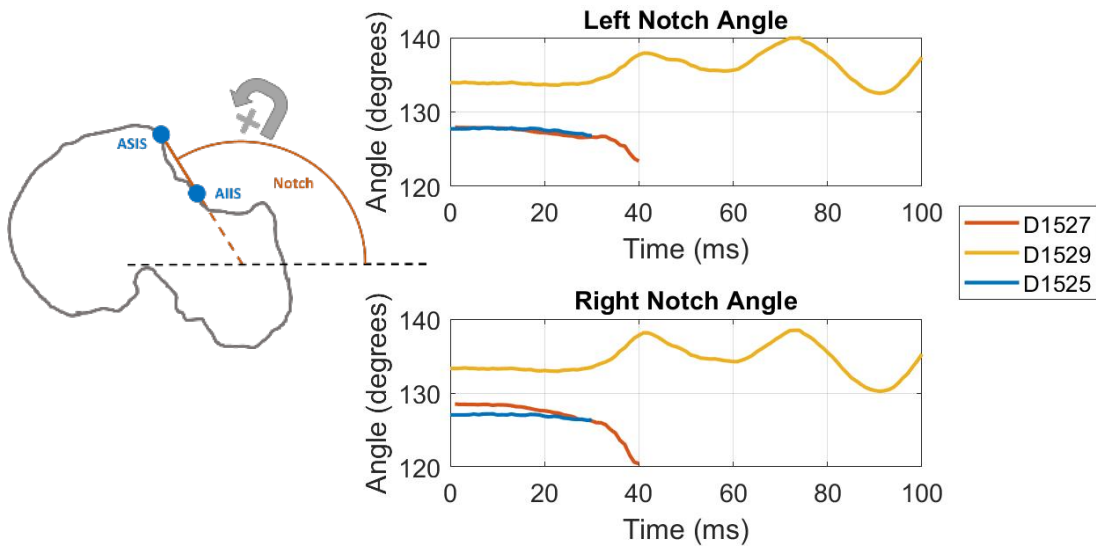
4.2.1.2.1-1 Notch Angle Time Histories
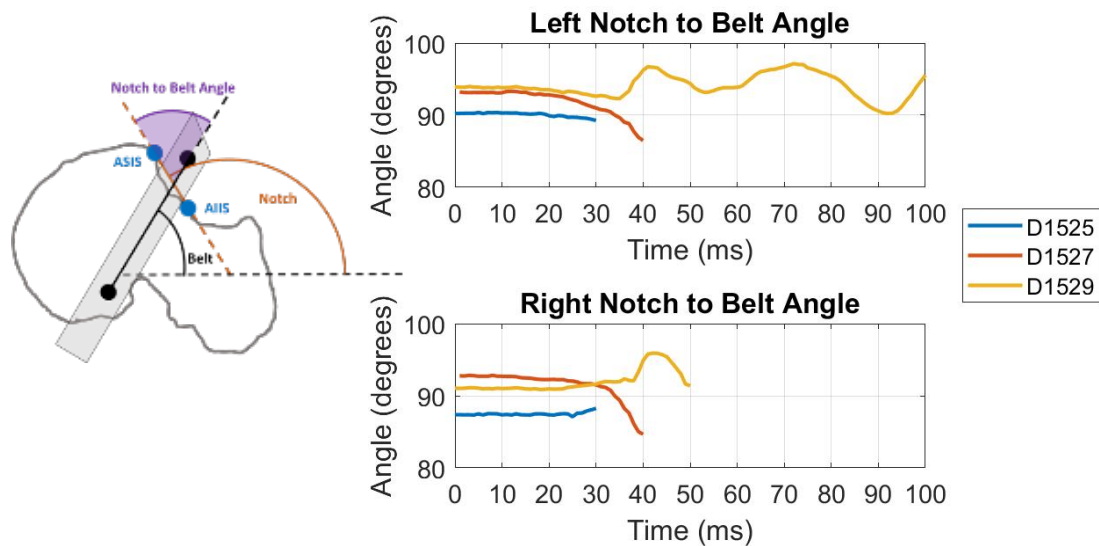
4.2.1.2.1-2 Notch to Belt Angle Time Histories

4.2.1.2.2. Lap Belt Displacements and Forces

In tests D1525, D1527, and D1529, the force limit of 8.0 kN was not reached. Peak belt forces can be seen in Table 4.2.1.2.2-1. In test D1525 the belt had displaced 32 mm on each side at time of peak force. After the time of peak force, the belt continued to displace until reaching a maximum displacement of 94 mm on the right side and 86 mm on the left side. In test D1527 the belt displaced 43 mm on each side at time of peak force. The belt continued to displace until a maximum displacement of 110 mm was reached on each side. In test D1529 the belt displaced 38 mm on each side at time of peak force. The belt continued to displace until a maximum displacement of 125 mm was reached on the left side and maximum displacement of 139 mm was reached on the right side.
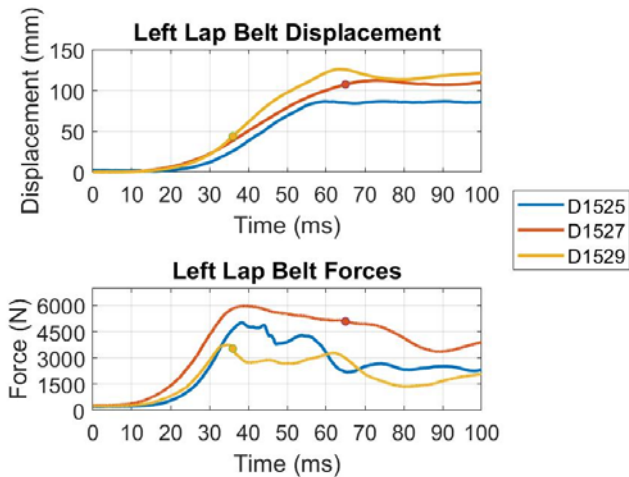
4.2.1.2.2-1 Lap Belt Data, Left Side   **4.2.1.2.2-2 Lap Belt Data, Right Side**
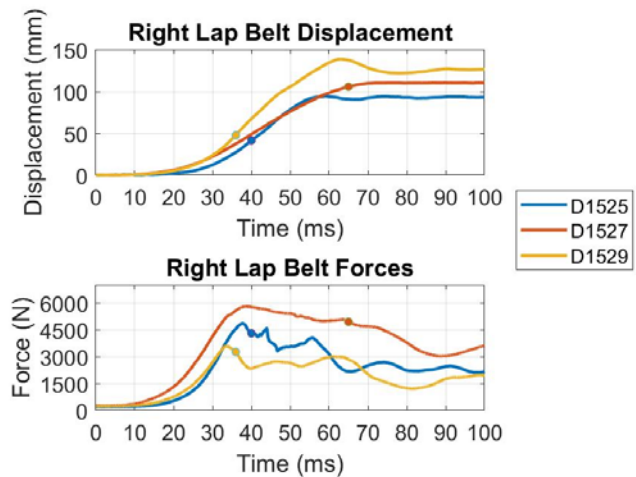
Table 4.2.1.2.2-1 Peak Lap Belt Force Data

Test Number	Peak Force Left (N)	Time (ms)	Peak Force Right (N)	Time (ms)
D1525	5016	38.3	4857	37.7
D1527	5961	38.9	5804	38.5
D1529	3754	34.7	3592	33.8

4.2.1.2.3.   Injury and Submarining Outcomes; Strain Data

Subject UVA_663 (test D1525) exhibited a large pelvis fracture at the right iliac wing between the ASIS and AIIS landmarks and a left sacral wing fracture. Subject UVA_1001M (test D1527) exhibited a small pelvis fracture at the right iliac wing between the ASIS and AIIS landmarks, while also exhibiting a left superior iliac fracture extending across the sacrum, minimally displaced superior right pubic rim fracture, and non-displaced inferior right pubic rim fracture. Subject UVA_895 (test D1529) exhibited no pelvis fractures. These findings were identified and confirmed from post-test CT scans and autopsy.

When possible, injury timing was determined through strain gauge data (Figure 4.2.1.2.3-1). Subject UVA_663 experienced fracture on the right side at around 40 ms, as

61

shown by a severe drop in strain. This is after the time of peak force, and occurred at 4.3 kN. Time of injury was not able to be determined for Subject UVA_1001 through the strain data as there were no severe drops in strain. Subject UVA_895 submarined at 36 ms at 3.2 kN of force. While no pelvis injuries occurred, the subject had severe lap belt "burn," and the subcutaneous fat had sheared from the fascia layer in regions superficial to the iliac wings. Strain gauges in each rosette failed for nearly every strain gauge of these tests, either from mechanical failures at the start of the test or due to the loading.
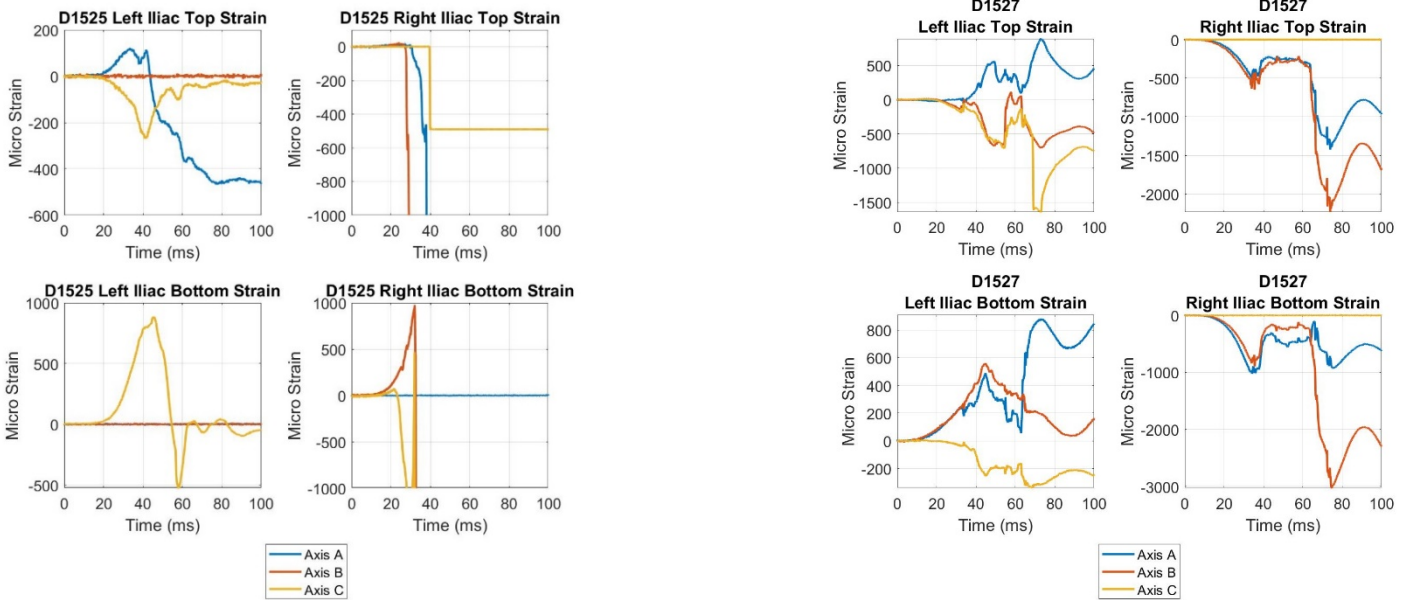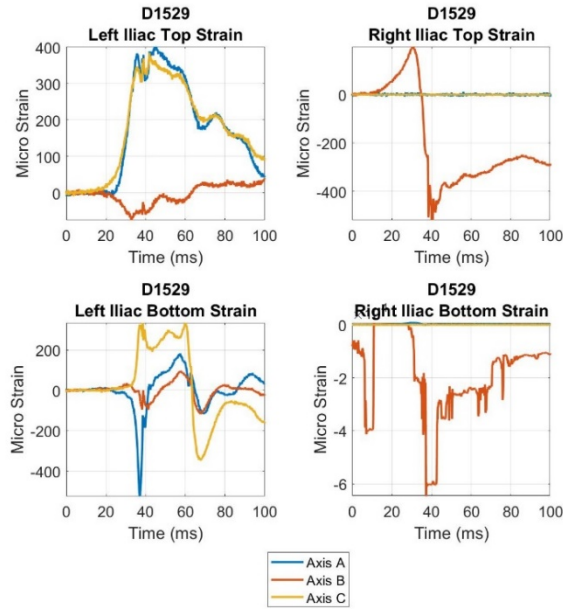
4.2.1.2.3-1 Strain Gauge Data from High Force Tests

4.2.2. Low Force Tests

4.2.2.1. Positioning

In the low force tests, the Notch Angle and Spine Angle targets relative to the world were the same as the high force tests (130 degrees and 45 degrees, respectively). Two tests were run; in both tests, the same Spine Angle (46 degrees) and Notch Angle (132 degrees) was achieved for both tests, meaning that the subject was oriented in the same way for both tests.

In the first low force test, the same target Notch to Belt Angle of 90 degrees was tested. Then, a test was run with a more vertical lap belt angle (and thus a smaller Notch to Belt Angle). This Notch to Belt Angle target was 75 degrees, but due to limitations in seat fixture, the lap belt anchors could only move to a maximum lap belt angle of ~ 54 degrees. Thus, the Notch to Belt Angle for test D1532 was 79 and 78 degrees, respectively.

Table 4.2.2.1-1 Initial Positioning for Low Force Tests

Test Number	Subject Number	Force Limit (kN per side)	Spine Angle (Deg)	Belt Angle (Deg)		Notch Angle (Deg)		Notch to Belt Angle (Deg)	
D1531	UVA_990	1.0	46	Left: 39	Right: 41	Left: 132	Right: 132	Left: 89	Right: 91
D1532	UVA_990	1.0	46	Left: 53	Right: 54	Left: 132	Right: 132	Left: 79	Right: 78

Three-dimensional reconstructions show that the lap belt midline was placed in the desired location for both tests. The midline of the lap belt passes through the Notch area. However, in test D1532, the lap belt was placed slightly lower than in test D1531. This is perhaps due to the more vertical lap belt angle, which allowed lower placement of the belt to occur.
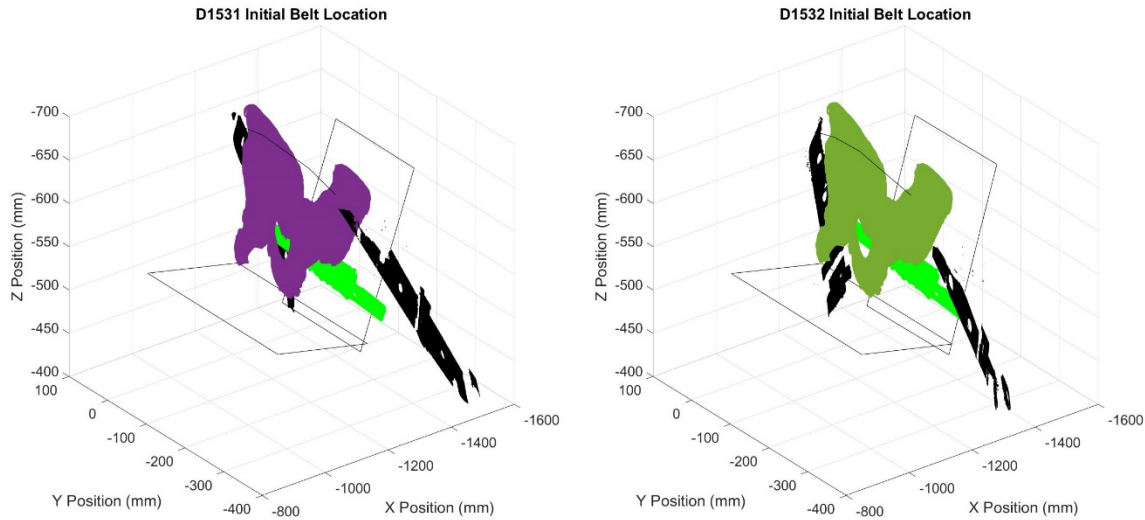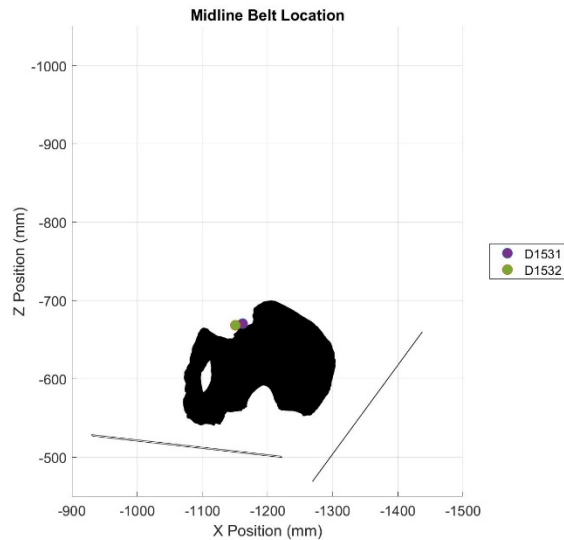
4.2.2.1-1 Initial Lap Belt Positions for Low Force Tests

4.2.2.2.   Data Traces

4.2.2.2.1.   Pelvis Kinematics

In both the low force tests (D1531-D1532), the pelvis did not translate relative to the seatback. In tests D1531 and D1532, the pelvis rotated slightly rearward relative to the sagittal plane. The rotation increased as a result of a more vertical lap belt angle (one degree of peak rearward rotation vs two degrees peak rearward rotation). Rearward rotation increased as belt force increased, and then dropped off as belt force decreased.

In tests D1531 and D1532, the left and right side Notch to Belt Angles change in different directions. The change in loading direction for both tests is always less than 3 degrees. Polarity differences can be attributed to twist in the lap belt cables that occurred during the pulse.
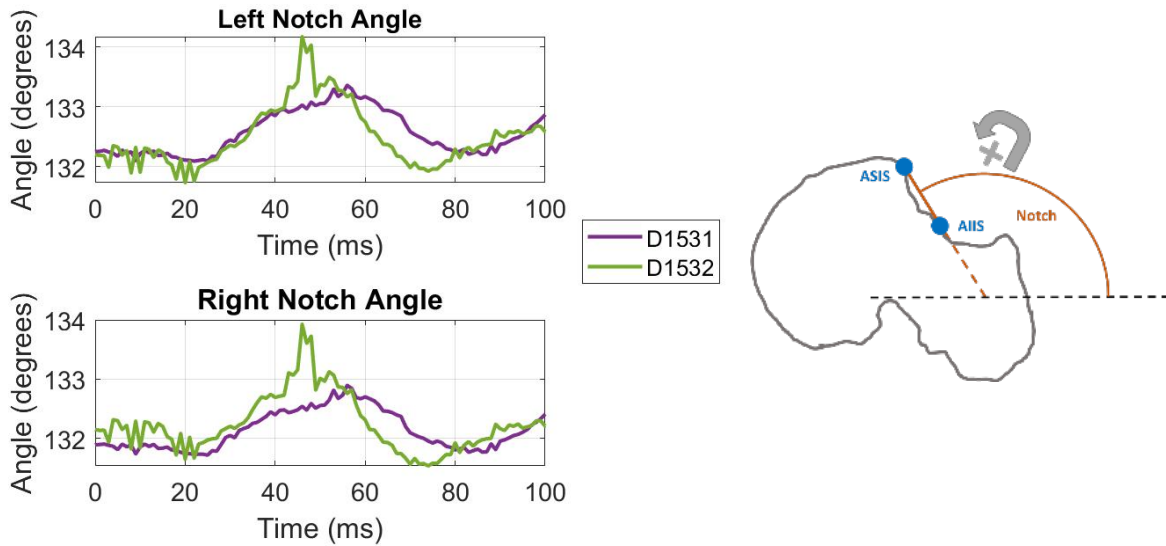
4.2.2.2.1-1 Notch Angle Time Histories, Low Force Tests
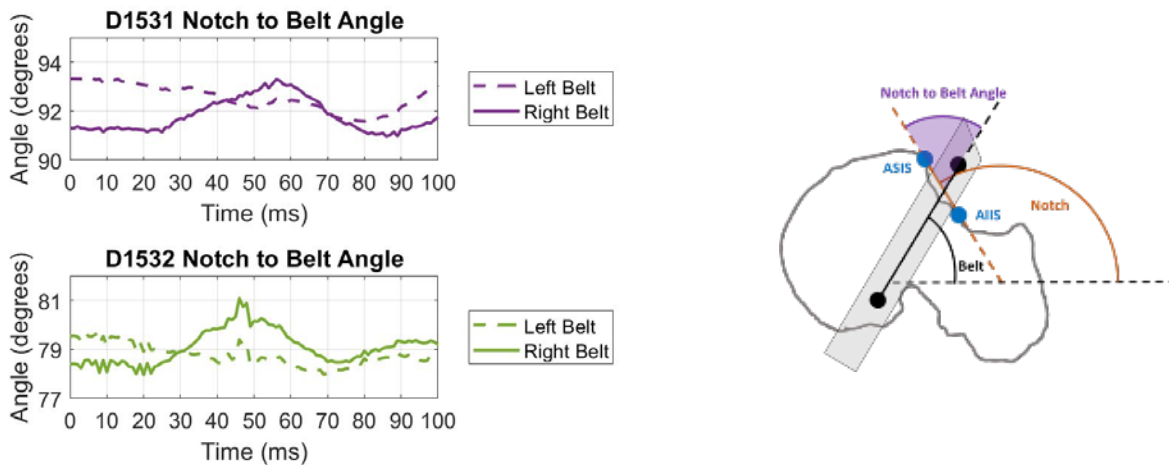
4.2.2.2.1-2 Notch to Belt Angle Time Histories, Low Force Tests

4.2.2.2.2. Lap Belt Displacement and Forces

In tests D1531 and D1532, the force limit of 1.0 kN per was reached. In test D1531, the belt reached its maximum displacement of 15 mm at the time of peak force. In test D1532, the belt reached its maximum displacement of 10 mm at the time of peak force. Overshoot in the system occurred as a result of inertial movement in the honeycomb fixture, causing lap belt forces to reach greater

magnitudes than 1.0 kN despite the force limiting features of the honeycomb itself.
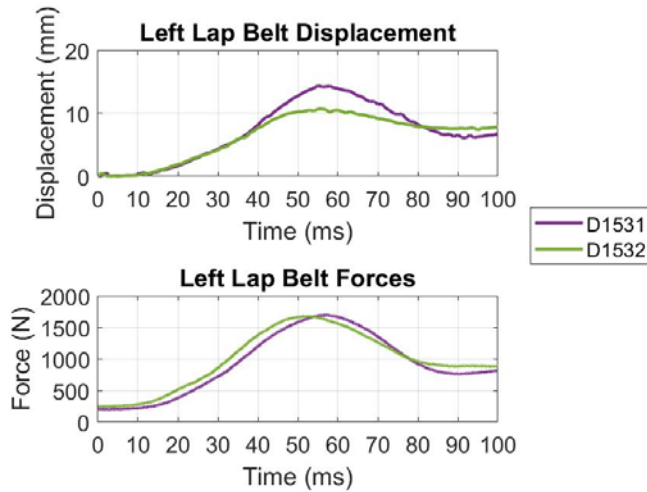
4.2.2.2.2-1 Lap Belt Data, Left Side
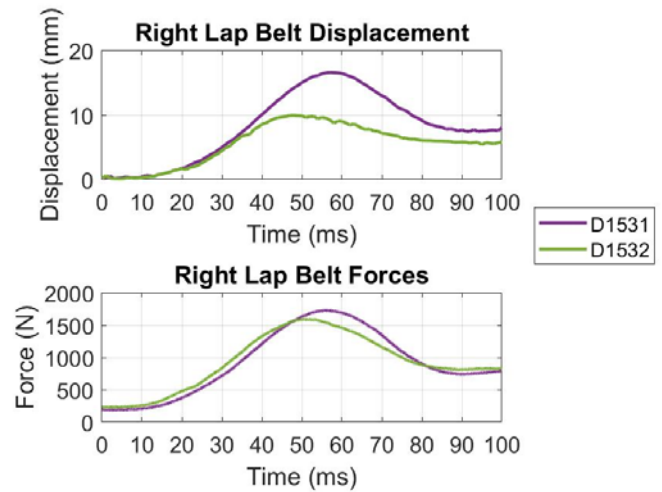
4.2.2.2.2-2 Lap Belt Data, Right Side

Table 4.2.2.2.2-1 Peak Lap Belt Force Data

Test Number	Peak Force Left (N)	Time (ms)	Peak Force Right (N)	Time (ms)
D1531	1701	56.9	1731	55.7
D1532	1680	52.6	1590	50.6

4.2.2.2.3.   Strain Data

For tests D1531 and D1532, strain data was captured to understand the difference in material response due to a change in lap belt to Notch orientation. Mechanical failures occurred for 4 out of the 5 strain gauges in test D1532, either due to damage from test D1531 or due to moisture. Between the two tests, the magnitude of strain measured at Left Iliac Extra (the only gauge that survived both tests) increased as a result of a change in lap belt angle. In addition, the

direction of principal strain at peak force changed by 5 degrees with a change in belt angle of 13 degrees.
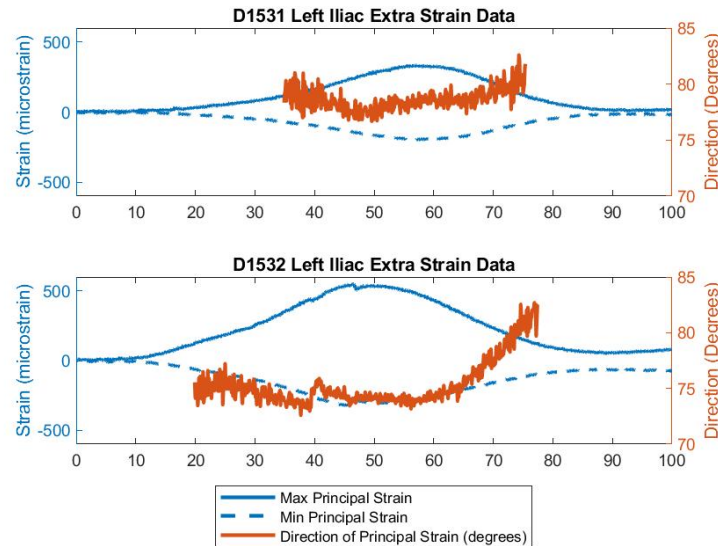
4.2.2.2.3-1 Left Iliac Extra Strain Data, Tests D1521 and D1532

4.3. Discussion

The subject positioning procedure laid out in this test series allowed for maximum flexibility and accuracy in targeting postures of mid sled impact test positions. The motion tracking markers on the pelvis mount and spine constraint beam allow for fine tuning to match targeted positions accurately and repeatedly. The impactor system was able to apply loading rates to the pelvis that are similar to loading rates seen in frontal sled tests. Rigid constraint of the thorax while supporting the pelvis using the seat pan and seatback plate kept the pelvis orientation and position near target values while the lap belt was pulled. The pelvis tracking mount was mostly designed for the ability to position the pelvis as close to a target orientation as possible. In tests D1525 and D1527, the pelvis mount integrity was compromised by interaction with the seat belt catching or the seat back support plate. Cable

twisting caused bilateral lap belt twist in all tests, and in test D1529 caused the loss of lap belt angle tracking at 50 ms.

4.3.1. High Force Tests

4.3.1.1. Injury Outcomes

Two of the three subjects tested using the high force pulse sustained fractures between the ASIS and AIIS. In test D1525, an iliac wing injury similar to Richardson et al 2020 Subject 1 and Subject 3 was sustained. However, the force at which this fracture was sustained was much lower (4.3 kN compared to 7.8 kN and 6.6 kN from Subjects 1 and 3 respectively). This may be in part to the poor bone quality of the subject, but illustrates the large range in forces that are required for the injury to occur. In test D1527, the pelvis translated due to the lack of support on the posterior side of the pelvis. As a result, the pelvis crashed into the seatback, and large, posterior pelvis fractures occurred. Because of these fractures, it was nearly impossible to determine the force at which the fracture of interest that occurred on the anterior side of the pelvis between the ASIS and AIIS occurred. For this reason, it must be treated as a censored data point, occurring somewhere below peak force of around 6 kN. The fracture sustained during this test was not the same type of fracture seen in Richardson et al 2020, but appeared to be the very beginning of a fracture at this area. The location of the fracture, however, matches up exactly between the ASIS and AIIS.

In test D1529, submarining occurred due to the lap belt placement relative to the pelvis. While every effort was made to place the lap belt low on the pelvis so that the midline of the lap belt was in line with the Notch region, the pre-tensioning procedure

caused the lap belt to ride up the subject. The soft tissue was compressed in such a

way that an upward force was created, causing the lap belt to slide along the flesh

until the lap belt caught on the ASIS. While no pelvis injuries occurred, soft tissue

damage did result because of the submarining, even causing a layer of subcutaneous

adipose tissue to be sheared off from the fascia layer.

Table 4.3.1.1-1 Injury Reconstructions from High Force Tests

Subject	Frontal	Right	Left
UVA_663			
UVA_1001			
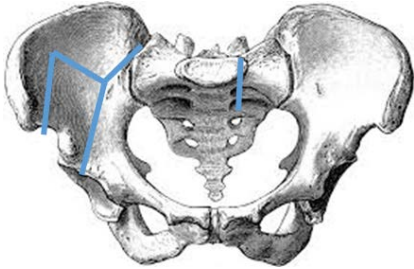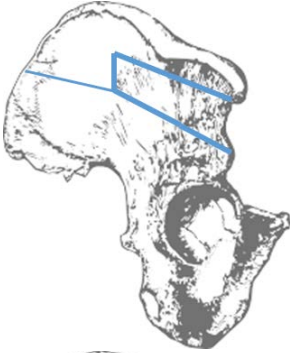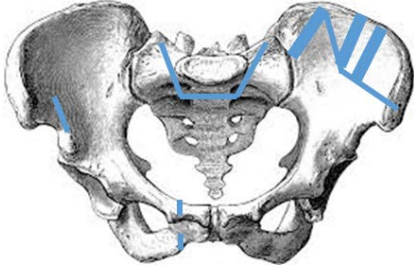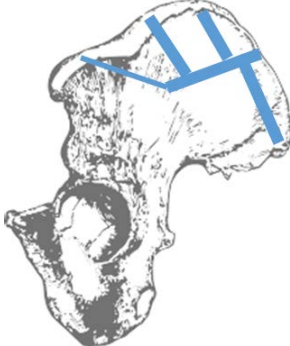
4.3.1.2.   Comparison to Richardson et al 2020

The test environment created in this task was designed to replicate the lap belt

loading conditions that caused fracture in Richardson et al 2020. Section 4.3.1.1 showed

that one of the three subjects sustained similar fractures to those seen in the Richardson

2020 sled tests. In addition, as shown in Figure 4.3.1.2-1, lap belt loading rates were also

similar to those from the sled tests. Certain differences can be seen in the Figure due to

the simplified loading environment created in Task 2. First, there was no pre-tensioner fired at the start of the pulse; rather, as seen in the Figure, pre-tensioning occurred before the test was run. This causes the lap belt force values to start above 0 N. However, for the main loading phase of the pulse, the loading rates lie right on top of each other. Peak forces are not the same as in the sled tests, but that can be attributed to pelvis fracture in test D1525, lack of pelvis support in test D1527, and submarining occurring in test D1529.
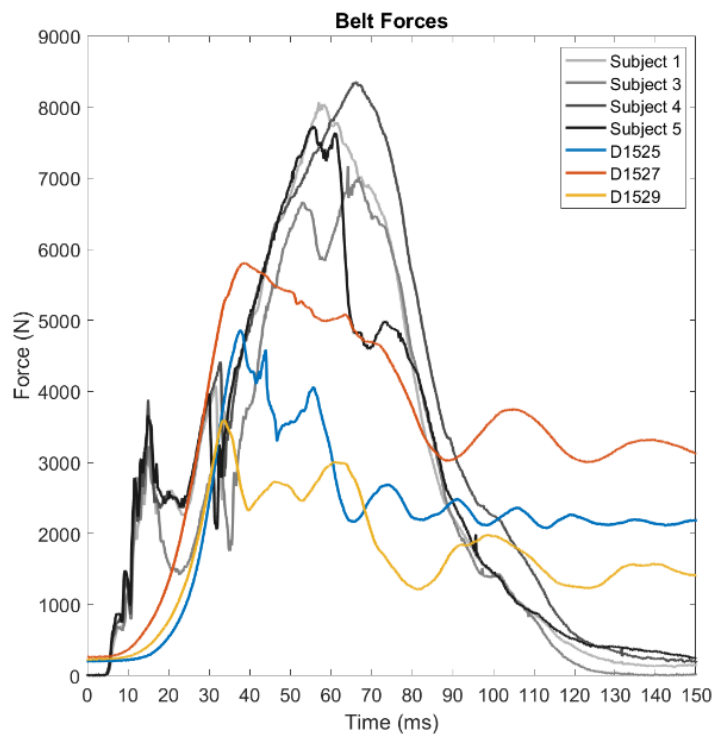
4.3.1.2-1 Lap Belt Force Comparison from High Force Tests to Richardson et al 2020 Outboard Lap Belt Forces

4.3.1.3.   Limitations

The main limitation of the High Force Tests from Task 2 is that only three PMHS were tested. Only one test has an exact censored replica of the targeted injury of this part of the study. The posterior support to the pelvis was crucial in keeping the pelvis

as still as possible throughout the loading pulse. This was not achieved for test D1527; as a result, the translation that occurred clouded the data able to capture the one fracture that did occur in the location of interest, and caused superficial injuries to the posterior side of the pelvis that are not representative of what occurs in a sled test. Submarining occurred in test D1529 due to a higher lap belt starting location despite all efforts to position the lap belt the same way. In a perfect world, all three subjects would have had the exact same boundary conditions in terms of posterior support and lap belt placement, but this did not occur.

Another limitation to the study was the pelvis mount design and the lap belt cables. While every effort was made in ensuring that the pelvis mount would not interact with the lap belt, it was difficult to control due to the sheer size of the pelvis mount. In order for the infrared cameras to pick up the markers, the mount needed to be quite long. While flexibility in the orientation of the physical array was given, it was nearly impossible to tell if the seatbelt would interact with the mount or not due to twist that occurred in the cables connecting the force limiting honeycomb system to the lap belt buckle on each side. The twist in the cable cause the lap belt to twist, which made it more likely to hit the pelvis mount.

In addition, the lap belt twist made calculation of the initial lap belt angle difficult. As the belt was pre-tensioned, the belt twisted as a result of the cables twisting. Thus, the lap belt angle also changed due to rotation of the infrared markers in space. It was decided that the lap belt would be placed below any abdominal tissue pannus; while this made securing the belt to the pelvis more likely, it also clouded the lap belt tracking capabilities of the system. Curvature of the belt around the subject

could only be found through 3-D reconstruction of the initial position; no information

is present for how the lap belt changes over time during the pulse. The amount of

physical lap belt visible was completely dependent on the size of the pannus; in test

D1525, there was only room to place three infrared markers on each side of the lap

belt. The limited distance between markers made small changes due to rotation of the

lap belt cause large changes in the measured lap belt angle. A better way to measure

the lap belt angle, whether it be through removing the cable twist or by relying only

on the manual measuring capabilities, would be better.

The lap belt loading environment was intended to be symmetric on both sides of

the occupant for simplification. However, no shoulder belt or the ability to stagger the

lap belt anchor sheaves to create asymmetric loading is also a limitation of this

environment. In the fleet (or in a sled test), the outboard and inboard side of the

occupant will have more of a discrepancy between the forces at each side, along with

the angle of the belt on each side, due to the presence of the shoulder belt pulling up

at the buckle on the inboard side. In Richardson et al 2020, Subject 5 submarined on

this side, partially hypothesized because the shoulder belt was pulling the lap belt

upwards at this location. Luet et al 2012, Uriot et al 2015, and Troseille et al 2018,

however, all used separate shoulder belt and lap belt restraint systems rather than one,

connected system. The environment created in this Task is more similar to the

restraint system of those tests, where there is more equivalent loading of the pelvis on

each side. It is possible that asymmetric loading would have changed the outcomes of

some of these tests.

4.3.2. Low Force Tests

4.3.2.1. Strain Distribution Interpretation and Limitations

The strain data captured in tests D1531 and D1532 was created to evaluate how well the simplified environment created in Task 3 matched the boundary conditions created in Task 2 of the thesis. Test D1531 generated strain data at multiple strain gauges that can be compared to the Task 3 environment by isolating the relative distribution of the magnitude of strain between the gauges, as well as the direction of principal strain at those gauges. By running tests at multiple Notch to Belt Angles, it was shown that loading direction does change the strain distribution in at least one location on the pelvis (where Left Iliac Extra was placed). This provides support that the injury risk function may be different dependent on the angle of load application.

However, the main limitations of these tests were the failures of the strain gauges. While the Data Acquisition System showed no errors in the gauges, it is clear that looking at the below figures that the strain data is completely different between tests. This is not expected; shapes of the graphs are jagged and inconsistent, indicating that the gauges themselves were damaged or removed from the surface of the bone between the end of the first test and the beginning of the second test.
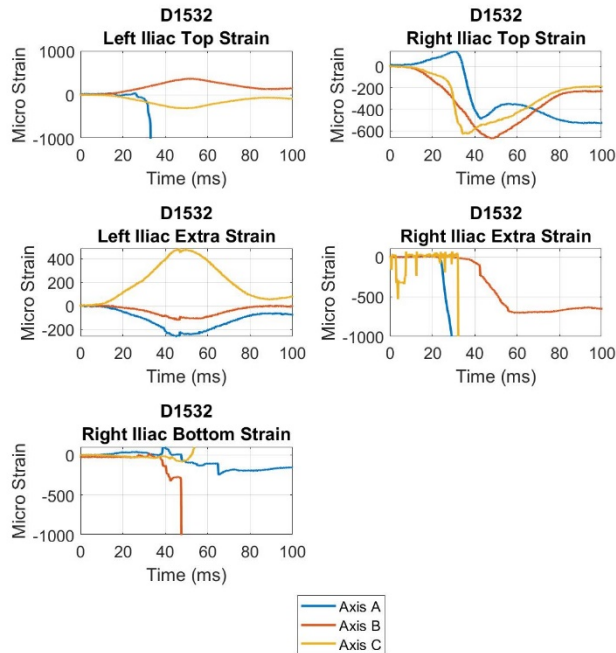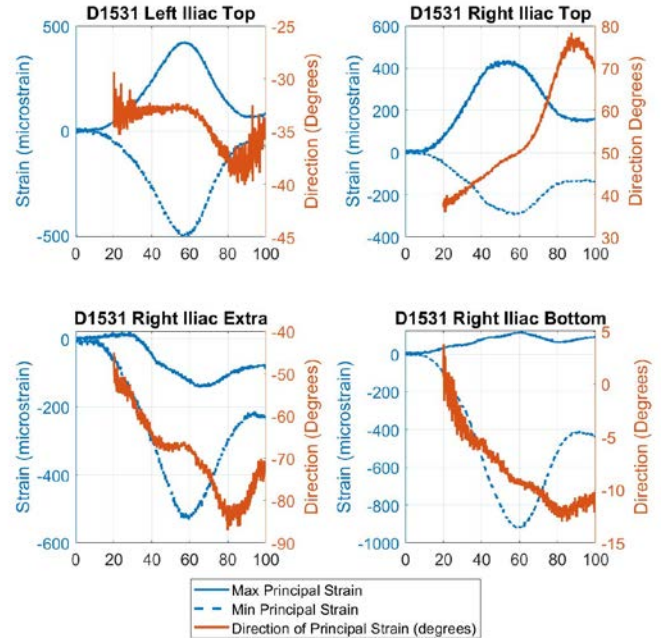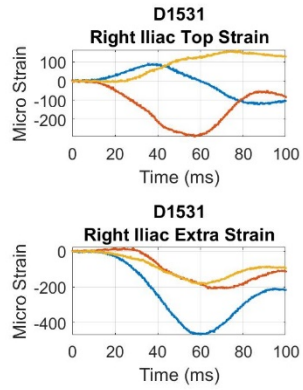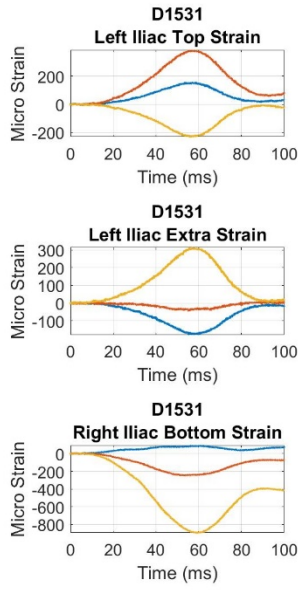
4.3.2.1-1 Strain Data from Low Force Tests

4.4. Summary and Conclusions

This tasked aimed to replicate the environment that caused fracture in the Richardson et al sled tests. A test fixture was developed that was able to match the targets that were isolated in Chapter 3. Two sets of test were run in this environment. One set was designed to replicate the fractures that were described in Chapter 2, and were seen in the Richardson et al sled tests. The second set was intended to capture material response data of the pelvis under lap belt loading. This second set of tests will provide information that can evaluate the component level test fixture used in Chapter 5 that will be used to determine the injury tolerance of the pelvis.

The data presented in Chapter 4 shows that these goals were achieved:

- Test D1525 resulted in the same fracture that Subjects 1 and 3 sustained in Richardson 2020 et al.

- Test D1527 resulted in a fracture in the location of interest, however due to poor support of the pelvis which resulted in the pelvis crashing into the seatback, exact fracture timing was unable to be determined.

- Section 4.3.1.2 shows the lap belt loading rates were similar to that of the sled test.

- The low force tests provided strain data to evaluate the boundary conditions of the environment generated Chapter 4 with the environment created in Chapter 5.

5. Task 3: Component Level Pelvis Testing

The goal of this task is to generate iliac wing fractures on isolated pelvic wings under frontal lap belt loading conditions. In Chapter 3, the lap-belt-to-pelvis loading environment at the time of fracture in the Richardson et al sled tests was isolated. In Chapter 4, material response data was captured that characterized the pelvis under this lap belt loading condition. In this chapter, a simplified loading environment will be manufactured that would ideally load pelvises the same way that they were loaded in Chapter 4. Subinjurious tests on the same pelvis tested in Chapter 4 will be conducted at various loading angles to determine the similarity between the two environments. Then, twenty two pelvic wings will be tested to failure with the goal of isolating injury between the ASIS and AIIS. Injury tolerance data will be collected and analyzed in Chapter 6 to develop an injury risk function for frontal loading of the pelvis.

5.1. Methods

5.1.1. Test Fixture Description

An Instron 8800 bi-axial testing machine (Axial-Torsion Servohydraulic Fatigue Testing System, FastTrack 8800 Materials Test Control System, Instron Corporation, Norwood, MA, USA) was used to apply load to the component pelvises. The Instron is both force and displacement controlled. In this study, displacement control was used because it was unclear exactly what force would be needed to fracture the pelvis. In addition, geometric constraints of the fixture may be present so a displacement limit was required, as it was necessary to ensure only the seatbelt was loading the specimen and not the tines of the fork which are metal. Thus, the displacement target was subject dependent based on the physical geometry of the specimen in the potting cup. The Instron has a 10 kN load limit, and displacement rates of the Instron can approach 1 m/s. While these are

constraints to the loading rate and level of the Instron, it was expected that these values

would be enough to fracture all pelvises at loading rates similar to those seen in sled tests.
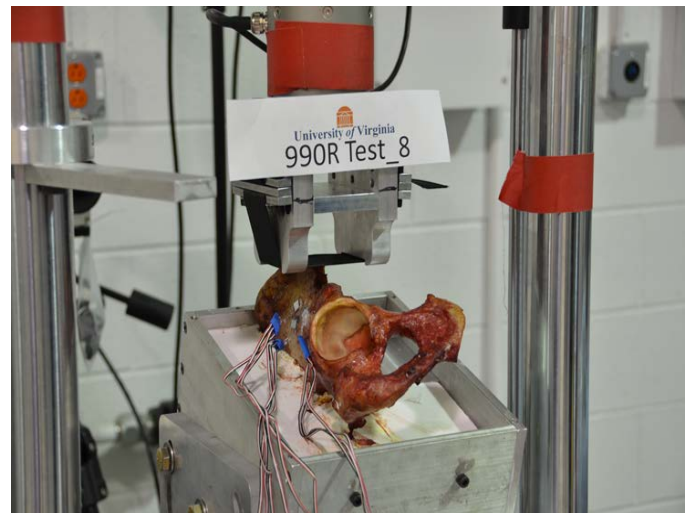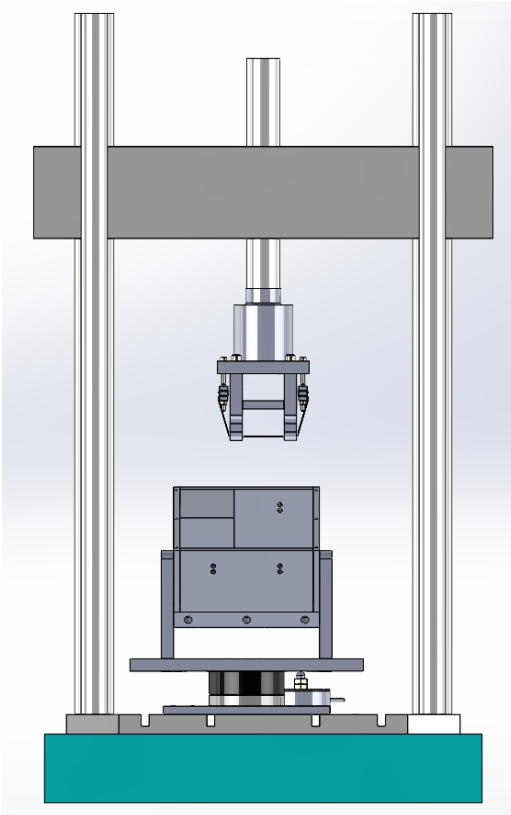
5.1.1-1 Component Pelvis Injury Test Fixture

In an effort to load the pelvises in the same way they are loaded in a sled test, it was

decided that a seat belt should be the mechanism to deliver the load. To achieve maximum

positioning capability as well as simplifying the environment for modelling purposes in the

future, the loading device used was a "fork "directly attached to the Instron head. Seatbelt

webbing could stretch between two, reinforced aluminum tines. Screws on each side of the belt

fork provided the ability to clamp the seatbelt webbing using steel plates to prevent slippage

during loading. Then, jack screws on both sides of the fork tines allow the belt to be pre-

tensioned. Due to the size of the fork, it was impossible to get a belt tension gauge positioned to

read the belt force during the test, as well as during pre-tensioning. For that reason, each tension

bolt was torqued to 4 ft-lbs using a torque wrench to provide a consistent starting tension for the
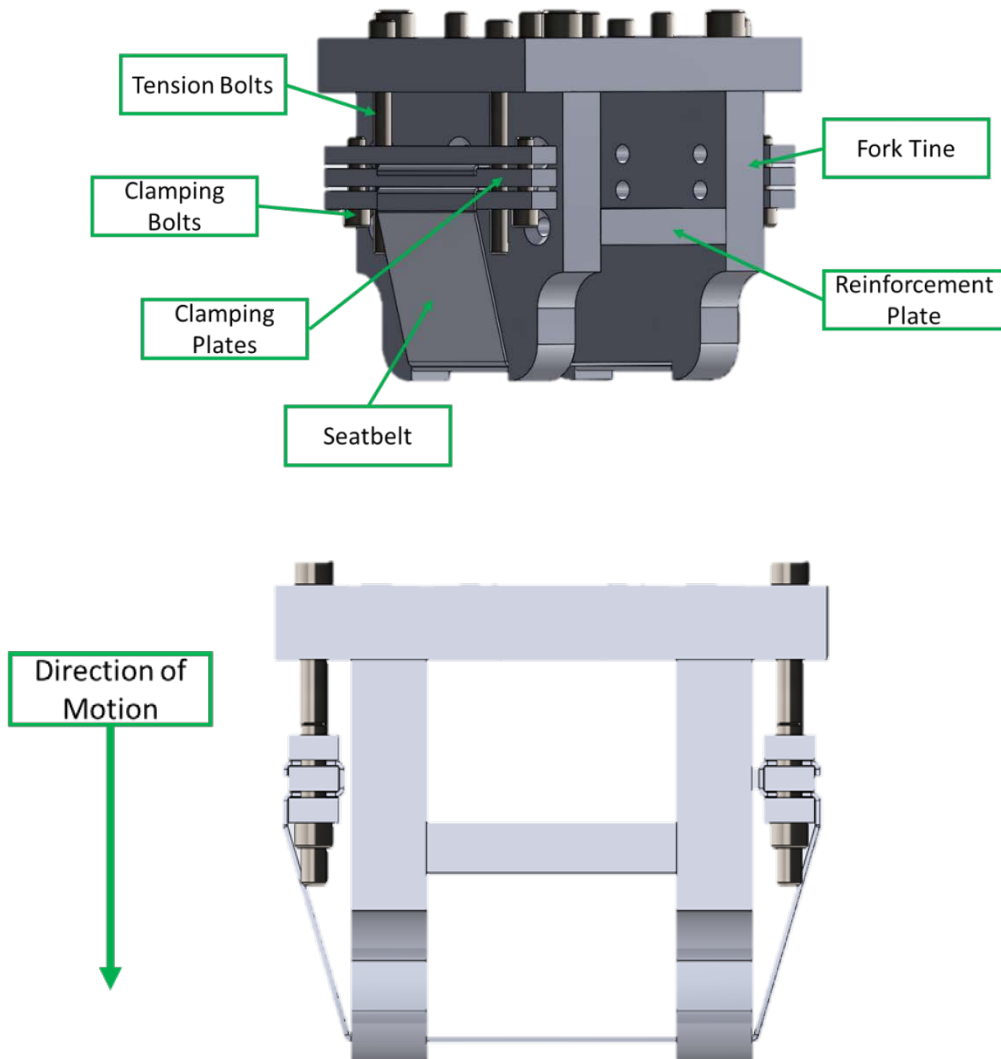
5.1.1-2 - Belt Fork Tine CAD

seatbelt in all tests. The seatbelt was replaced before every test. To achieve a consistent

startinposition for the load, the Instron was positioned to read 10 N at the start of every test.

5.1.2. Potting Procedure and CT Analysis

An aluminum potting cup was developed to hold the pelvis rigidly in position while it

was loaded. Due to the complex geometry of the pelvis, a consistent, mechanical potting

jig to make an identical potting procedure was nearly impossible. However, it was necessary to pot the pelvises in a consistent manner to ensure that they were loaded similarly. To achieve this, plungers were made to hold the pelvis still while the potting material was poured. A consistent procedure was attempted in potting by:

1) Aligning the Notch plane (denoted by a line connecting the ASIS to the AIIS) as parallel with the top of the potting cup as possible.

2) Minimize the overall bend of the wing above the potting material to promote a pure compressive load.
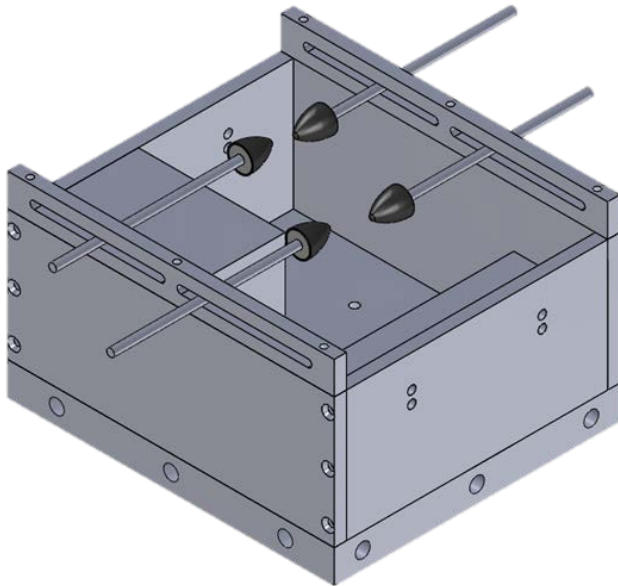
5.1.2-1 – Potting cup; plungers helped hold the pelvic wing in place while pouring the resin to ensure that the wing did not move as it was secured into its desired oreintation.

The potting material used was Smooth-Cast 300Q. The material data specifications can be found in the Appendix. The potting material was a two part low-viscosity resin that allowed for maximum flexibility in pouring capability. This was important because the material had to flow around the complex features of the pelvis shape to create a form fitting hold onto the pelvis. After mixing the two piece resin

together, the chemical reaction would begin to take place, and after a few minutes would become a solid.

Due to the size of the pelvis, the potting cup had to be quite large. Because of this, there was concern that the pre-test computed tomography (CT) scans would become saturated with scatter. Thus, it was necessary that the CT scan had to be taken without the potting cup. However, the relationship between the Notch Plane and the potting cup had to be known in order to adjust the pelvis to the correct loading angle. To achieve this, threaded inserts were placed in the potting material to mimic the horizontal plane of the potting cup. By creating a coordinate system based on the locations of the threaded inserts, the angle of the Notch plane relative to the potting cup could be found so that the potting cup could be adjusted in the test fixture to ensure the target loading direction was achieved. In addition, the threaded inserts provided locations for bolts to be inserted into the side of the potting material to ensure that the potting material was rigidly connected to the potting cup itself.

The potting cup was clamped to the Instron base via clamping plates and bolts. These plates could be attached on either side of the potting cup to allow for rotation in different directions (only one direction at a time, however). The rotation capabilities were +/- 22.5 degrees, which allowed ample room for correcting the difference between the angle of the Notch Plane and the potting cup. The pelvis was positioned in a way that would maximize the total stroke available. Because pelvis geometry is so variable, it was decided that the top edge of the seatbelt would always align with the most anterior, superior part of the Iliac Spine. This was to ensure consistent contact surface between pelvises of different shape.
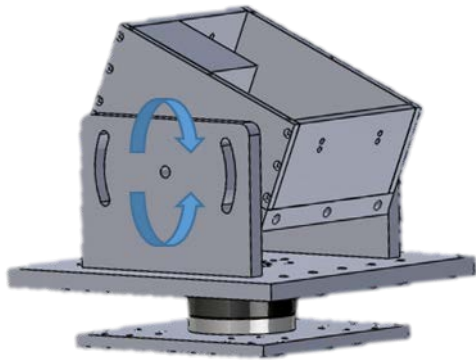
5.1.2-2 - Potting Cup Adjustment Used to Account for Potting Variability

5.1.3. PMHS and Fixture Instrumentation

A 6-axis load cell, along with two, single axis load cells, captured the reaction load delivered by the Instron to the pelvis. A string potentiometer measured the displacement of the belt fork tine loading device. In addition, a Micro-Measurements ® C2A-06-062WW-350 strain gauge rosette was affixed to the lateral surface of each iliac wing between the ASIS and AIIS landmarks. The resulting in-plane maximum and minimum principal strains and direction of principal strain were computed when possible, however the main function of the strain gauge was to identify fracture timing.

5.2. Results

5.2.1. Positioning Details

As stated previously, due to the complex geometry of the pelvis, a mechanical way of potting each pelvic wing was nearly impossible. A subjective, visual representation of "straight" for the wing needed to be used as the target to keep the pelvis loaded in as much compression as possible. For this reason, it was necessary to characterize how different each pelvis was potted.

Most importantly, the roll angle (or how much the wing was bent laterally or medially) needed to

be characterized to understand if certain pelvic wings may have been more susceptible to

bending failures. To do this, two coordinate systems were developed: one that was independent

of the potting material and one that was depending on the potting material.

Both coordinate systems had origins at the ASIS. Construction of the potting independent

coordinate system was done by connecting a line between the ASIS and AIIS, and a line between

the ASIS and a point 50 mm below the lowest point of the "Notch." This coordinate system was

anatomic based, meaning that it would measure the roll angle as a function of the pelvis

geometry relative to the threaded inserts. The lateral Y direction of the coordinate system was

found by the cross product of these two vectors.
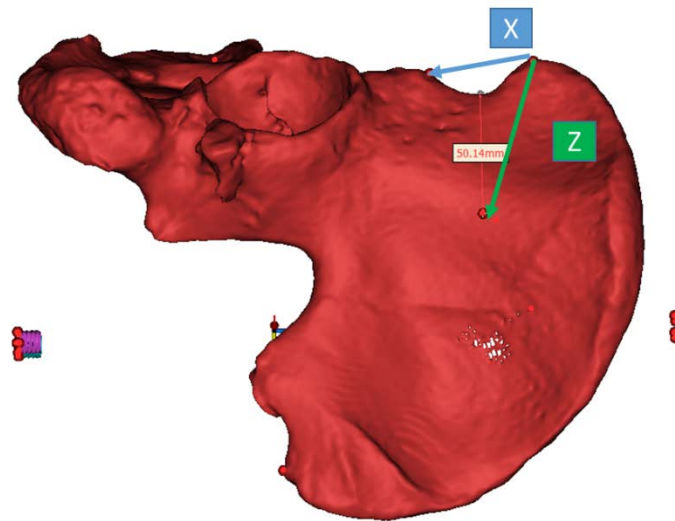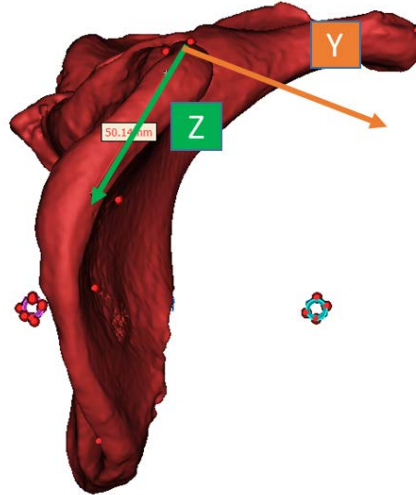
5.2.1-1 Potting Indpendent Coordinate System

The potting dependent coordinate system changed the Z vector to rely on the level of the potting interface. This point is not at a consistent distance relative to the ASIS, as it is completely dependent on the size of the pelvis, how much potting material was put in, and any possible tilt that was present in the potting material as it set. However, in an effort to characterize bending, it was necessary to look at a coordinate system that relied on the potting interface, as the bending would occur at the boundary of the rigid potting connection.
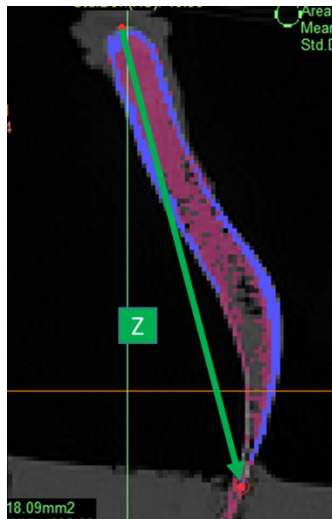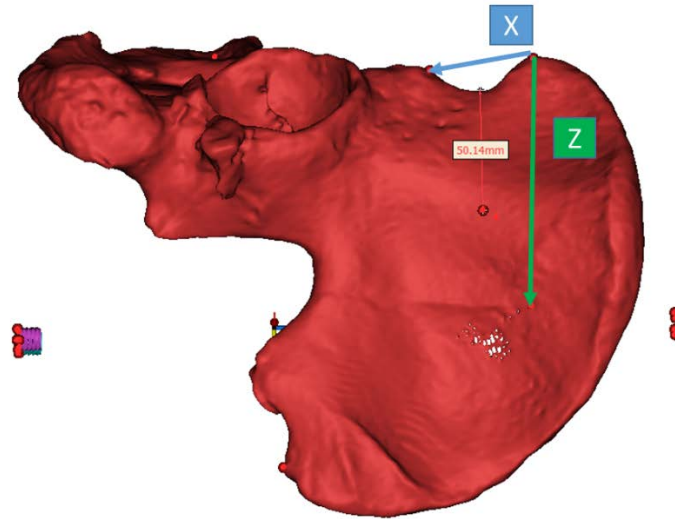
5.2.1-2 - Potting Dependent Coordinate System

In addition to the roll angle, the notch angle relative to the potting cup was calculated so that test day adjustments could be made to rotate the pelvis to the correct Notch to Belt angle. The evaluation of the roll angle and Notch to Belt angle can be seen in Table 5.2.1-1:

Table 5.2.1-1 Injurious Testing Positioning Details

Test Number	Test Condition (deg)	A: Notch Angle wrt Instron (deg)	B: Notch to Belt Angle (deg)	C: Roll Angle wrt Instron Potting Dependent CS (deg)	D: Roll Angle wrt Instron Potting Independent CS (deg)
714L	90	0.0	90.0	10.3	3.6
714R	90	0.0	90.0	-20.9	3.1
715L	90	0.0	90.0	19.3	5.3
715R	75	15.0	75.0	-24.8	-2.8
990L	90	0.0	90.0	6.1	-1.5
990R	75	14.9	75.1	-13.9	-4.9
713L	75	14.8	75.2	20.6	2.8
713R	90	0.0	90.0	-18.3	-5.4
716L	75	15.1	74.9	2.3	6.7
716R	90	0.0	90.0	-2.9	-10.8
792R	90	0.0	90.0	-10.7	7.7
1000R	90	-0.1	90.1	-7.3	-1.5
1000L	90	0.0	90.0	14.8	-2.3
998R	75	14.9	75.1	-11.6	1.0
792L	75	13.8	76.2	16.8	6.3
998L	90	-0.1	90.1	22.0	8.1
997L	75	14.8	75.2	10.4	3.2
999L	90	0.1	89.9	8.5	7.6
798L	75	14.9	75.1	11.8	2.4
997R	75	14.6	75.4	1.5	3.2
999R	75	15.0	75.0	3.8	-0.6
798R	75	14.9	75.1	-12.6	-8.7
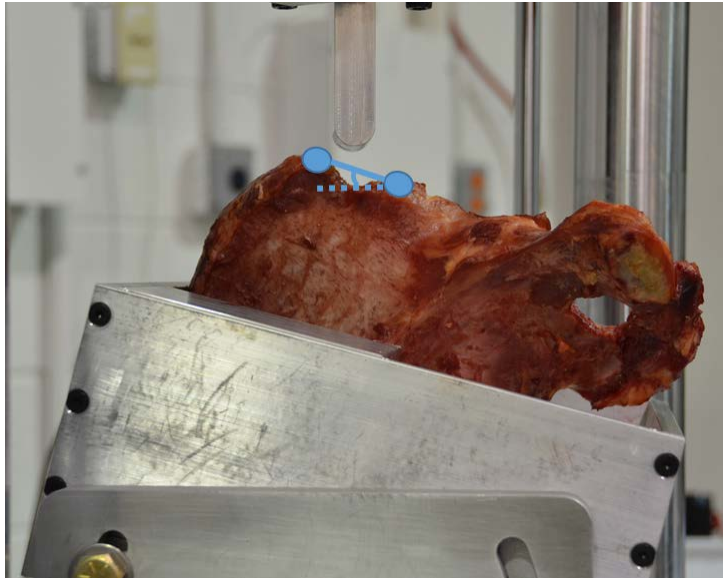
Figure 5.2.1-3 Notch Angle wrt Instron (Measurement A, Blue)
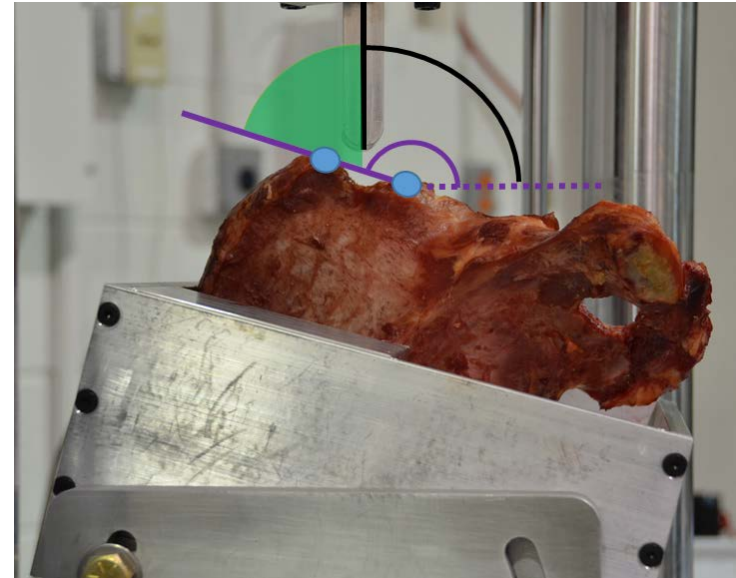
Figure 5.2.1-4 Notch to Belt Angle (Measurement B, Green)
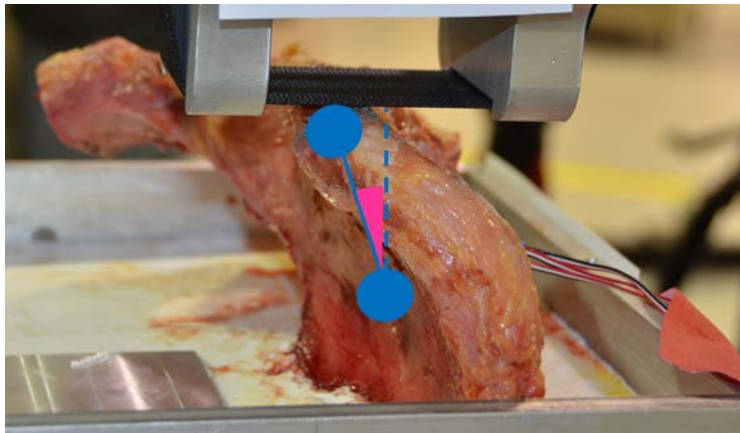
Figure 5.2.1-5 Potting Independent Roll Angle wrt Instron (Measurement C, Pink)
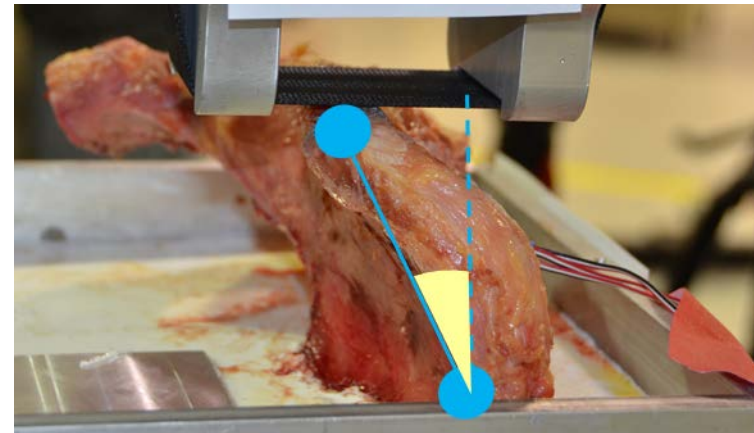
Figure 5.2.1-6 Potting Dependent Roll Angle wrt Instron (Measurement D, Yellow)

Table 5.2.1-2 - Positioning Data Summary

Notch to Belt Angle Target	Absolute Value Average Roll Angle Potting Independent CS	Standard Deviation Potting Independent CS	Absolute Value Average Roll Angle Potting Dependent CS	Standard Deviation Potting Dependent CS	Average Notch to Belt Angle	Standard Deviation Notch to Belt Angle
90	5.2	3.0	12.8	6.6	90.0	.1
75	3.9	2.5	11.8	7.3	75.2	.4

5.2.2. Evaluation of Boundary Conditions (Sensitivity Analysis)

5.2.2.1. Motivation

In an effort to check if the simplified loading environment on the Instron (Task 3) could be related to the Task 2 whole-body tests, a sensitivity analysis was completed on the same pelvis tested in Task 2 to check if the strain distributions could be matched. Exact magnitudes of strain were not intended to be matched, as this number is directly proportional to the amount of force applied. However, general trends in the amount of strain at each strain gauge, as well as the direction of strain, were the target metrics to be investigated. A summary can be found here:

1) In test D1531, the right side strain gauges measure the most strain (looking at minimum principal strain) at Right Iliac Bottom, then Right Iliac Extra, and then the last at Right Iliac Top. This pattern is different on the left side, where Left Iliac Top measured more minimum principal strain than Left Iliac Extra.

2) Between tests D1531 and D1532, the overall magnitude of strain measured at Left Iliac Extra increased, and the direction changed by around 5 degrees with a 13 degree change in load angle.

In the Task 2 tests, a mechanical force limiter was present to assist in preventing any overshoot of the system during repeated tests to ensure injury did not occur. With the simplified environment developed in Task 3, this just was not the case. For this reason, quasi-static tests were completed to avoid any overshoot in the Instron system that could cause injury.

In an effort to find the condition that most closely matched the strain data from Task 2, each pelvis wing was tested in five different conditions. Two conditions were the same Notch to Belt Angles (75 degrees and 90 degrees) tested in Task 2, which was predicted to be the two conditions that would result in the same strain distributions. However, to mimic the arc of the seatbelt in a whole body test, a condition that changed the lateral-to-medial loading direction was also checked to see whether adjustments in that direction would be necessary to better match the strain distribution (Figure 5.2.2.1 and Figures 5.2.1-3 through Figures 5.2.1-6).
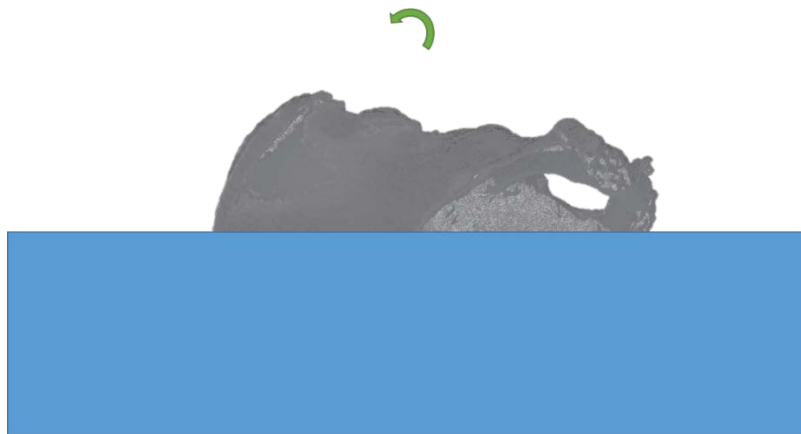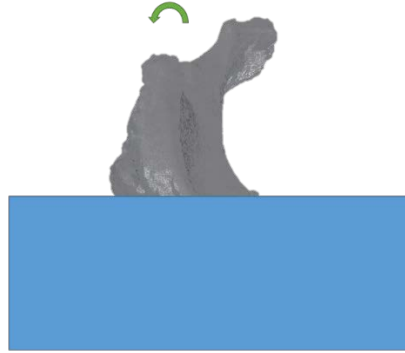
5.2.2.1-1 Notch Angle Adjustment Direction (top) and Roll Angle Adjustment (bottom)

Five, subinjurous tests were run on each side of the pelvis in an attempt to isolate the loading environment that most closely matched the strain distribution from the Task 2 tests. The same set-up procedure was followed, with the same displacement target for each test. Each specimen was preloaded to 10 N, and the test was run after that. Variable force levels were seen as a result of orientation changes.

5.2.2.2. Data Analysis

The goal of the subinjurious tests was to capture strain data in various configurations of load to pelvis orientation to compare to the data collected in Task 2. The thought behind this part of Task 3 was to understand if the potted pelvis loaded in the simplified environment could be completely representative to the way the pelvis is loaded in sled tests. If the sensitivity analysis would show that the strain data is similar, then the injury risk function developed in Task 3 would be representative of how the pelvis is loaded in a sled test environment.

Analysis of the strain data in Task 3 shows the following trends:

1) The overall magnitude of strain captured for similar peak loads is often times much lower than the Task 2 tests. This makes calculations of principal strain direction very difficult, because there is large error due to the noise in the signal.

2) In all tests, Right Iliac Bottom strain gauge had larger magnitude of strain than Right Iliac Extra, and both of these strain gauges had large magnitude of strain that Right Iliac Top. This trend is the same as that seen in the Task 2 tests.

3) Changing the Notch to Belt angle load direction by 15 degrees resulted in a 4 degree change in the direction of principal strain, which is similar to that of Task 2 where a 13 degree change in loading direction resulted in a 5 degree change in strain.

4) The condition that had the most similarities to the Task 2 test was the 90 degree Notch to Belt Angle test case.

However, this goal of showing that the loading environment in Task 2 is the same as Task 3 is not achieved. Data from these tests can be found in Appendix 8.6. The strain magnitude captured by the strain gauges is too small to rise above the noise band in the signal, making direction calculations have large variation. In addition, because of the low magnitude of strain, drawing confident conclusions about which strain gauge sees more strain is difficult on all of the left side tests that were completed. When the strain magnitudes are large enough to saturate the gauges enough to get rid of the noise in the signal, the directions of principal strain are not the same. This could be due to the fact that the strain gauges themselves had to be replaced after Task 2, and may have not been put in the exact same spot or orientation. In addition, it could be because the boundary conditions of a potted, denuded pelvis with no muscle attachments or other tissue is different than the boundary conditions of a posteriorly supported pelvis in a whole body test.

For this reason, the sensitivity analysis is inconclusive for showing whether the loading environment created in Task 3 is directly comparable to that from Task 2. As a result of this, the injury risk function developed in Task 3 cannot be immediately implemented into sled

tests. It must be assumed that the boundary conditions of the two loading environments are different. Further analysis must be done to work backwards from the tests completed in the rest of the report to the belt load applied to the pelvis in a sled test.

5.2.3. Injurious Testing

5.2.3.1. Results

Of the 22 pelvic wings tested, 19 sustained fractures. Of the 19 that sustained fracture, exact time and force of fracture was determined for 17 of them. This summarizes to a breakdown of 17 exact data points, 2 left censored data points, and 3 right censored data points. No fractures occurred at the level of the potting material; all fractures occurred (and started) at the interface between the belt webbing and the pelvis, or in the middle of the pelvic wing.

Data traces for the tests can be found in Appendix D, which includes force time histories, moment time histories, displacement time history, strain data, and fracture diagrams.

Table 5.2.3.1-1 Force and Time of Fracture (Main Event and First Event)

Subject	Force First Event (N)	Time First Event (ms)	Censoring	Indicator	Injury Type (Publication)
714L	1899	16	Exact	Dip in force; piece seen breaking off on lateral side of pelvis in video	Richardson 2020
714R	1906	18	Exact	HS video shows large fracture break event; large drop in force	Uriot 2015
715L	6878	41	Left	No clear indicator of event	Moreau 2021 (Test D1527)
715R	8242	39	Right	No Fracture	N/A
990L	5085	24	Exact	Drop in force, fracture caught in HS video	Richardson 2020
990R	5356	22	Exact	Change in slope on force trace, small bits of bone seen in HS video near AIIS	Richardson 2020
713L	2608	19	Exact	Change in slope of force; small piece seen giving way closer to AIIS in video	Richardson 2020
713R	2890	15	Exact	Dip in force; small piece seen giving way closer to AIIS in video	Uriot 2015
716L	8430	35	Exact	Drop in force; HS video shows small event occurring	Moreau 2021 (Test D1527)
716R	8895	40	Exact	Drops in force and strain; HS video shows large movement of wing	Moreau 2021 (Test D1527)
792L	6985	35	Exact	Drop in force; HS video shows pieces of bone flying out after this time	Moreau 2021 (Test D1527)
792R	3350	18	Exact	Change in slope of force; piece of bone moving on back side of belt in HS video closer to AIIS	Uriot 2015
798L	2476	22	Exact	Drop in force followed by visible HS video event	Richardson 2020
798R	8034	38	Left	No clear indicator of event	Moreau 2021 (Test D1527)
997L	2886	28	Exact	Only one force peak; aligns with strain gauge failure and visible event in video	Richardson 2020
997R	2717	26	Exact	Strain gauge rail, small force drop, fracture initiates on medial side of pelvis in HS video	Richardson 2020
998L	5266	26	Exact	Strain gauge rail; large drop in force; HS video sees large fracture	Richardson 2020
998R	5851	27	Exact	Drop in force; large fracture seen in HS video; strain gauge failure	Richardson 2020
999L	1463	20	Exact	Plateau in force followed by small piece coming off lateral side of pelvis in HS video	Richardson 2020
999R	1487	20	Exact	Blip in force trace followed by pieces coming off medial side of pelvis in HS video	Richardson 2020
1000L	9570	41	Right	No Fracture	N/A
1000R	8431	40	Right	No Fracture	N/A

The fractures that occurred in Task 3 can be broken down into three categories.

The first type of fracture that occurred can be described as a large break where the top

half of the pelvic wing breaks off from the rest of the bone. It appeared like the

superior piece of the wing bent and "snapped" off from the bone. This type of fracture

occurred in tests 714R, 713R, and 792R. These fractures were not the same seen in

Richardson et al 2020, but have been documented in Uriot et al 2015.

5.2.3.1-1 Fracture Diagram of Test 713R ("Snapping" Fracture). Blue boxes indicate the top and bottom edge of the seatbelt webbing

In tests 715L, 716L, 716R, 792L, and 798R, only small, localized

fractures between the ASIS and AIIS were documented. These fractures were

similar in shape, location, and size to the fracture documented from Task 2, test

D1527, between the ASIS and AIIS. Again, these fractures were different than the

fractures that occurred in Richardson et al 2020, but shows the large variation in

the types of fractures that occur in this region. For the most part, the specimens

that sustained this style of fracture required larger forces to fracture than the other specimens, indicating that they were stronger pelvises to begin with. For the most part, these fractures were difficult to determine from High Speed Video, and required post test review of the pelvis to determine whether fracture actually occurred or not. Two of these tests were the left censored data points, where exact time and force of fracture was unable to be determined.
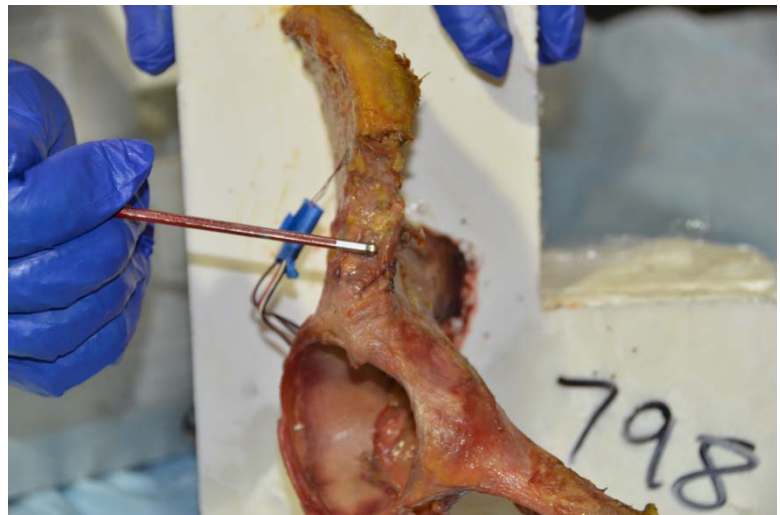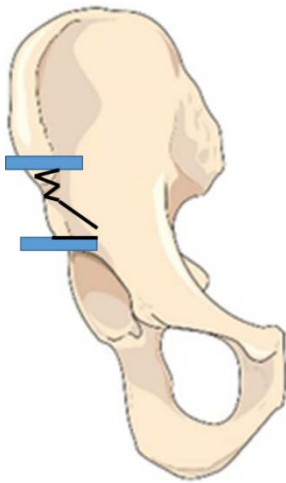
5.2.3.1-2 Fracture Diagram of 798R ("Localized" Fracture.) Blue boxes indicate the top and bottom edge of the seatbelt webbing

All other tests where pelvis fractured sustained the "crushing" fracture between the ASIS and AIIS that were noted in Richardson et al 2020 (n = 11). These fractures were similar in shape, size, and severity to the fracture documented in Task 2, test D1525. These were the targeted style of fracture, and were successfully replicated over 50% of the time.
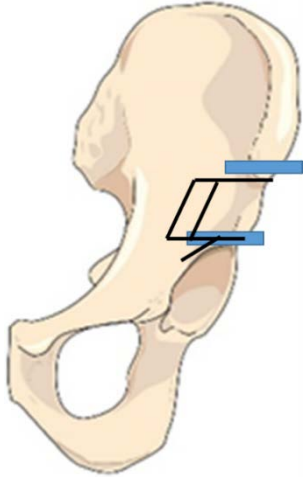
5.2.3.1-3 Fracture Diagram of 997L ("Crushing" Fracture.) Blue boxes indicate the top and bottom edge of the seatbelt webbing

5.3. Limitations

The largest limitation of this testing was that the environment created in Task 2 was unable to be directly connected to the environment in Task 3. Potting the pelvic wing was too much of a different boundary condition to conclude that the way the pelvis was loaded in each environment was the same. This means that the forces collected in Task 3 cannot be directly connected to the lap belt load data generated in Task 2. Further work will need to be done to connect the lap belt force metric to the force measured at the anterior pelvis. Human body models would be the best method to do so. It has been shown using the THUMS SAFER model that the force measured at the ASIS was around 50% of that measured at the lap belt (Mroz 2020). However, further investigation of consistency between HBMs will need to be completed to validate such statement. The injury risk function developed in the next chapter of the thesis will be based on force measured at the pelvis; however, in a vehicle setting, the real metric of interest would be the lap belt force applied to the pelvis. Some ATDs (THOR M-50 and HIII small female) have implanted ASIS load cells that can read

data where the IRF could be applied, but alternative load paths between the ATD and a human may not be the same. Unpublished research completed with the THOR dummy in the Task 2 environment showed that the ASIS load never surpassed 80% of the belt load, which is a much larger proportion of the belt load than the THUMS SAFER HBM reported in Mroz 2020. Thus, while this is a first step in understanding the fracture tolerance of the pelvis, it will require further development to get into a useable form for the field.

The Instron bi-axial loading device provided some flexibility in positioning for the pelvic wings. However, its stroke limit often limited the total displacement that the head could go, thus limiting the force applied to the pelvis. A lower profile potting cup clamp, or an increased range of the Instron, would have solved this issue. Along the same line, the metal belt fork tines were sometimes not wide enough to avoid hitting the pelvis at certain displacements, limiting the total displacement that could be achieved. However, this could not be extended because the belt would lose tension, and thus cause issues in creating enough force to fracture the pelvis. No belt tension gauge could be routed between the belt fork tines to capture the belt load over time; had this data been available, it may have been more useful in developing a belt load based injury risk function.

5.4. Summary and Conclusions

A test environment was developed to load isolated, denuded pelvic wings with a seat belt until failure occurred. This environment was created to replicate the two loading conditions tested in the subinjurious tests of Task 2, which were presented in Chapter 3. Evaluations of the strain data from a pelvis tested in the Task 2 and Task 3 environments were completed to understand if the two loading environments were similar. Twenty-two pelvic wings from

eleven pelvises were tested to failure. Of the twenty-two pelvises tested, nineteen fractured. I was able to determine the exact force of fracture in seventeen of those nineteen. CT analysis allowed for rotation of a potted pelvic wing to ensure loading directions matched the targets determined in Task 1. The tolerance data generated in this chapter will be used to create in injury risk function in Chapter 6.

The conclusions drawn from this chapter are:

- Potting the pelvis in Task 3 loaded the isolated pelvic wing differently than a supported, whole pelvis in a whole-body PMHS.

- Despite that they could not be directly related, the same lap-belt-to-pelvis loading angles tested in Task 2 were applied to 20 pelvic wings in the Task 3 environment. Of the 20 wings tested, 17 sustained fracture. All fractures occurred in the area of interest; none occurred at the level of the potting.

- Three, distinct injury patterns were observed. These injuries were representative of the injuries seen in Richardson et al 2020, Uriot et al 2015, and of the injury seen in test D1527 of Task 2.

- I conclude that the injury tolerance data collected in this task is representative of lap belt induced injuries and accurately characterizes the injury tolerance of the iliac wing under frontal loading.

6.   Task 4: Injury Risk Function Development

Injury tolerance data created in the previous chapter will be statistically analyzed in this chapter to develop an injury risk function for anterior loading of the pelvis. First, a new methodology for measuring bone quality from CT scans will be presented. Then, discussion of the statistical analysis completed will be presented to determine the best-fit injury risk function. At the end of this chapter, the first injury risk function for the anterior portion of the pelvis under frontal loading will be created. Limitations and next steps will also be provided at the end of this chapter.

6.1. Measuring Bone Density

In this study, not all specimens had a dual-energy x-ray absorptiometry (DXA) scan taken. A DXA scan is used to measure bone density, and is often used to identify risk of osteoporosis through analysis of the intensity of the x-rays collected in a scan. The scan uses various landmarks (most often, the femoral heads, femoral neck, and lumbar spine) to calculate scores of certain body regions, and then give an overall measure of the quality of the bone in the body. However, the scan can be influenced by a variety of things. For instance, calcified growths in body regions can artificially increase the score. In scanning PMHS, it is usually impossible to move the specimen into the orientation that a live human can be positioned at to get the most accurate reading. In addition, the scan is unable to be performed on denuded specimens because it relies on there being tissue present.

For this study, it was necessary to calculate bone quality in a different way in order to have a comparable metric across the population. Some specimens had DXA scans completed in similar fashion, while others only had one measurement available. Four specimens came pre-denuded, which prevented DXA from being complete (specimens 997-1000). Specimen

1000 was the only subject to have both wings withstand fracture, and sustained between 8.5-9.5 kN of force. In addition, some specimens fractured below 2 kN of force. So, having something consistent to measure bone quality among the specimens was imperative in understanding if this phenomenon was driven by bone quality.

To achieve a consistent measurement procedure, an electron density phantom (EDP) was used in each pre-test CT scan. An EDP (pictured below) is a measurement device used to provide landmark intensities of Hounsfield units (HU). Hounsfield units are the measure of the amount of scatter given off by a pixel in a CT scan. The higher the scatter, the higher the measured HU, which leads to a higher BD measurement. In an EDP, various tubes of known BD are placed in a known configuration. Then, in post processing of CT scans, measurements of the HU in a given area can be taken. Since the BD of that section is known, a linear fit between these points can be created, and a BD measurement of any HU point along that line can be found through extrapolation. However, CT scanners are recalibrated almost every day. So, slight variations in the measured HU for the same BD landmark can occur. For this study, every scan taken had the EDP present in the scan so that all points could be aggregated into one, linear fit model and account for this variation.
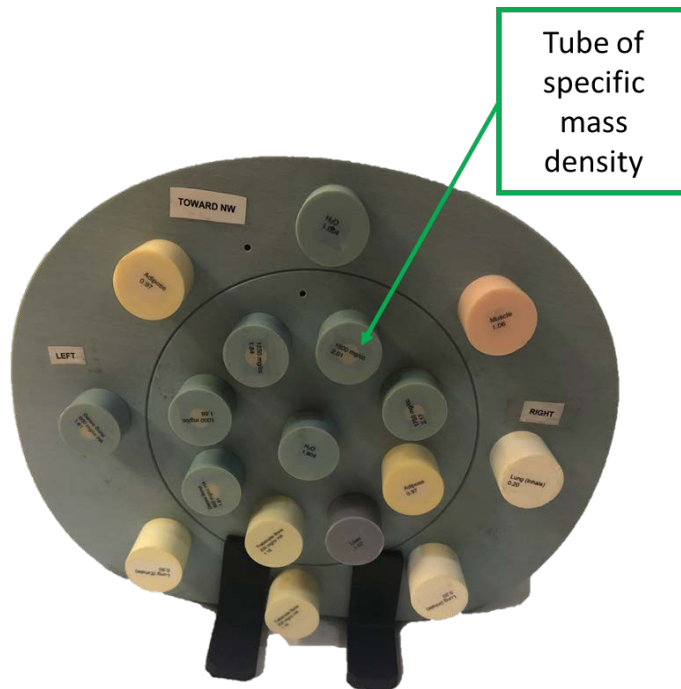
6.1-1 Electron Density Phantom
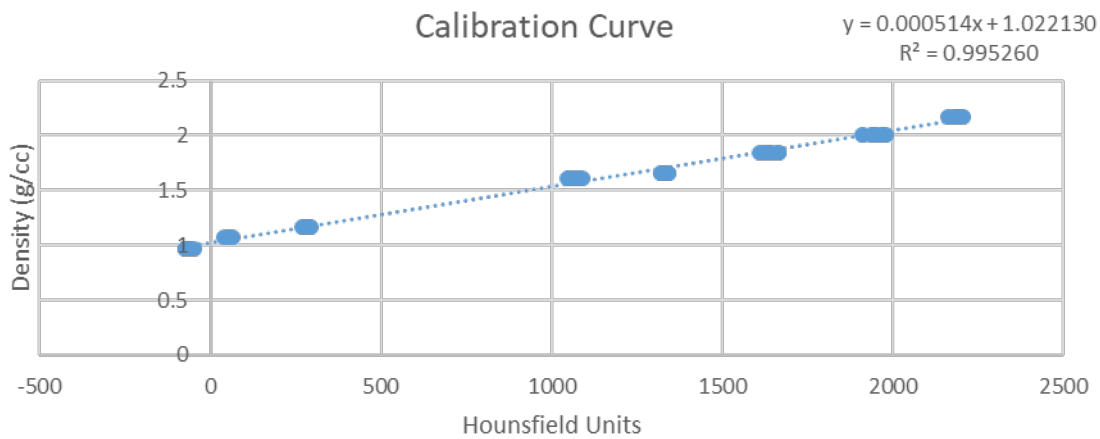
6.1-2 - BD Linear Extrapolation Function

Using MIMICS Research 21.0, CT objects of specified HU can be created. Using pre-defined HU ranges, objects of "Strong Bone" (HU of 662-1988) and "Weak Bone" (HU of 148-661) can be generated for each pelvis. Then, from those objects, the average value HU can be found, as well as the number of pixels in each object. From here, the ratio of strong

bone and weak bone can be found by adding the number of pixels in each object, and

dividing each object pixel count by the total pixel count:

$$Ratio \ of \ Bone \ Type = \frac{Number \ of \ Pixels \ in \ Object}{Number \ of \ Pixels \ in \ Strong \ Bone \ Object + Number \ of \ Pixels \ in \ Weak \ Bone \ Object}$$

Table 6.1-1 - Hounsfield Unit Measurements from Mimics

Subject	Cortical Ave HU	Cortical Pixels	Trabecular Ave HU	Trabecular Pixels	Ratio: Strong to all	Ratio: Weak to all
714L	1075	168315	316	410125	0.29	0.71
714R	1080	132636	315	337102	0.28	0.72
715L	1149	219777	328	396421	0.36	0.64
715R	1157	185577	324	349879	0.35	0.65
990L	1131	189532	332	310017	0.38	0.62
990R	1150	224267	331	346696	0.39	0.61
713L	1107	113170	315	276862	0.29	0.71
713R	1116	150602	319	372348	0.29	0.71
716L	1154	222071	321	324565	0.41	0.59
716R	1152	205499	324	307044	0.40	0.60
792L	1181	240584	344	281279	0.46	0.54
792R	1187	277853	341	357612	0.44	0.56
998L	1088	185108	342	270794	0.41	0.59
998R	1079	149120	348	200678	0.43	0.57
1000L	1163	202601	352	293221	0.41	0.59
1000R	1169	209763	350	291640	0.42	0.58
798L	1174	254355	339	318245	0.44	0.56
798R	1168	254763	339	310737	0.45	0.55
997L	983	54805	301	485937	0.10	0.90
997R	986	50908	300	472345	0.10	0.90
999L	1118	109861	336	205735	0.35	0.65
999R	1115	117691	336	219303	0.35	0.65

In addition, the average HU for each object can correlate to a BD measurement using the

function found in Figure 6.1-2. So, an average BD for the strong bone and an average BD for the

weak bone can be calculated. Using the ratios determined by the number of pixels, a weighted

BD value can be measured by:

$$Weighted\ BD = Ratio_{Trabecular} * BD_{Trabecular} + Ratio_{Cortical} * BD_{Cortical}$$

Table 6.1-2 - BD Measurements from Mimics

Subject	Ratio: Strong to all	Ratio: Weak to all	BD (Cortical)	BD (Trabecular)	BD (Weighted Average)
714L	0.29	0.71	1.57	1.18	1.30
714R	0.28	0.72	1.58	1.18	1.30
715L	0.36	0.64	1.61	1.19	1.34
715R	0.35	0.65	1.62	1.19	1.34
990L	0.38	0.62	1.60	1.19	1.35
990R	0.39	0.61	1.61	1.19	1.36
713L	0.29	0.71	1.59	1.18	1.30
713R	0.29	0.71	1.60	1.19	1.30
716L	0.41	0.59	1.62	1.19	1.36
716R	0.40	0.60	1.61	1.19	1.36
792L	0.46	0.54	1.63	1.20	1.40
792R	0.44	0.56	1.63	1.20	1.39
998L	0.41	0.59	1.58	1.20	1.35
998R	0.43	0.57	1.58	1.20	1.36
1000L	0.41	0.59	1.62	1.20	1.37
1000R	0.42	0.58	1.62	1.20	1.38
798L	0.44	0.56	1.63	1.20	1.39
798R	0.45	0.55	1.62	1.20	1.39
997L	0.10	0.90	1.53	1.18	1.21
997R	0.10	0.90	1.53	1.18	1.21
999L	0.35	0.65	1.60	1.19	1.33
999R	0.35	0.65	1.60	1.19	1.33

While this BD measurement may not be clinically accurate to what would be found in DXA scan, it gives a comparable way to have a measure of BD among the pelvises tested in this study. It allows for a comparison of the pelvises in the tested population, allowing for general conclusions about "stronger" pelvises and "weaker" pelvises based on the BD calculated from the HU intensities of the CT objects. A table of values for the BD from this population is provided below (all in g/cc):

Minimum	Q1	Mean	Median	Q3	Max
1.211	1.312	1.337	1.351	1.370	1.397

6.2. Function Development

Through the analysis of injury timing, an injury risk function was developed as force as the predictor variable and fracture as the outcome. A survival analysis of the data in the table in section 5.2.3.1 was completed, using a Weibull distribution. It is often used in the analysis of biomechanical data as it is often used in reliability analysis (Kent 2004, McMurry 2015). Statistical analysis was done using R version 3.6.2, but all plotting was done in MATLAB.

As previously stated, the form of the function created was a Weibull distribution. Assuming two variables to denote subject (i=1,2,…,11) and side (s=1,2), the function becomes:

$$Equation\ 1: Force_{is} \sim_{iid} Weibull(\kappa, \lambda)$$

The cumulative distribution function of each Weibull distribution was first formed with no covariates to understand the general trend and shape of the function. After that, two covariates to the function were considered. The first covariate that was included was the independent variable of loading angle. In Task 1 of this test series, it was determined that a 13 degree change in load angle created a 5 degree change in the principal strain. So, in this test series, two load angles were tested to determine if this made a difference on the fracture tolerance of the pelvis. This should be included in the function in order to tell whether it was a significant factor or not. Through post analysis of the data, it was

determined that there was a large correlation between the bone density measurements and the fracture tolerance of the pelvis. For this reason, UVA thought it to be wise to incorporate this effect into a separate model to understand if this had a large effect on the injury risk prediction of the function. Scatterplots of the data to show correlation can be found in Appendix 8.6.

$$Equation\ 2: Weibull\ Distribution\ CDF = 1 - e^{-(x)^{\kappa}}$$

$$Equation\ 3: Shape\ (\kappa) = 1/e^{Log(Scale)}$$
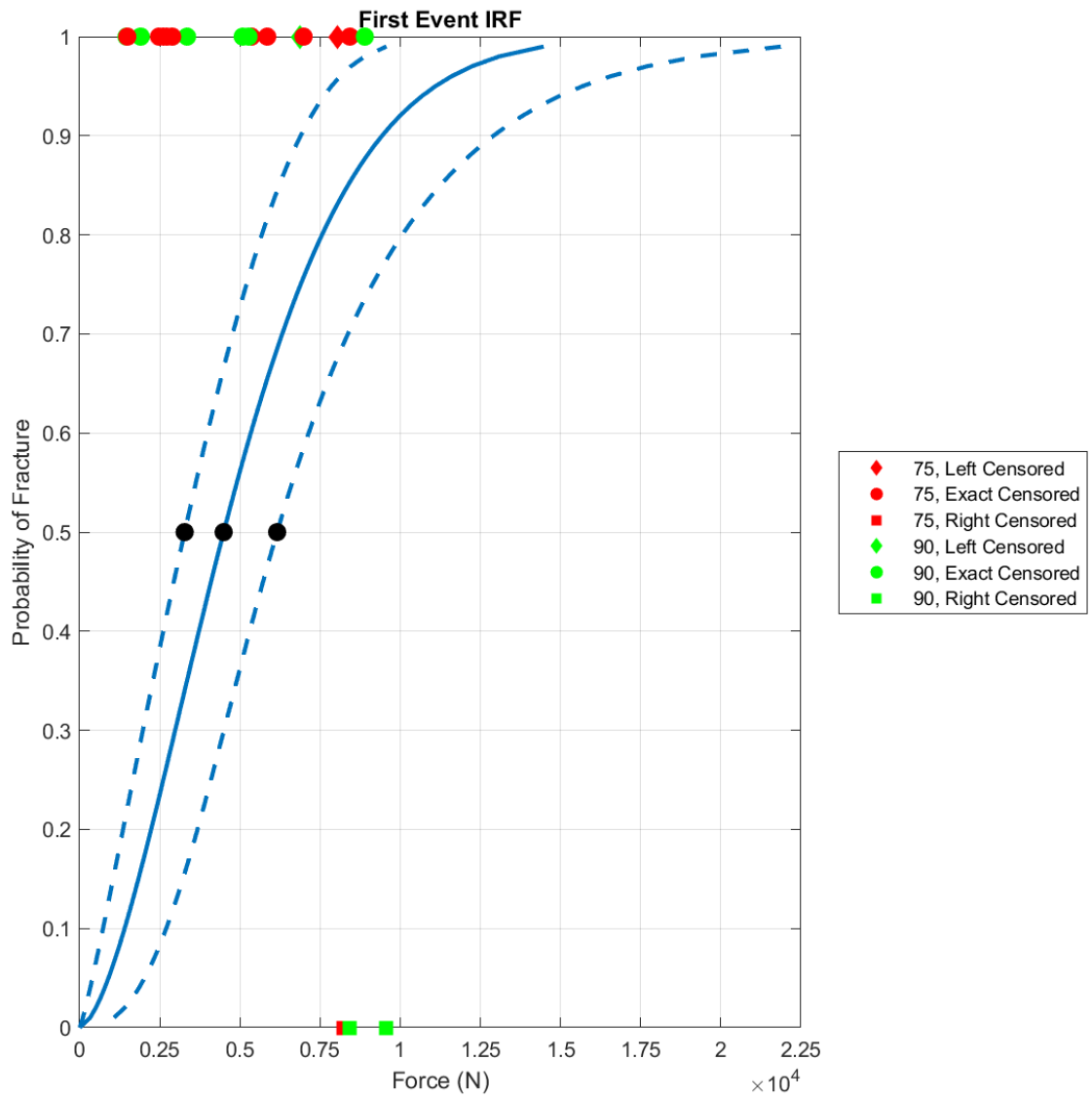
6.2-1 - First Event Injury Risk Function, No Covariates

50% Risk (N)	Upper Confidence Interval 50% Risk (N)	Lower Confidence Interval 50% Risk (N)
4492	6160	3276
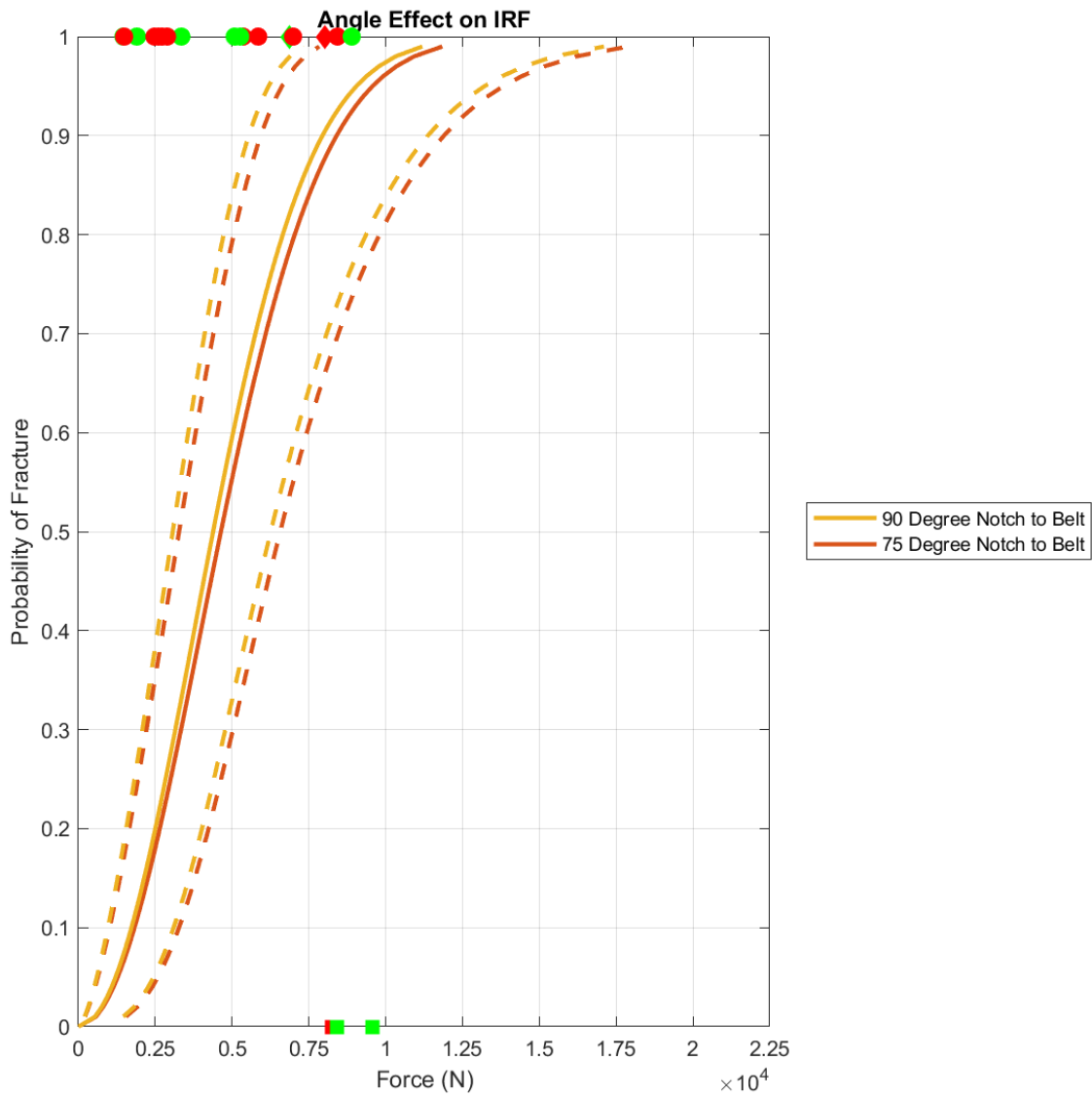
6.2-2 – Two Covariate Injury Risk Functions to illustrate the Load Direction Effect on Injury Tolerance. The bone density term was set to the mean value of the population. Illustration above shows that angle did not have a significant effect on injury tolerance.

Angle Parameter (75 Degree Notch to Belt Angle)	Upper Confidence Interval	Lower Confidence Interval
.0565	-.434	.547
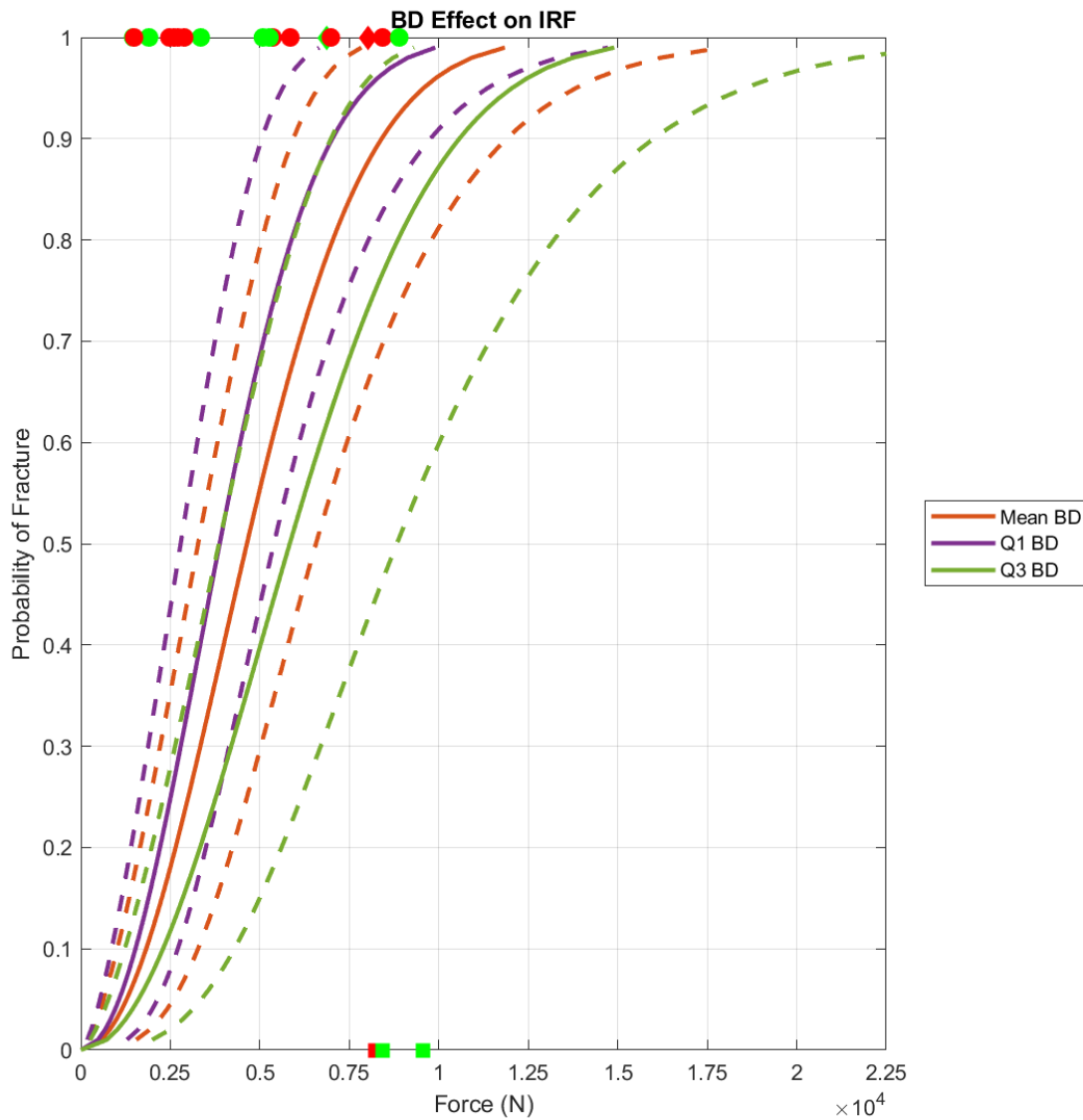
6.2-3 – Two Covariate Injury Risk Functions to illustrate the BD Effect on Injury Tolerance. The angle term was set to 75 degree Notch to Belt Angle. Illustration shows large variation in injury tolerance dependent on bone density.

BD Parameter	Upper Confidence Interval	Lower Confidence Interval
7.0475	11.334	2.761

6.2.1. Discussion of Model Choice

Based on the plots in section 6.2, it is clear that BD has a large effect on the prediction of injury tolerance, while angle does not. However, at this point, is unclear which model is "best" to fit the data. To check this, a corrected, Second-order Akaike Information Criterion (AICc) test was run to account for the small sample size in this study. The models checked were the model without any covariates, a model with a covariate for angle, a model with a single covariate for BD, and a model with two covariates for angle and BD (Table 6.2.1-1). A lower value of AICc means a better fit to the data. All calculations were completed in R version 3.6.2. Table 6.2.1-2 shows the model coefficients and formulations based on the analysis.

Table 6.2.1-1 Corrected AICc results

Model Name	Model Input	AICc
Base	$x = Force * e^{-\beta_{intercept}}$	328.6
BD	$x = Force * e^{-(\beta_{intercept}+(\beta_{BD}*BD))}$	324.5
Angle	$x = Force * e^{-(\beta_{intercept}+(\beta_{Angle}*Angle))}$	331.1
Angle and BD	$x = Force * e^{-(\beta_{intercept}+(\beta_{BD}*BD)+(\beta_{Angle}*Angle))}$	327.5

Table 6.2.1-2 Models and Model Coefficients

Model Name	Shape (κ)	$\beta_{intercept}$	β_{BD}	β_{Angle}	Equation
Base	1.6193	8.637	N/A	N/A	$P(Fracture) = 1 - e^{-(Force*\,e^{-(8.637)})^{1.6193}}$
BD	2.0158	-0.570	6.854	N/A	$P(Fracture) = 1 - e^{-(Force*\,e^{-(-.570+6.854*BD)})^{2.0158}}$
Angle	1.6274	8.696	N/A	-.117	$P(Fracture) = 1$ $- e^{-(Force*\,e^{-(8.696-.117*ANGLE)})^{1.6274}}$
Angle and BD	2.02	-0.8585	7.0475	0.0565	$P(Fracture)$ $= 1 - e^{-(Force*\,e^{-(-.8585+7.0475*BD+.0565*ANGLE)})^{2.02}}$

The tables above suggest that the model that best fits the data would be the model where BD is the only covariate. This model has the lowest AICc value, using the survival analysis completed. However, it is important to note that the actual BD value that would have to go into the function would need to follow the calculation measurement outlined in Section 6.1. It is still unclear how the BD measurements created from the methodology outlined in Section 6.1 relate and/or compare to BD measurements from a DXA scan, or any other testing metric. For the use of this IRF, statistics from the population tested are provided in Section 6.1 to provide the range of BD values determined in this study. It is incorrect to use any other BD measurement as an input into the injury risk function.

In addition, a subset of the data was put through a matched pair t-test to show the lack of significance that angle had on the injury tolerance of the pelvis. The data from this test can be found in Table 6.2.1-1, and shows that angle is not significant.

Table 6.2.1-3 Matched Pair T-Test results for pelvises where each side was tested at a different Notch to Belt Angle*

90 Degree Notch to Belt Angle Side	Force First Event (N)	75 Degree Notch to Belt Angle Side	Force First Event (N)	Difference First Event (N)
990L	5085	990R	5356	271
713R	2890	713L	2608	282
716R	8895	716L	8430	465
792R	3350	792L	6985	3635
998L	5266	998R	5851	585
999L	1463	999R	1487	24

Average Difference (N)	Standard Deviation (N)	Paired T-Test P Value
877	1365	.36

*Note: Does not include subject 715 (Left and Right) because both sides were censored data points.
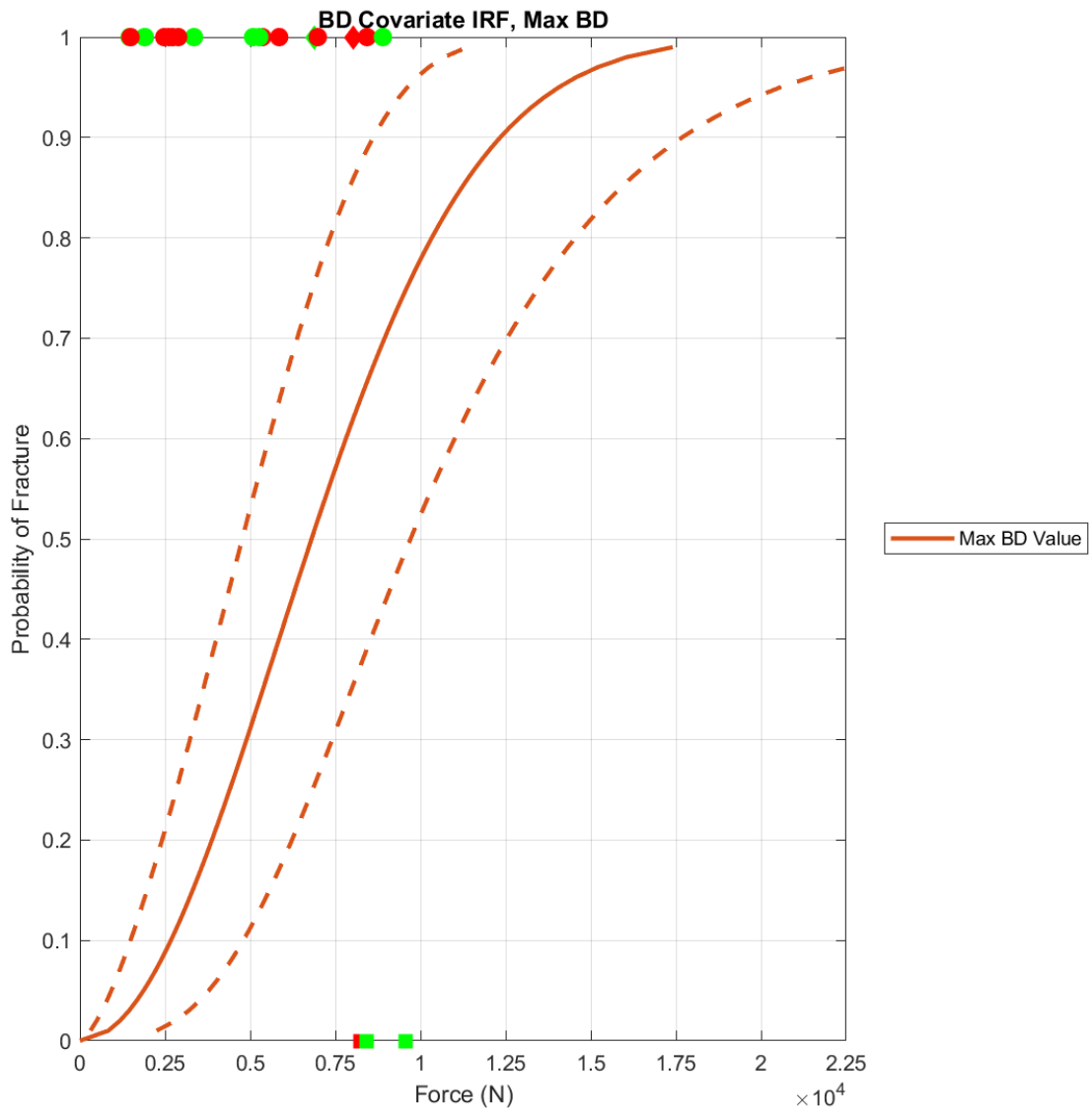
6.2.1-1 IRF developed using the maximum BD measurement from the population. BD is the only covariate in the model

Force at 50% Probability of Injury (N)	Upper Confidence Interval	Lower Confidence Interval
6801	9707	4765
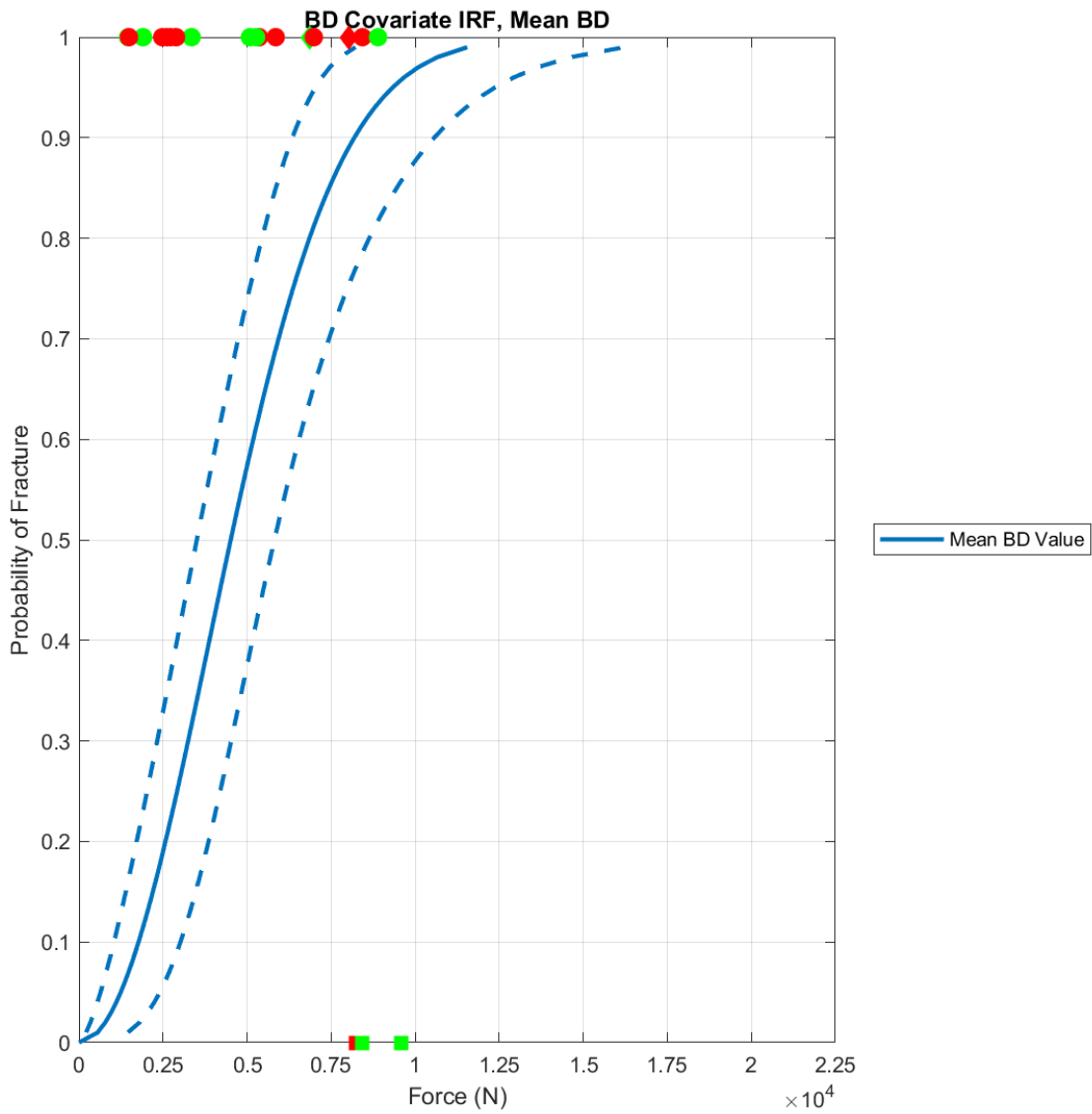
6.2.1-2 - IRF developed using the mean BD measurement from the population. BD is the only covariate in the model

Force at 50% Probability of Injury (N)	Upper Confidence Interval	Lower Confidence Interval
4512	5812	3503
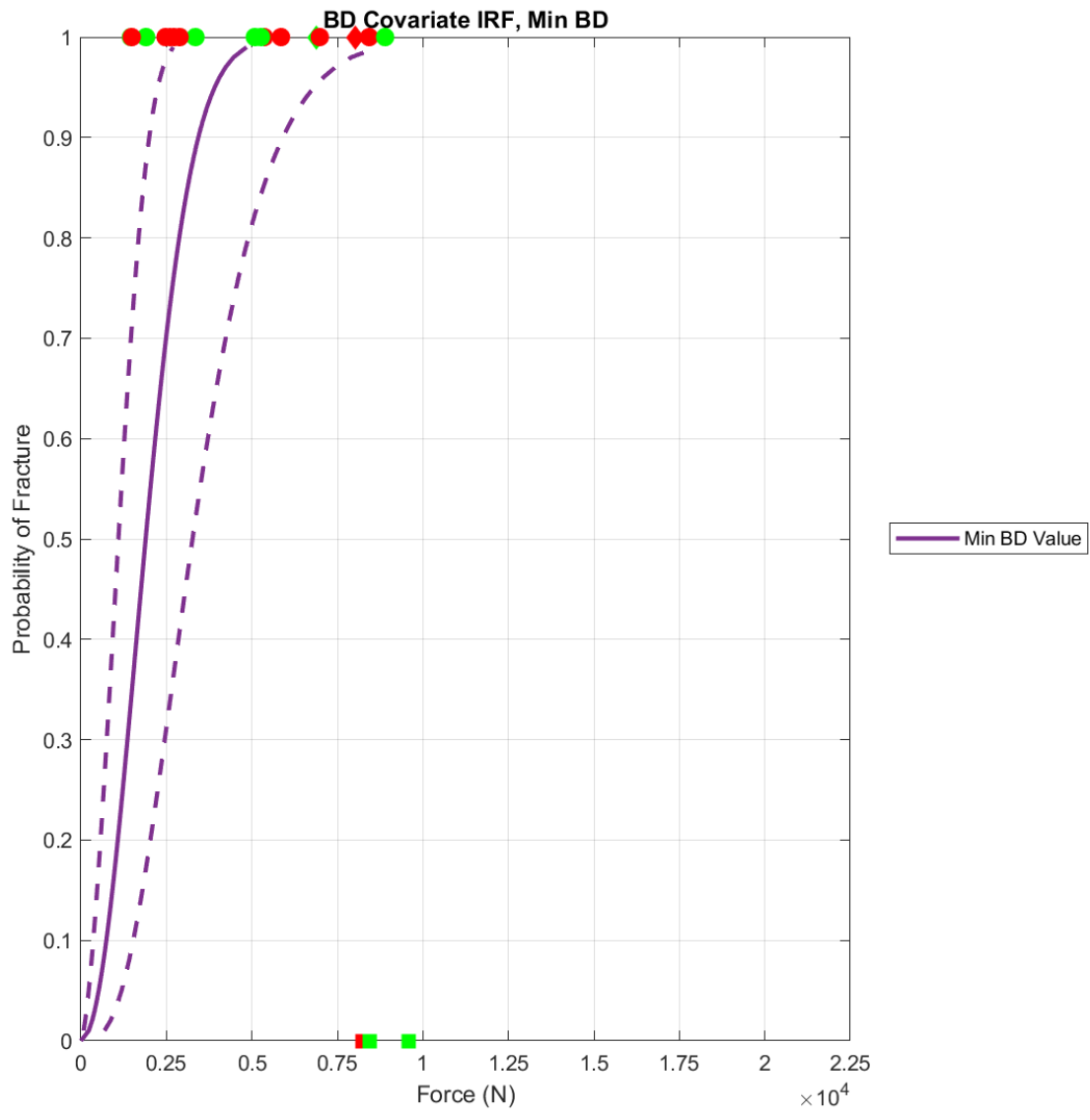
6.2.1-3 - IRF developed using the minimum BD measurement from the population. BD is the only covariate in the model

Force at 50% Probability of Injury (N)	Upper Confidence Interval	Lower Confidence Interval
1892	3264	1097

6.3. Limitations

The injury risk function developed in Task 4 is a force-at-pelvis injury risk function. This means that further work must be completed to relate the force-at-pelvis to the force-at-lap belt, which is a more easily measurable metric in a sled test. In addition, the BD measurements created as a part of Task 4 have yet to be related to any other BD measurement determined from literature or a DXA scan.

Analysis of the data using a different statistical formulation could be done. The analysis completed in this study followed many of the steps laid out in McMurry et al 2015, which describes in detail an perform survival analysis and construct injury risk curves on datasets with small sample sizes. However, post-test analysis of the data clearly shows that there is a large correlation between the left and right sides of the same subject. In Figure 6.3-1, it can be seen that pelvic wings from the same subject generally fracture at similar forces. This can be determined by the distance between the dots for the same subject. Thus, the subject also has an effect on the injury tolerance. Some of the subject effect may be accounted for by accounting for BD, but early analysis of other statistical models (such as frailty models) shows that the subject effect may take away some of the statistical significance of BD. It's possible that the "classic" Weibull survival analysis could be improved upon if other statistical processes are used, such as switching to a Bayesian statistical method.
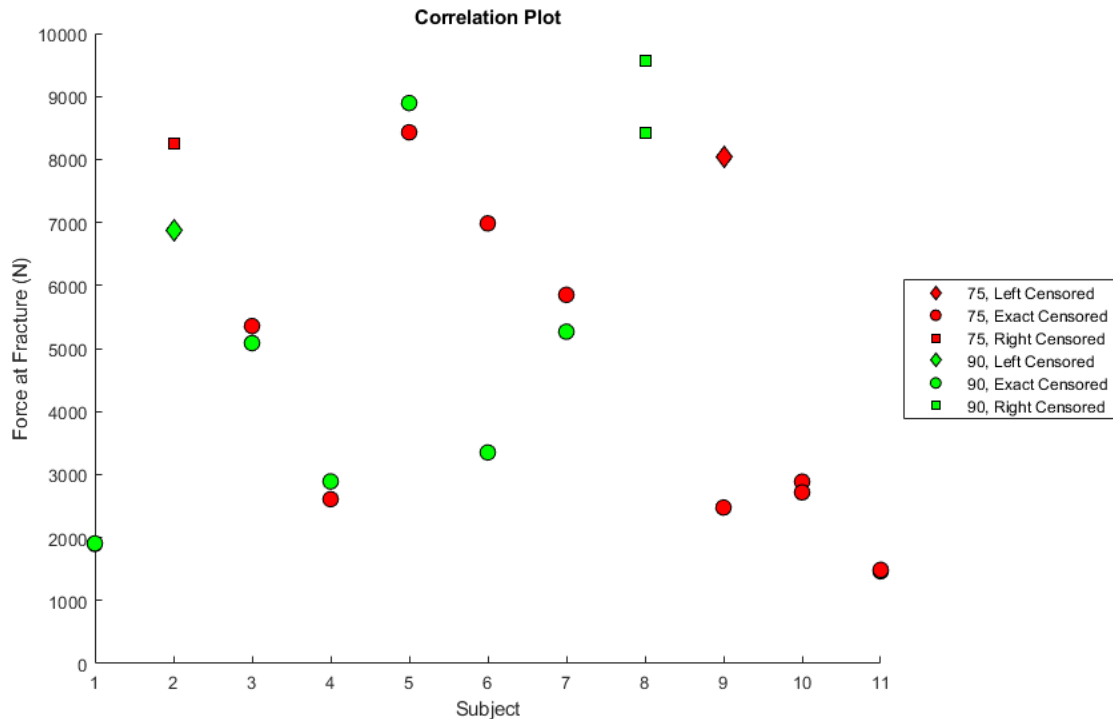
6.3-1 Correlation plot of force at fracture for each subject. In plot, the measured force at fracture (or peak force for those that did not fracture) is plotted for the left and right sides of the same subject. It clearly shows that left and right sides are correlated to each other and, generally, not random.

6.4. Summary and Conclusions

Task 4 outlines the process completed to develop an injury risk function after completed a survival analysis using a Weibull distribution which is a common statistical analysis completed in the injury biomechanics field (McMurry 2015, Kent 2004). Through this analysis, a 50% probability of injury translates to 4492 N of force (confidence interval of 3276, 6160) without including any covariates. Angle of applied load (ie, Notch to Belt Angle) did not have a significant effect on the injury tolerance of the pelvis (Figure 6.2-2). Bone density was calculated by creating a calibration curve from an electron density phantom and the use of thresholded pelvis objects of specific HU ranges determined to be

116

strong bone (cortical) and weak bone (trabecular). A weighted BD value was created by multiplying the volumetric ratio of bone strength type by the BD value based on the average HU of that bone type. If included as a covariate in the model, weighted BD shows to be a significant predictor of failure tolerance of the pelvis. A larger BD value (thus indicating a stronger bone quality) correlated to a higher force at 50% fracture. Figures 6.2.1-1 – 6.2.1-3 show the variation in the predicted injury values based on BD values from the tested population. The force values at 50% probability of injury ranges from 1892 N for the minimum BD values, 5812 N for the mean BD value, and 6801 N for the maximum BD value.

7. Conclusions, Contributions, and Future Work

7.1. Summary of Work

The overall goal of this thesis was to recreate lap belt induced pelvis fractures and develop a prediction tool for those injuries. I introduced the motivation for the research in Chapter 1 as a potential future problem with new, HAV interiors, as well as postulating the necessary steps to best understand how these fractures occur. I provided the relevant background information for this work in Chapter 2, with a large focus on reviewing previous sled tests studies where pelvis fractures occurred. In addition, relevant computational studies were summarized to clarify the role of the knee bolster as a restraint system component; not only would lap belt forces increase as a result of knee bolster removal, but the occurrence of submarining could also increase. A query of the CIREN database showed that 14 cases of frontal impacts where iliac wing fractures were sourced to lap belt loading, meaning this injury has been shown to currently occur in the field. I developed a new way of describing pelvis orientation relative to the world and pelvis orientation relative to the lap belt, which helped to develop targets to replicate from Richardson et al 2020 in Chapter 3. I described the development of a test fixture that can isolate a mid-sled test posture and recreate a similar lap belt loading environment on whole-body PMHS in Chapter 4. In this environment, pelvis fractures occurred in 2 out of 3 tests. I described the development of a test fixture in Chapter 5 that isolated the same belt to pelvis angles tested in Chapter 4, but on 22, isolated pelvic wings to make a reaction force based injury risk function. I investigated the development of an injury risk function in Chapter 6, and showed that bone density is a significant factor in the prediction of injury.

7.2. Contributions

The following points describe the contributions of this graduate thesis:

7.2.1. Injury Risk Function Development

The injury risk functions developed as a part of this thesis are the first of any kind to predict fracture between the ASIS and AIIS caused by distributed frontal loading. This information will be crucial in the development of restraint systems for HAVs moving forward, as the seat belt system may be required to prevent occupant motion as it has never had to before due to the removal of knee bolsters and other devices that assist in restraining occupant motion. It has been assumed that the pelvis is one of the strongest bones in the human body, which is why seat belt restraint systems have been designed to load the pelvis as a way of decelerating the body. However, the tolerance of the pelvis has actually not been tested under distributed frontal loading; the data provided in this thesis takes the first step in understanding what the threshold value may be.

7.2.2. Test Fixture Development: Task 2

The test fixtures developed for Task 2 of this thesis can be used for a variety of other testing, not detailed as a part of this thesis. For example, unpublished data was collected using the THOR M-50 ATD using the same test fixture in Task 2 to understand how well the ASIS load cells present in the THOR M-50 ATD capture the belt load read at belt load cells. From this investigation, it was found that a maximum of 80% of the lap belt load was read at the ASIS load cell, and was usually lower due to the occurrence of the lap belt being split in half by the ASIS load cells or by the occurrence of submarining. This is important, as it was a metric to understand how much lap belt force was directly delivered to the pelvis. The THOR ASIS load cells, however, are only unidirectional;

perhaps if other channels were present, the percentage of lap belt load to ASIS load would change. This is an important finding, as it is still unknown as to how much lap belt load gets delivered to the pelvis of a human. HBMs differ from THOR, as in Mroz 2020 where ~ 50% of the lap belt load was recorded at the pelvis.

In addition, a submarining threshold for THOR at two different recline angles was found.by changing the lap belt angles relative to the pelvis. Future studies can use this test fixture to investigate the submarining threshold of different ATDs or of PMHS. The test fixture and accompanying DSD pulse tuning procedure that was created in Task 2 has maximum flexibility in its use of investigating lap-belt-to-pelvis interaction.

7.2.3. Test Fixture Development: Task 3

The test fixture developed in Task 3 of this thesis was created to be as simple as possible to facilitate computational modeling of the tests. The procedure of potting the pelvis, along with the accompanying CT analysis, was extremely accurate in generating the correct Notch to Belt loading angles. The roll angle was difficult to control, due to the unique geometries of the pelvis; however, the procedure allowed for this measurement to be made. While the test fixture was found not to create the same boundary conditions for the pelvis in Task 2, it did always provide good support for the pelvis. No fractures occurred at the potting level, which was important in generating the same, localized fractures on the front of the iliac wing seen in the literature. The loading device of a belt-fork tine allowed the ability for the fracture pattern to be similar to that of the fractures seen in the sled tests, since the physical loading belt was the same.

As a part of Task 3, a new potting material had to be used. A crucial part of this test fixture required the pelvic bone to stay rigidly fixed on the posterior surface so that

the Notch to Belt Angle did not change as the loading occurred. In addition, this rigid

fixation needed to occur without screws entering into the bony surface because it was

important that fractures didn't artificially start as a result of instrumentation. Due to

various factors, a new potting material needed to be found because production of the

original FastCast material had stopped. Various different two part resins were tested prior

to testing to test how well the material would adhere to biological material. In the end,

SmoothCast 300Q was the best material. Not only is it an effective material at holding the

pelvis rigid, especially for such a complex geometry, but its ability to free form around

shapes, and the usability factor of the two part resin, made it a very effective substitute.

Future studies will benefit from this potting material investigation, as it is readily

available and does not appear to have supply issues.

7.2.4. Bone density via CT Data and Mimics Measurement Methodology

The BD measurement methodology created in this thesis can be used in any other

PMHS component level test series in the future. While work still has to be done to correlate

the value of the BD calculated from the phantom to a BD value calculated from DXA or

other measurement devices, the procedure lined out in this thesis allows sample populations

to be compared in a similar format. This is especially important because, even in whole-

body DXA scans, the scan measurements are only taken from certain areas (none of which

are the pelvis). The methodology outlined in this thesis allows any component to have a BD

measurement calculated. At this point in time, it is unclear if this exact HU to BD function

developed could be used in any test series moving forward. Validation of the function

should be done in a future study at UVA on the same CT scanner to check whether the

measured HU from the EDP match with the measured HU from this study. This is because

the CT scanner undergoes a large recalibration once or twice a year that could change the measured HU for the same BD calibration tube. For Task 3, no large recalibration occurred in the test series, so there is large confidence that the function is reliable for this sample population. Checking to see how the large calibration changes the linear function would be important; if it ends up that the linear function does not change by much, it could be possible to use the function and masking method developed for any test series moving forward. It is unlikely that the exact function created in this test series could be used for other labs with other CT scanners; however, the methodology presented is detailed and will allow any other research group to complete the same analysis at their labs.

7.2.5. Publication Plan

The publication plan surrounding this thesis is as followed:

1. IRCOBI Conference publication surrounding the data presented in Task 2 of the thesis. This full conference paper has been accepted, and a presentation was be given in September of 2021.

2. A journal publication regarding the data presented in Task 3, regarding the development of the injury risk function. Exact journal has yet to be decided, but publication will ensue after discussion of the best way to present the data is decided among the UVA team. It is expected that the journal will be the Journal of Biomechanics. Timeline for submission looks to be Fall of 2021 or Winter of 2022.

3. Unpublished work, not included directly in this thesis (but referenced multiple times) surrounding the testing of THOR M-50 ATD in the Task 2

environment will be published at either a conference or in a journal in the
near future.

7.3. Future Research

The following items describe some of the potential future research directions that would relate to the work completed in this thesis:

7.3.1. Computational Modeling of Task 3 Testing

Evaluation of the current HBM pelvises in the test environment created in Task 3 could not only evaluate how the HBM pelvises compare to the test data, but also allow for a different form of the IRF. For example, a strain based injury criteria could be developed for HBMs, as FE modeling capabilities allow for that. Some HBMs currently have failure properties of bone available; the force of failure of the HBMs could be tuned based on the data collected in the experiments run in Task 3. In addition, the load across the section of a seat belt model could be measured in the FE model, so relating the belt load to the pelvis load could be completed. Sensitivity analysis could also be completed where other factors not looked at in this study could be changed, such as variations in the location of load.

7.3.2. Relating Belt Load to Pelvis Load

Since there was no room for a belt gauge in the testing of Task 3, the load in the lap belt piece between the belt fork tines could not be measured. For this reason, the injury risk function was a pelvis-force based injury risk function. This measurement is very difficult to obtain in a whole-body PMHS sled test, or with any ATD that does not have ASIS load cells. An easier measure (and prediction tool) to develop the IRF would be the lap belt load, measured externally by seat belt gauges. This would require some

assumptions (ie, that the lap belt is actually loading the pelvis). Validation of this assumption could be completed through the use of 3-D motion tracking markers, or video analysis where the markers are not present. However, this also assumes that every surrogate would have the same proportion of measured lap belt load to measured pelvis load. This assumption should be tested; the easiest way to do that would be in modeling the tests completed in Task 2. By modeling the environment, parameters such as soft tissue material properties, amount of soft tissue, tissue attachment type, etc can be changed to understand how the measured lap belt load effects the load delivered to the pelvis. Mroz 2020 showed that, in the THUMS SAFER HBM, a measured lap belt force of between 6.6-7.8 kN was shown to have 3.6-4.4 kN of force at the right ASIS (Mroz 2020). However, how this relates when changes to the size of the occupant occurs, or changes to the actual HBM used occurs is still unknown. This gap could be filled with a future computational study.

7.3.3. Submarining Threshold Testing

Further testing could be completed in the fixture developed in Task 2 to understand the submarining threshold of various occupants (PMHS or ATD). The flexibility created in positioning of the occupant allows for many mid-sled test postures to be created. The development of the Notch Angle metric of pelvis orientation provides a better measure of how the anterior portion of the pelvis that engages with the lap belt is oriented relative to the direction of loading, and may be a better predictor of submarining than other pelvis orientation metrics. With boundary conditions that matched the testing completed in Task 2, lap-belt-to-pelvis angle could be isolated as the metric that causes submarining.

7.3.4. Additional Field Data Work/Clinical Investigation

Much of this thesis revolves around understanding an injury that is currently uncommon in the field, and is only predicted to occur more frequently with open cabin designs of HAVs. While I was successfully able to recreate the fractures seen in sled tests in this thesis to provide important data in the development of new restraint systems, further field data analysis could be completed to understand the gravity of the injury in the field. The difficulty with this field analysis stems from the fact that the AIS code 856151.2 encompasses many types of pelvis injuries, not just iliac wing injuries.

Discussion with two, UVA Orthopaedic Trauma surgeons about this injury type presented was completed to try to understand the clinical side of this injury. One surgeon said he had never seen the injury before, and one said he may have seen it a few times. One surgeon said:

"…these [injuries] are likely rare occurrences in the real world due to some fairly large muscle groups in these areas and likely reduced bone density with limited muscle protection in the cadaveric model which allows the seat belt to slide into the area between ASIS and AIIS and create a crush injury… We probably do see a few iliac wing fractures (a little more proximal then on your cadaver) caused by seat belts but would be difficult to separate this as cause vs intrusion from door or impact with console without detailed analysis of the specific crash… These are also rarely surgical in nature and typically heal with minimal sequelae."

Both surgeons agreed that the injury type would likely not require surgery, but one stated that it would likely be very debilitating in the short term. Further discussions with trauma surgeons from other institutions could be conducted to get a better idea of

125

how this type of injury would be treated, and what the associated recovery times would be.

7.3.5. Instrumentation Development

Strain gauges have been used in various sled test studies to determine the time of fracture occurrence (Richardson et al 2020, Uriot et al 2015, Luet et al 2012, Trosseille et al 2018). Strain gauges assisted in the fracture time determination in both Task 2 and Task 3 of this thesis, but often times were damaged in a way that was not diagnosable by the data acquisition system. For this reason, some gauges "passed" diagnostics, but did not collect any data. This is extremely valuable information that was lost when determining the time of first fracture. A more robust (although albeit most likely a larger one) strain gauge could be used to assist in gathering more meaningful data without failing.

In addition, the strain gauge data was the link between Task 2 and Task 3. Strain gauges used in any environment that is not on a flat, metal sheet is beyond the scope of their capabilities, let alone on biological material of varying curvature in a moist environment. Again, a more robust strain gauge may do a better job at collected data because it may be better at withstanding some of the environmental factors it was not designed to face.

7.4. Injury Risk Function Development

Future statistical analysis avenues were presented in Chapter 6. The use of Bayesian statistics could provide the ability of the development of a frailty model. A frailty model accounts for repeated measures on the same subject. As shown in Chapter 6, the left and right sides of the pelvis from the same subject are extremely correlated. For

126

this reason, the current injury risk function may not be portraying the data as accurately as possible, since it currently counts each wing as independent. Further investigation in using Bayesian statistics as the method of survival analysis may provide a better representation of the injury data. Cutcliffe et al 2012 showed that Bayesian formulations of injury risk functions often were better than the "standard" analysis using the same data. Moving to the Bayesian formulation for injury risk functions also showed better results when small samples sizes (even a sample size of 1) were used. The injury biomechanics field may want to push towards this method of statistical analysis, since small sample sizes are usually always used in PMHS testing.

7.5. Conclusions

- I was able to successfully isolate the exact lap-belt-to-pelvis (Notch to Belt Angle) instance where fracture occurred in a sled test series.

- I was able to develop a fixture that could create the same pelvis fractures at the same Notch to Belt Angle from the sled test series on whole body PMHS

- I created a simplified methodology to measure bone quality of component pelvis specimens which I call a weighted bone density.

- I created a simplified loading environment to measure the tolerance of isolated pelvic wings to loading conditions similar to a sled test. In these tests, I had great success and fractured 19/22 specimens

- I created the first injury risk function for frontal distributed loading of the iliac wings. Loading angle did not have a significant effect on the fracture tolerance of the pelvis, but the weighted bone density measurement was a significant predictor of fracture tolerance.

  - The IRF is: $P(Fracture|BD) = 1 - e^{-\left(Force * e^{-(-.570+6.854*BD)}\right)^{2.0158}}$

References

Adomeit D, Heger A. Motion Sequence Criteria and Design Proposals for Restraint Devices in Order to Avoid Unfavorable Biomechanic Conditions and Submarining. SAE Technical Paper 751146, 1975. doi: 10.4271/751146

Cutcliffe H, Schmidt A et al. How Few? Bayesian Statistics in Injury Biomechanics. 56th Stapp Car Crash Conference, 2012, Savannah, GA.

Fayon A, Tarriere C, Wasfish G, Got C, Patel A. Thorax of 3-Point Belt wearers During a Crash (Experiments with Cadavers). 19th Stapp Car Crash Conference, 1975, San Diego, CA.

Forman J, Lin H et al. Occupant Safety in Automated Vehicles: Effect of Seatback Recline on Occupant Restraint. Japan Society of Automotive Engineers. 2018

Gepner B, Draper D et al. Comparison of Human Body Models in Frontal Crashes with Reclined Seatback. Proceedings of the 2019 IRCOBI Conference. Florence, Italy.

Gepner B, Rawska K et al. Challenges for Occupant Safety In Highly Automated Vehicles Across Various Anthropometries. 26th International Technical Conference on the Enhanced Safety of Vehicles (ESV), 2019. Eindhoven, Netherlands.

Ji P, Huang Y, Zhou Q. Mechanisms of Using Knee Bolster to Control Kinematical Motion of Occupant in Reclined Posture for Lowering Injury Risk. 2017 International Journal of Crashworthiness. 22(4):415–424.

Jorlöv S, Bohman K, Larsson A. Seating Positions and Activities in Highly Automated Cars – A Qualitative Study of Future Automated Driving Scenarios. Proceedings of IRCOBI Conference, 2017, Antwerp, Belgium.

Kent R et al. Assessment of a Three-Point Restraint System with a Pre-tensioned Lap Belt and an Inflatable, Force-Limited Shoulder Belt. 55th Stapp Car Crash Conference, 2011, Dearborn, Michigan.

Kent R et al. The Influence of Superficial Soft Tissues and Restraint Condition on Thoracic Skeletal Injury Prediction. 45th Stapp Car Crash Conference, 2001, San Antonio, Texas.

Kent R, Funk J. Data Censoring and Parametric Distribution Assignment in the Development of Injury Risk Functions from Biomechanical Data. SAE Technical Paper, 2004-01-0317. 2004.

Kim T, Park G et al. Abdominal characterization under lap belt loading. 24th International Technical Conference on the Enhanced Safety of Vehicles (ESV), 2015, Gothenburg, Sweden.

Kitagawa Y, Hayashi S et al. Occupant Kinematics in Simulated Autonomous Driving Vehicle Collisions: Influence of Seating Position, Direction and Angle. 61st Stapp Car Crash Conference, 2017, Charleston, SC.

Koppel S, Octavio J et al. Seating Configuration and Position Preferences in Fully Automated Vehicles. Traffic Injury Prevention, 2019, Volume 20: 103-109.

Luet C, Trosseille X et al. Kinematics and Dynamics of the Pelvis in the Process of Submarining using PMHS Sled Tests. 56th Stapp Car Crash Conference, 2012, Savannah, GA.

McMurry T, Poplin G. Statistical Considerations in the Development of Injury Risk Functions. Traffic Injury Prevention, 2015, Volume 16, 618-626

Mroz K et al. Effect of Seat and Seat Belt characteristics on the Lumbar Spine and Pelvis Loading of the SAFER Human Body Model in Reclined Postures. Proceedings of the 2020 IRCOBI Conference.

Nyquist G, Patrick L. Lumbar and Pelvic Orientations of the Vehicle Seated Volunteer. SAE
Transactions, Volume 85, Section 4: 76012-160934. 1976.

Östling M, Larsson A. Occupant Activities and Sitting Positions in Automated Vehciels in China
and Sweden. 26th International Technical Conference on the Enhanced Safety of
Vehicles (ESV), 2019, Eindhoven, Netherlands.

Rawska K, Gepner B et al. Submarining Sensitivity Across Varied Anthropometry in an
Autonomous Driving System Environment. Traffic Injury Prevention, 2019. Volume
20:S123–S127

Rawska K, Gepner B et al. Submarining Sensitivity Across Varied Seat Configurations in an
Autonomous Driving System Environment. Traffic Injury Prevention, 2020. Volume 21:
S1-S6

Richardson R, Donlon J P et al. Kinematic and Injury Response of Reclined PMHS in Frontal
Impacts. 64th Stapp Car Crash Conference, 2020, Denver, CO.

Richardson R, Donlon J P et al. Test Methodology for Evaluating the Reclined Seating
Environment with Human Surrogates. 26th International Technical Conference on the
Enhanced Safety of Vehicles (ESV), 2019, Eindhoven, Netherlands.

Richardson R, Jayathirtha M et al. Pelvis Kinematics and Injuries of Reclined Occupants in
Frontal Impacts. Proceedings of IRCOBI Conference, 2020, Munich, Germany.

Richardson R, Jayathirtha M et al. Thoracolumbar spine kinematics and injuries in frontal
impacts with reclined occupants. Traffic Injury Prevention, 2020, Volume 21: 1-7.

Schmidt G, Kallieris D, Barz J, Mattern R. Results of 49 Cadaver Tests Simulating Frontal
Collision of Front Seat Passengers. 18th Stapp Car Crash Conference, 1974, Ann Arbor,
MI.

Shaw G, Lessley D et al. Pelvic Restraint Cushion Sled Test Evaluation of Pelvic Forward

    Motion. Traffic Injury Prevention, 2018. Volume 19: 250–255.

Stitzel J et al. A Population-Based Comparison of CIREN and NASS Cases Using Similarity

    Scoring. Association for the Advancement of Automotive Medicine, 2007, Volume 51,

    395-417

The U.S. Department of Transportation's: Automated driving systems 2.0 a vision for safety,

    September 2017. https://www.nhtsa.gov/sites/nhtsa.dot.gov/files/documents/13069a-

    ads2.0_090617_v9a_tag.pdf

Trosseille X, Petit P et al. Reference PMHS Sled Tests to Assess Submarining of the Small

    Female. 62nd Stapp Car Crash Conference, 2018, San Diego, CA.

Uriot J, Potier P et al. Reference PMHS Sled test to Assess Submarining. 59th Stapp Car Crash

    Conference, 2015, New Orleans, LA.

8.   Appendix

8.1. Appendix A: Task 2 Specimen Information

General Information				
Cadaver ID Number	663	1001	895	990
Age at Time of Death	64	68	73	75
Sex	Female	Male	Male	Male
Cause of Death	Chronic Heart Failure	COPD	COPD	Dementia
Preservation Method	Freezing	Freezing	Freezing	Freezing
Immunology				
HIV Assay	Negative	Negative	Negative	Negative
Hepatitis B	Negative	Negative	Negative	Negative
Anthropometry (all measurements in mm unless otherwise stated)				
Weight (kg)	70	76.6	68	71.2
Stature	159	180	175	183
Vertex-to-Symphision Length	91	102	99	98
Top of Head-to-Trochacterion	81	93	89	82
Shoulder (Acromial Height)	137	157	155	161
Waist Height – ASIS	85	100	97	106
Waist Depth - Umbilicus	22	20	20	16.5
Waist Breadth	36	33	35	32
Shoulder Breadth (Biacromial)	33	37	36	35
Chest Breadth: 4th Rib	35	38	31	33
Chest Breadth: 8th Rib	33	35	32	33
Chest Depth: 4th Rib	20	21	21	20
Chest Depth: 8th Rib	22	22	22	21
Hip Breadth	32	34	31	30.5
Buttock Depth	18	19	18	17
Shoulder-to-end of amputation	13	0	0	0
Tibiale Height	42	50	49	52
Ankle Height (Outside)	8	8	9.5	10
Foot Breadth	8	8	8	9
Foot Length	21	26	23	26
Head Length	18.5	22	18.5	20
Head Breadth	14.5	15	15	16.5
Head Height	23	23	21	24
Head Circumference	52	58	57	59
Neck Circumference	40	47	45	43
Chest Circumference: 4th Rib	106	107	99	101
Chest Circumference: 8th Rib	102	101.5	97	98
Waist Circum: At Umbilicus	109	101	96	87

Waist Circum: 8cm above Umbilicus	106	105	97	88
Waist Circum: 8cm below Umbilicus	109	95	98	97
Buttock Circumference	100	97	99	98
Thigh Circumference	52	49	52	53
Lower Thigh Circumference	39	37	36	38
Knee Circumference	38	40	36.5	38
Calf Circumference	35	29	30	32
Ankle Circumference	25	25	23	26
Scye (Armpit) Circumference	93	N/A	43	47
Femur Length	39	41	38	48
Shoulder to elbow length[a]	N/A	N/A	36	37
Forearm to hand length[a]	N/A	N/A	46	46
Bicep circumference[a]	N/A	N/A	29	28
Elbow circumference[a]	N/A	N/A	27	30
Forearm circumference[a]	N/A	N/A	24	31
Wrist circumference[a]	N/A	N/A	17	17

a: Measurements were taken when possible, prior to amputation.

8.2.   Appendix B: Task 2 Post Test CT Report

Patient ID: **Autosafetylab, F00663DA13**
Type of specimen: Whole Body
Type of scan/read: **Post-Test, RCCADS Belt Pull**
Specimen Number: 663

Scan Date: 10/22/2020

Comparison: 10/20/2020

Additional clinical data: COD – congestive heart failure

Technique: Helically acquired imaging was obtained from the vertex to the toes. Axial, coronal, and sagittal reformations were provided, including dedicated reformats of the spine.

FINDINGS

SKULL / BRAIN:
Normal appearance of the skull and facial bones. No displaced fracture or mass lesion. Expected postmortem appearance of the soft tissues. Intracranial contents are within normal limits.

CHEST:
Lungs/Pleura: Expected postmortem appearance of the lungs and pleural cavity. No mass lesion.
Mediastinum: Expected postmortem appearance.
Heart: Expected postmortem appearance.
Bones: Multiple bilateral anterior rib fracture involving second through a right bilaterally with non-displaced sternal fractures, these are similar to pretest imaging. No joint malalignment. No significant degenerative changes. Normal bone mineralization. No focal bone lesions. No hardware or prosthetic devices.
Extrathoracic Soft tissues: No focal abnormality.

CERVICAL SPINE: (Degree of rotation of the cervical spine makes evaluation somewhat limited)
No spine fractures are evident. No spondylolisthesis. Vertebral body heights and intervertebral disc spaces are preserved. No significant degenerative changes. No focal bone lesions. No spinal hardware or prosthetic devices. The paravertebral soft tissues appear grossly normal.

THORACIC SPINE:
Vertebral T1 irregularity was air within the vertebral body likely sequela instrumentation. No spondylolisthesis. Vertebral body heights and intervertebral disc spaces are preserved. No

1

significant degenerative changes. No focal bone lesions. No spinal hardware or prosthetic devices. The paravertebral soft tissues appear grossly normal.

LUMBAR SPINE:
Left L1 non-displaced transverse process fracture as described above. No spondylolisthesis. Vertebral body heights and intervertebral disc spaces are preserved. Intervertebral disc calcification at L1-L2. No significant degenerative changes. No focal bone lesions. No spinal hardware or prosthetic devices. The paravertebral soft tissues appear grossly normal.

ABDOMEN/PELVIS SOFT TISSUES: Expected postmortem appearance. No mass lesion or focal abnormality.

PELVIS:
Complex segmental right iliac fracture involving the superior iliac crest with multifocal segment displacement worst along the anterior superior iliac and extending to the SI joint on the right. There is a non-displaced left sacral wing fracture that is likely extending from the inferior left transverse process of L5 and extending inferiorly along the left sacral wing of S1 and mild extension into S2. No significant degenerative changes. No hardware or prosthetic devices.

UPPER EXTREMITIES:
Left: No fracture in the visualized portion. Normal mineralization.
Right: No fracture in the visualized portion. Normal mineralization.

LOWER EXTREMITIES:
Left: No displaced fracture. No joint malalignment. Mild bilateral degenerative changes of the knee. Normal bone mineralization. No focal bone lesions. No hardware or prosthetic devices. Expected postmortem appearance of the soft tissues.
Right: Chronic avulsion fragment along the anterior talus. No joint malalignment. Mild bilateral degenerative changes of the knee. Normal bone mineralization. No focal bone lesions. No hardware or prosthetic devices. Expected postmortem appearance of the soft tissues.

IMPRESSION
1. Complex and segmented right iliac fracture involving the pelvic rim and extending posteriorly to the SI joint without involving the sacrum on the right, and anteriorly into the anterior inferior iliac spine.
2. Non-displaced new sacral week French 2 standing from the inferior left transverse process of L5 through the S1 sacral wing and likely involves the superior aspect of S2.
3. Multifocal bilateral anterior rib fractures as described above in addition to non-displaced sternal fractures, these are similar to pre-test imaging and likely represent traumatic injury sequela of CPR.
4. Cortical irregularity without high loss involving T1 vertebral body likely sequela of instrumentation.

2

135

Name: B11
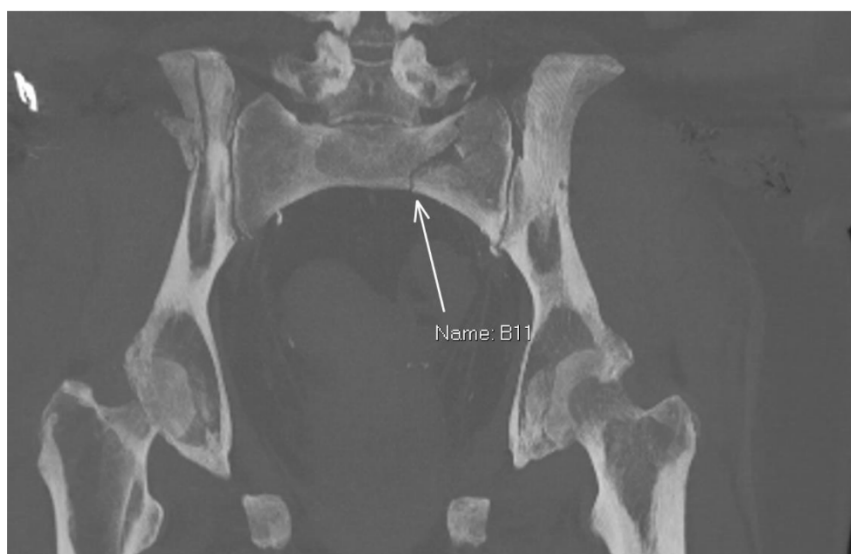
Mohammad A Halaibeh, M.D. – Resident Physician, UVA Department of Radiology

Patient ID: **Autosafetylab, M00895DA17**
Type of specimen: Whole Body
Type of scan/read: **Post-Test, RCCADS Belt Pull**
Specimen Number: 895

Scan Date: 11/12/2020

Comparison: 11/10/2020

Additional clinical data: COD – COPD
Specimen involved in auto accident simulation involving a lap seatbelt. Please pay special attention to any abnormalities in the lumbar spine and pelvis (especially around the ASIS?) – this test focused on the interaction of the occupant with the lap belt on impact.

Technique: Helically acquired imaging was obtained from the vertex to the toes. Axial, coronal, and sagittal reformations were provided, including dedicated reformats of the spine.

FINDINGS

SKULL / BRAIN:
Normal appearance of the skull and facial bones. No displaced fracture or mass lesion. Expected postmortem appearance of the soft tissues. Intracranial contents are within normal limits.

UPPER EXTREMITIES:
Right: No fracture in the visualized portion. Normal mineralization.
Left: No fracture in the visualized portion. Normal mineralization.

CHEST:
Lungs/Pleura: Expected postmortem appearance of the lungs and pleural cavity. No mass lesion.
Mediastinum: Expected postmortem appearance.
Heart: Expected postmortem appearance.
Bones: Chronic healed right and fourth anterior rib fractures. No joint malalignment. No significant degenerative changes. Normal bone mineralization. No focal bone lesions. No hardware or prosthetic devices.
Extrathoracic Soft tissues: No focal abnormality.

CERVICAL SPINE:
No spine fractures are evident. No spondylolisthesis. Multilevel degenerative disc disease with facet arthropathy involving C2-C3, and loss of disc space worst C5-C6 and C6-C7.   No focal

1

bone lesions. No spinal hardware or prosthetic devices. The paravertebral soft tissues appear grossly normal.

THORACIC SPINE:
Superior endplate compression fracture involving T4 new from prior. No spondylolisthesis. Vertebral body heights and intervertebral disc spaces are preserved. No significant degenerative changes. No focal bone lesions. No spinal hardware or prosthetic devices. The paravertebral soft tissues appear grossly normal.

LUMBAR SPINE:
Mild superior endplate fracture of L1 with minimal height loss. 2-column fracture of L2 vertebral body extending from the anterior inferior edge and terminating in the superior endplate with minimal height loss and no retropulsion. Non-displaced right L3 and L4 transverse process fractures. No focal bone lesions. No spinal hardware or prosthetic devices. The paravertebral soft tissues appear grossly normal.

ABDOMEN/PELVIS SOFT TISSUES: Expected postmortem appearance. No mass lesion or focal abnormality.

PELVIS:
No pelvic fractures are evident. No significant degenerative changes. No focal bone lesions. No hardware or prosthetic devices. No focal abnormality in the pelvic soft tissues.

LOWER EXTREMITIES:
Left: No displaced fracture. No joint malalignment. No significant degenerative changes. Normal bone mineralization. No focal bone lesions. No hardware or prosthetic devices. Expected postmortem appearance of the soft tissues.
Right: No displaced fracture. No joint malalignment. No significant degenerative changes. Normal bone mineralization. No focal bone lesions. No hardware or prosthetic devices. Expected postmortem appearance of the soft tissues.

IMPRESSION
1. No pelvic fractures.
2. Two-column fracture of L2 vertebral body with no significant height loss as described above.
3. Mild superior end plate fracture of T4 and L1.
4. Non-displaced right L3 and L4 transverse process fractures.

Mohammad A Halaibeh, M.D. – Resident Physician, UVA Department of Radiology

Patient ID: **Autosafetylab, M01001DA20**
Type of specimen: Whole Body
Type of scan/read: **Post-Test, RCCADS Belt Pull**
Specimen Number: 1001

Scan Date: 10/29/2020

Comparison: 10/27/2020

Additional clinical data: COD – COPD

Technique: Helically acquired imaging was obtained from the vertex to the toes. Axial, coronal, and sagittal reformations were provided.

FINDINGS

SKULL / BRAIN:
Normal appearance of the skull and facial bones. No displaced fracture or mass lesion.
Expected postmortem appearance of the soft tissues. Intracranial contents are within normal limits.

CHEST:
Lungs/Pleura: Expected postmortem appearance of COPD lungs and pleural cavity. No mass lesion.
Mediastinum: Expected postmortem appearance.
Heart: Expected postmortem appearance.
Bones: No displaced fracture. No joint malalignment. No significant degenerative changes. Normal bone mineralization. No focal bone lesions. No hardware or prosthetic devices.
Extrathoracic Soft tissues: No focal abnormality.

CERVICAL SPINE: (Degree of rotation of the cervical spine makes evaluation somewhat limited)
No spine fractures are evident. No spondylolisthesis. Vertebral body heights and intervertebral disc spaces are preserved. No significant degenerative changes. No focal bone lesions. No spinal hardware or prosthetic devices. The paravertebral soft tissues appear grossly normal.

THORACIC SPINE:
No spine fractures are evident. No spondylolisthesis. Vertebral body heights and intervertebral disc spaces are preserved. No significant degenerative changes. No focal bone lesions. No spinal hardware or prosthetic devices. The paravertebral soft tissues appear grossly normal.

LUMBAR SPINE:
No spinal hardware or prosthetic devices. The paravertebral soft tissues appear grossly normal. Diffuse osteopenia the bones with lumbar levoscoliosis centered at L3. There is worsening superior L2 fracture now distraction fracture involving the three columns along the superior margin without significant height change.
Minimally displaced left L2 transverse process fracture
Minimally displaced bilateral L3 transverse process fractures
Minimally displaced left, and displaced right L4 transverse processes
Complex fragmented bilateral L5 transverse process fractures

ABDOMEN/PELVIS SOFT TISSUES: Expected postmortem appearance. No mass lesion or focal abnormality.

PELVIS:
No significant degenerative changes. No hardware or prosthetic devices.
Complex left superior iliac fracture crossing the SI joint medially into the sacral ala and involving the left S2 foramina. The fracture then extend into the right sacral ala involving the S1 neural foramina. Minimally displaced superior pubic rim, and non-displaced inferior pubic rim fractures on the right.

UPPER EXTREMITIES:
Right: No fracture in the visualized portion. Normal mineralization.
Left: No fracture in the visualized portion. Normal mineralization.

LOWER EXTREMITIES:

Left: No displaced fracture. No joint malalignment. No significant degenerative changes. Normal bone mineralization. No focal bone lesions. No hardware or prosthetic devices. Expected postmortem appearance of the soft tissues.

Right: No displaced fracture. No joint malalignment. No significant degenerative changes. Normal bone mineralization. No focal bone lesions. No hardware or prosthetic devices. Expected postmortem appearance of the soft tissues.

IMPRESSION
1. Diffuse osteopenia with levoscoliosis centered at L3
2. Complex left superior iliac fracture crossing the SI joint medially into the sacral ala and involving the left S2 foramina. The fracture then extend into the right sacral ala involving the S1 neural foramina
3. There is worsening superior L2 fracture now distraction fracture involving the three columns along the superior margin without significant height change.
4. Minimally displaced superior pubic rim, and non-displaced inferior pubic rim fractures on the right.

2

140

5. Minimally displaced left L2 transverse process fracture,
6. Minimally displaced bilateral L3 transverse process fractures
7. Minimally displaced left, and displaced right L4 transverse processes
8. Complex fragmented bilateral L5 transverse process fractures

Mohammad A Halaibeh, M.D. – Resident Physician, UVA Department of Radiology

Addendum to 1001 Post Test Report

IMPRESSION:
1. Diffuse osteopenia with levoscoliosis centered at L3
2. Complex left superior iliac fracture crossing the SI joint medially into the sacral ala and involving the left
   S2 foramina. The fracture then extend into the right sacral ala involving the S1 neural foramina
3. There is worsening superior L2 fracture now distraction fracture involving the 3 columns along the
   superior margin without significant height change.
4. Minimally displaced superior pubic rim, and nondisplaced inferior pubic rim fractures on the right.
5. Minimally displaced left L2 transverse process fracture,
6. Minimally displaced bilateral L3 transverse process fractures
7. Minimally displaced left, and displaced right L4 transverse processes
8. Complex fragmented bilateral L5 transverse process fractures

Mohammad A Halaibeh, M.D.
UVA Radiology

Addendum to include additional fracture seen in the pelvis:

**Mildly displaced, comminuted fracture along the anterior aspect of the right iliac bone with
involvement of the anterior superior iliac spine.**

Matthew Schmidt, M.D.
UVA Radiology

8.4. Appendix C: Task 3 Specimen Information

Subject ID	Sex	Age	Weight (kg)	Stature (cm)	Cause of Death	BD (DXA, g/cm^2)*	Designation
990	M	75	71.2	183	Dementia	1.42	Strain Matching
713	M	75	61.2	188.0	Emphysema	.929	Injury Risk
714	M	61	122.4	177.8	CHF	.818	Injury Risk
715	M	50	108.8	182.9	GSW suicide	1.116	Injury Risk
716	M	52	101.1	185.4	Prescription drug overdose	1.040	Injury Risk
792	M	68	70.3	177.8	Malignant neoplasm of bile duct	1.356	Injury Risk
798	M	77	77.1	182.9	Bronchiectasis	1.048	Injury Risk
997	M	66	81.2	172.7	CHF	N/A	Injury Risk
998	M	59	76.6	175.3	Neck and throat cancer	N/A	Injury Risk
999	M	56	72.6	167.6	CHF	N/A	Injury Risk
1000	M	61	72.1	175.3	Cardiac arrest	N/A	Injury Risk

* DXA value location was not consistent among specimens. Reported number was

the value taken from DXA scan (some are femoral head/neck, some are lumbar spine)

8.5. Appendix D: Task 3 Data and Injury Diagrams

Table 8.6-1 990L 0 Degree Roll Subinjurious Test Data
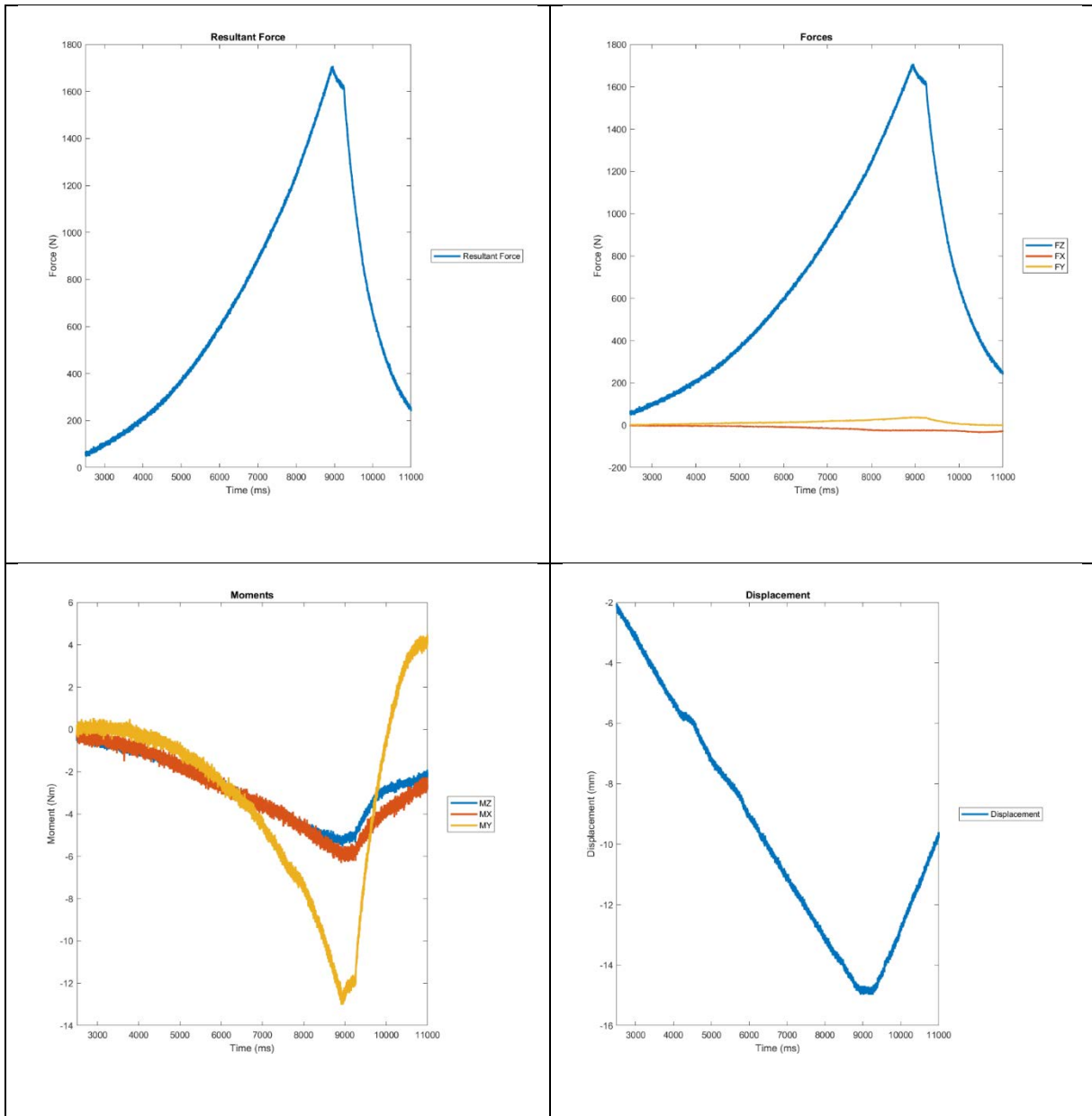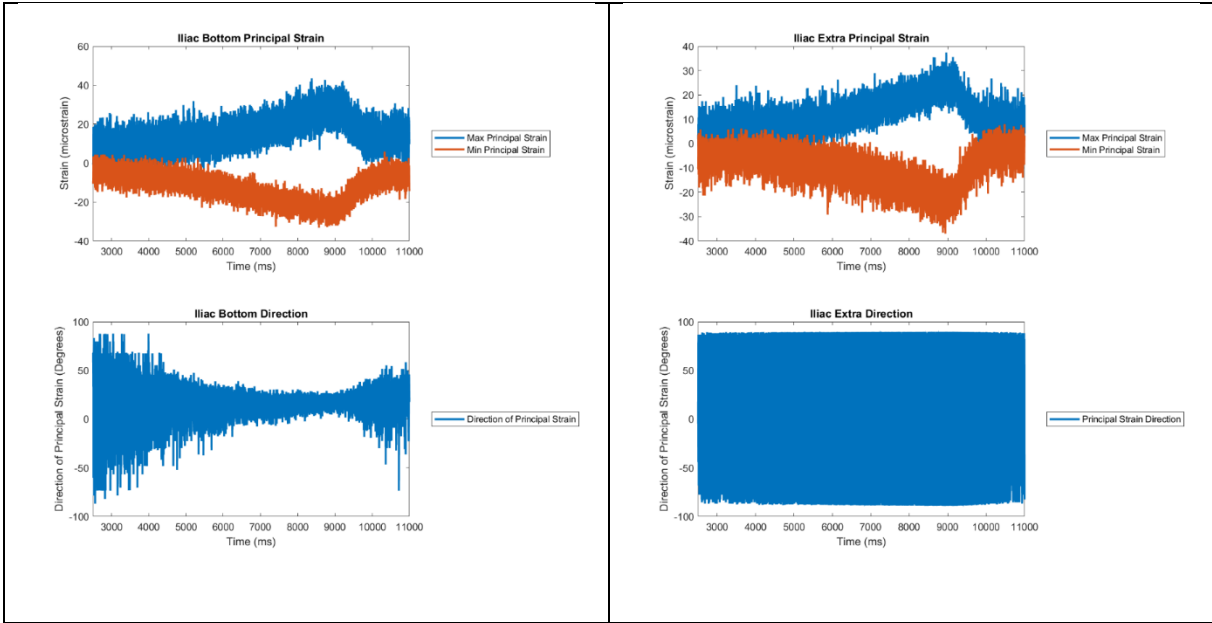
Table 8.6-2 - 990L +10 Degree Roll Subinjurious Test Data
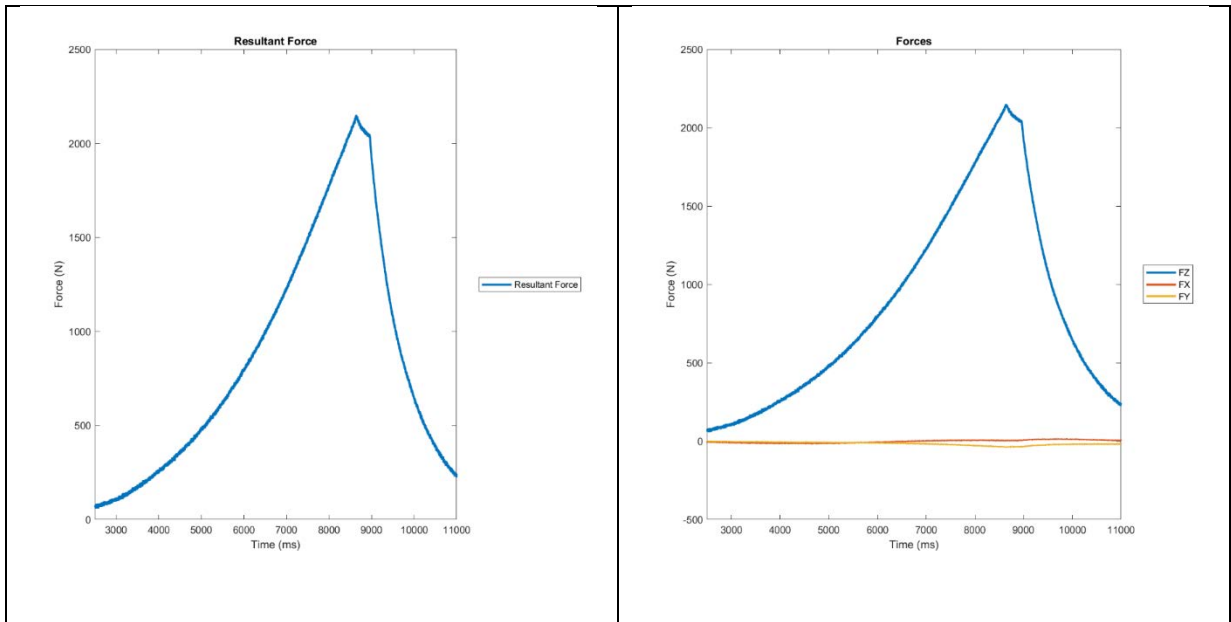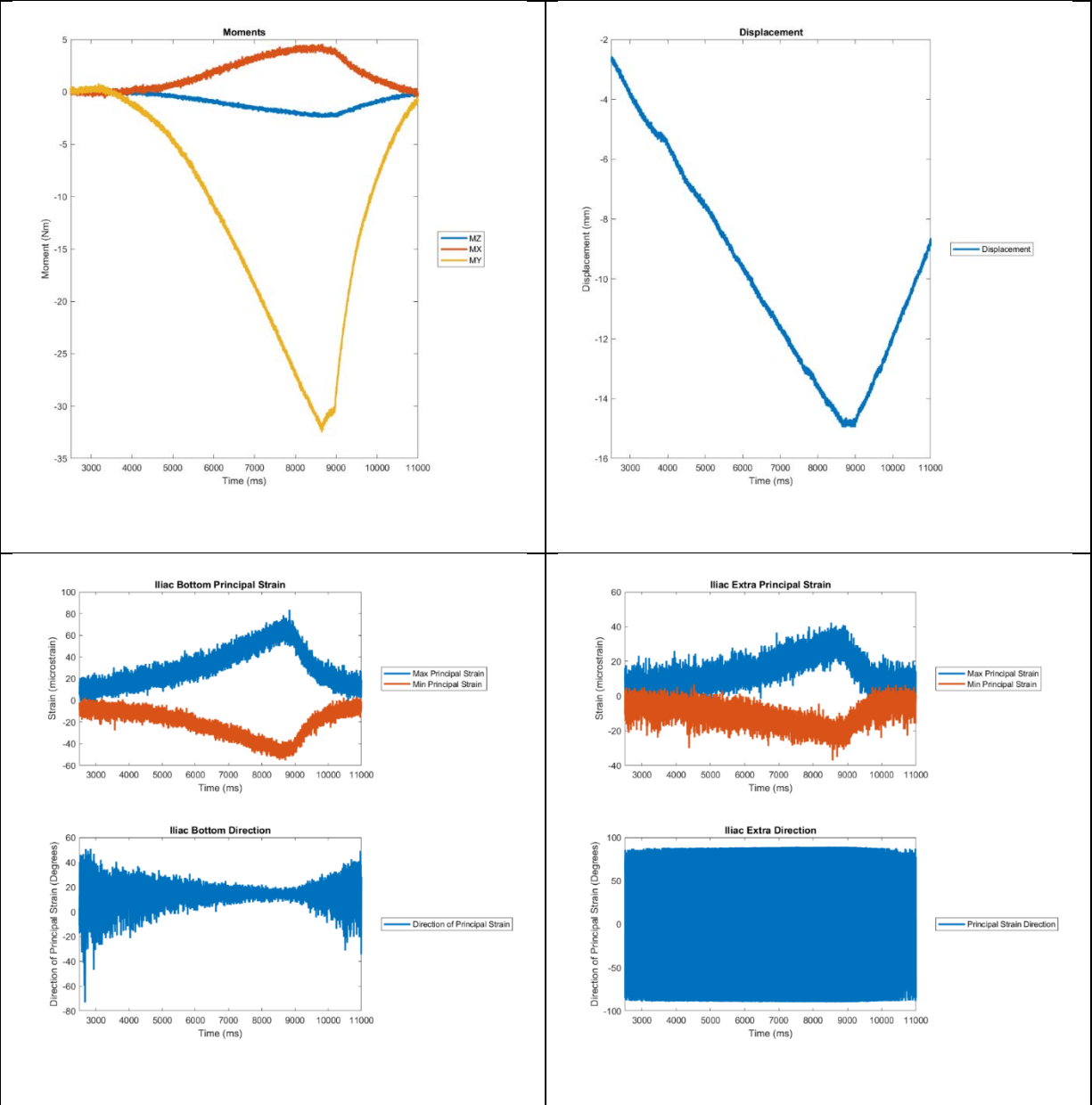
Table 8.6-3 - 990L -10 Degree Roll Subinjurious Test Data
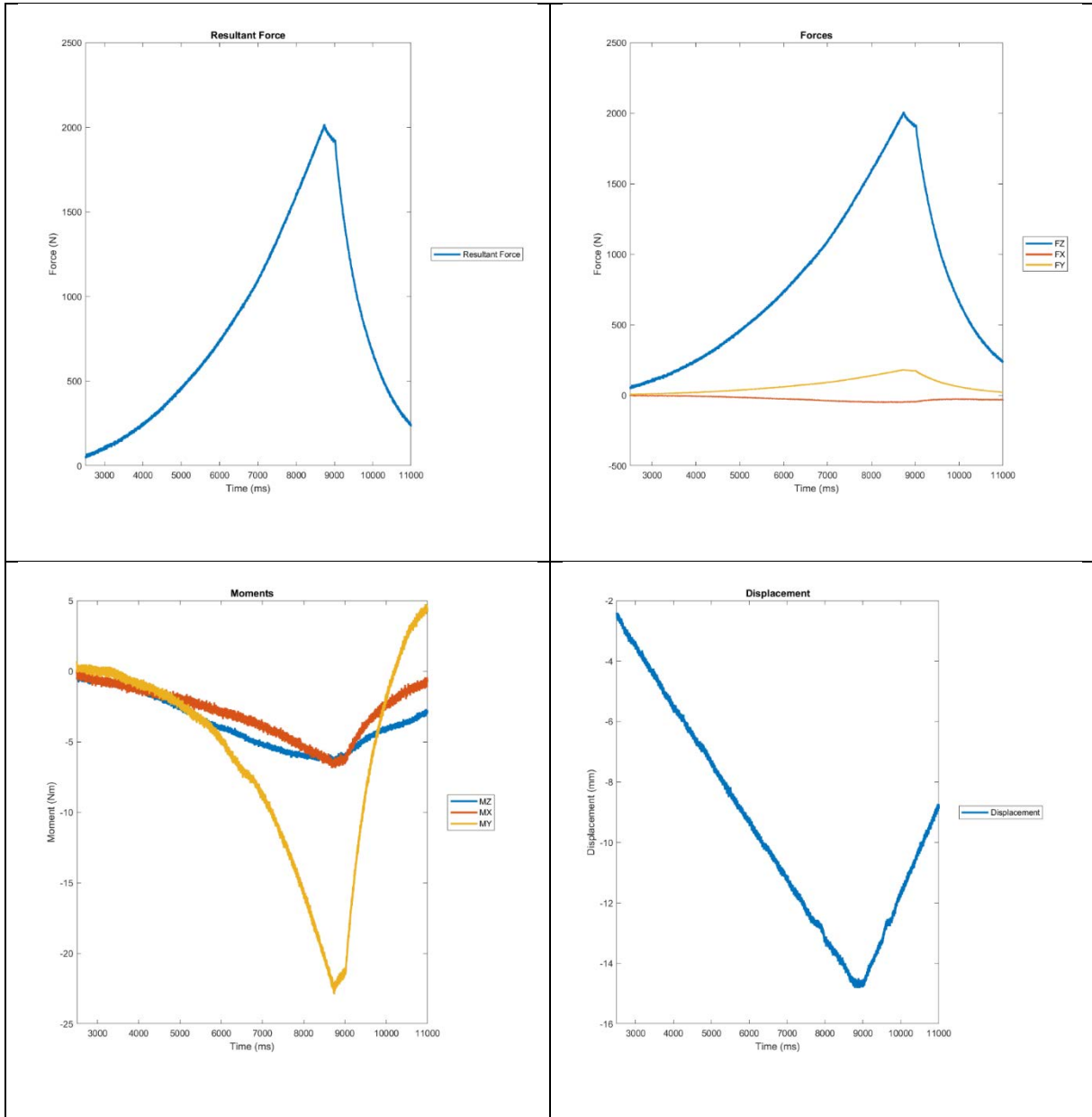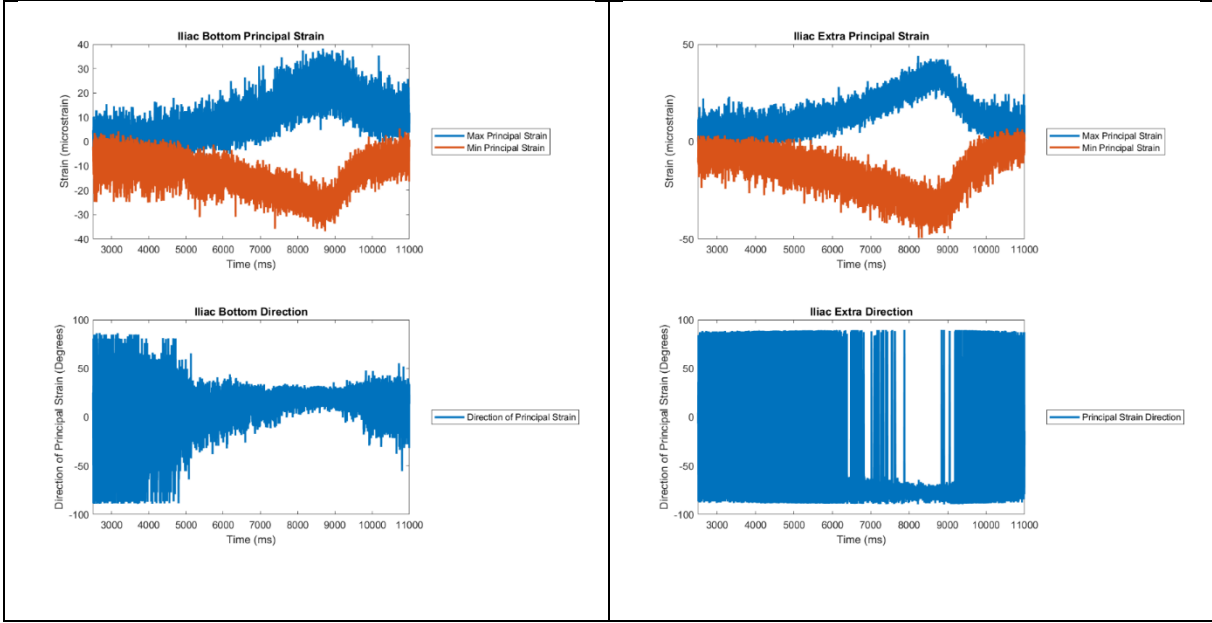
Table 8.6-4 - 990L 75 Degree Notch to Belt Angle Subinjurious Test Data
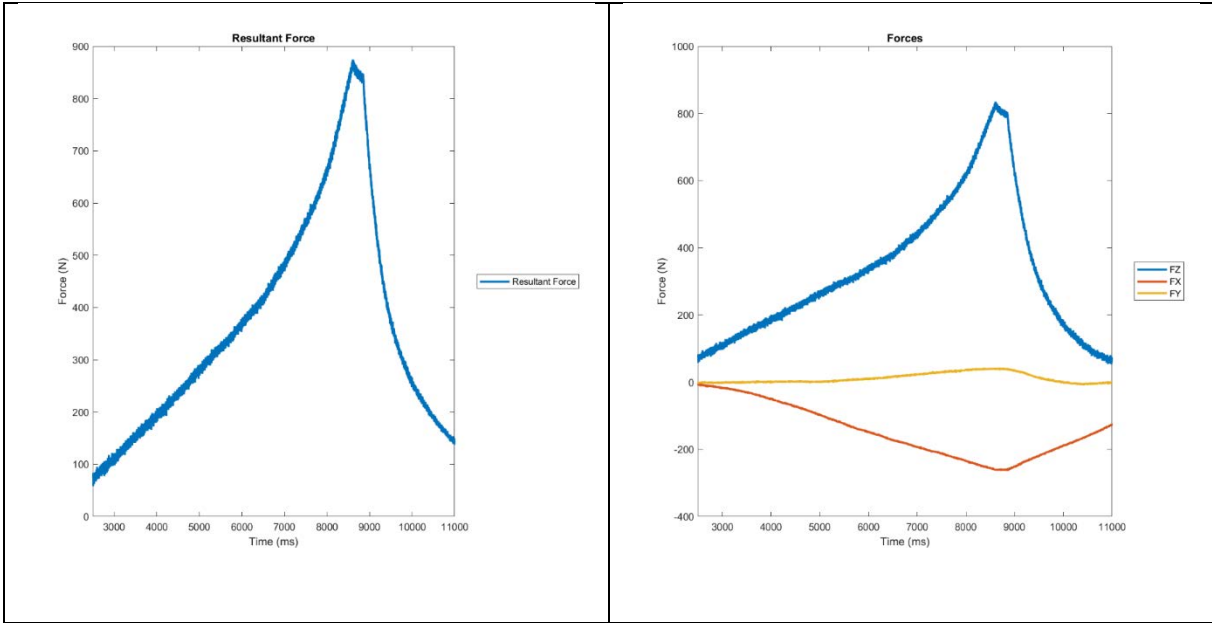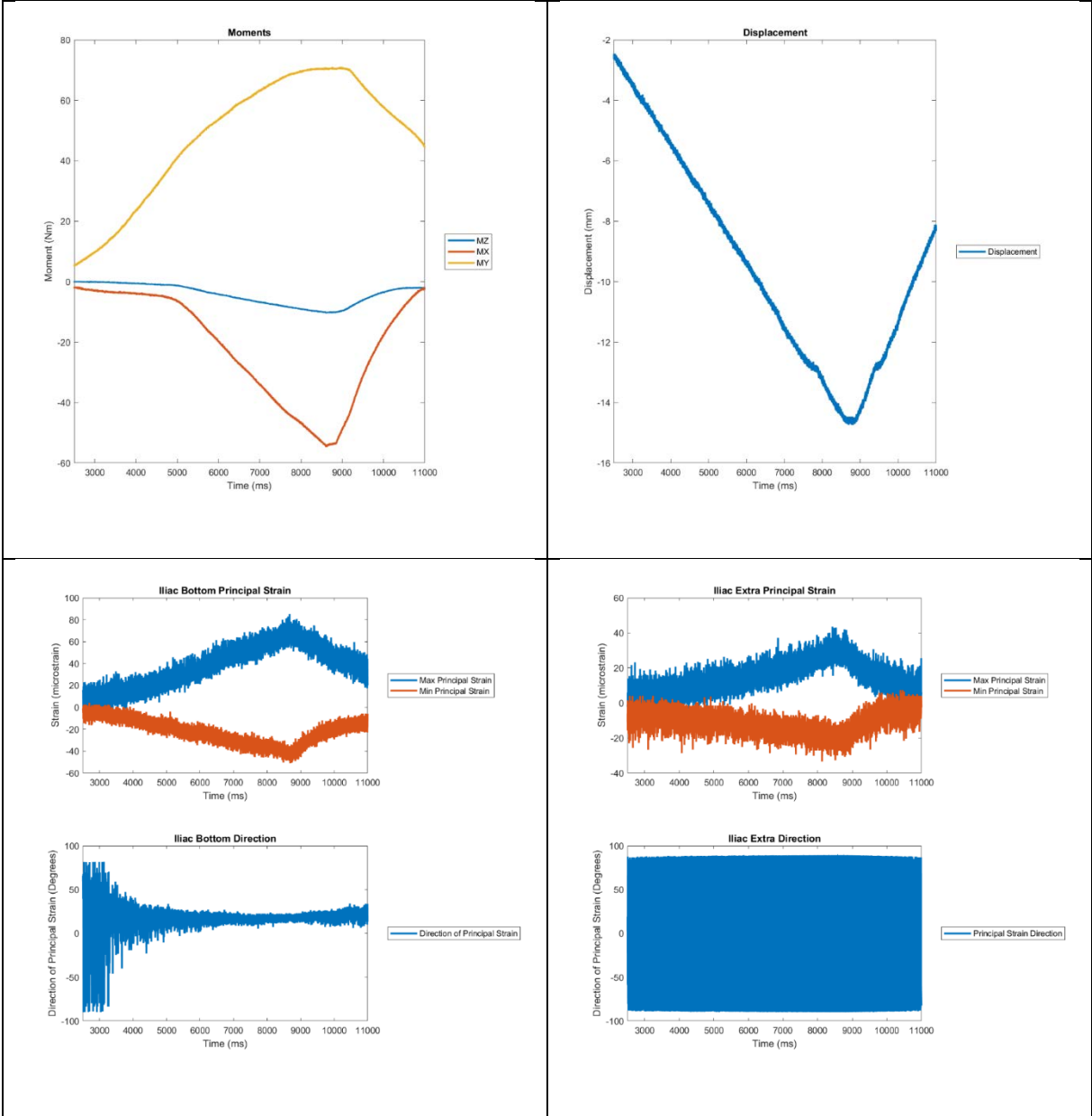
Table 8.6-5 - 990L 90 Degree Notch to Belt Angle Subinjurious Test Data
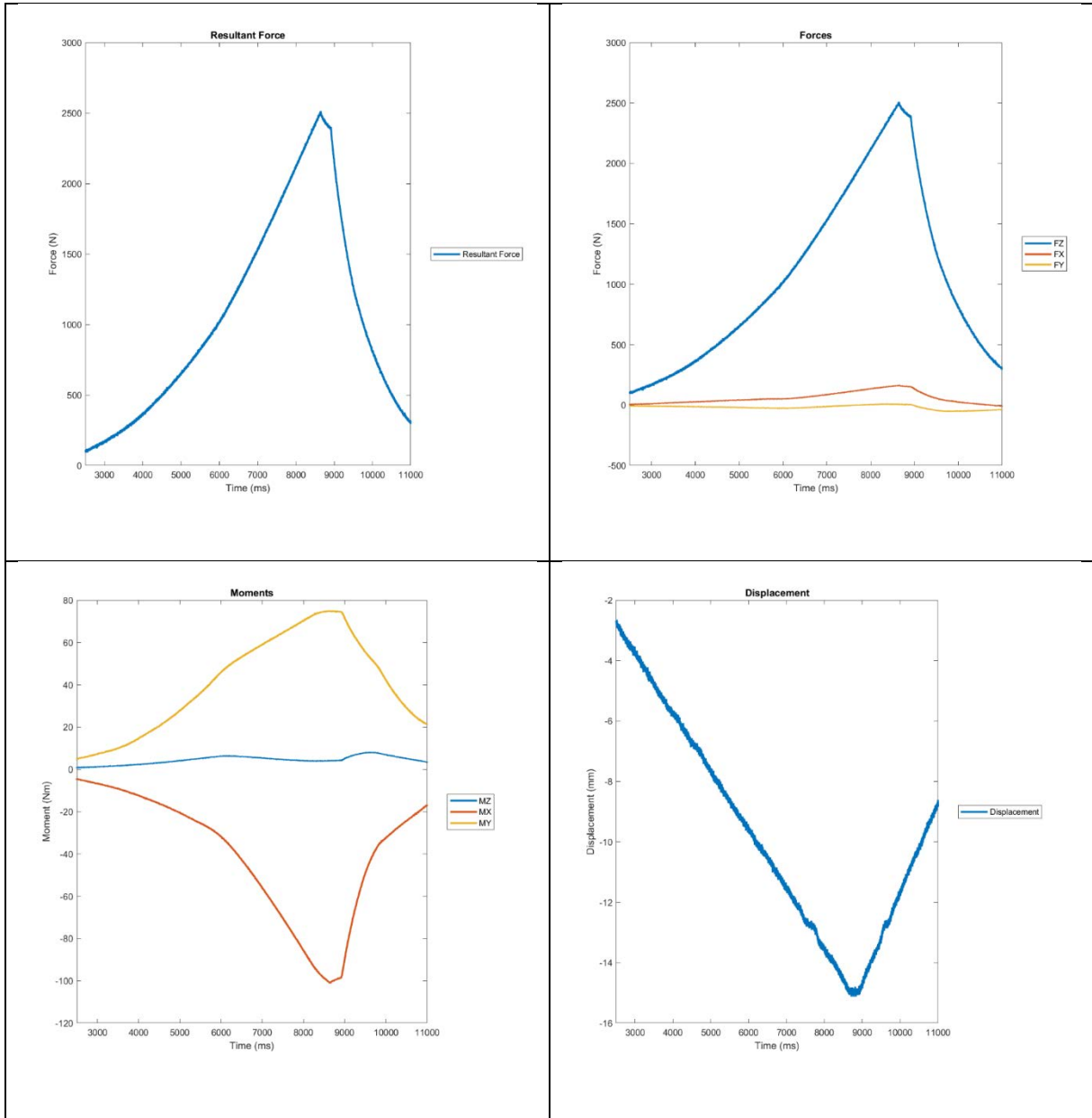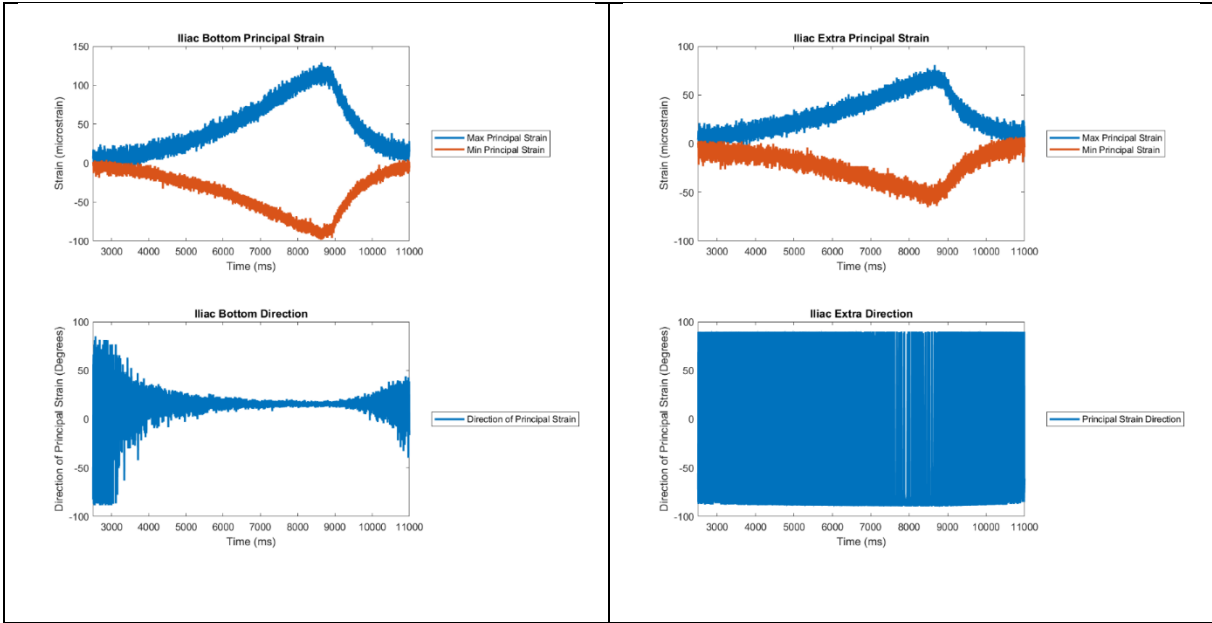
Table 8.6-6 - 990R 0 Degree Roll Angle Subinjurious Test Data
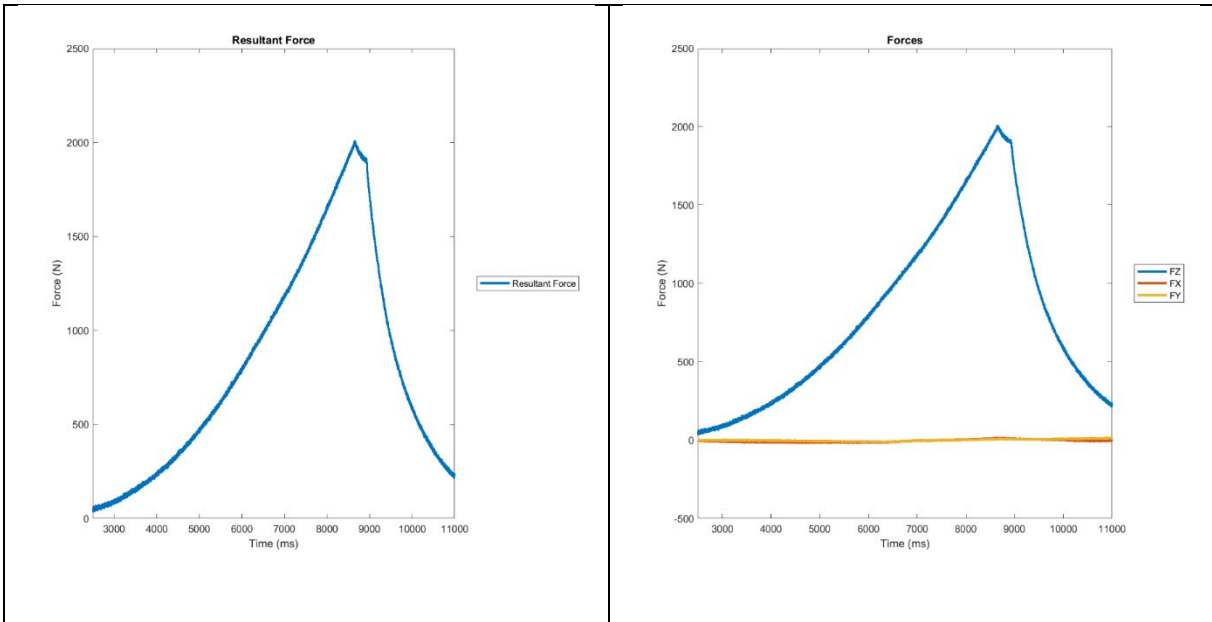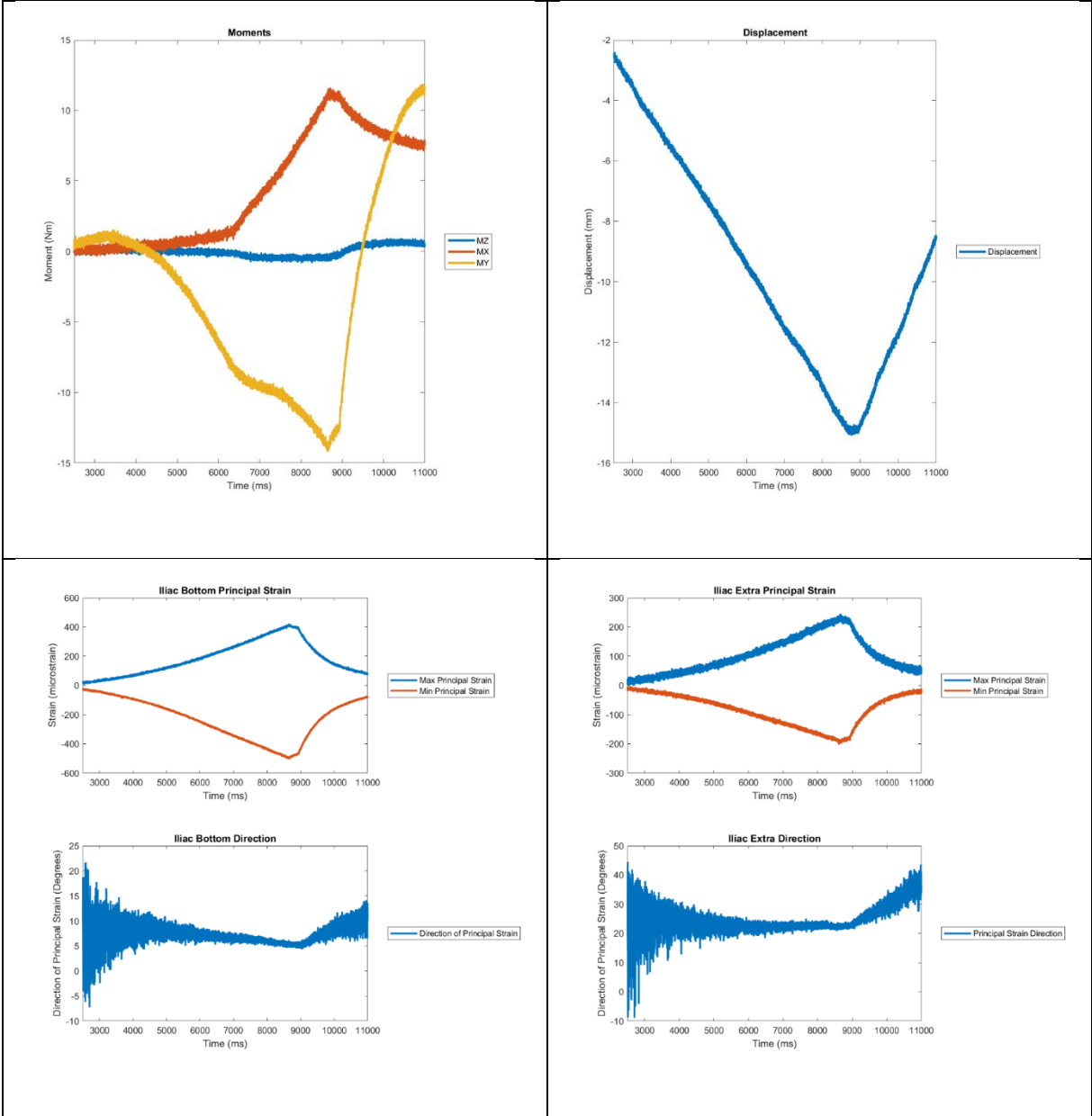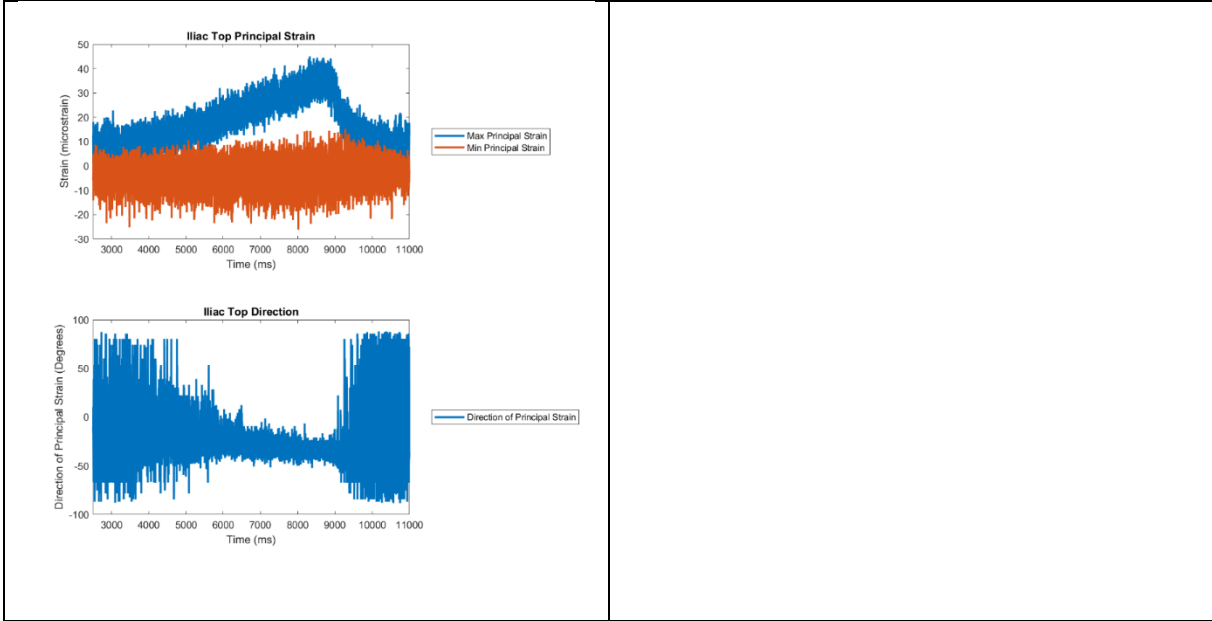
Table 8.6-7 - 990R +10 Degree Roll Angle Subinjurious Test Data
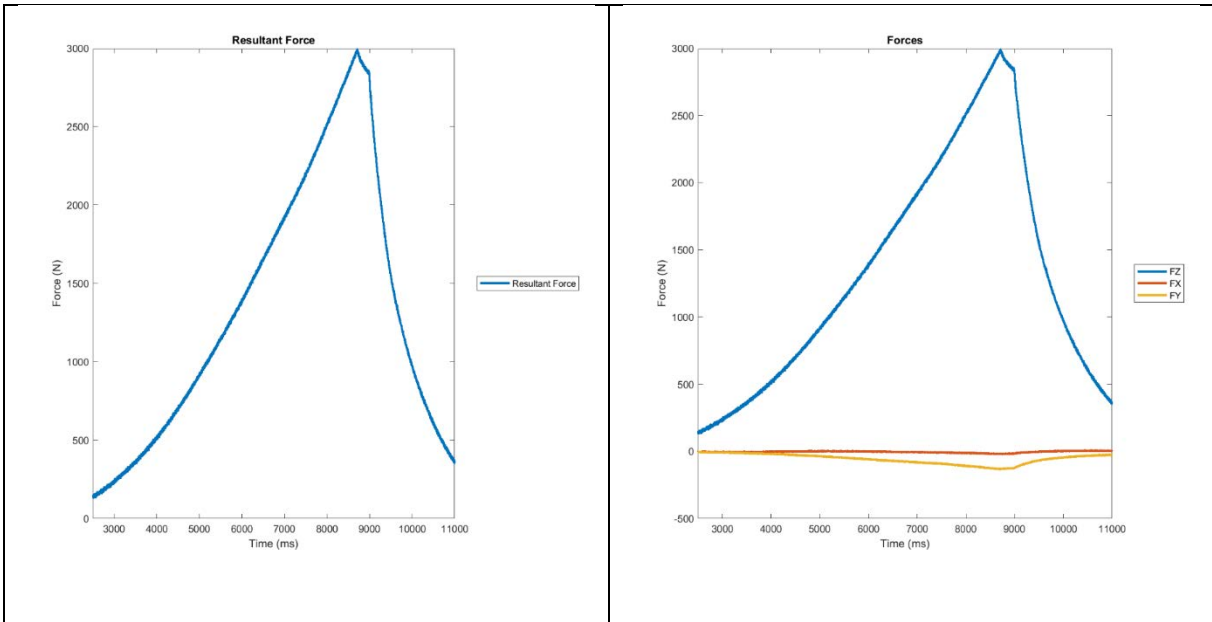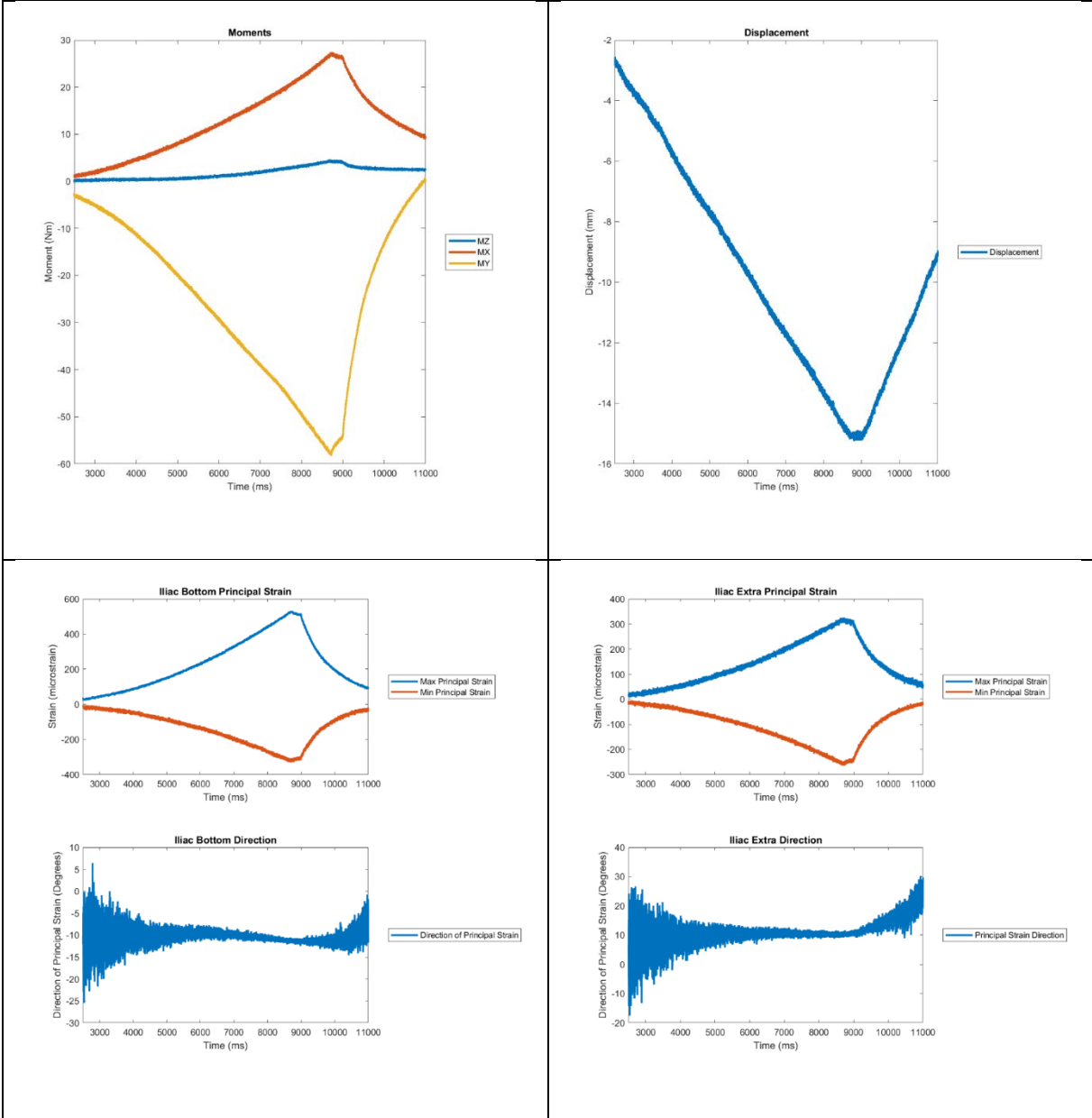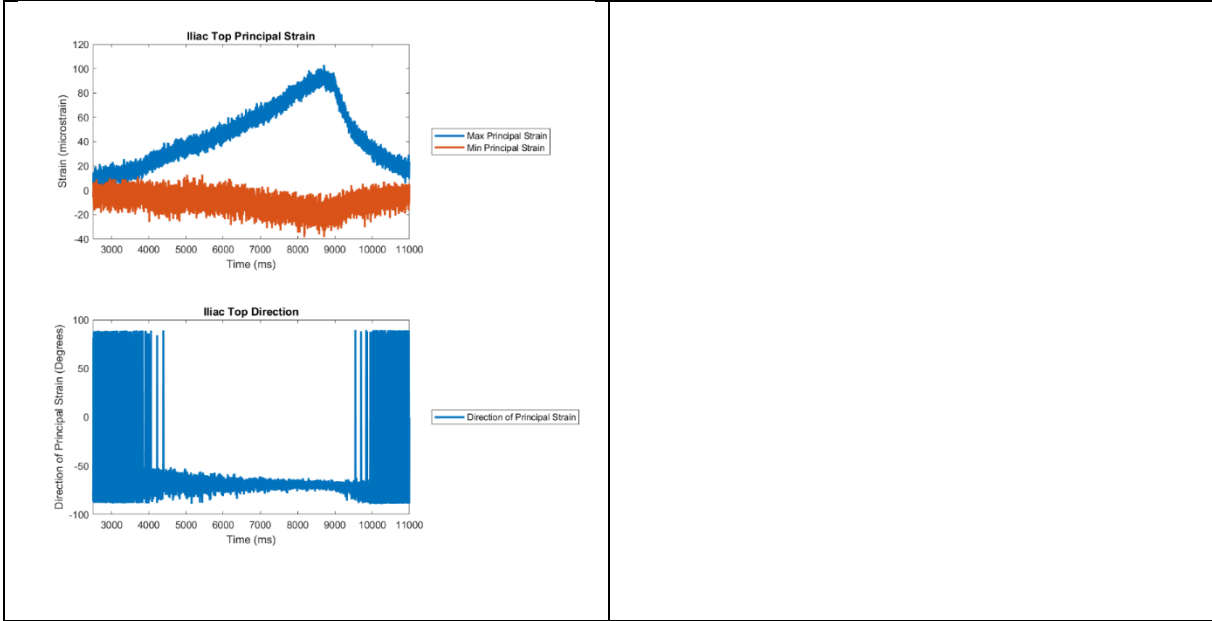
Table 8.6-8 - 990R -10 Degree Roll Angle Subinjurious Test Data
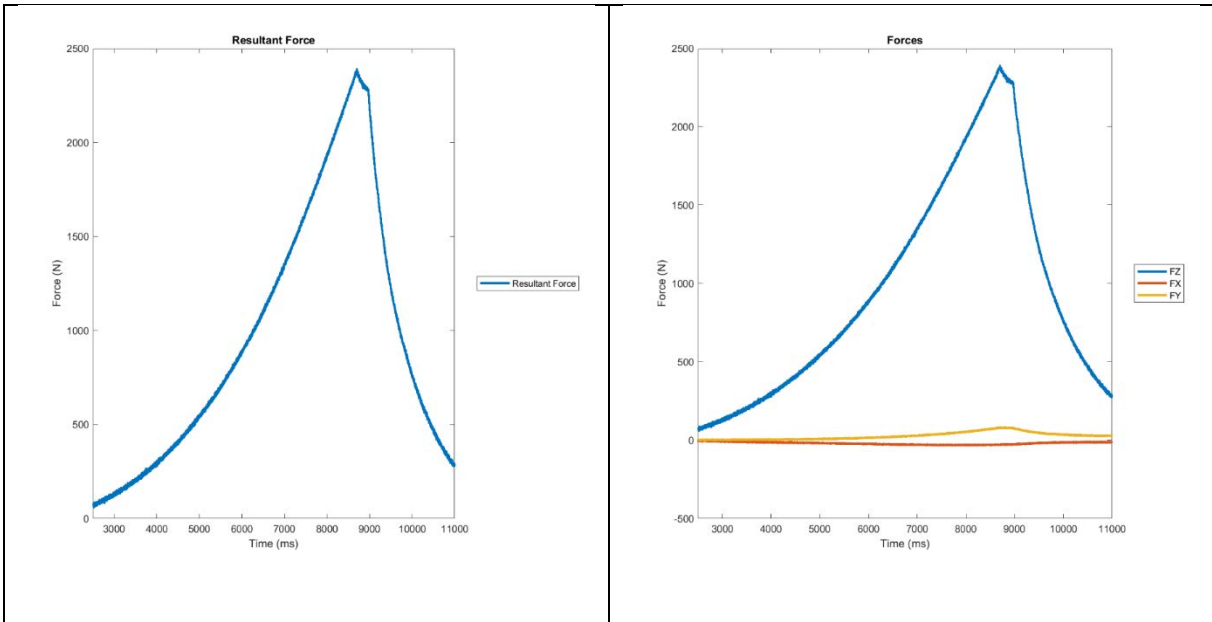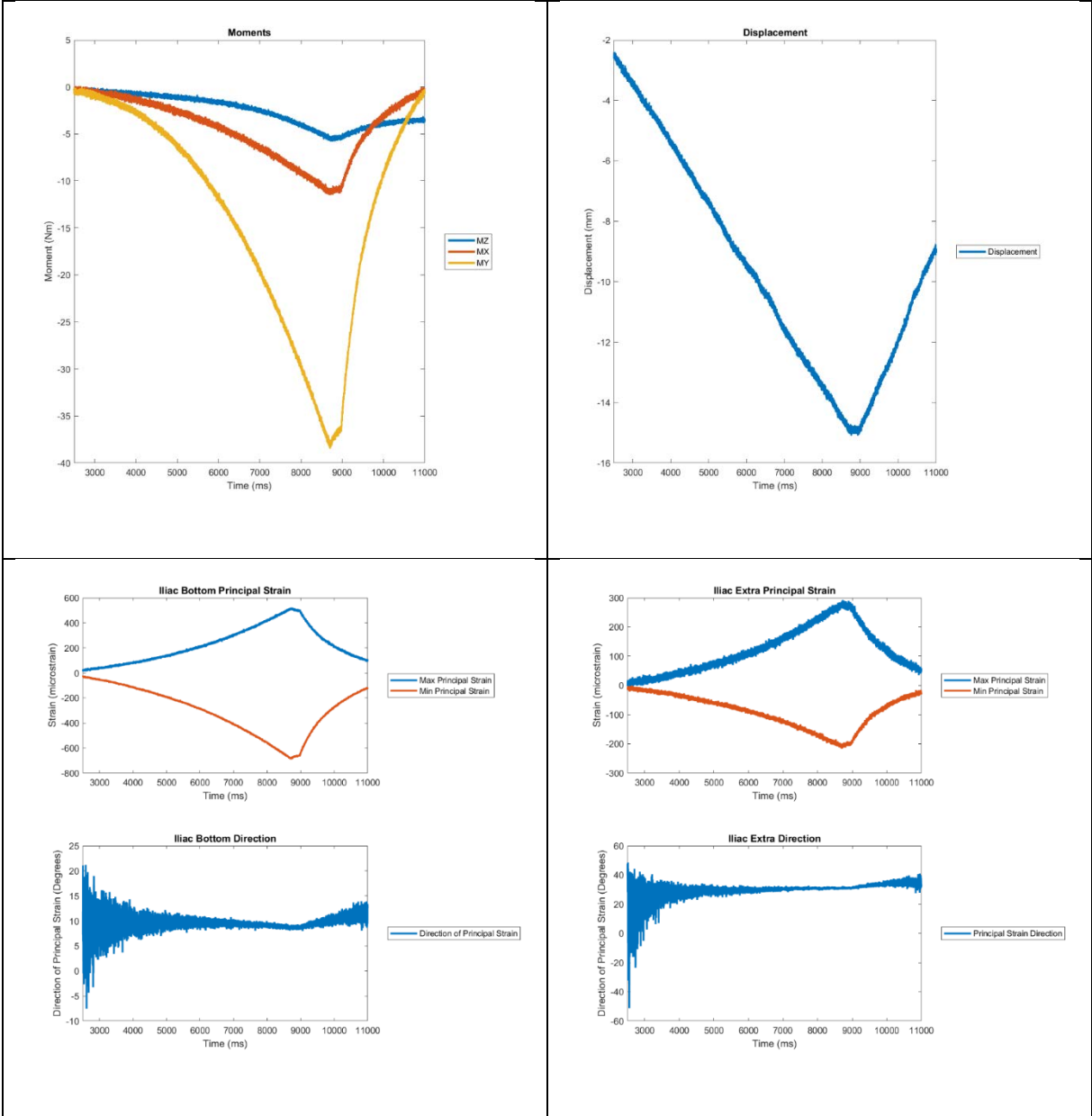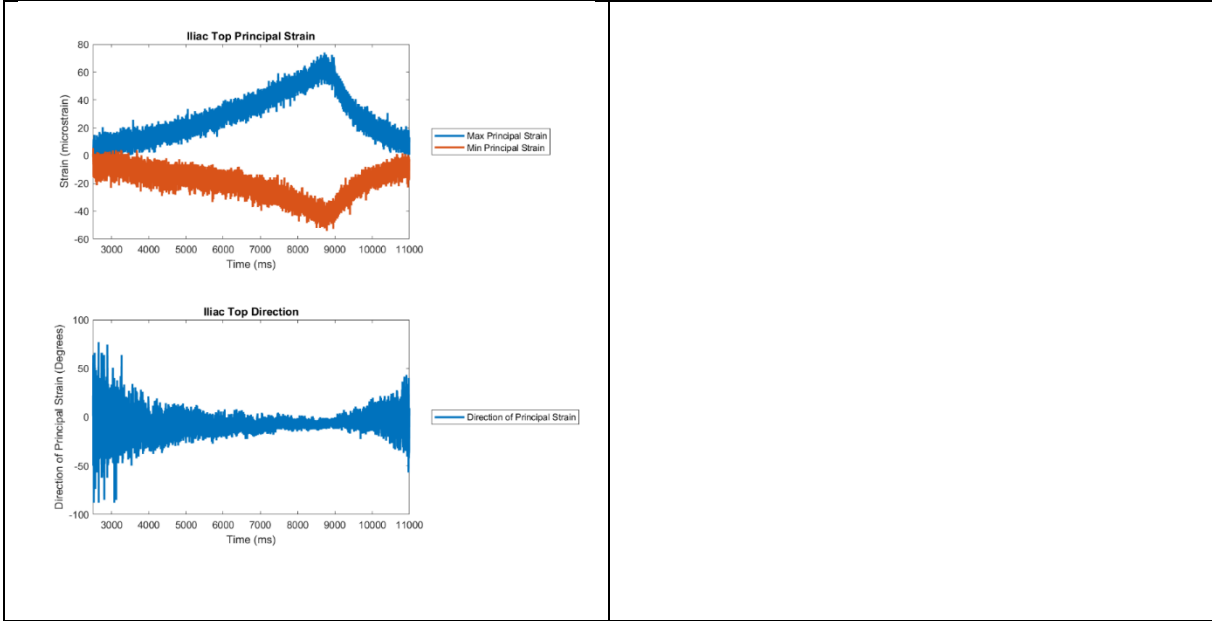
Table 8.6-9 - 990R 90 Degree Notch to Belt Angle Subinjurious Test Data
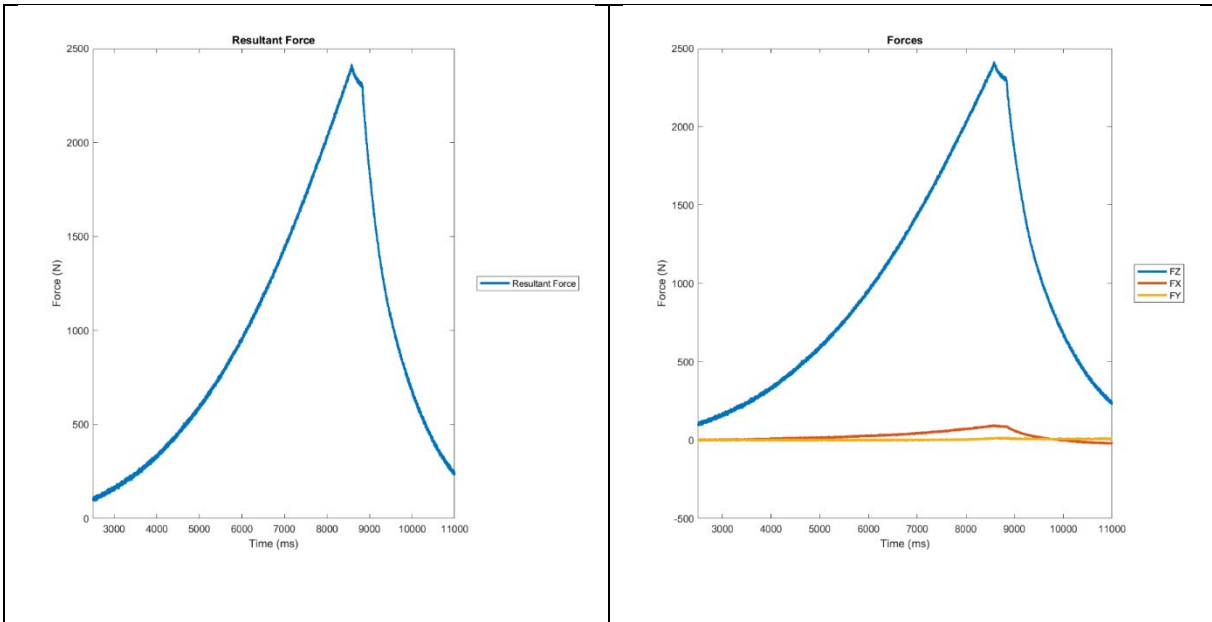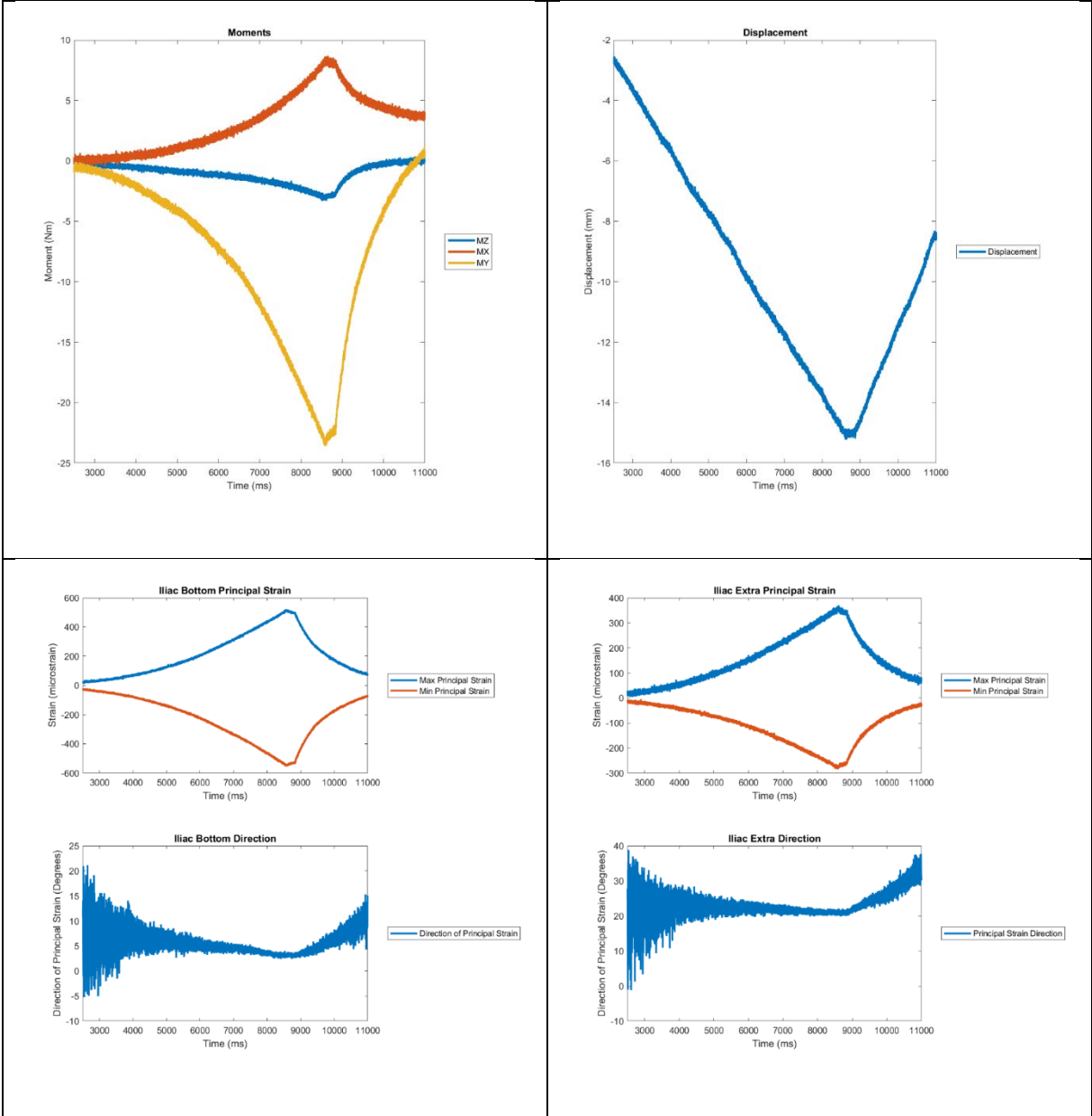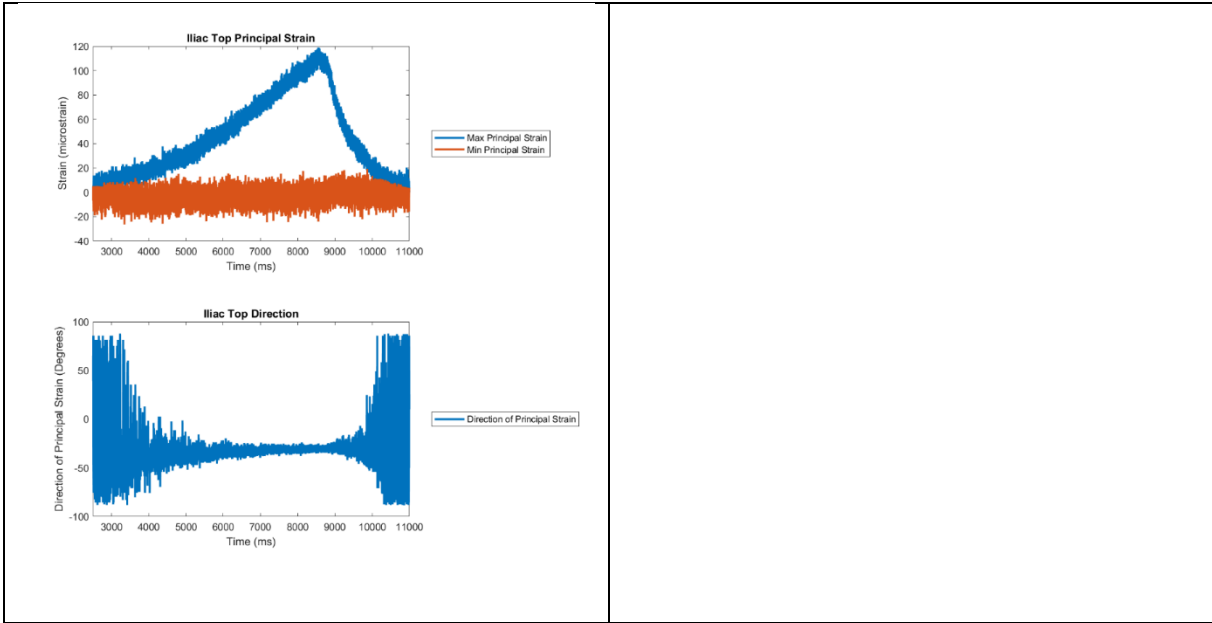
Table 8.6-10 - 990R 75 Degree Notch to Belt Angle Subinjurious Test Data

158
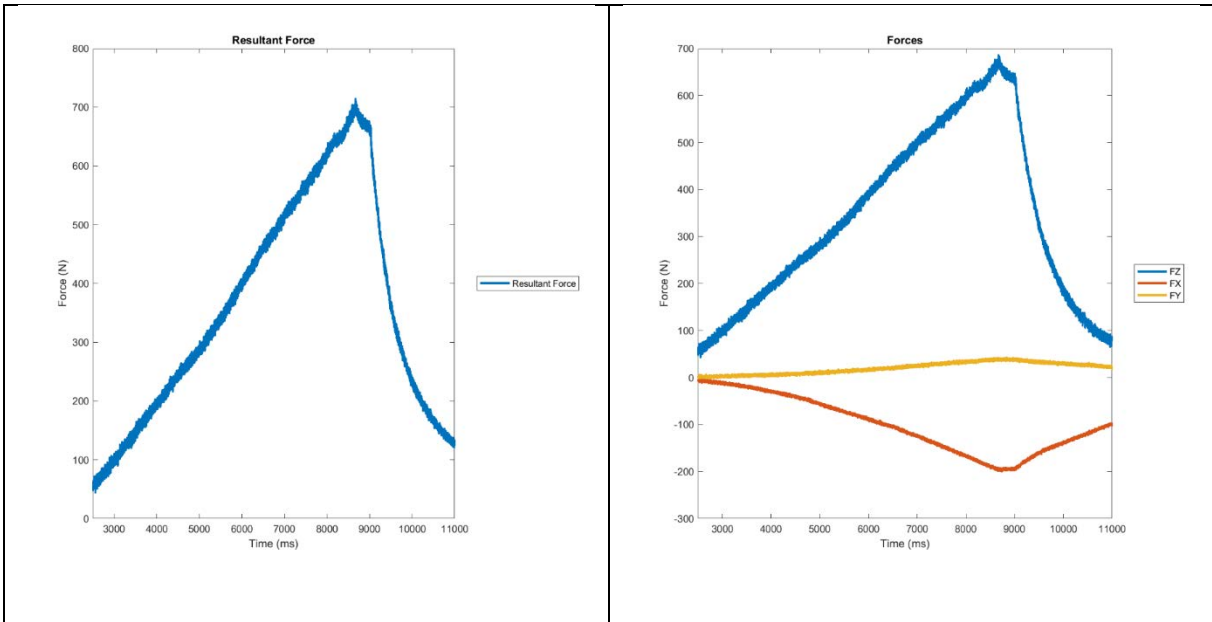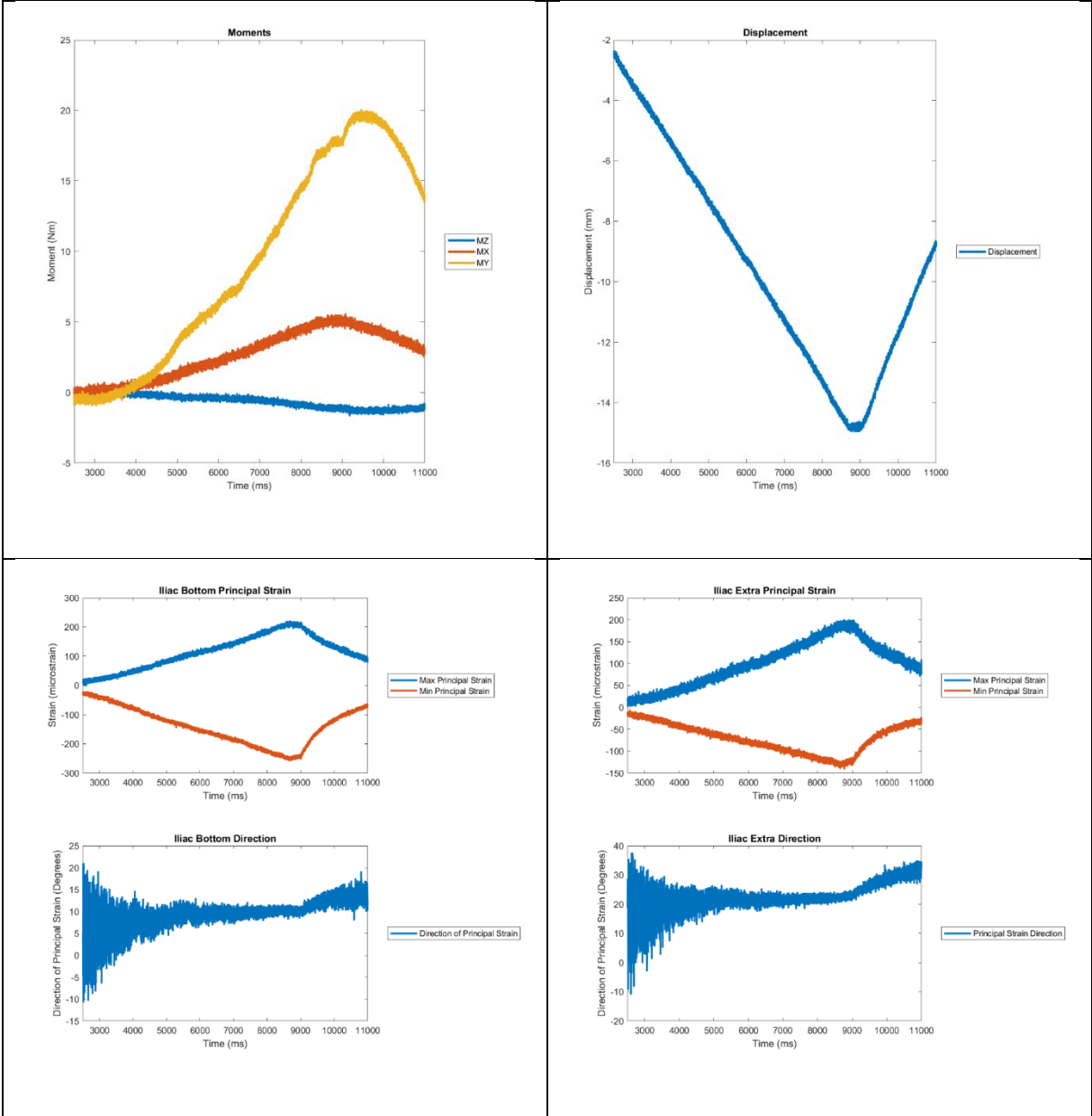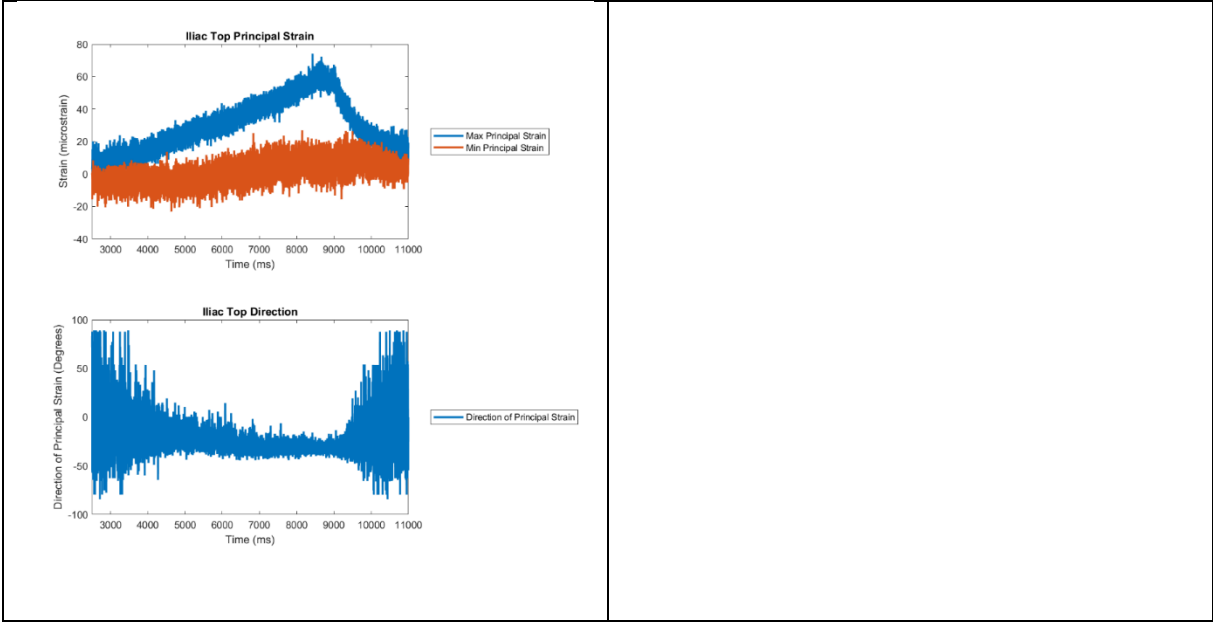
Table 8.6-11 - 990R Injurious Test Data
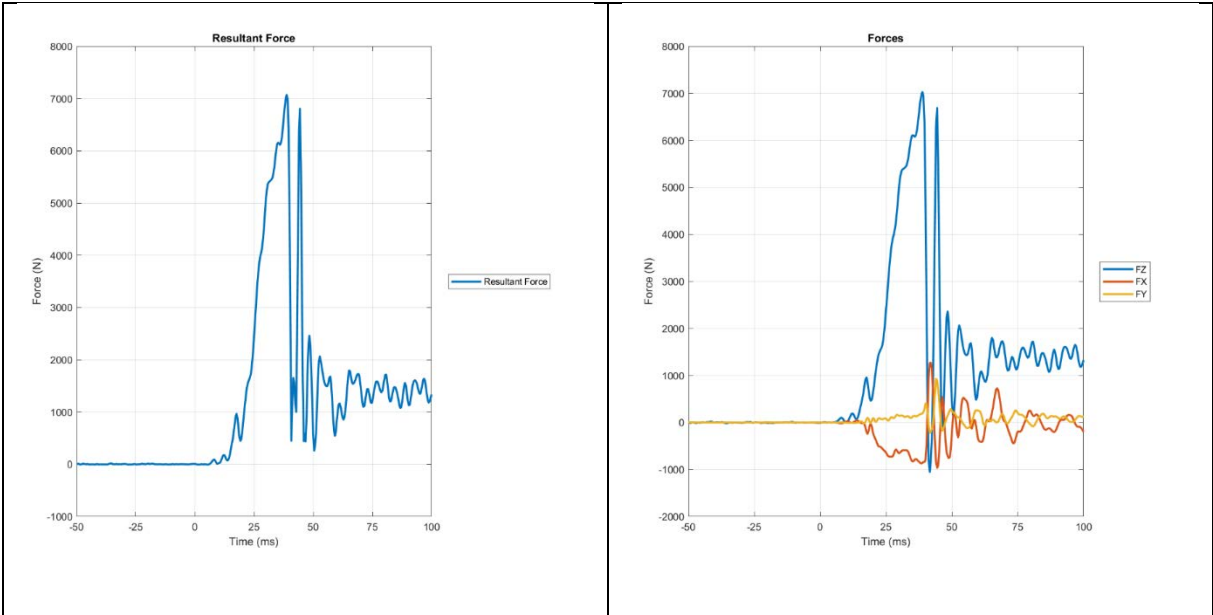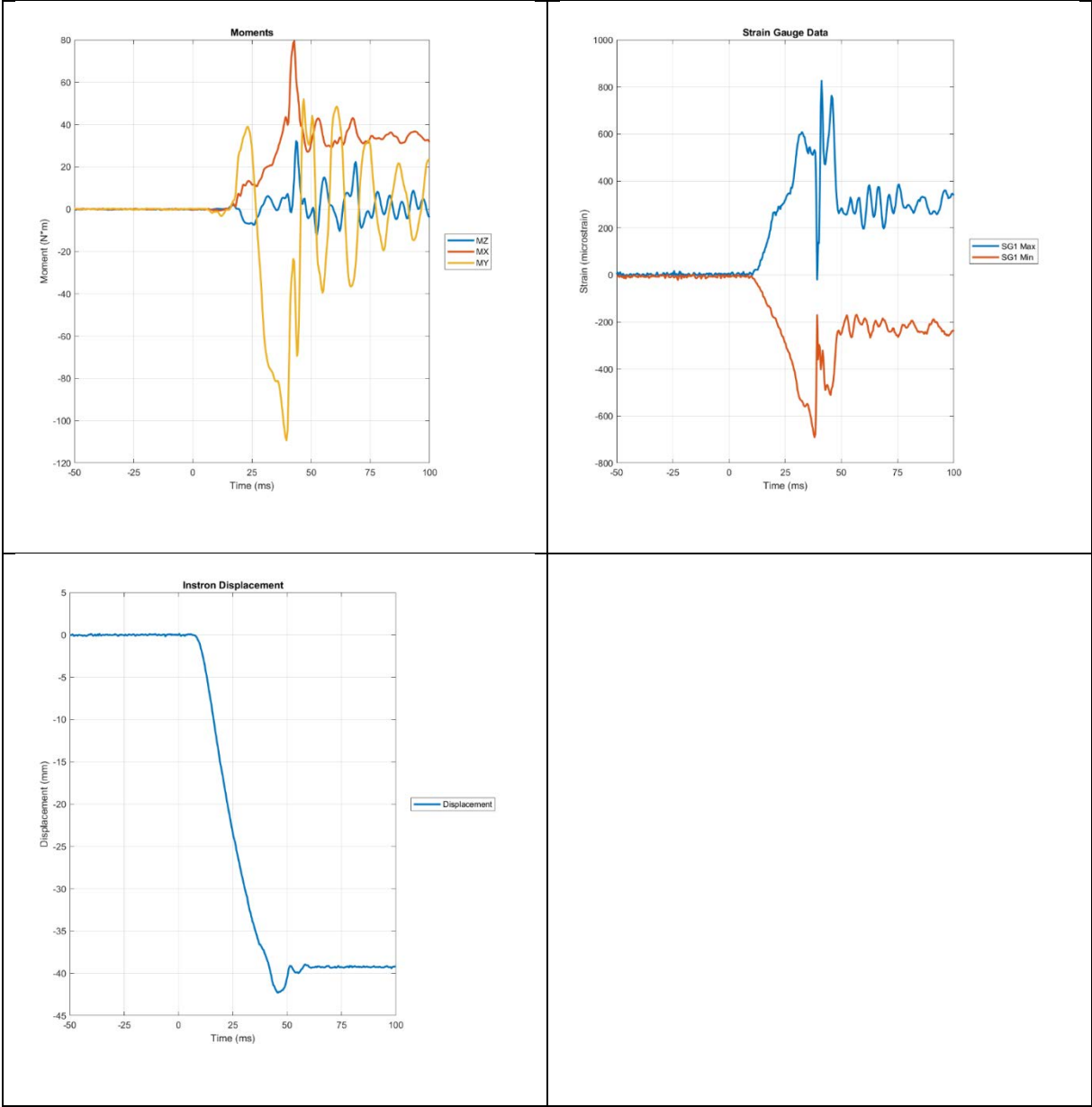
Table 8.6-12 - 990L Injurious Test Data
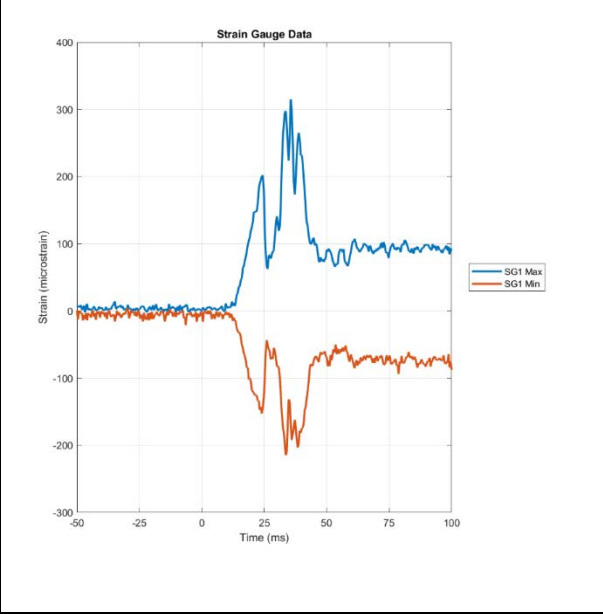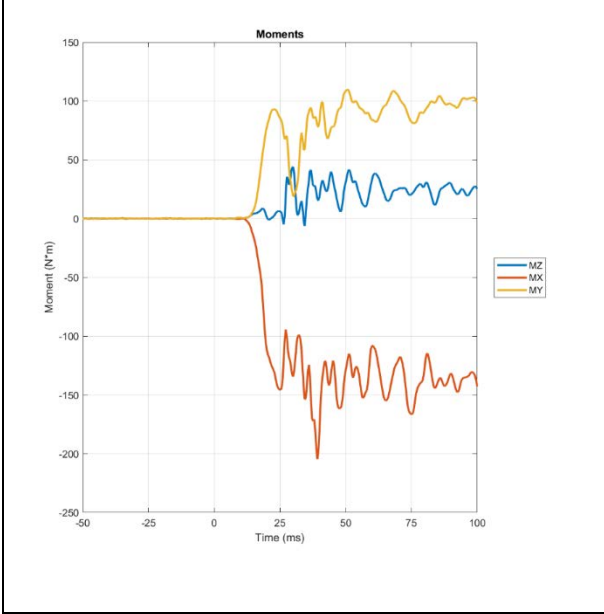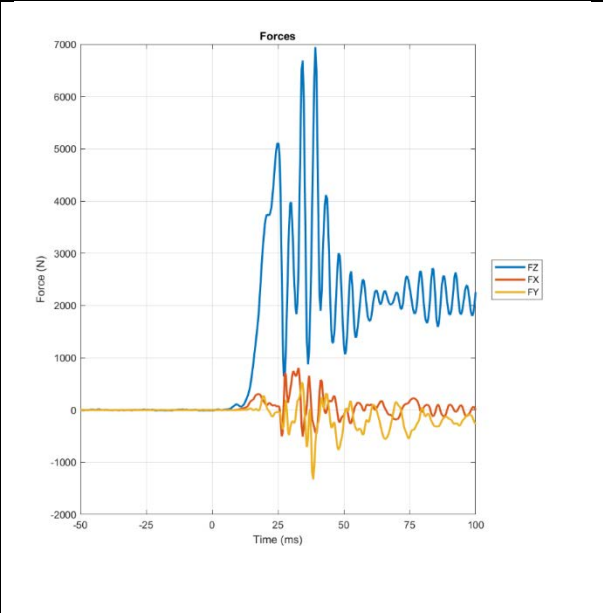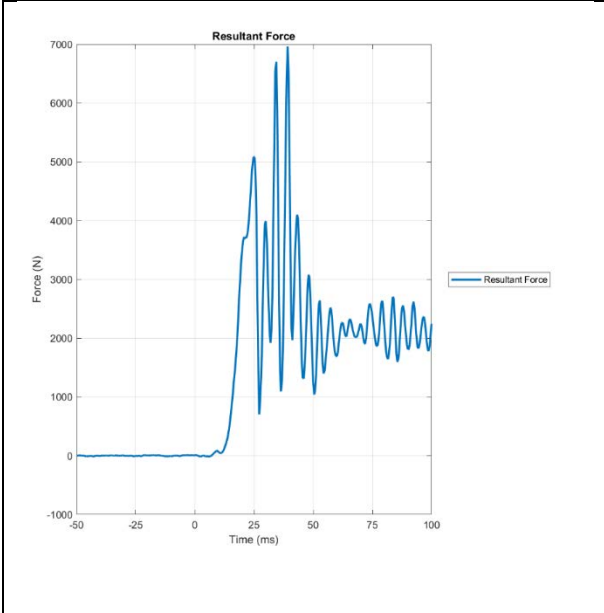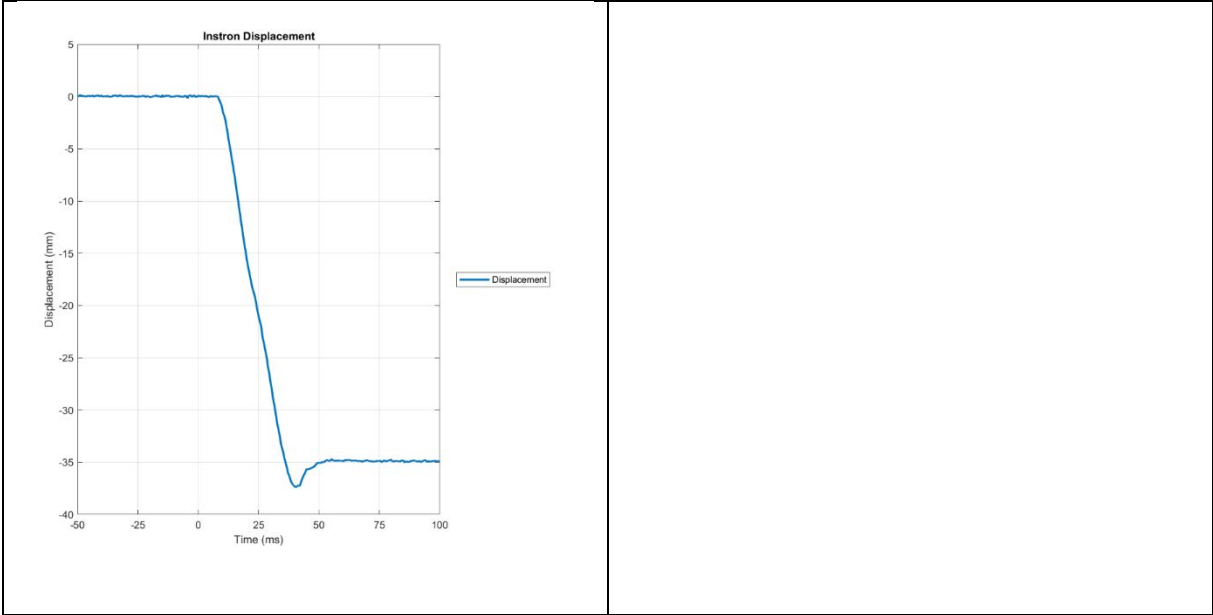
Table 8.6-13 – 714L Test Data
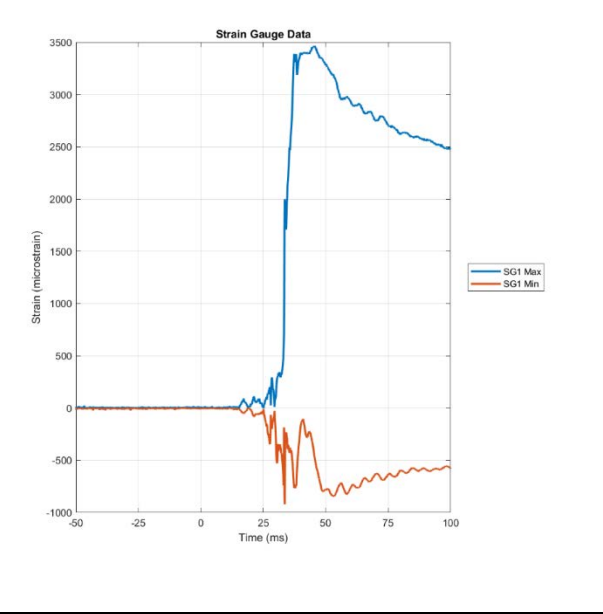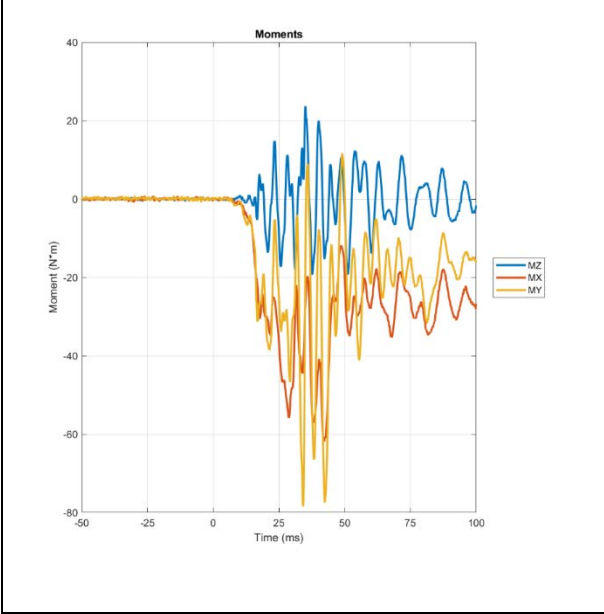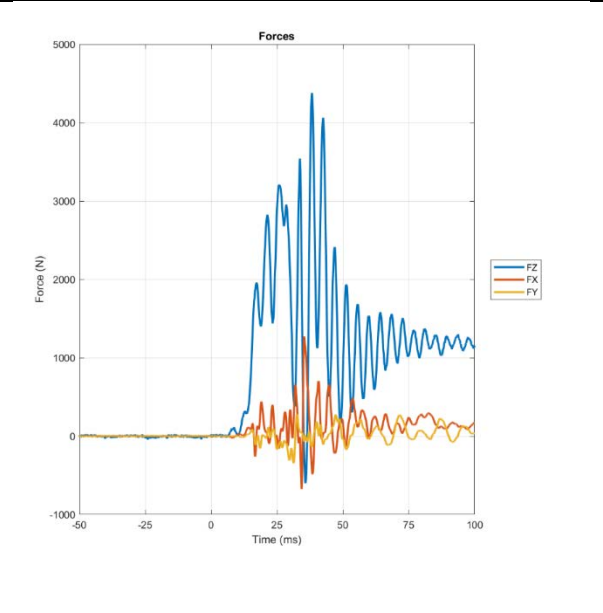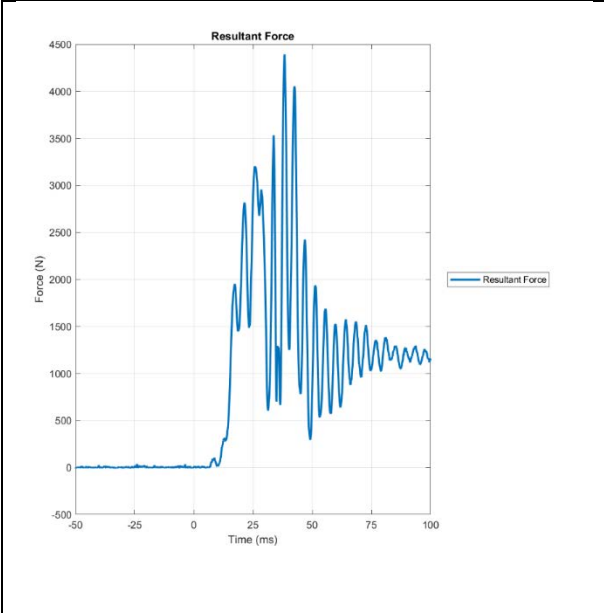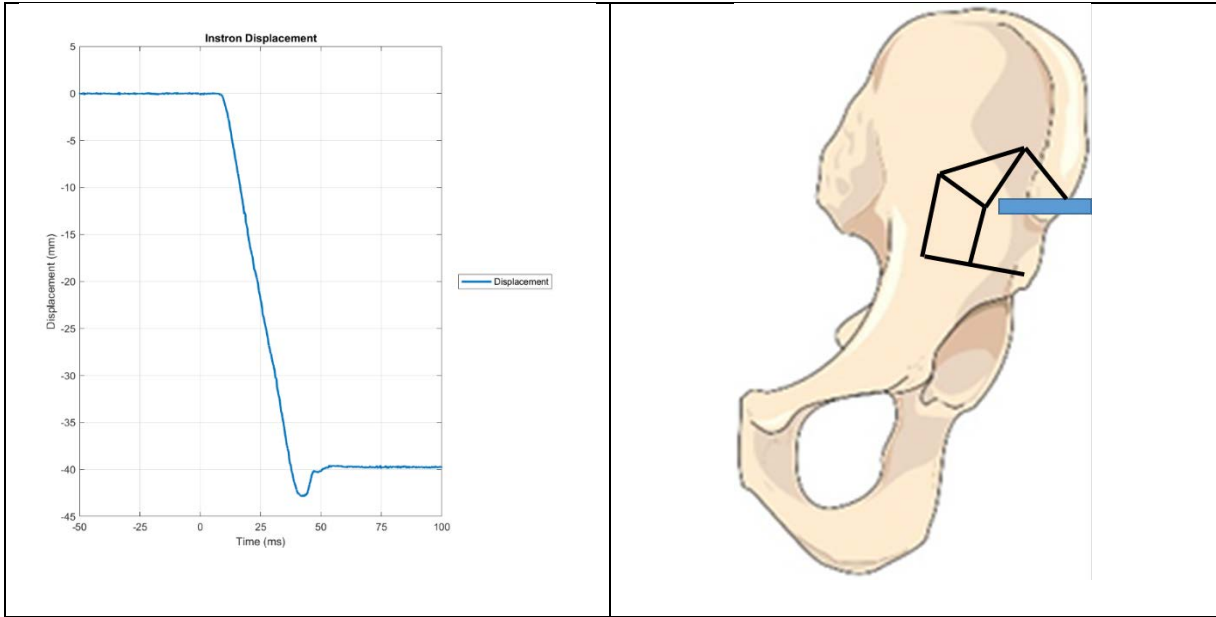
Table 8.6-14 - 714R Test Data
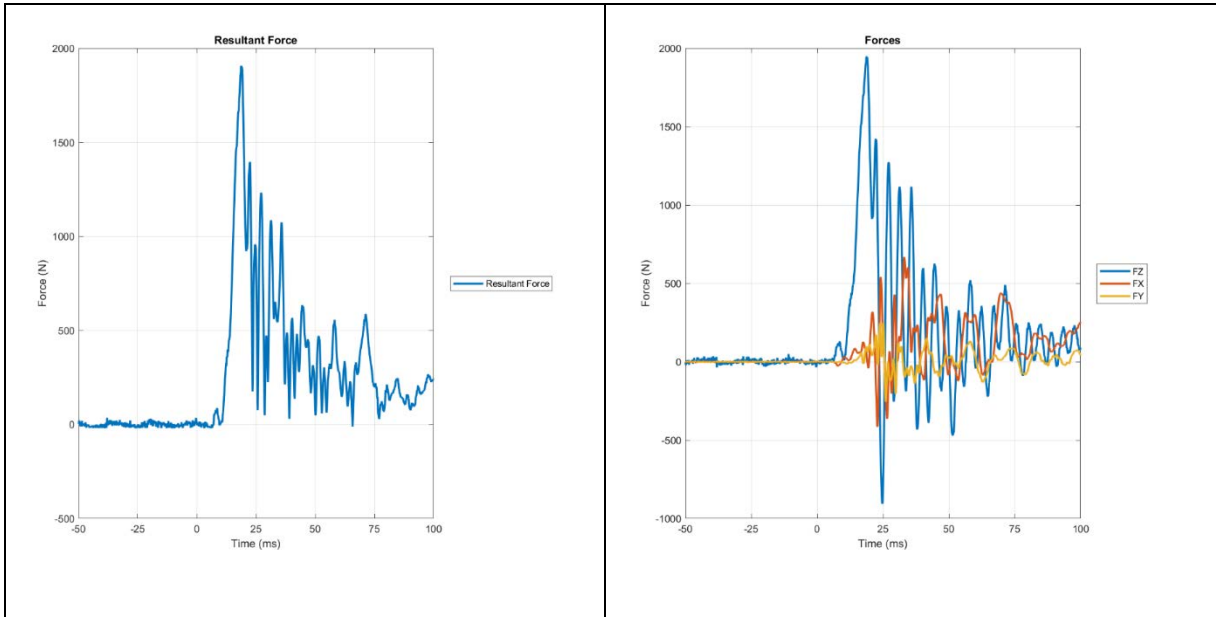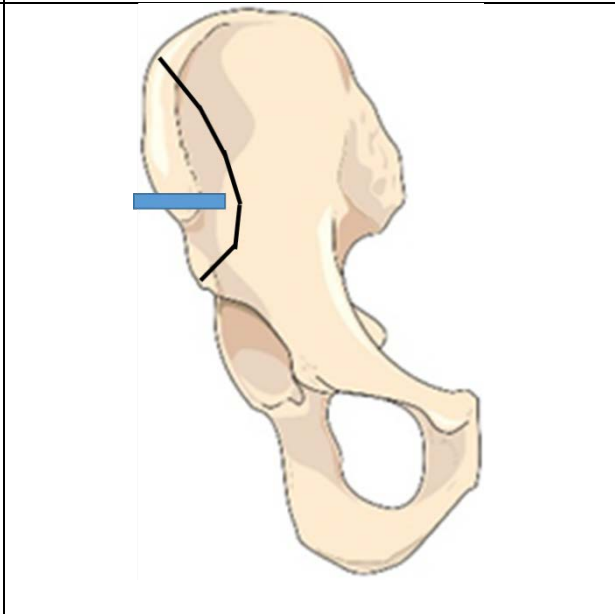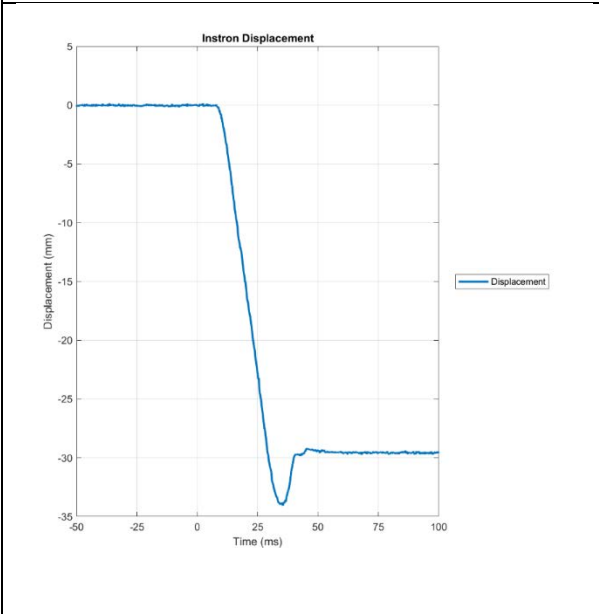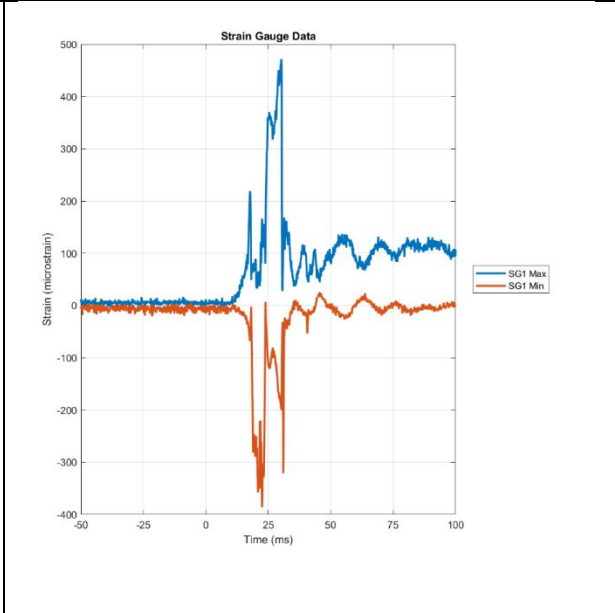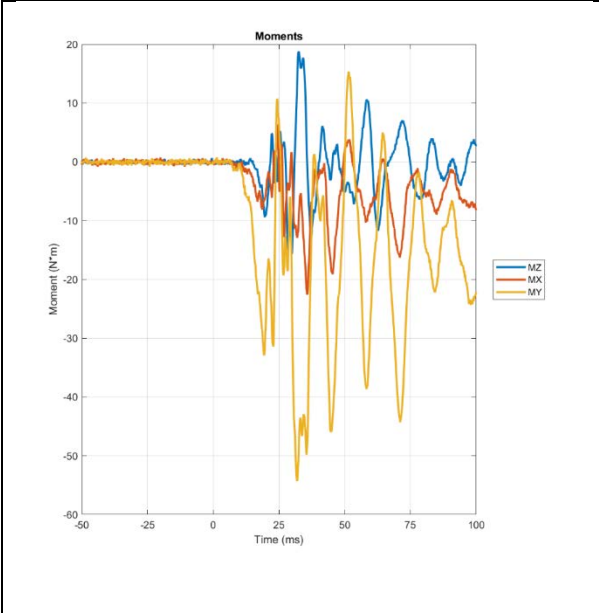
Table 8.6-15 - 715L Test Data
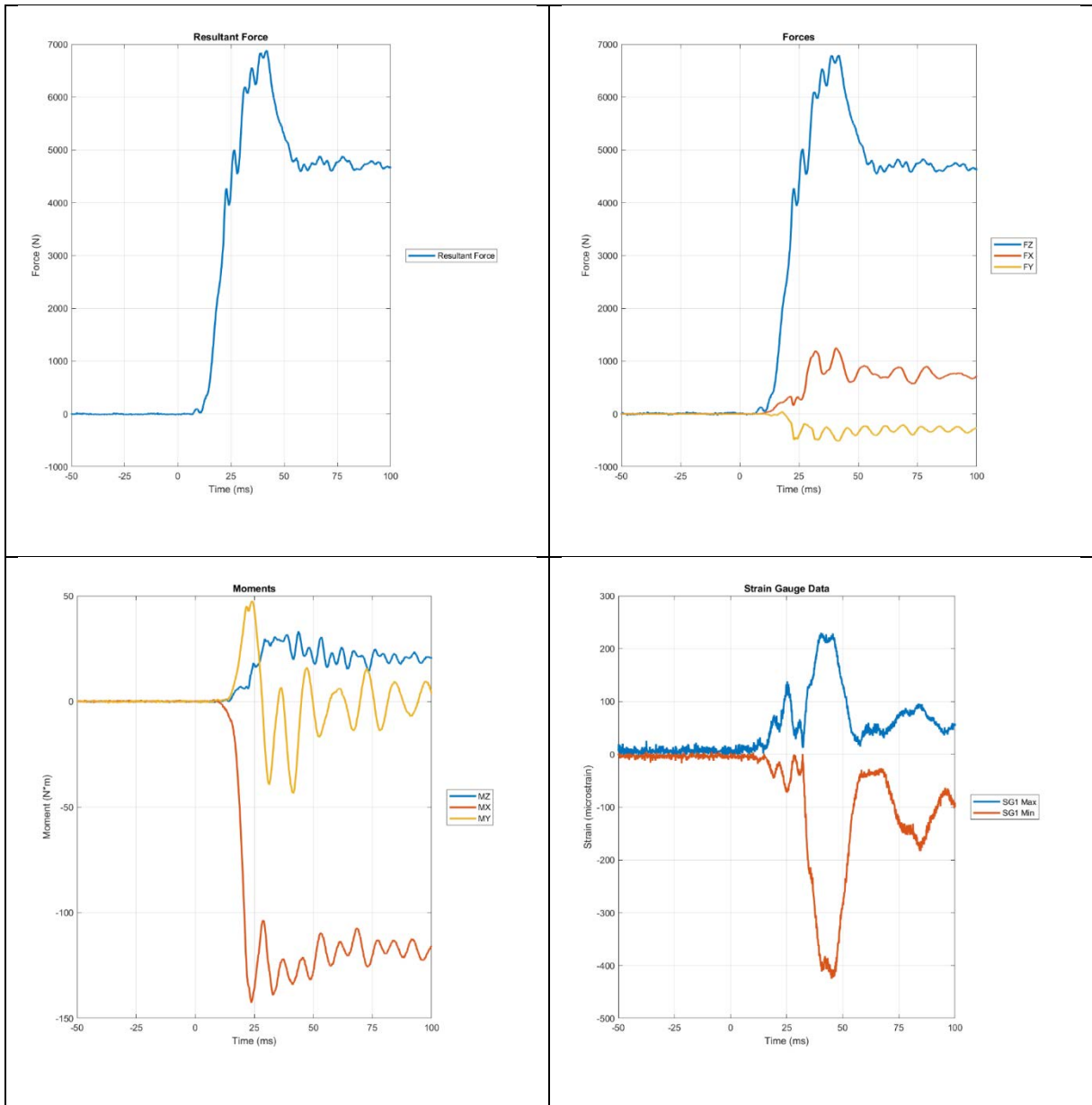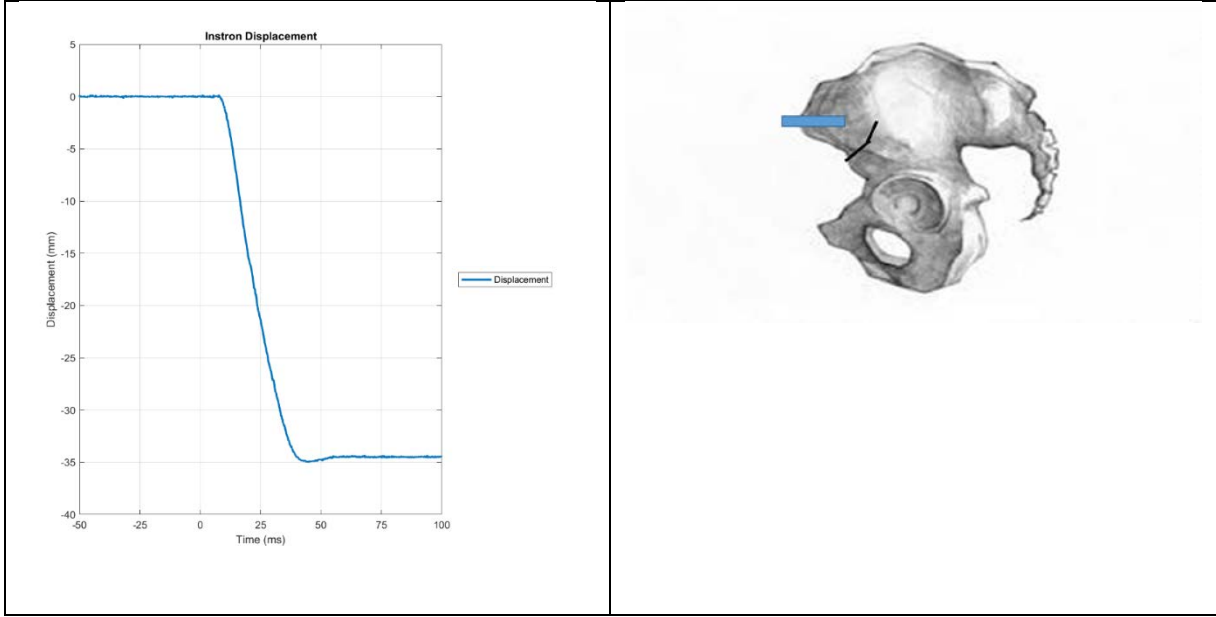
Table 8.6-16 - 715R Test Data
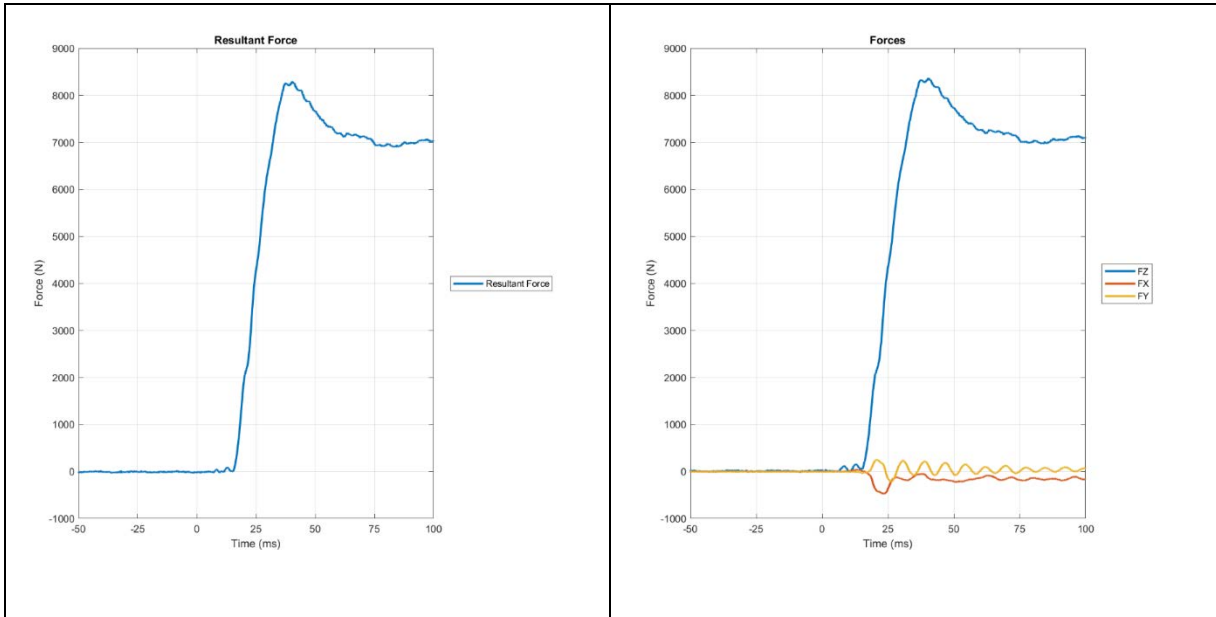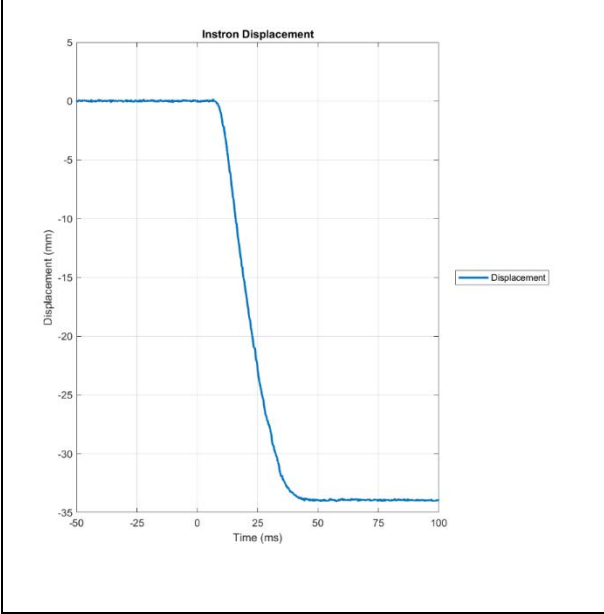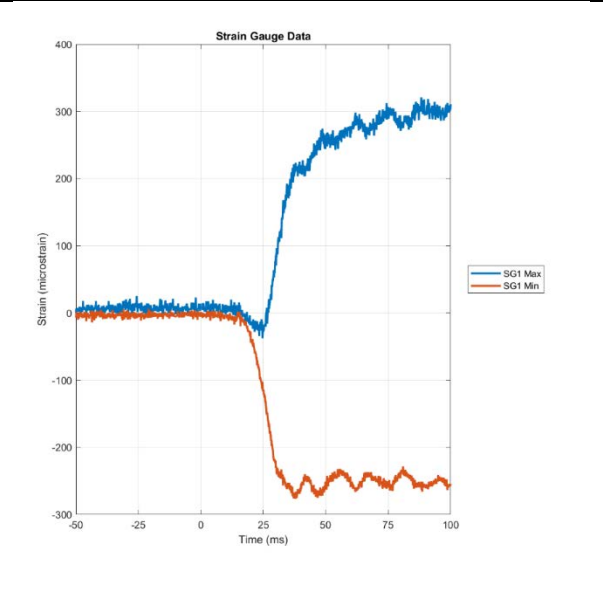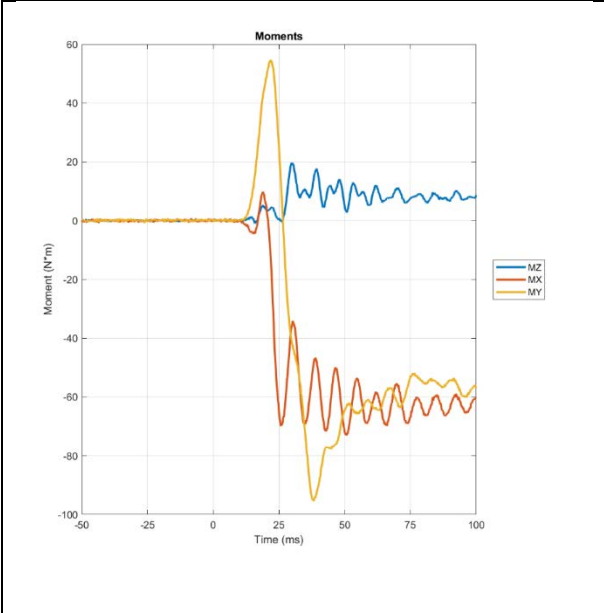
Table 8.6-17 - 713L Test Data
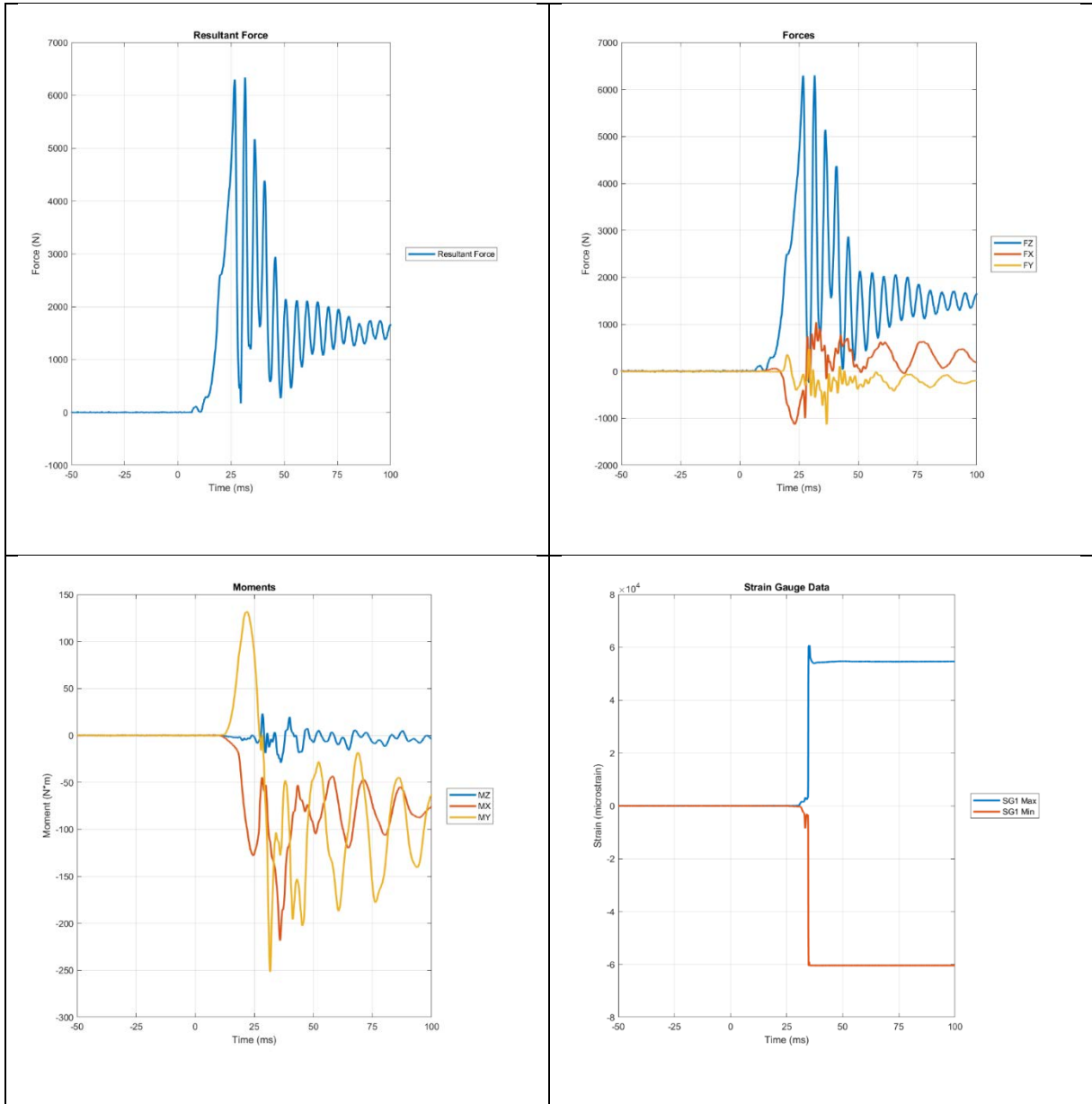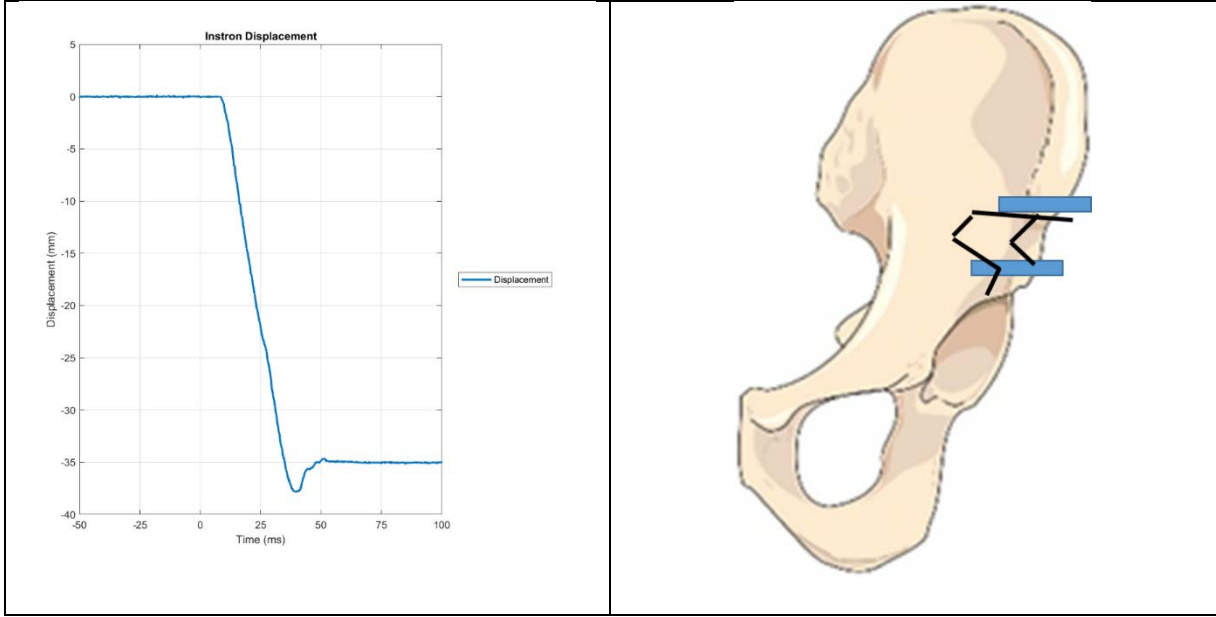
Table 8.6-18 - 713R Test Data
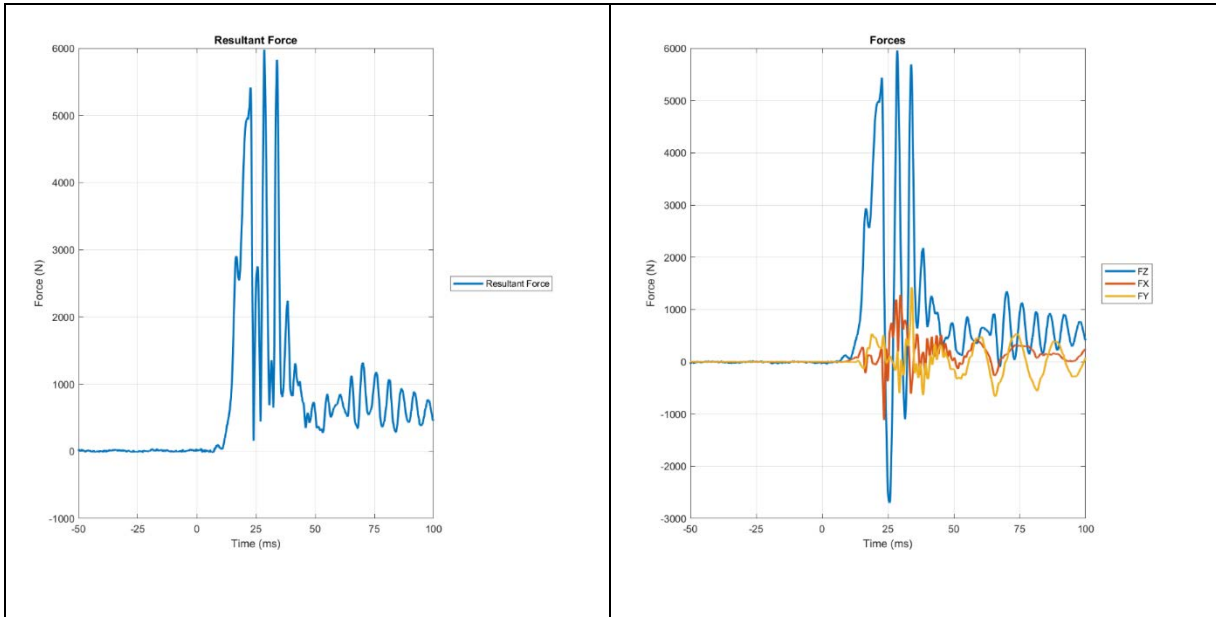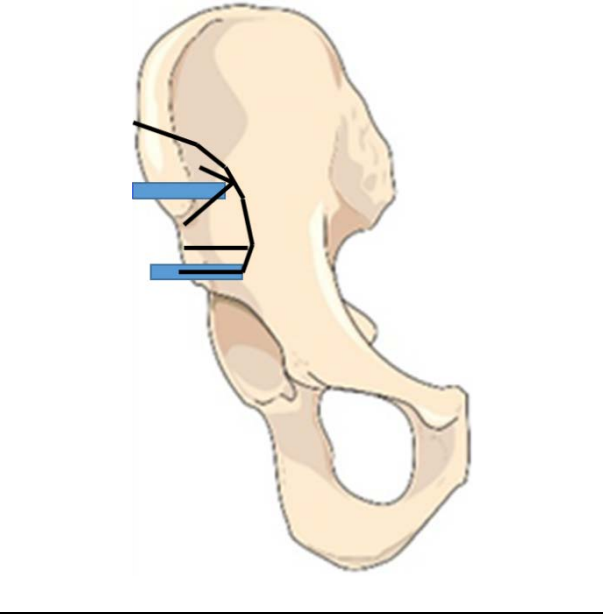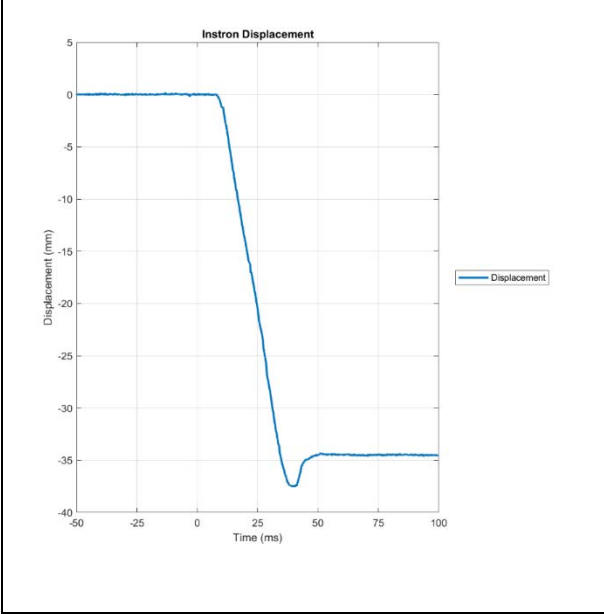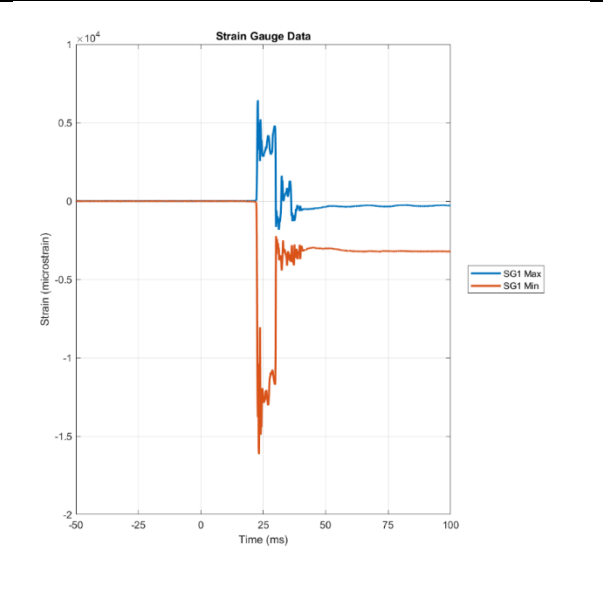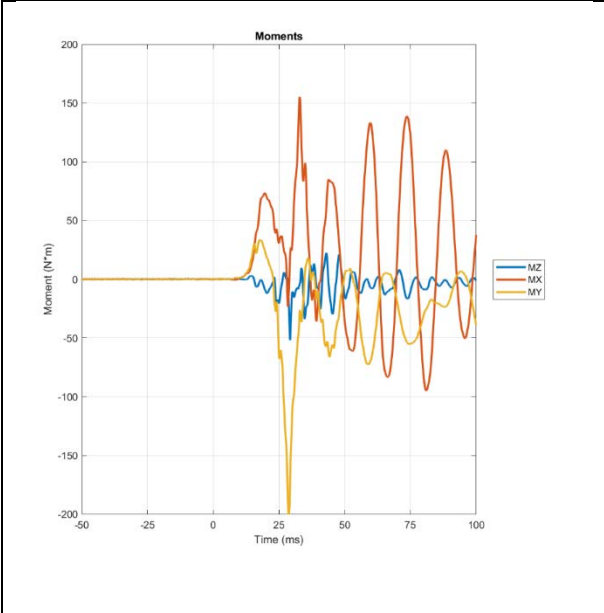
Table 8.6-19 - 716L Test Data
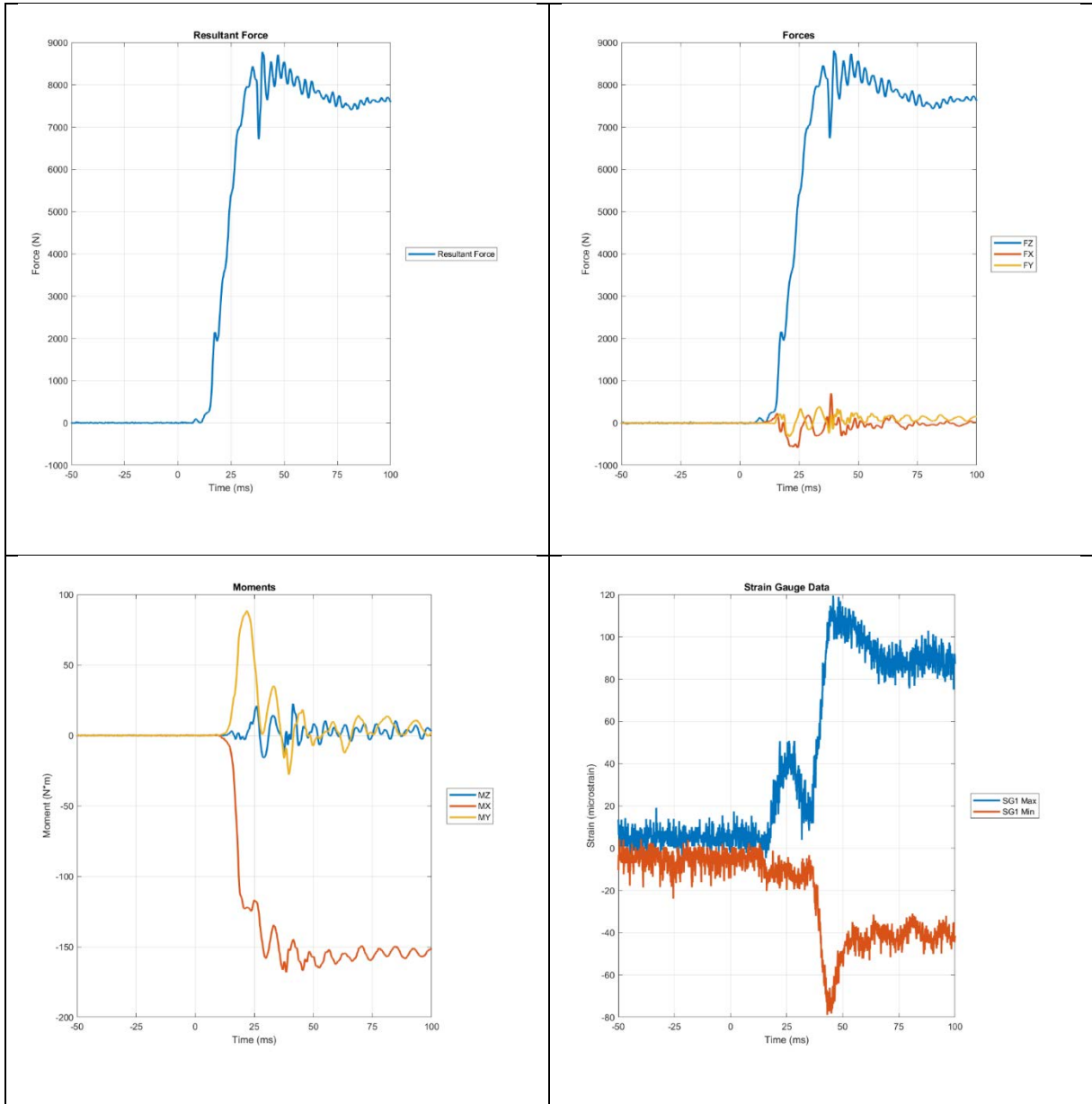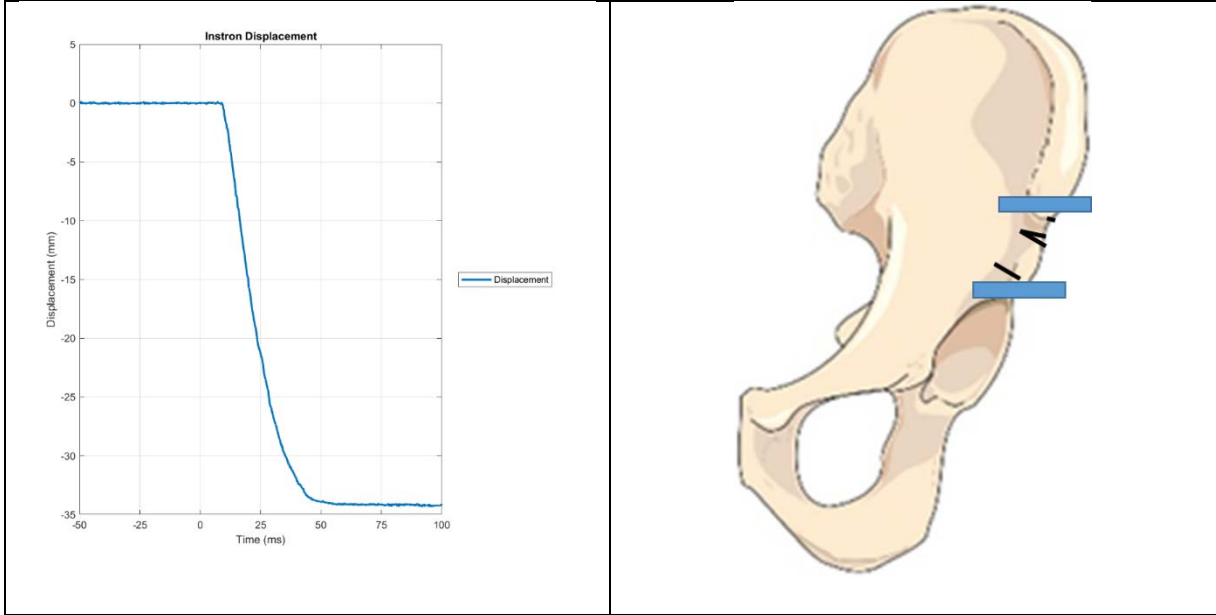
Table 8.6-20 - 716R Test Data
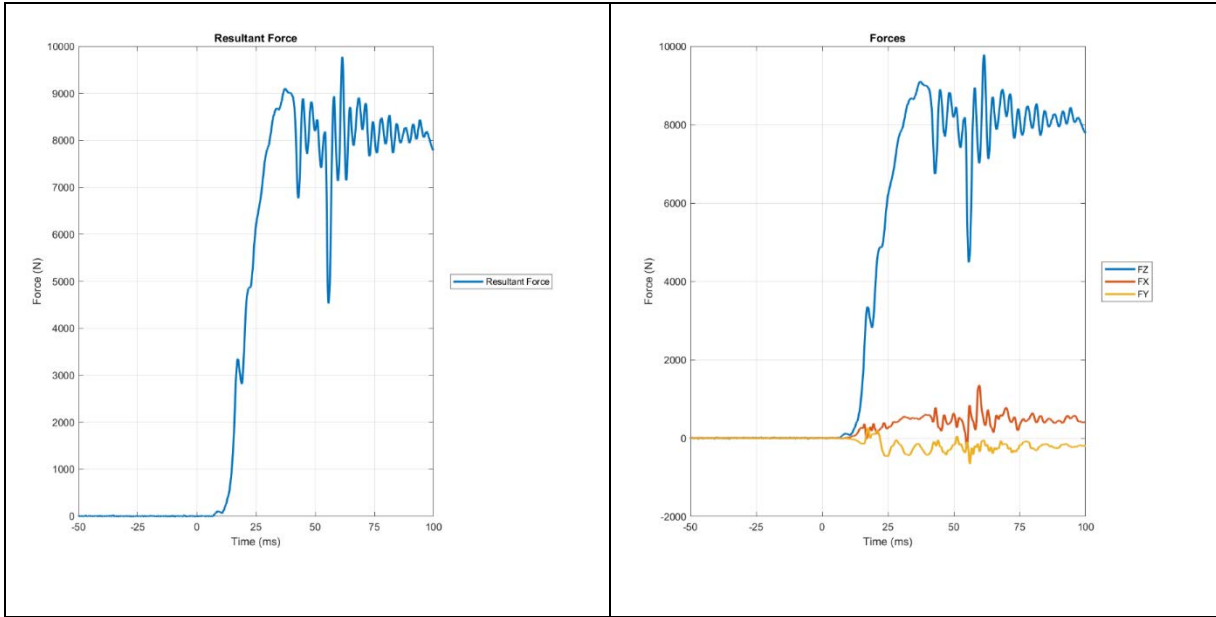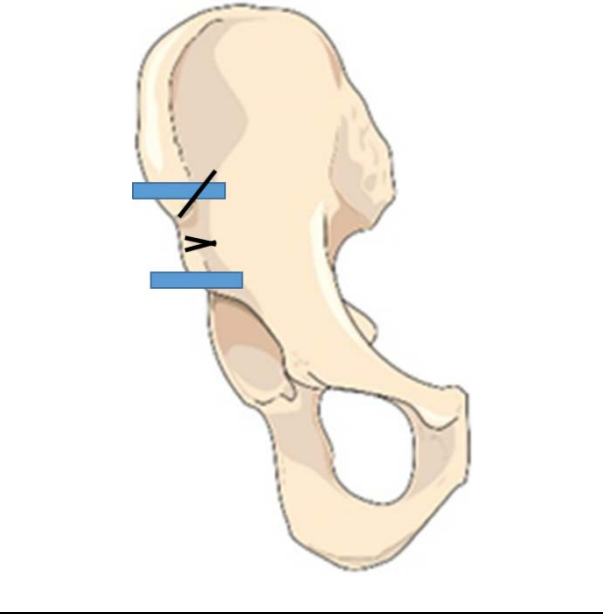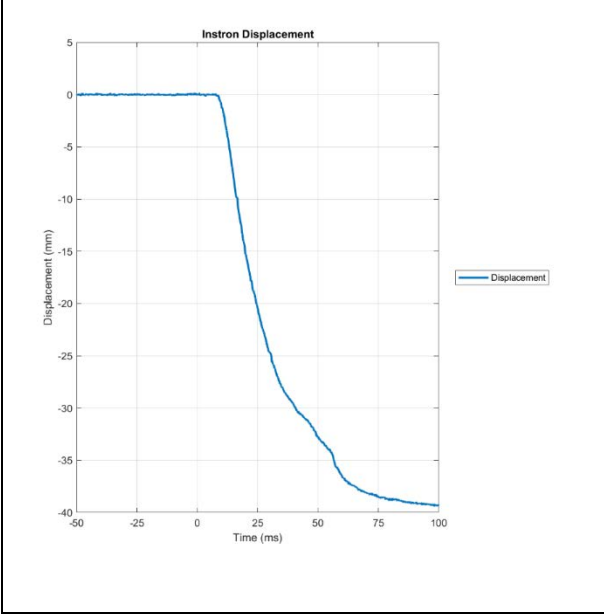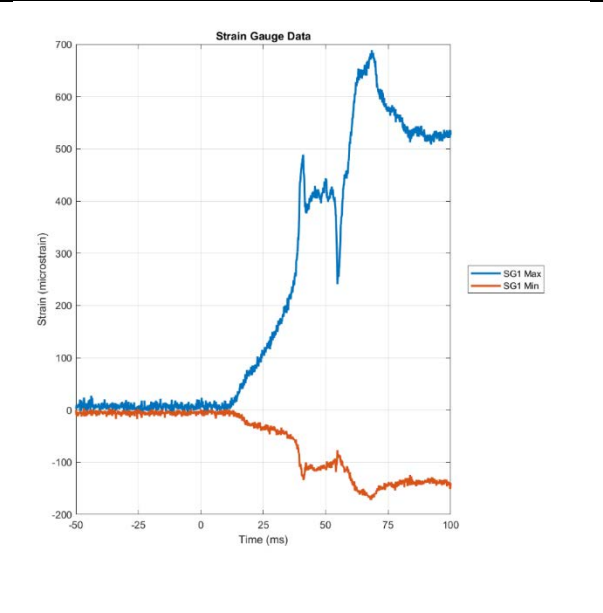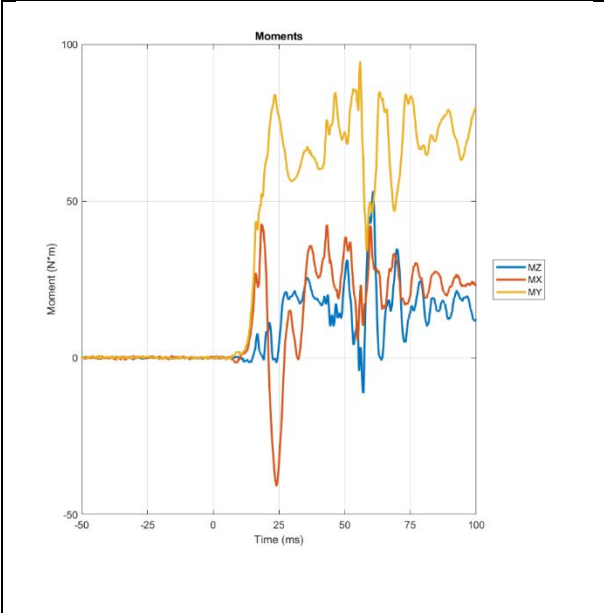
Table 8.6-21 - 792R Test Data
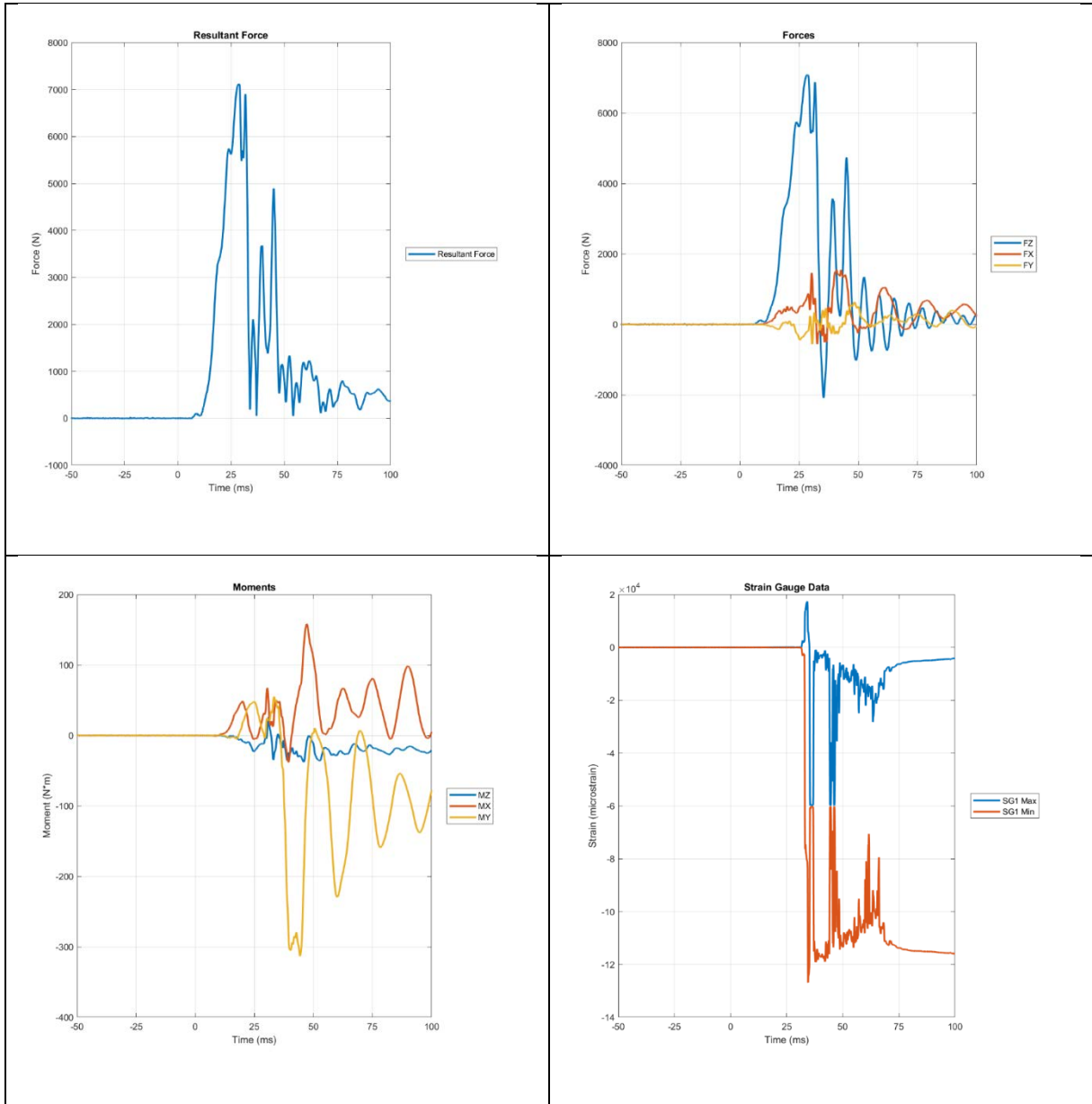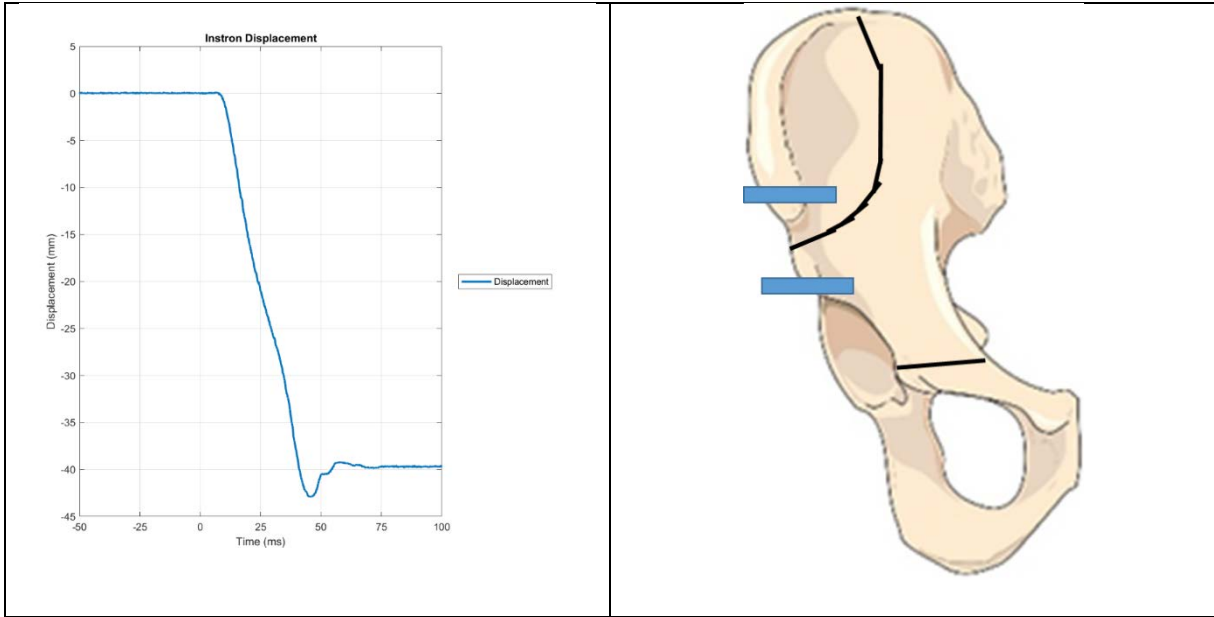
Table 8.6-22 - 792L Test Data
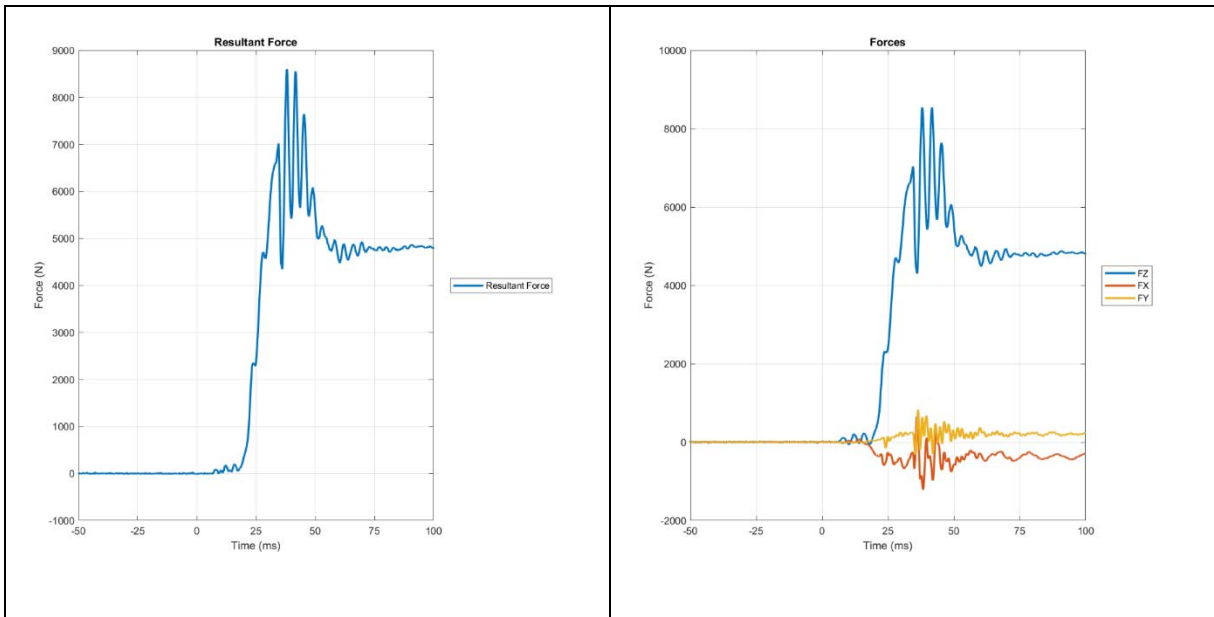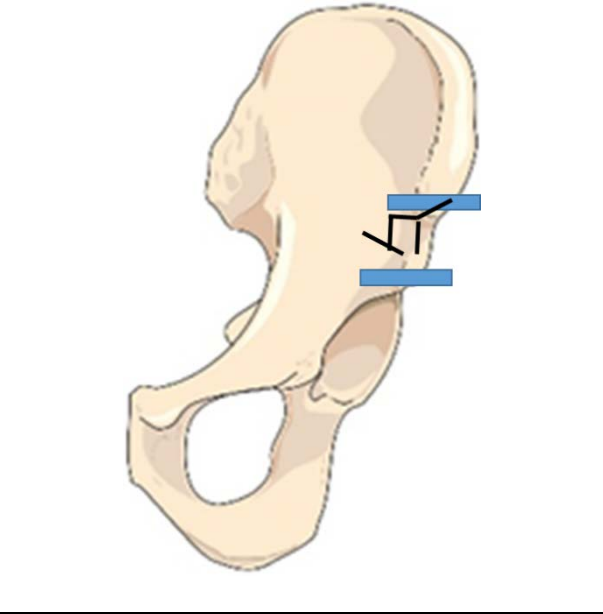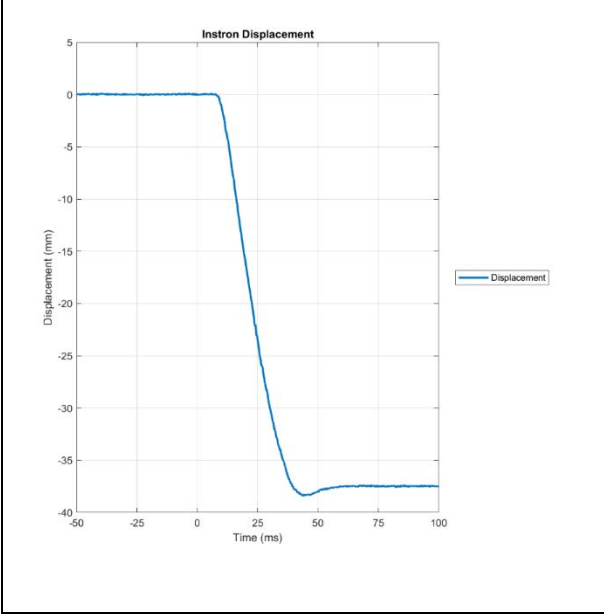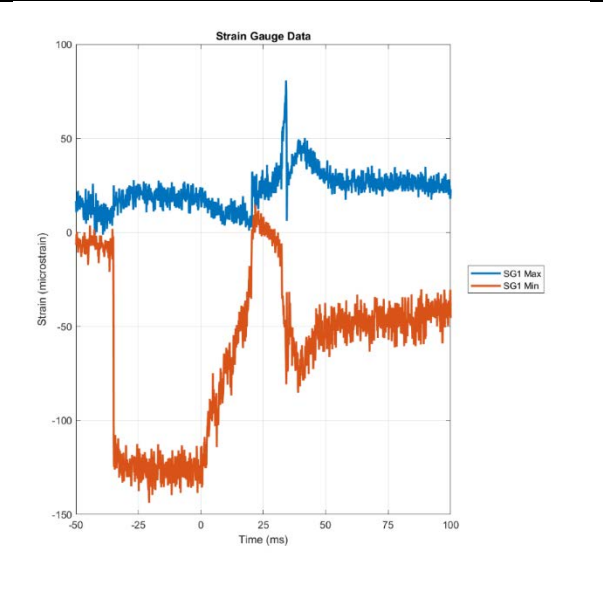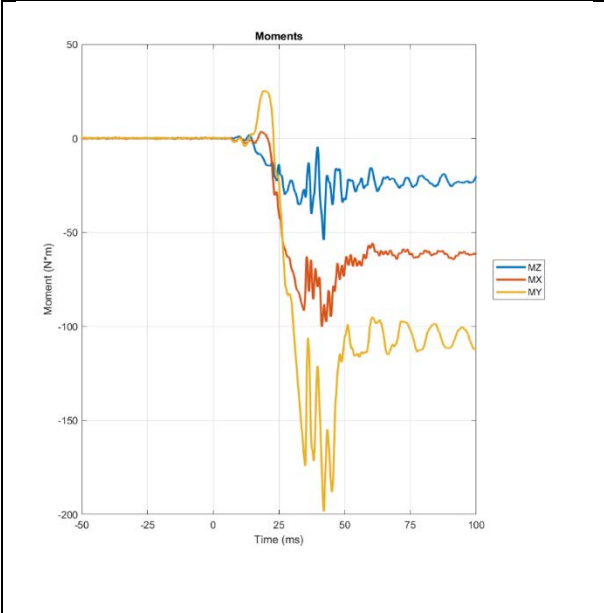
Table 8.6-23 - 798R Test Data
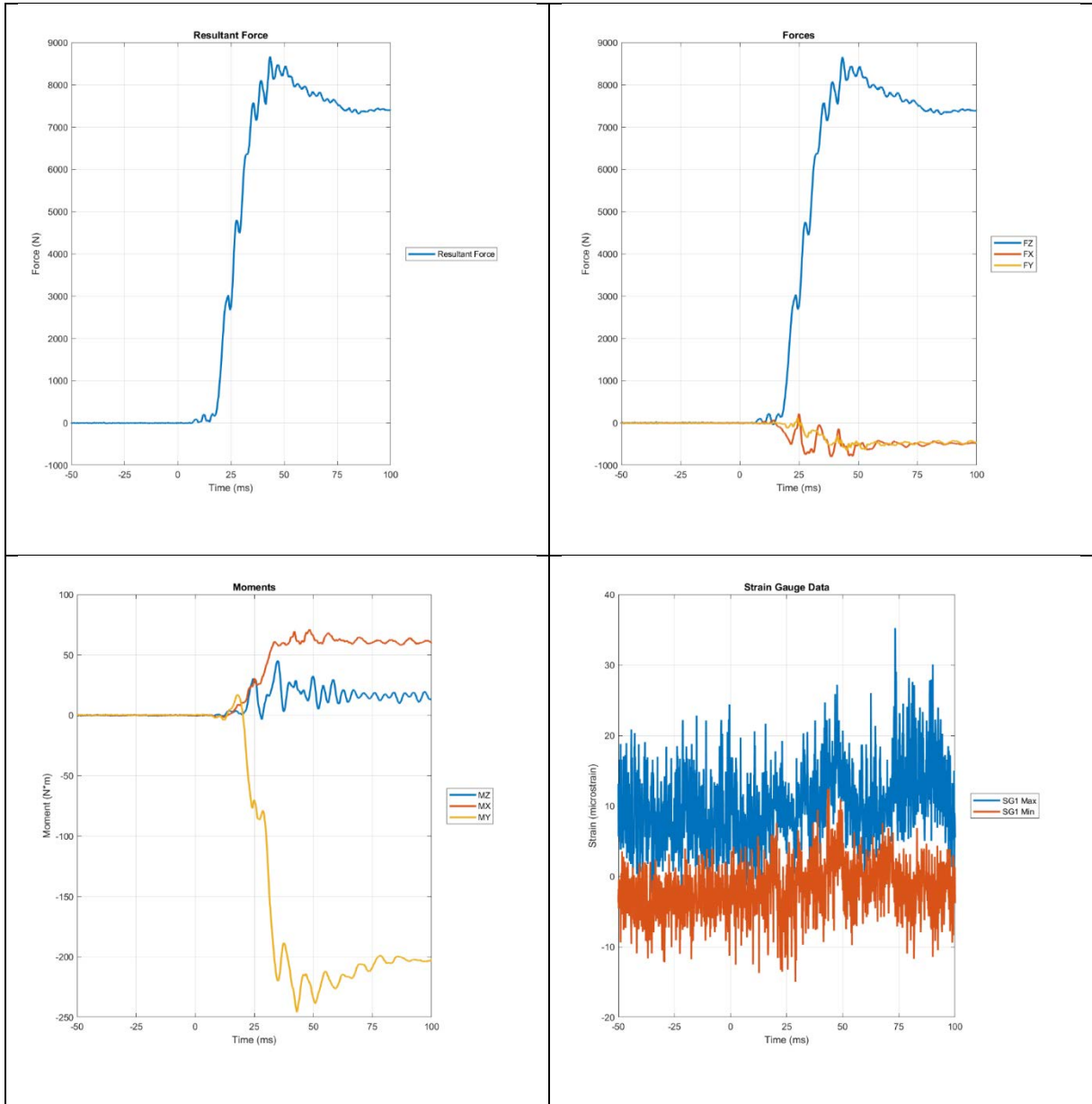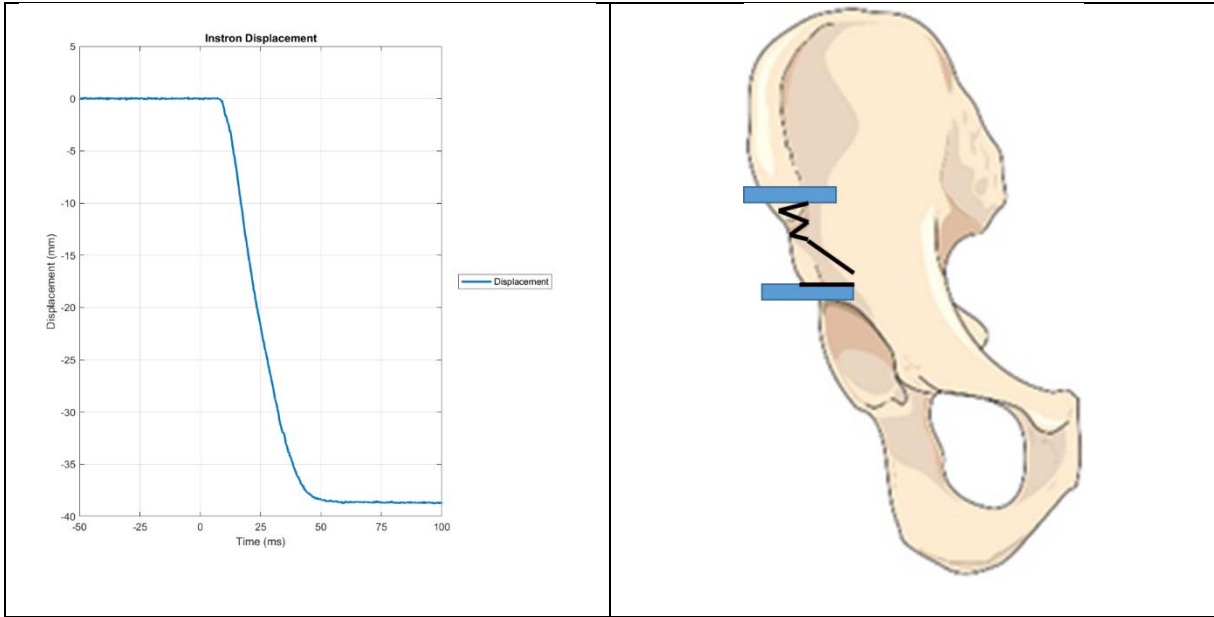
Table 8.6-24 - 798L Test Data
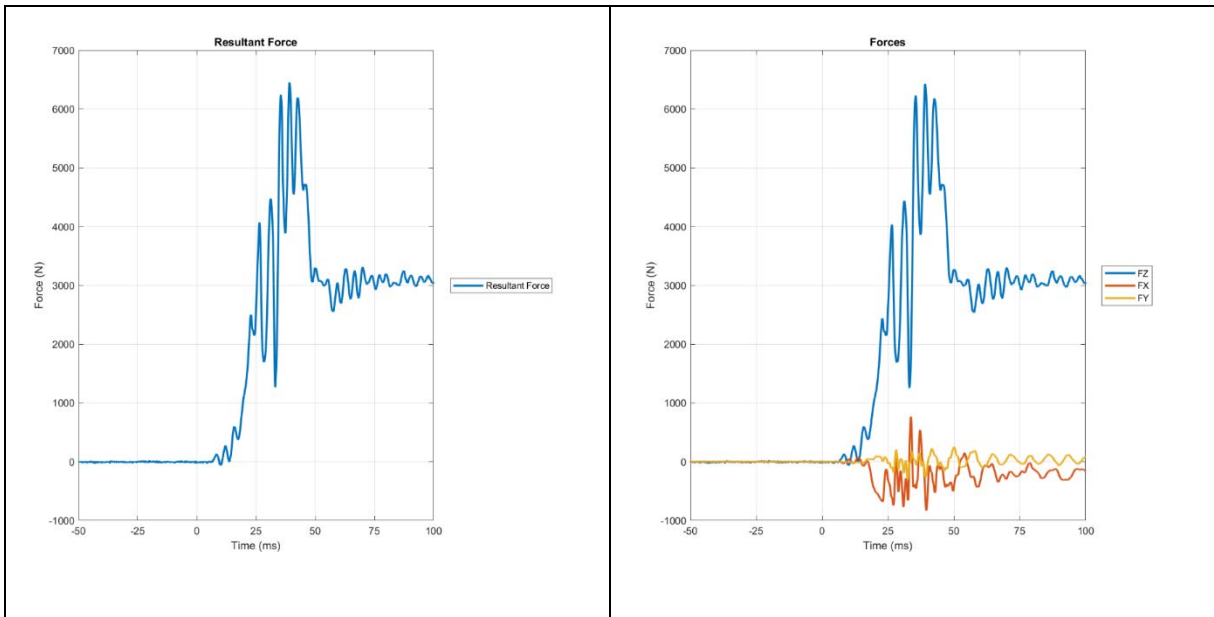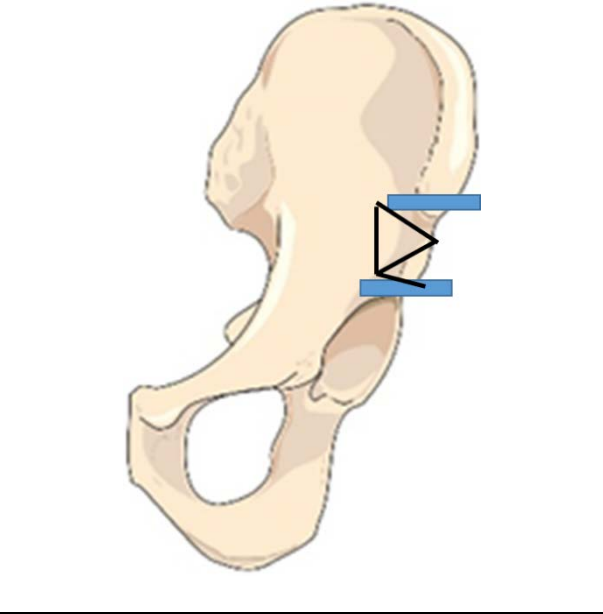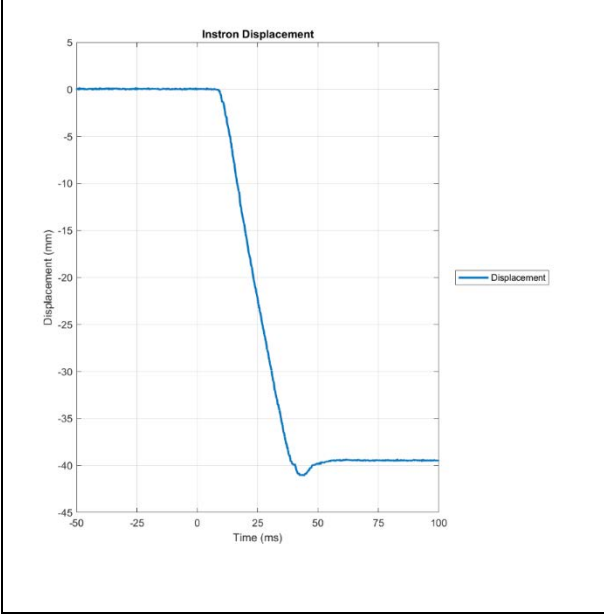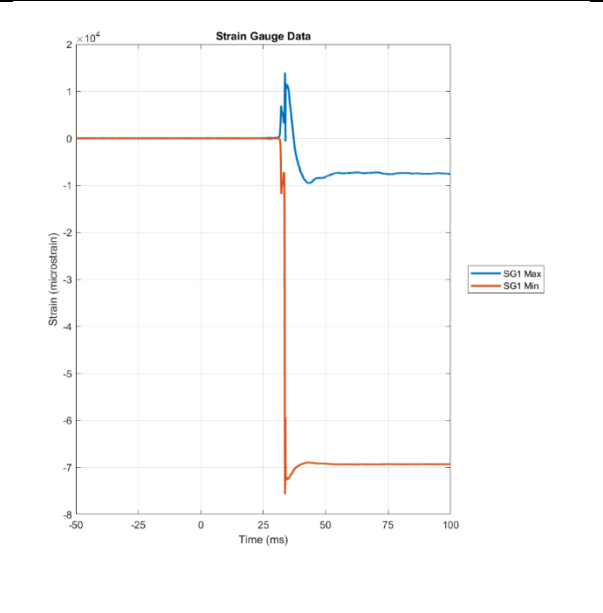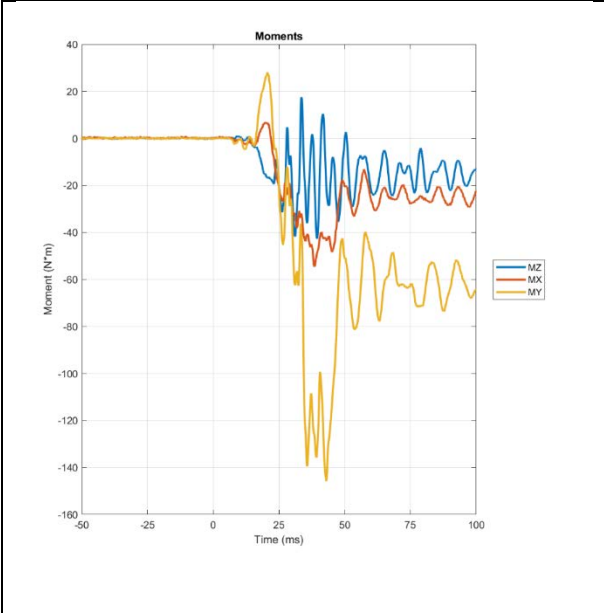
Table 8.6-25 - 997R Test Data
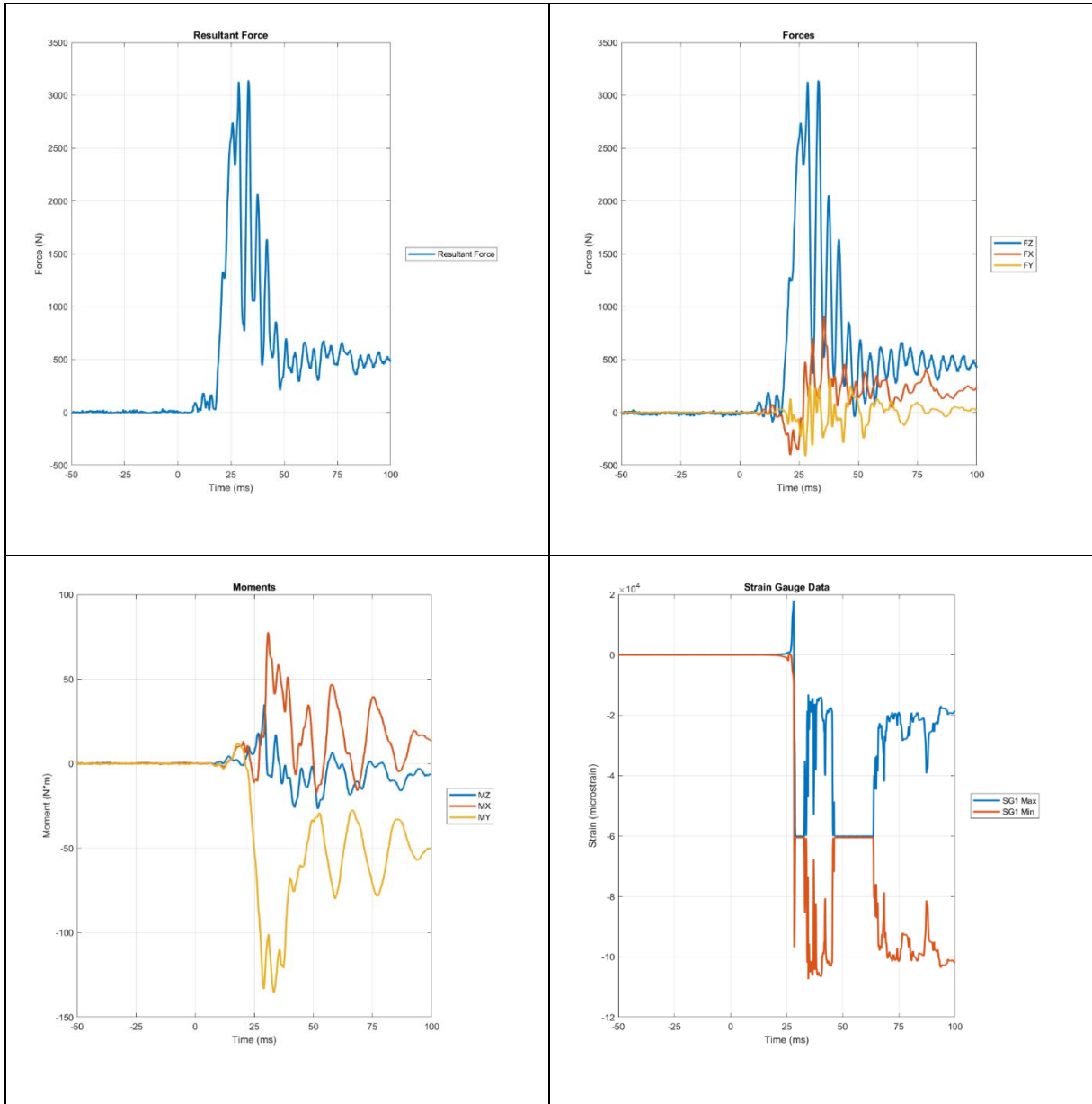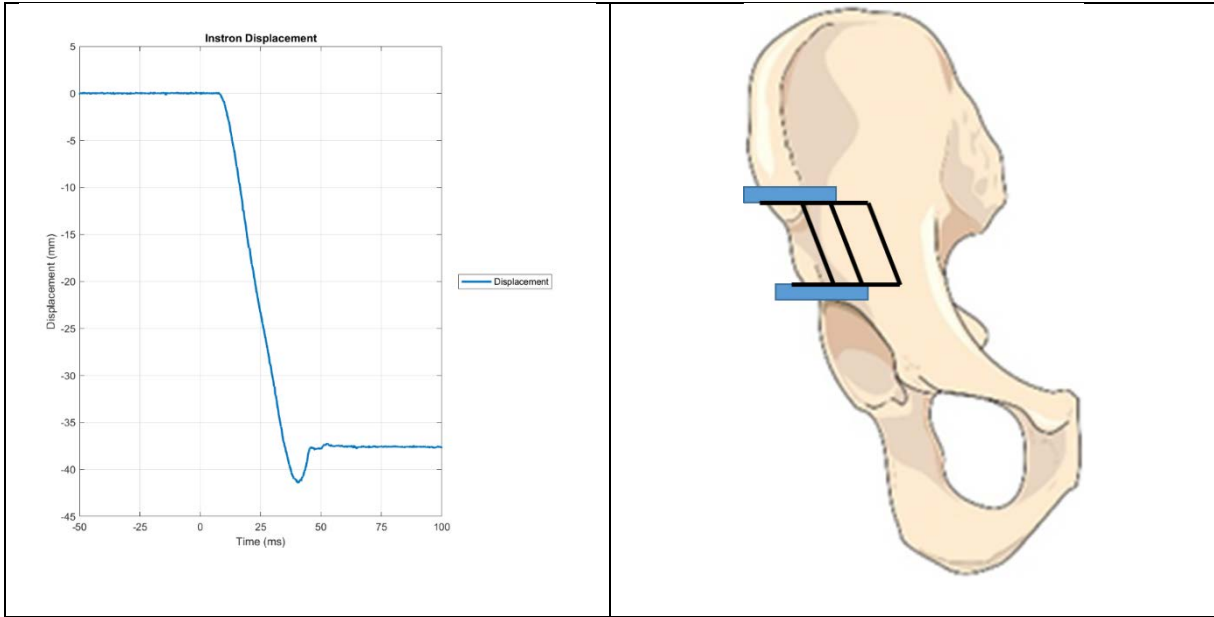
Table 8.6-26 - 997L Test Data
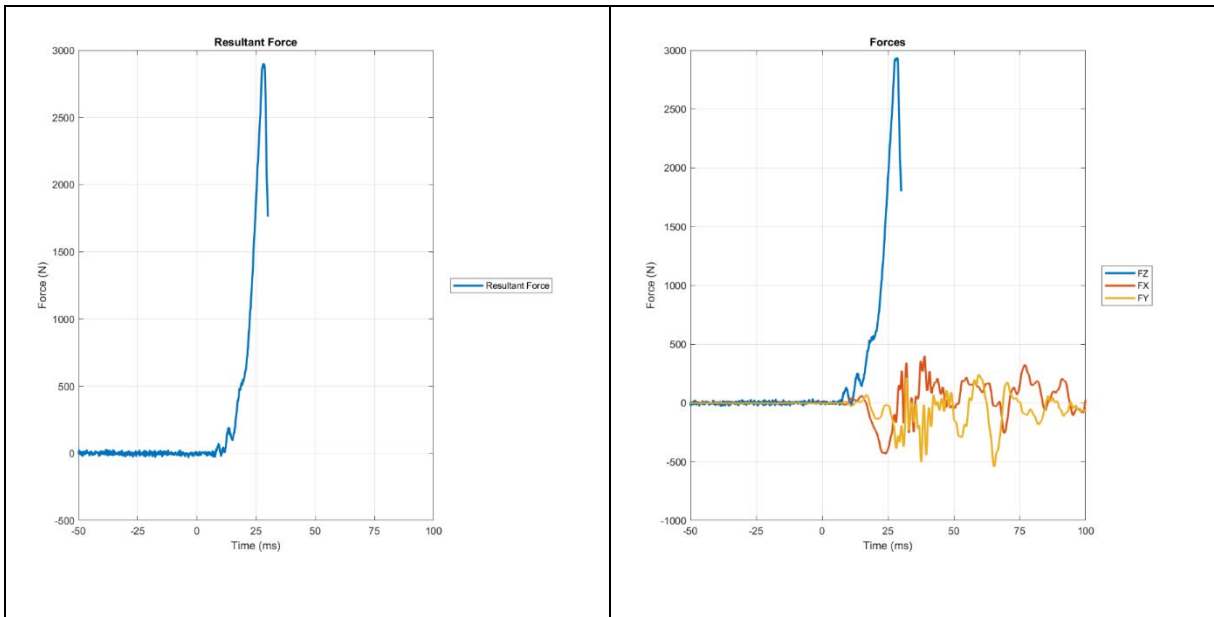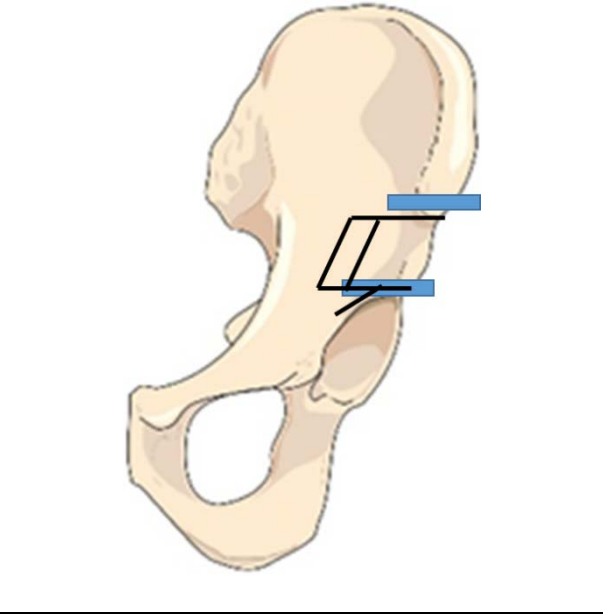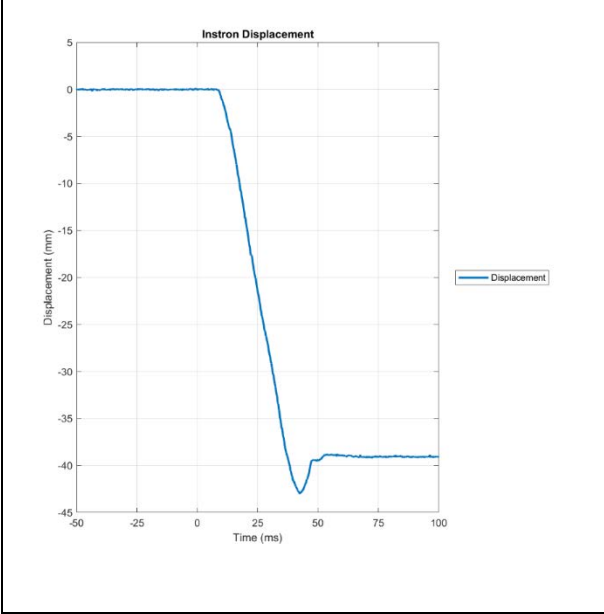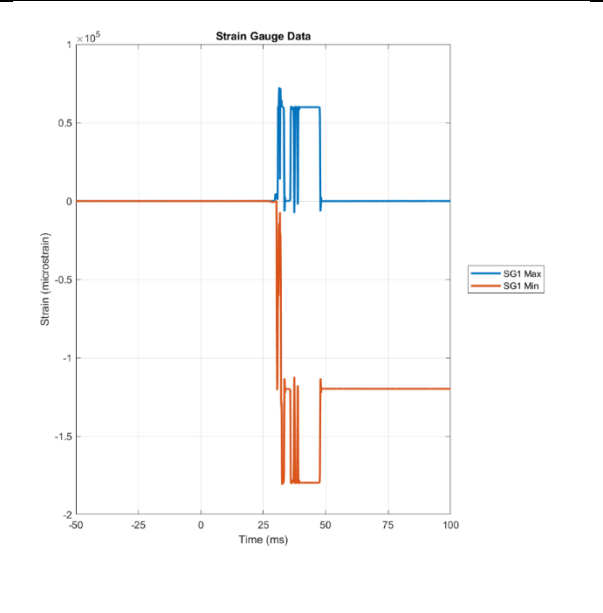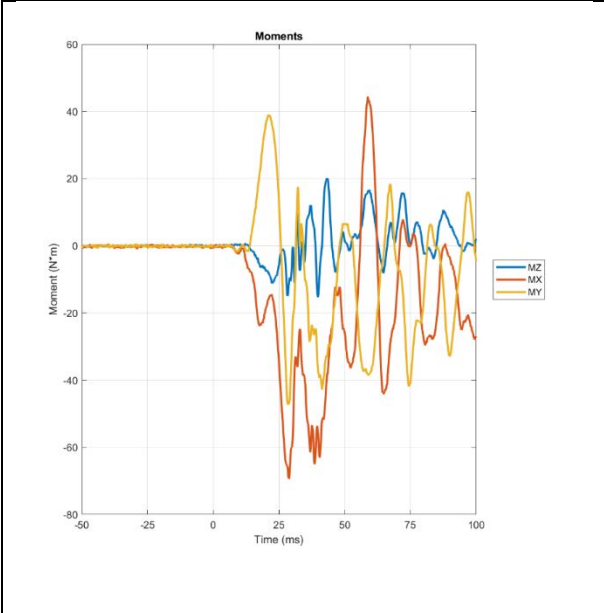
Table 8.6-27 - 998R Test Data
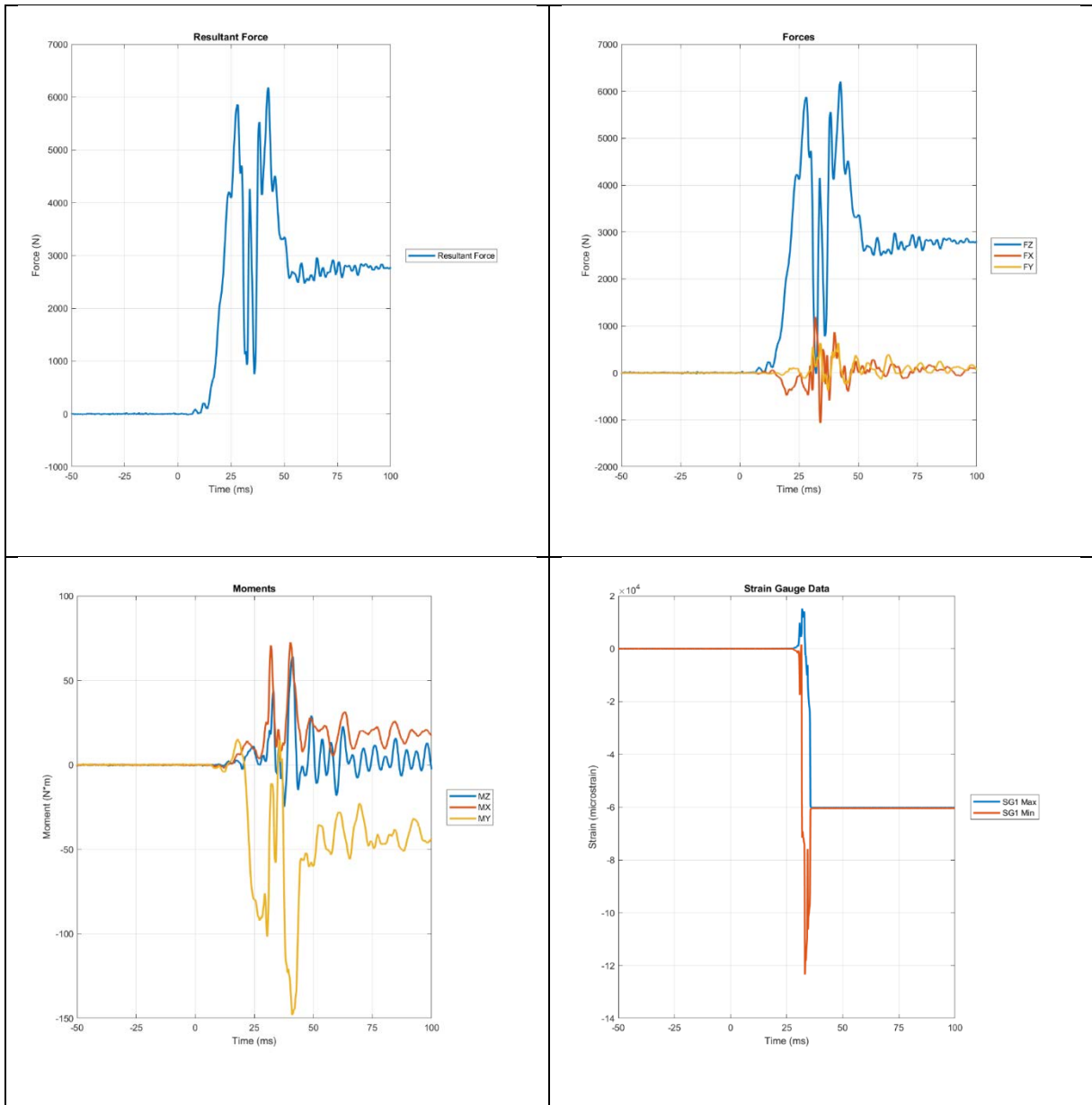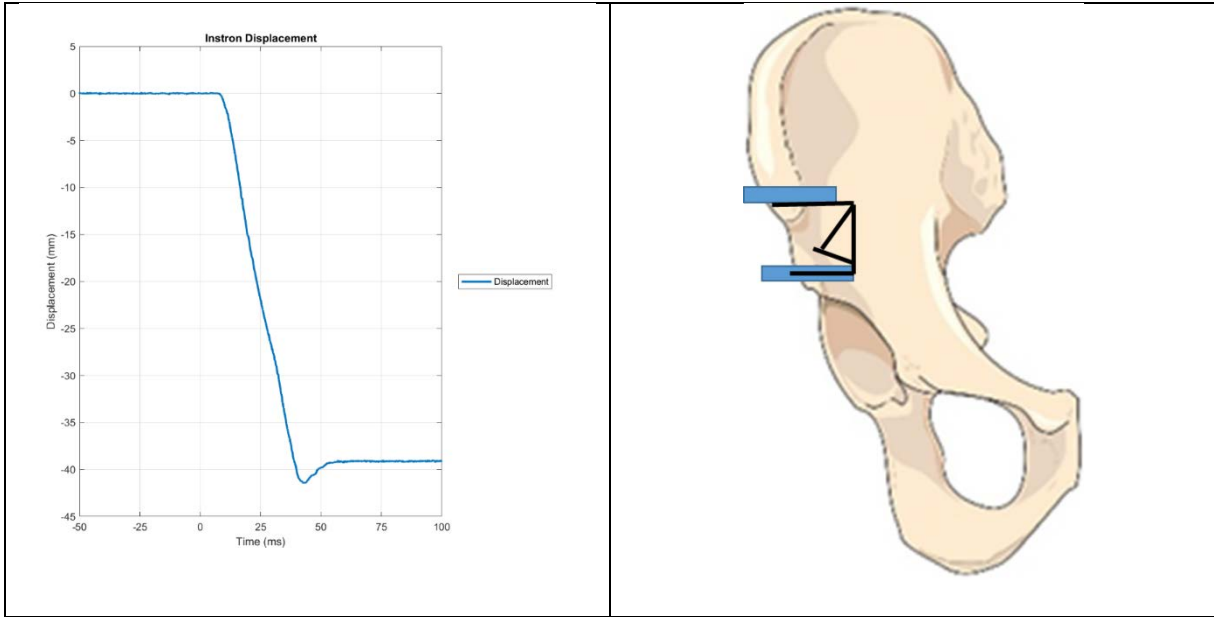
Table 8.6-28 - 998L Test Data
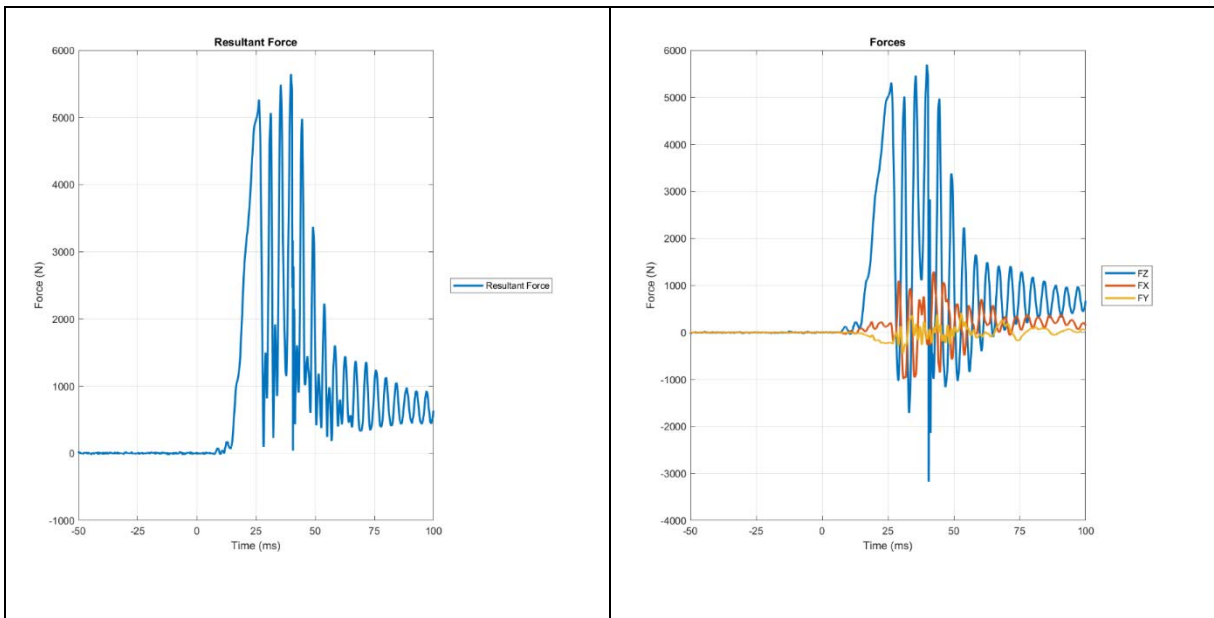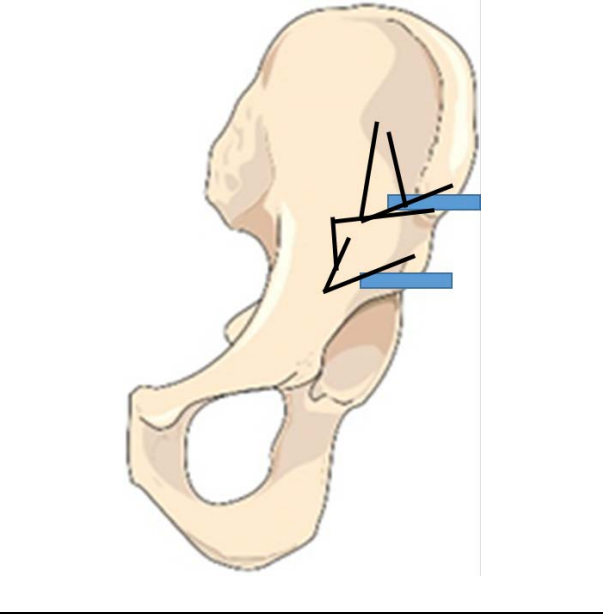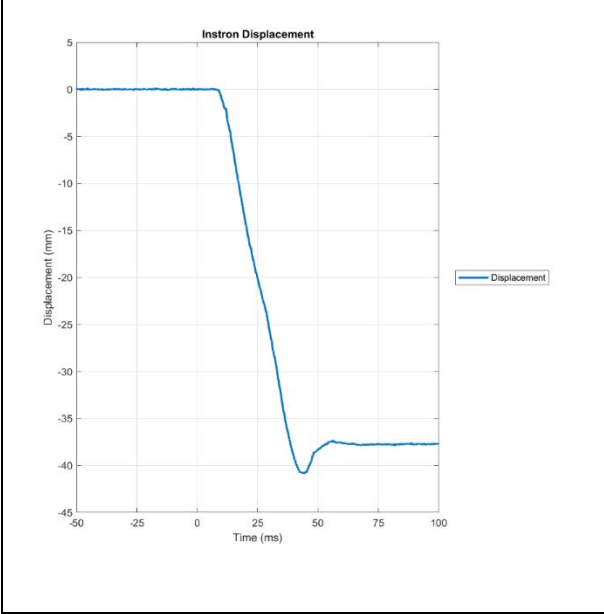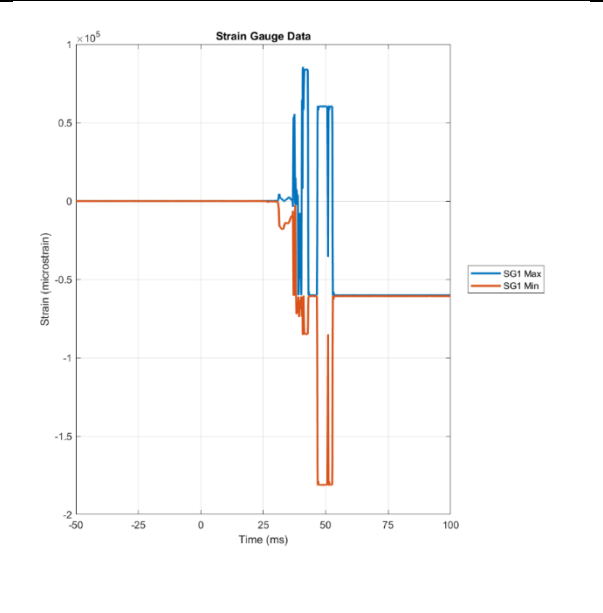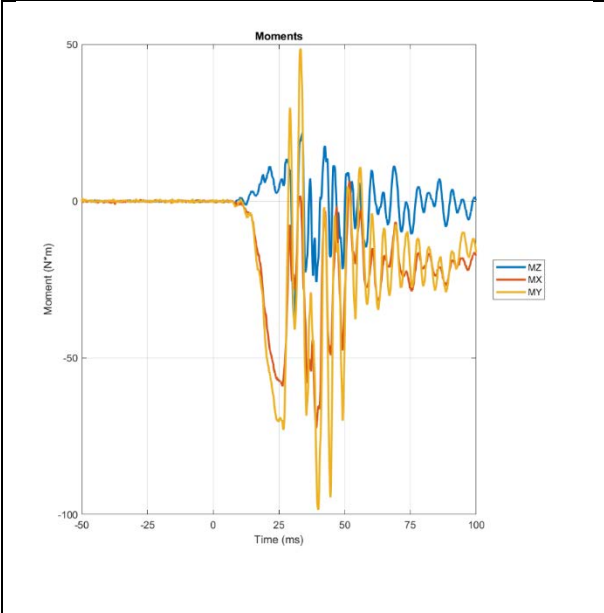
Table 8.6-29 - 999R Test Data
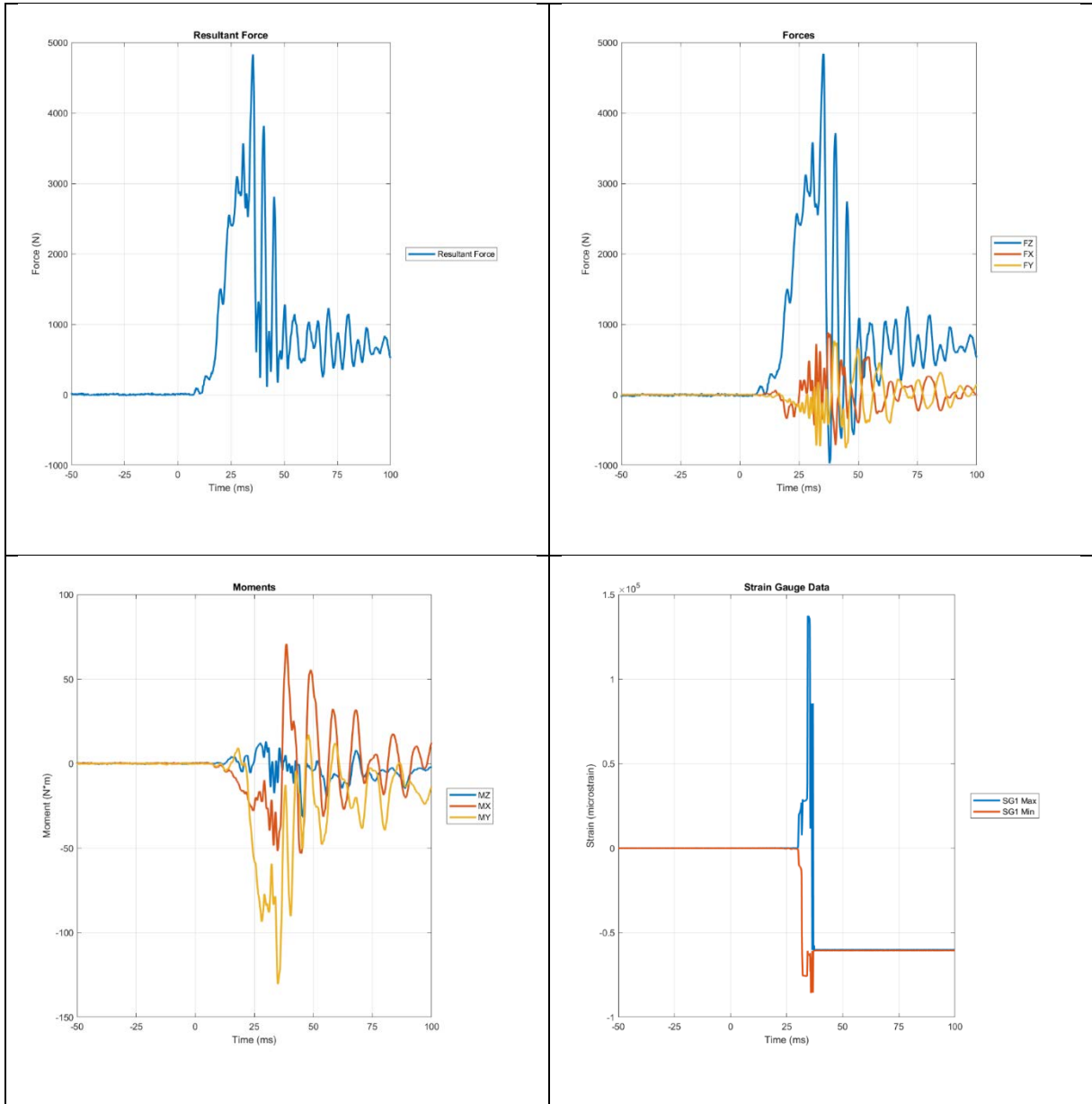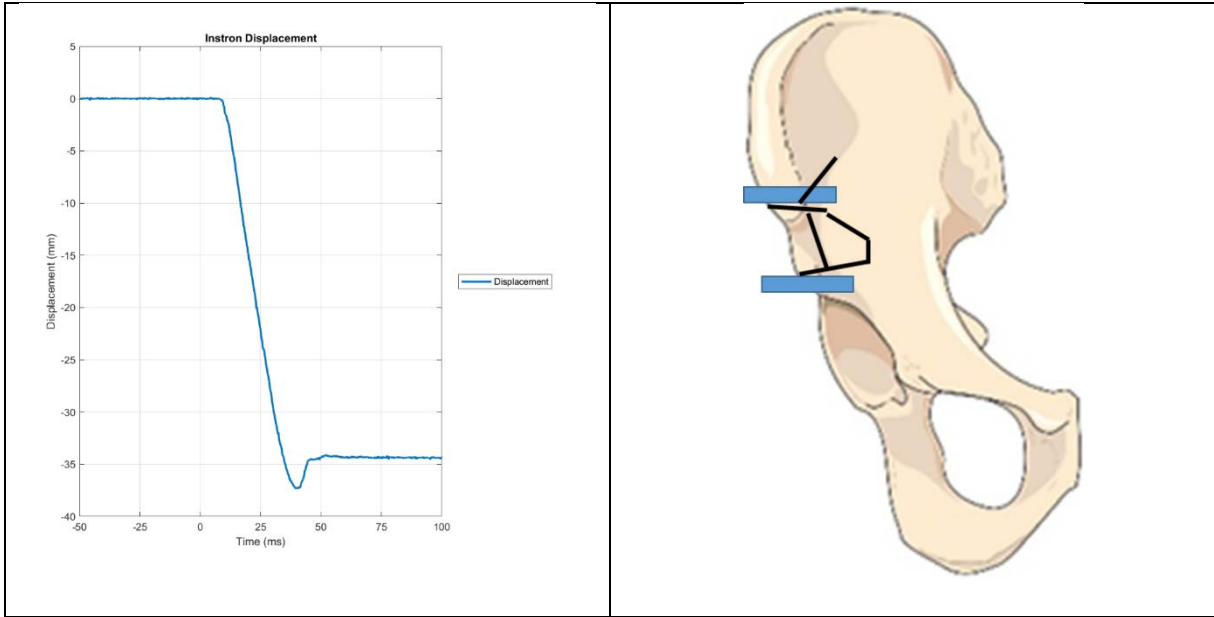
Table 8.6-30 - 999L Test Data
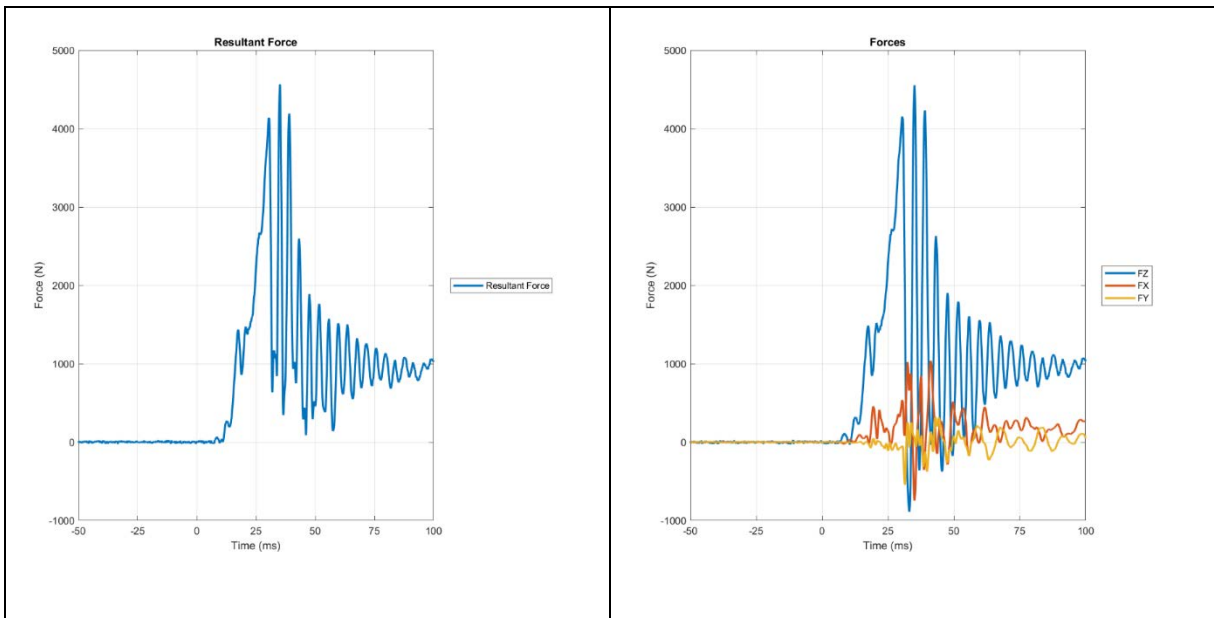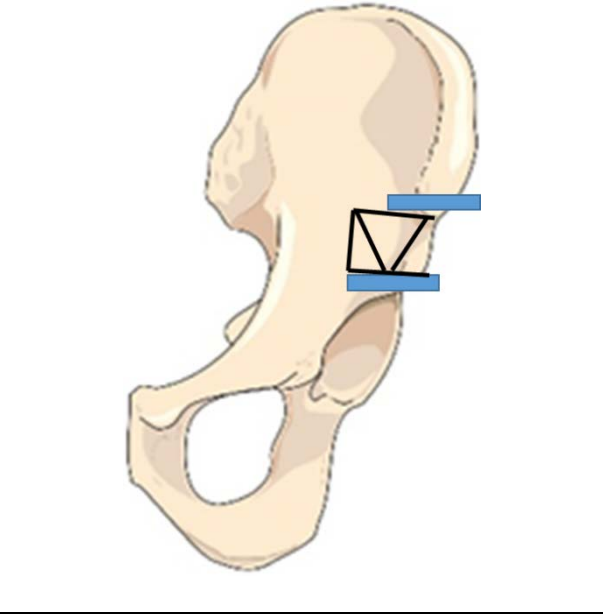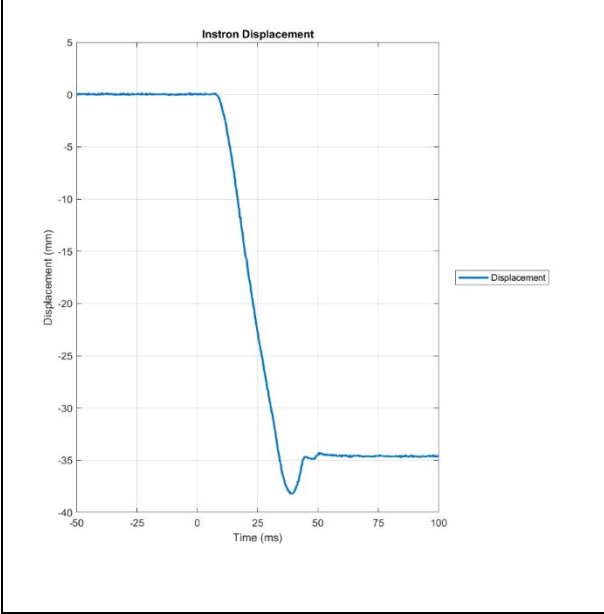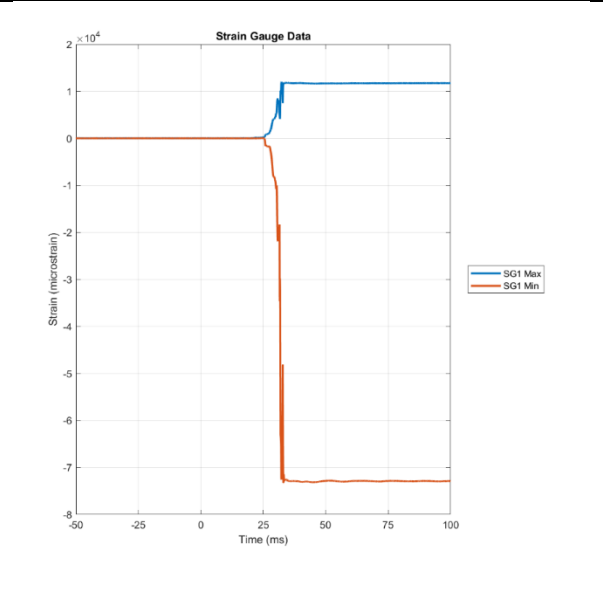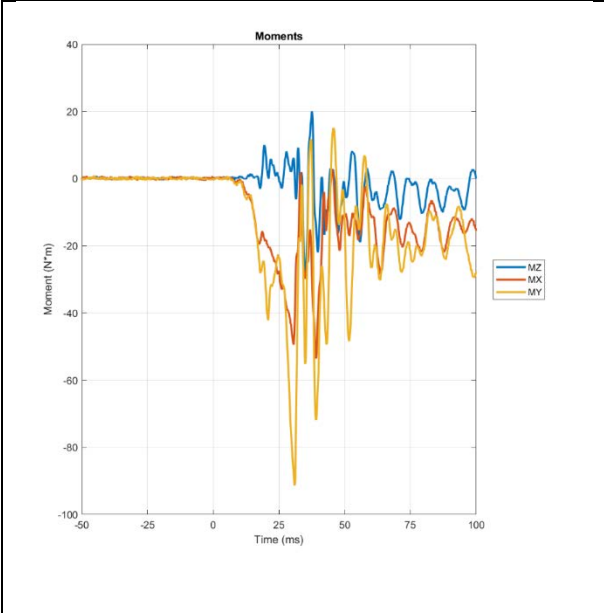
Table 8.6-31 - 1000R Test Data
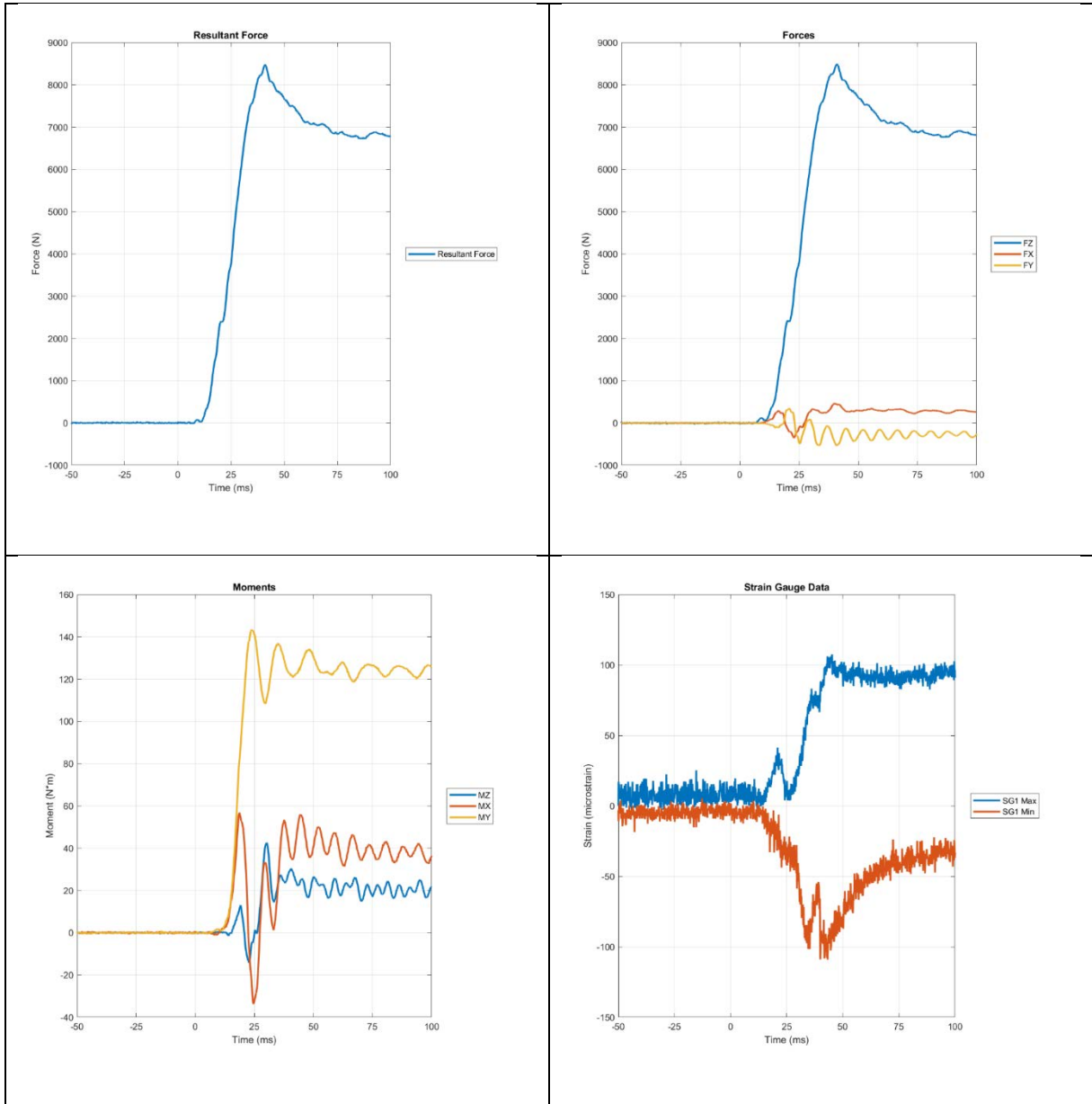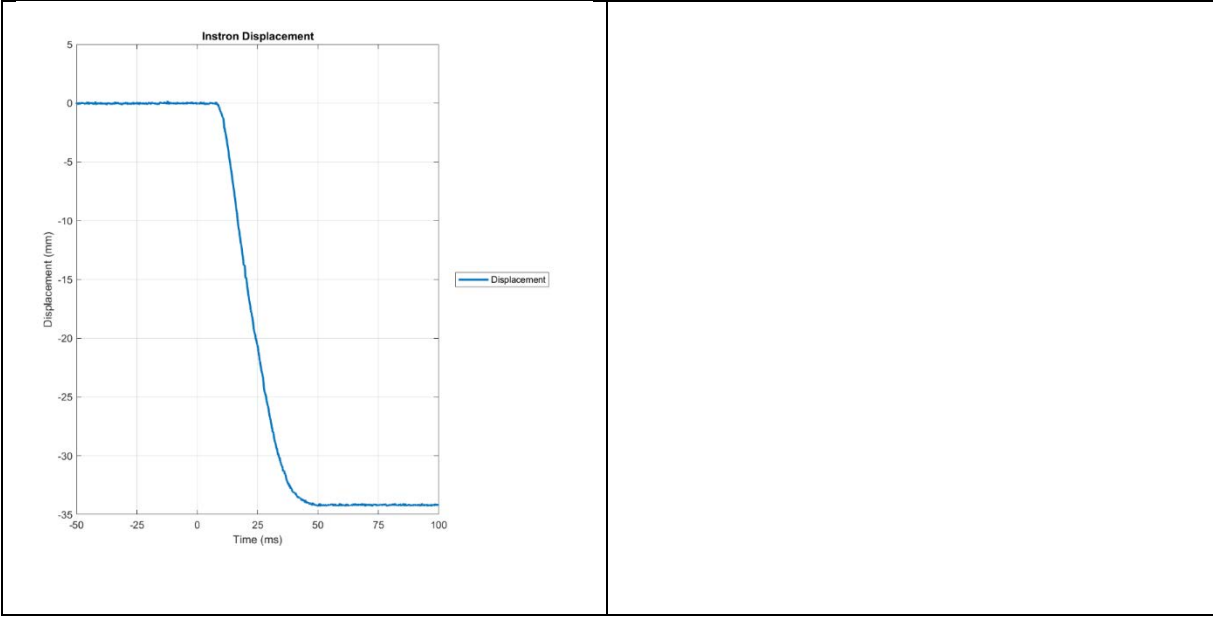
Table 8.6-32 - 1000L Test Data
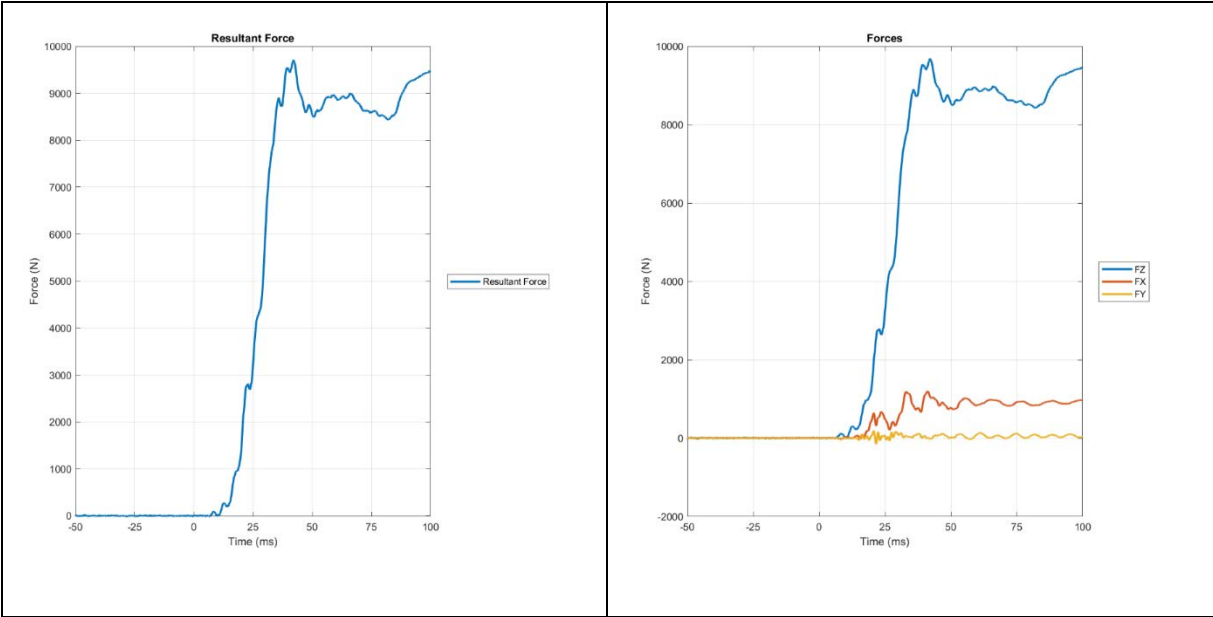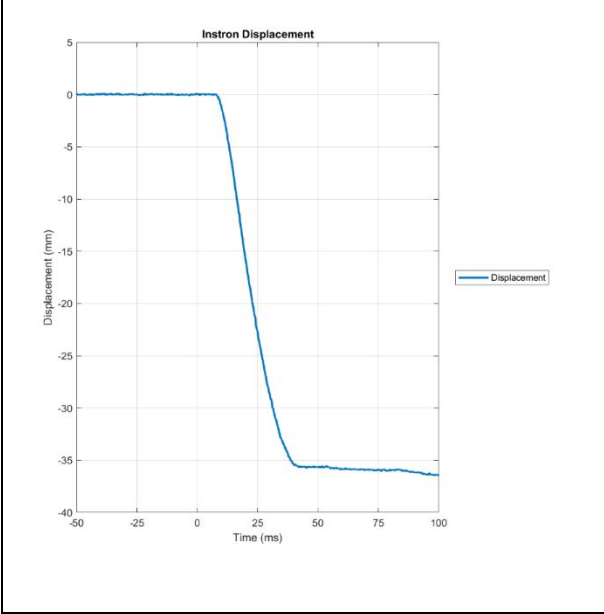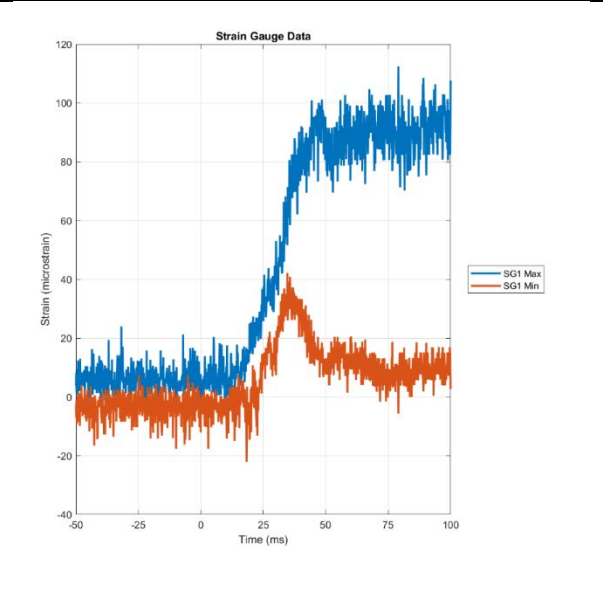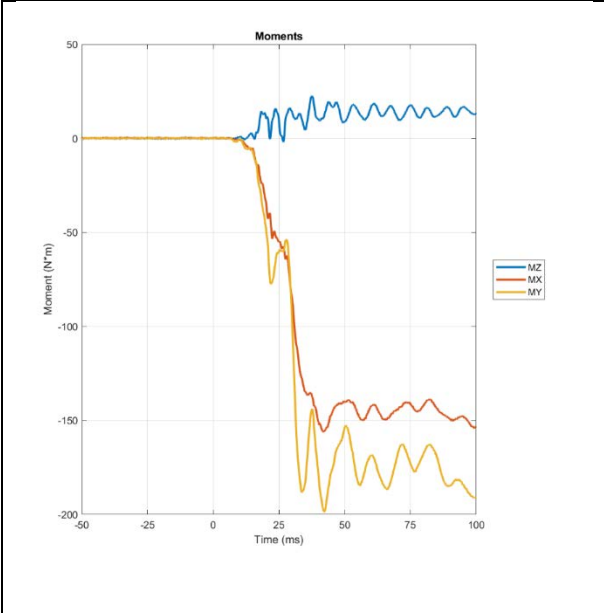
8.6. Appendix E: Scatterplots of Possible Covariates for IRF
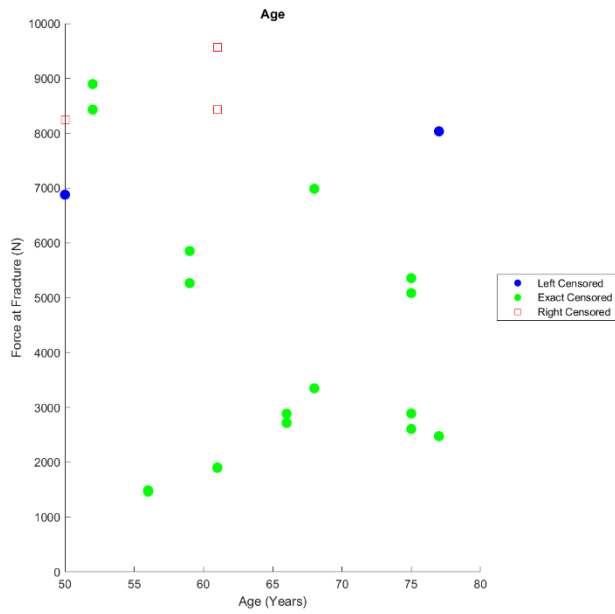
Correlation Value (R)	P Value of Slope
-.300	.1744
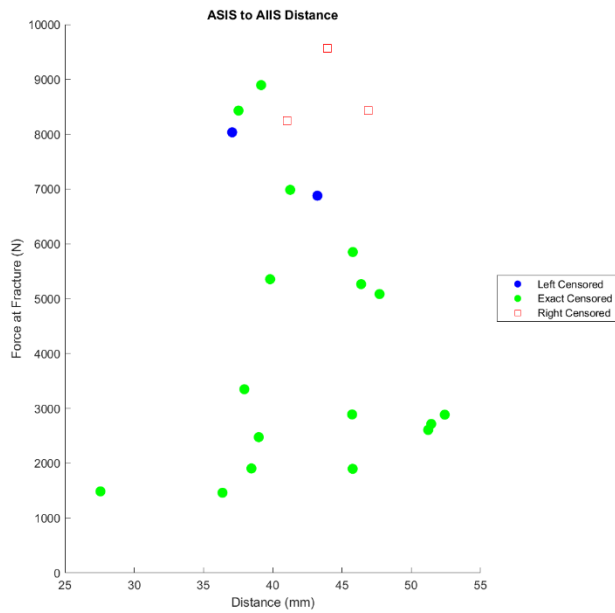
Correlation Value (R)	P Value of Slope
-.010	.963

ASIS to ASIS Distance
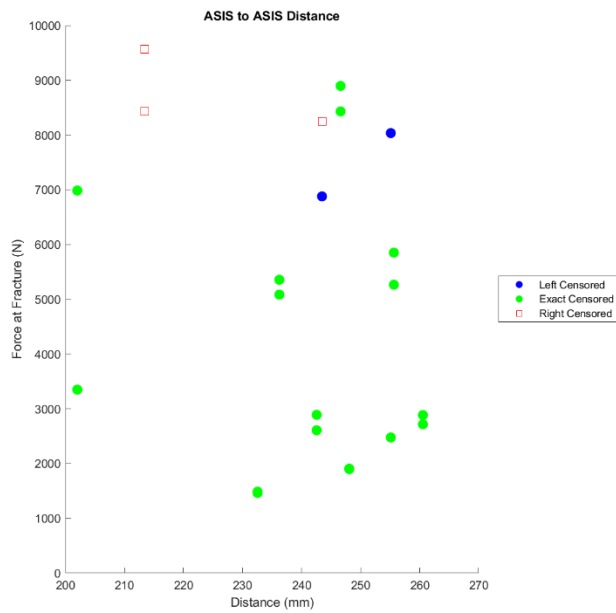
Correlation Value (R)	P Value of Slope
-.230	.303

ASIS to PC Distance
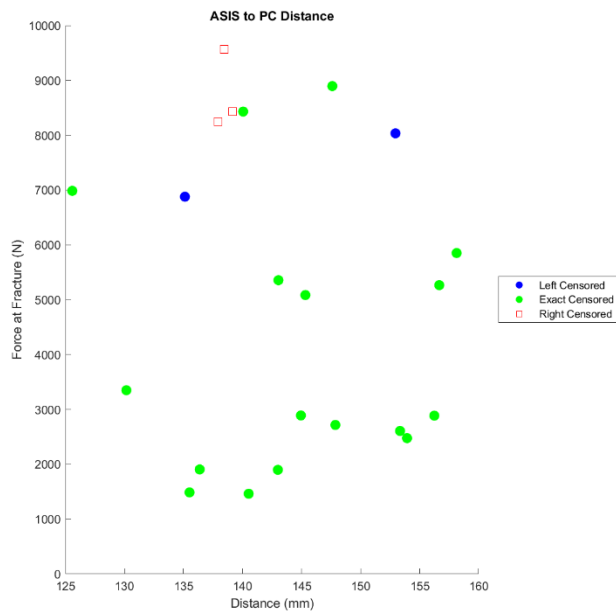
Correlation Value (R)	P Value of Slope
-.124	.582

ASIS to PSIS Distance
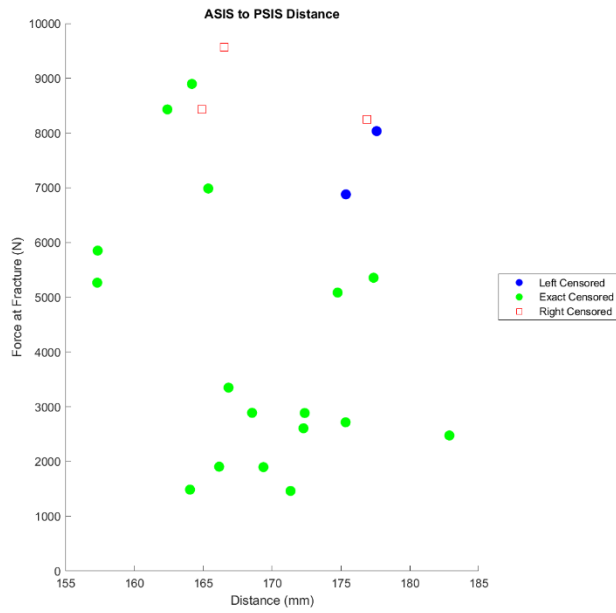
Correlation Value (R)	P Value of Slope
-.163	.469

Age vs BMD
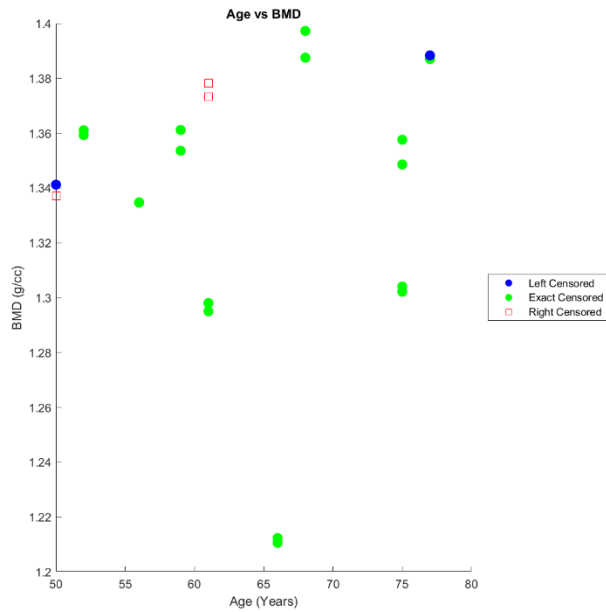
Correlation Value (R)	P Value of Slope
.01	.965

Cortical vs Trabecular
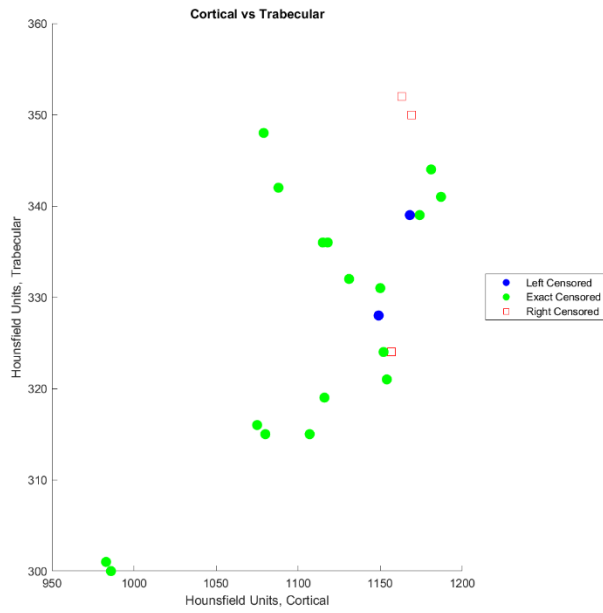
Correlation Value (R)	P Value of Slope
.69	**.0003**

Cortical HU
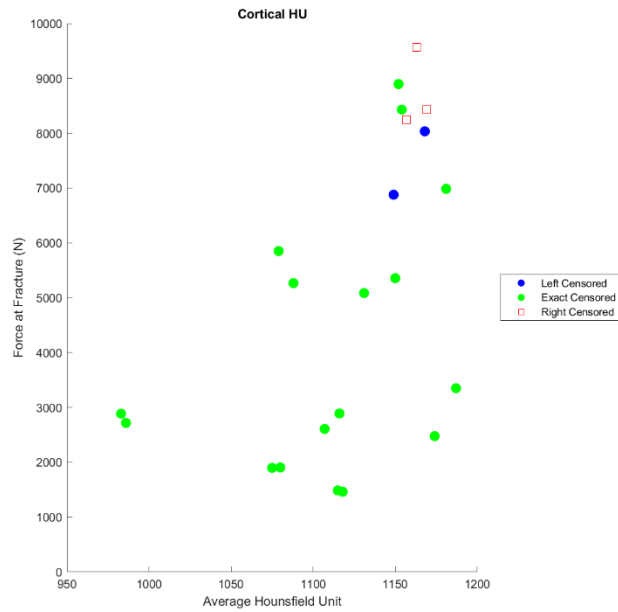
Correlation Value (R)	P Value of Slope
.518	**.0136**
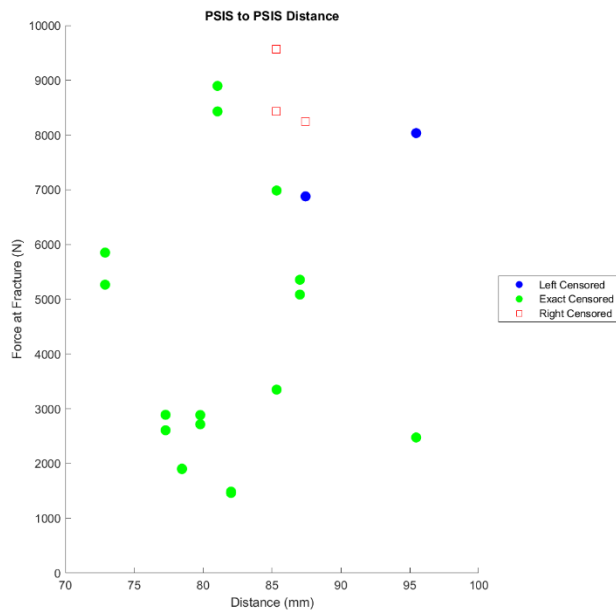
PSIS to PSIS Distance

Correlation Value (R)	P Value of Slope
.288	.194

Strong Bone Ratio

Correlation Value (R)	P Value of Slope
.501	**.016**

Trabecular HU
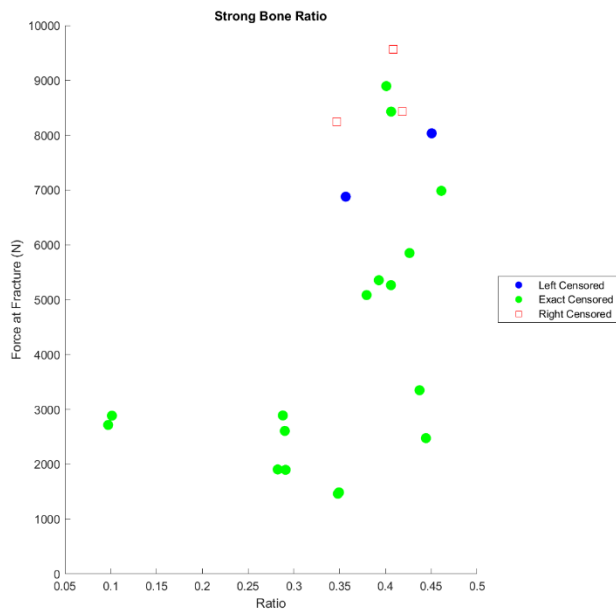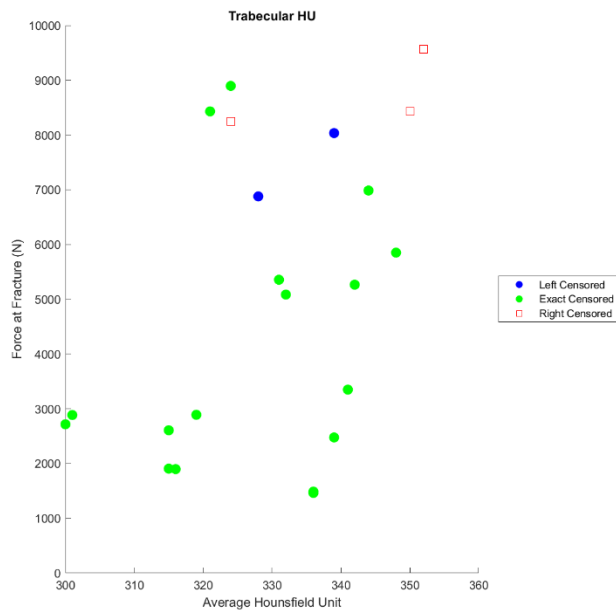
Correlation Value (R)	P Value of Slope
.422	.0504

Weak Bone Ratio

Correlation Value (R)	P Value of Slope
-.501	**.016**

Weight
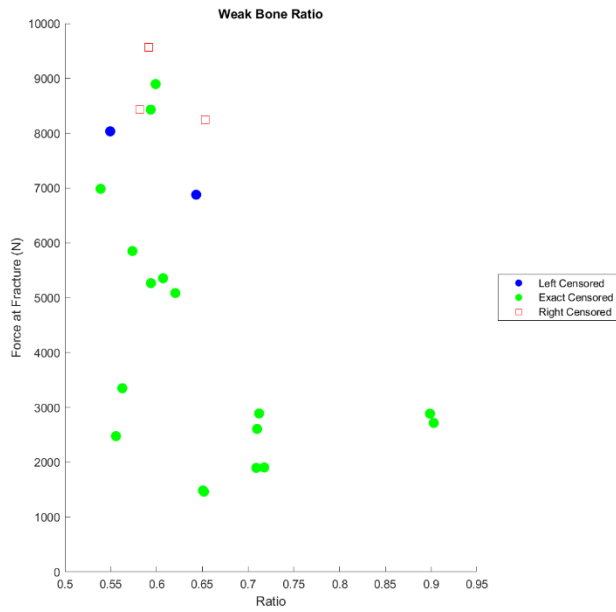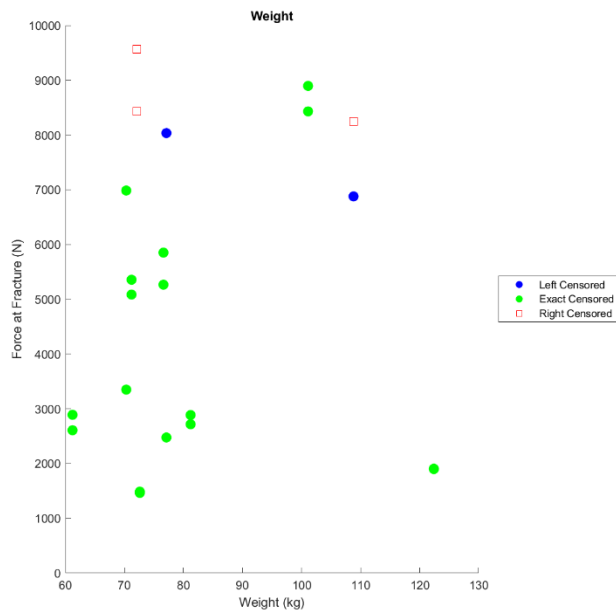
Correlation Value (R)	P Value of Slope
.086	.703

Weighted Average BD
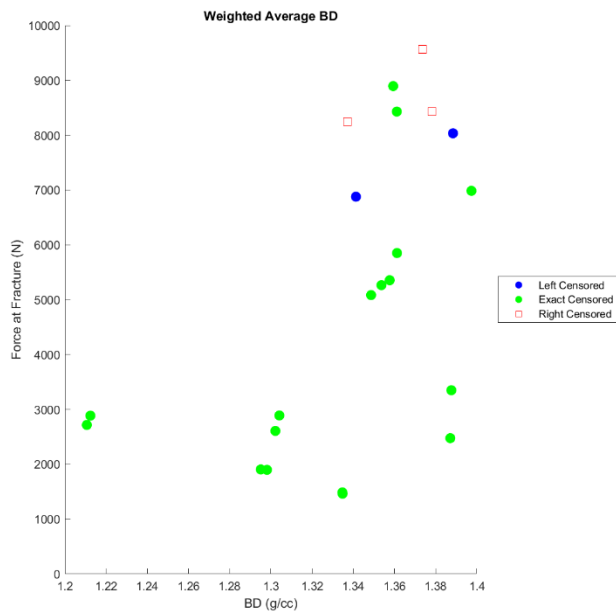
Correlation Value (R)	P Value of Slope
.528	**.0115**